Functional Assessment of Rare Genetic Variants of Complement Factor I in Age-Related Macular Degeneration

Thomas Edward Cox

Thesis submitted in partial fulfilment of the requirements for the degree of Doctor of Philosophy

Translational and Clinical Research Institute

Newcastle University

October 2021

Abstract

Age-related macular degeneration (AMD) is the leading cause of blindness in the developed world. There is no cure for the disease, and treatment options remain limited to anti-vascular endothelial growth factor (VEGF) therapeutics and dietary supplementation. Several pivotal studies have associated both rare and common genetic variants in complement factor I (*CFI*) with an increased AMD susceptibility, with rare variants carrying a particularly increased burden (Seddon *et al.*, 2013; Fritsche *et al.*, 2016).

Three rare genetic variants of *CFI* nominally associated with AMD were identified for further functional analysis (R406H, K441R and P553S). Their selection was based upon occurrence in the literature, in silico analysis and structural modelling within the alternative pathway (AP) regulatory trimolecular complex (TMC). Each of the three variants are secreted and are reported within the normal range for serum FI levels.

A simplified method was developed for the purification of both recombinant and plasma FI without the need for a polyhistidine tag. Recombinant protein production led to the generation of a mixture of proteins, Pro-I and FI. Pro-I is proposed to be functionally inactive, however this has not been proven. To facilitate the removal, and subsequent analysis of Pro-I, the generation of an antibody was attempted, however this was unsuccessful. Using ion-exchange chromatography, Pro-I could be purified from both plasma and supernatant and has been confirmed as completely inactive and incapable of forming the AP regulatory TMC.

Additionally, a novel method for generating completely processed, fully functional recombinant FI has been developed. Through the modelling of K441R, R406H and P553S on both a WT and inactive (S525A) *CFI* backbone, this has enabled the most extensive analysis of these variants recorded in the literature. K441R, R406H, P553S all demonstrate proteolytic activity, however P553S demonstrates a significantly reduced activity in a variety of fluid-phase cofactor assays. When modelled on the AP regulatory TMC, K441R performed similarly to WT, R406H demonstrated a slightly reduced response, and P553S exhibited noticeably decreased binding.

These results led to the hypothesis that patients carrying the variants P553S and R406H may benefit from complement inhibition or FI supplementation, due to a defect in AP regulation which may exacerbate their disease.

Declaration

I declare that no work presented in this thesis has been submitted elsewhere for the award of any other degree or qualification. The work presented has been carried out by me, unless otherwise stated, and all sources of information have been acknowledged by reference.

Thomas E. Cox

Acknowledgements

I would first like to start my thanking my funders the Medical Research Council, and the Discovery Medicine North (DiMeN) Doctoral Training Partnership, for giving me this opportunity.

Secondly, I would like to express my gratitude towards both of my supervisors, Professor David Kavanagh and Professor Kevin Marchbank, for their continued academic support, patience, and guidance throughout this project.

I am incredibly grateful to all members of the Complement Therapeutics Group, who have provided technical support, advice and friendship over the last five years. In particular, I would like to give thanks to Professor Claire Harris, Dr Edwin Wong, Dr Thomas Hallam, Mrs Harriet Denton, Dr Yi Yang and Dr Isabel Pappworth.

I would also like to extend my thanks to the staff in the Comparative Biology Centre at Newcastle University for their support and assistance with the animal work.

Thank you also to my friends and family for their help, support and understanding for the last five years.

Last, but by no means least, I would like to thank my partner, Georgie. I really could not have done this without you. You are my rock.

Contents

Table of Figures

List of Tables

Abbreviations

2ME	β Mercaptoethanol
Ab	Antibody
ABCA1	ATP-binding cassette transporter 1
aHUS	Atypical haemolytic uremic syndrome
AMC	7-amino-4-methylcoumarin
AMD	Age-related macular degeneration
AP	Alternative pathway
APOE	Apolipoprotein E
AREDS	Age-related eye disease study
ARHGAP21	RhoGAP Rho GTPase Activating Protein 21
ARMS2	Age-related maculopathy susceptibility protein 2
ARPE-19	A spontaneously arising retinal pigment epithelia 19
ATP	Adenosine triphosphate
B3GALTL	Beta-1,3-glucosyltransferase
BM	Bruch's membrane
BRB	Blood-retinal barrier
BSA	Bovine serum albumin
C[n]	Complement component [number]
C1-INH	C1 esterase inhibitor
C3G	Complement 3 glomerulopathy
C3INA	C3 inactivator
C4BP	C4 binding protein
CADD	Combined annotation dependent depletion

CCP	Complement control protein
CD	Cluster of differentiation
cDNA	Complementary deoxyribonucleic acid
CETP	Cholesteryl ester transfer protein
CFD	Complement fixation diluent
CFH	Complement factor H
CFHR	Complement factor H receptor
CFI	Complement factor I
CFID	Complete FI deficiency
CHO	Chinese hamster ovary cell
CL-4B	Cross-linked agarose, 4%, spherical
CNV	Choroidal neovascularisation
COL8A1	Collagen type VIII alpha 1 chain
COS-1	CV-1 in origin carrying SV40 -1
CP	Classical pathway
CR[n]	Complement receptor [number]
CRA	Closely related antigens
CRP	C-reactive protein
CSE	Cigarette smoke extract
CTC	C-terminal C3b
CV	Column volumes
DAA	Decay-accelerating activity
DAF	Decay-accelerating factor
DDD	Dense deposit disease

DMEM	Dulbecco's modified eagle medium
DMSO	Dimethyl sulfoxide
DNA	Deoxyribonucleic acid
dNTP	Deoxynucleoside triphosphate
DPBS	Dulbecco’s phosphate-buffered saline
EA	Sensitised erythrocytes
EA-C3b	C3b-coated sensitised sheep erythrocytes
ECL	Enhanced chemiluminescence
ECM	Extracellular matrix
EDC	N’-ethylcarbodimide hydrochloride
EDTA	Ethylenediaminetetraacetic acid
ELISA	Enzyme-linked immunosorbent assay
EUGENDA	European genetic database
FB	Factor B
FBS	Foetal bovine serum
Fc	Fragment crystallisable region
FD	Factor D
FH	Factor H
FHL-1	Factor H like protein 1
FI	Factor I
FIMAC	Factor I membrane attack complex domain
FLFH	Full-length Factor H
GA	Geographic atrophy
GAG	Glycosaminoglycan

GlcNAc	*N*-Acetylglucosamine
GVB	Gelatin veronal buffer
GWAS	Genome-wide association studies
HAT	Hypoxanthine aminopterin thymidine
HEK293	Human embryonic kidney 293 cells
HEPES	4-(2-hydroxyethyl)-1-piperazineethanesulfonic acid
HRP	Horseradish peroxidase
HSPG	Heparan Sulphate Proteoglycan 2
HTRA1	High temperature requirement A serine peptidase 1
HuCAL	Human combinatorial antibody libraries
HUVEC	Human umbilical veinendothelial cells
IAMDGC	International AMD genomics consortium
ICAM-1	Intercellular adhesion molecule-1
IFA	Incomplete Freund's adjuvant
Ig	Immunoglobulin
IL	Interleukin
Inr	Initiator element
IP	Intraperitoneal
iPSC	Induced pluripotent stem cells
IRES	Internal ribosomal entry site
IV	Intravenous
KAF	Conglutinogen-Activating Factor
kDA	Kilo Dalton
KLH	Keyhole limpet hemocyanin

LB	Luria Bertani
LC-MS	Liquid chromatography tandem mass spectrometry
LD	Linkage disequilibrium
LDLRA	Low-density lipoprotein receptor class A
LP	Lectin pathway
M	Molar
MAC	Membrane attack complex
MAF	Minor allele frequency
MASP	Mannose-binding lectin-associated serine proteases
MBL	Mannose-binding lectin
MCP-1	Monocyte chemoattractant protein-1
MCP	Membrane cofactor protein
MG	Macroglobulin
mL	Millilitre
MPGN	Membranoproliferative glomerulonephritis
mRNA	Messenger ribonucleic acid
MS	Mass spectrometry
MSVI	Moderate or severe vision impairment
mUA	Milli-absorbance unit
NHS	N-hydroxysuccinimide
OD	Optical density
OR	Odds ratio
PBS	Phosphate buffered saline
PBS-T	Phosphate buffered saline with tween

PCR	Polymerase chain reaction
PD-10	Protein desalting-10
PDEF-*CFI*	Polyhistidine tagged complement factor I
PEG	Polyethylene glycol
pH	Potential hydrogen
PLEKHA1	Pleckstrin Homology Domain Containing A1
POS	Photoreceptor outer segments
PNGase	Peptide-*N*-Glycosidase
Pro-I	Precursor to factor I
PRM	Pattern recognition molecule
PVDF	Polyvinylidene Fluoride
RA	Rheumatoid arthritis
RCA	Regulators of complement activity
RNA	Ribonucleic acid
RNase	Ribonuclease
ROS	Reactive oxygen species
RPE	Retinal pigment epithelium
RPM	Rotations per minute
RPMI	Roswell Park Memorial Institute media
RT	Room temperature
RU	Refractive unit
SC	Subcutaneous
SDM	Site directed mutagenesis
SDS PAGE	Sodium dodecyl sulphate-polyacrylamide gel electrophoresis

SERPING1	Serpin (serine protease inhibitors) Family G Member 1
SLE	Systemic lupus erythematosus
SNP	Single nucleotide polymorphism
SOC	Super optimal broth
SP	Serine protease
SPR	Surface plasma resonance
SRCR	Scavenger receptor cysteine-rich domain
SV40	Simian virus 40
TAE	Tris, Acetic acid, EDTA
TCC	Terminal complement complex
TED	Thioester domain
TMB	Tetramethylbenzidine
TMC	Trimolecular complex
TMP3	Recombinant human fusion protein 3
TNF	Tumour necrosis factor
UV	Ultraviolet
VCAM-1	Vascular cell adhesion molecule-1
VEGF	Vascular endothelial growth factor
WT	Wildtype

Chapter 1. Introduction

1.1. Age-Related Macular Degeneration

Age-related macular degeneration (AMD) is a progressive degenerative disease of the macula, resulting in a loss of central vision and irreversible blindness. AMD is the most common cause of irreversible blindness in the developed world, the fourth leading cause of blindness globally and the third leading cause of moderate or severe vision impairment (MSVI) in adults aged 50 years and older (Bourne *et al.*, 2021). Previous projections have suggested that approximately 170 million people are currently affected by some form of AMD (Xu *et al.*, 2020), with around 1.5 million individuals afflicted in the UK (Macular Society, 2018) and 18 million in the US (Rein *et al.*, 2022). However more recent estimates suggest that the number of affected individuals may be much lower, with approximately 8 million people experiencing vision loss as a result of AMD in 2020. Of the 33.6 million adults aged 50 years or older who were blind in 2020, around 1.84 million (1.34 to 2.42) people were blind due to AMD, and of the 206 million people with MSVI, 6.22 million (5.03-7.57) experienced MSVI as a consequence of AMD (Bourne *et al.*, 2021). Whilst these figures cast doubt onto the previously projected 196 million affected individuals in 2020 (Pascolini and Mariotti, 2012; Wong *et al.*, 2014), AMD continues to have a significant impact on society, particularly due to the prevalence of the untreatable dry form of AMD (Flaxel *et al.*, 2020; Schultz *et al.*, 2021), and increasing burden due to an ageing population (Bourne *et al.*, 2021).

Due to its debilitating nature and global prevalence, AMD is a disease with a significant societal impact. Fortunately, new therapeutic strategies are beginning to emerge fuelled by strong genetic associations and an improved understanding of the disease, which may relieve some of the burden of this condition. Increasingly, it seems that a personalised approach to the treatment of AMD will provide the best course of action, due to the ability to pinpoint the specific aspect of the disease mechanism, in such a complex multifactorial disease.

1.1.1. The Retina

AMD pathology affects five major layers of the human retina: the choroid, the choriocapillaris, Bruch's membrane (the basement membrane (BM) of the retina), the retinal pigment epithelium (RPE), and the photoreceptor cells (rods and cones). The primary region affected in AMD patients is that of the macula, the central region of the retina, which consists of the BM, RPE cells and the inner and outer neuronal layers. This area contains the highest proportion of photoreceptor cells and is responsible for responding to photons and for the transmission of electrical signals to the visual cortex via the optic nerve. The macula itself is an oval, heavily pigmented area, approximately 5.5 mm in diameter. The macular area can be further subdivided into several zones: the fovea, the foveloa, the capillary-free zone/ foveal avascular zone, the umbo, the parafoveal area and the perifoveal area (Provis *et al.*, 2005). The fovea is located at the centre of the macular and is comprised of the highest density of cone photoreceptor cells. Surrounding the fovea is the parafoveal area, which is predominately populated by rod photoreceptor cells (Curcio, Medeiros and Millican, 1996). Rod photoreceptor cells are responsible for low light vision, and have low spatial acuity, whereas the cone photoreceptor cells capable for colour vison and have high spatial acuity.

Blood is supplied to the cells of the macular by the choroid, a process which is regulated by the blood ocular barriers, a two-barrier system consisting of the blood-aqueous barrier and the blood-retinal barrier (BRB), which function to keep the eye a privileged site within the body (Cunha-Vaz, Bernardes and Lobo, 2010). The BRB consists of an inner and outer component. The inner component comprises of the endothelial cells of the retinal capillary vessels, and the outer component consists of a monolayer of RPE cells attached to an extracellular BM. The BRB regulates the movement of ions, water, and metabolic end products from the ocular vascular bed and to the retinal tissues, through the use of tight junctions between neighbouring RPE cells (Hussain *et al.*, 2010). Additional to the role in maintaining retinal homeostasis, the RPE cells are also responsible for the phagocytosis of photoreceptor outer segments, facilitating maintenance of the visual pigment (Kevany and Palczewski, 2010). On the basal (choroid) side of the RPE cells, is the BM, a five layered acellular extracellular matrix. The BM both supports the RPE physically and also contributes to the selectivity of the BRB dictating the diffusion of proteins, and therefore offering protection from inflammatory proteins and some anaphylatoxins (Clark *et al.*, 2017). The outermost layer of BM is the choroidal vasculature, a three-layered network consisting of the anterior choriocapillaris, the Sattler's layer of intermediate vessels, and the outermost Haller's layer; responsible for maintaining the metabolic demands of the RPE and photoreceptor cells (Lutty *et al.*, 2010).

1.1.2. Ageing in the Eye

During the ageing process, several physiological changes occur in the retina, predisposing the eye to developing AMD. With increasing age, rod photoreceptor density is decreased by 30% both in the extrafoveal area and in the fovea. This degeneration can be observed in macroscopically healthy eyes from the age of 34 years, and increases with age, with the greatest degeneration observed in the ninth decade (Curcio *et al.*, 1993). Additional to the loss of photoreceptors, RPE cells are also affected by the ageing process and undergo pigmentary changes (Delori, Goger and Dorey, 2001), decreases in mitochondria size and number (Feher *et al.*, 2006), and accumulation of lipofuscin, a metabolic debris (Terman and Brunk, 1998; Delori, Goger and Dorey, 2001). Ageing also leads to the thickening of the BM, due increased deposition, and the crosslinking of collagen fibres (Pauleikhoff *et al.*, 1990). Further to this is the accumulation of advanced glycation end-products, consisting of oxidised proteins and lipids (Handa *et al.*, 1999). Together these changes lead to a decrease in membrane permeability, altering the nutritional flow from the choroidal vasculature to the cells of the retina (Hussain, Rowe and Marshall, 2002). The nutrient and oxygen supply to the retina are also affected by changes that occur to the choroid vascular itself. Over time the choroid begins to thin due to decreased choriocapillaris density and a reduction in lumen diameter (Ramrattan *et al.*, 1994), leading to an hypoxic environment stressing the cells of the RPE (Chirco *et al.*, 2017).

1.1.3. Pathophysiology of AMD

AMD results in the degeneration of the macular resulting in a loss in the central field of vision and visual acuity, significantly impacting patient quality of life (Coleman *et al.*, 2010). Clinical findings associated with AMD include drusen deposition, RPE abnormalities and detachment, geographic atrophy, choroidal neovascularisation, and disciform scaring (Age-Related Eye Disease Study Research Group, 1999). As outlined by the Age-Related Eye Disease Study (AREDS) research group, AMD progression can be classified into three clinical stages: early, intermediate, and late stage. AREDS also defined a severity scale which is used to score each eye between 0-4 based upon a variety of clinical risk factors, whereby a score of 0 suggests a low risk or developing late stage AMD, and a score of 4 is suggestive of a high risk for developing late stage AMD over a five year period (Ferris *et al.*, 2005).

The early stages of the disease are characterised by the accumulation of sub-retinal debris, known as drusen, between the BM and the basal lamina of the RPE (Hageman *et al.*, 2001; Crabb *et al.*, 2002). The components of drusen include amyloid beta (Luibl *et al.*, 2006), apolipoprotein E, esterified cholesterol, phospholipids, immunoglobulin light chains, and complement proteins (Mullins *et al.*, 2000). Using fundus microscopy, drusen can be seen as circular yellow deposits in the macular (Figure 1-1). Whilst small drusen deposits are considered to be part of the normal ageing process, and are most identified in individuals over 55 (Sarks *et al.*, 1999), drusen which exceed 63µm in diameter are used to form the diagnosis of early AMD (Ferris *et al.*, 2013). In addition to their size and number, drusen morphology is also used in the diagnosis of AMD, with early drusen classified as 'hard' with distinct well-defined edges, and later stage drusen, associated with AMD, classified as 'soft' due to a lack of distinct boarders (Bird *et al.*, 1995; Sarks *et al.*, 1999). Progression from early AMD to intermediate AMD is defined by the presence of greater than 15 intermediate drusen (64-124 µm) or the presence of large (> 125 µm) drusen, but with no RPE cell abnormalities (Ferris *et al.*, 2005; Liew *et al.*, 2016).

Late stage (advanced) AMD can be further divided into two forms, the "dry" and the "wet". The "dry" form is characterised by islands of RPE cell death, known as geographic atrophy (GA), and the degeneration of the photoreceptor cells of the macular. Whereas the "wet" form is characterised by disordered choroidal neovascularisation (CNV), resulting in sub-RPE haemorrhages and RPE detachment, dry AMD is the most common form of late AMD and is responsible for ~80% of all AMD cases - with the wet form responsible for ~20% of cases (Hussain *et al.*, 2019). Despite the differences in pathophysiology observed for the two late stages of the disease, both forms eventually lead to a total loss of central vision through the photoreceptor degeneration (Curcio, Medeiros and Millican, 1996).

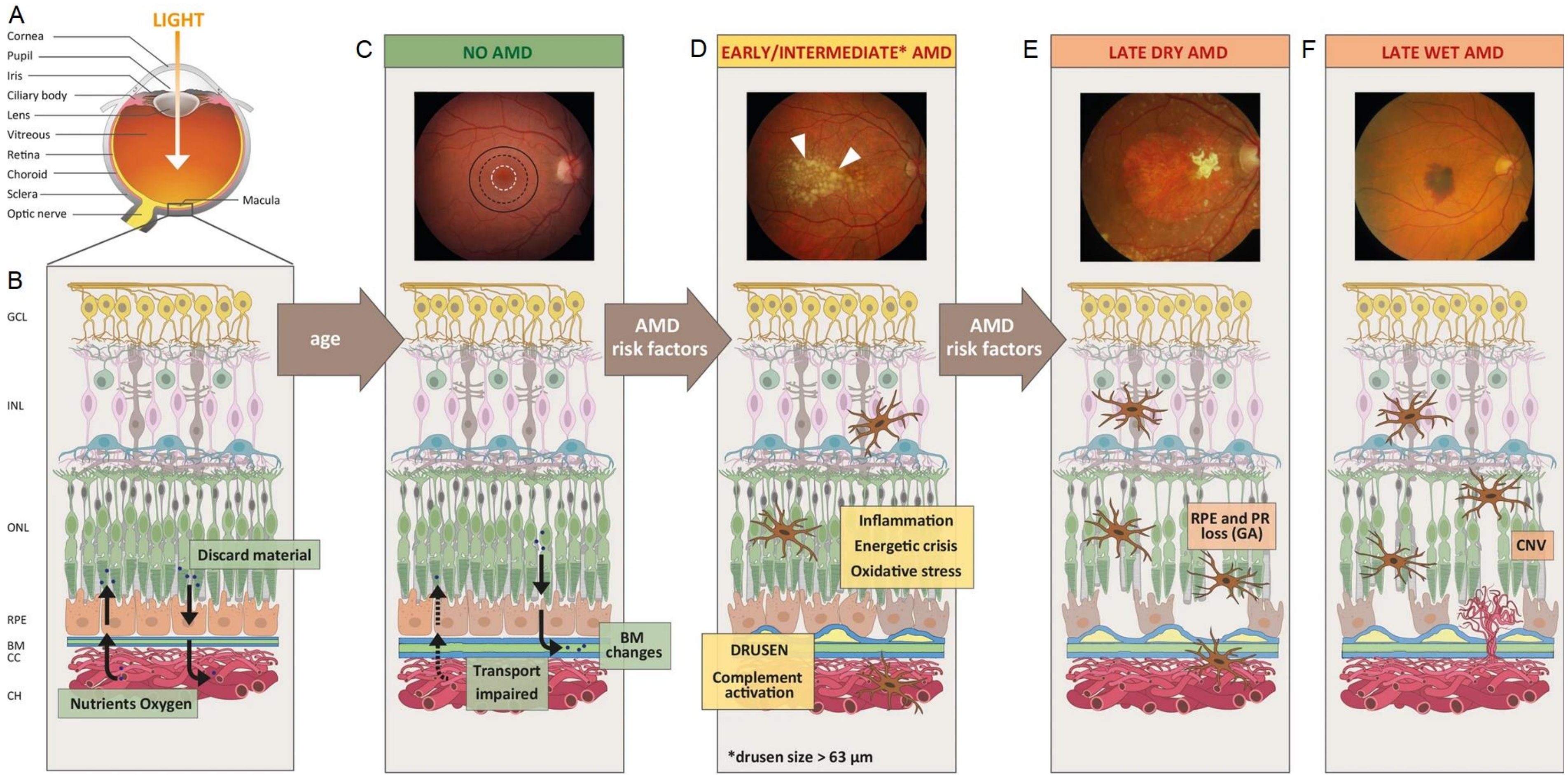

Figure 1-1 Schematic of the human eye in health and AMD (from Armento *et al.*, 2021).

(A) The anatomical features of the human eye. (B) A healthy human retina with its cell layers and transport of nutrients across BM. (C-F) Progression of AMD shown by fundus images (from the Macula Reading Centre, University of Tübingen) and schematic changes within the retinal cell layers. (C) Example of an older patient without AMD. (D) Visible inflammation, oxidative stress, energetic crisis, complement activation and drusen formation. Drusen visualised in fundus images as yellow spots (white arrows). (E) Late dry AMD with geographic atrophy (GA) characterised by defined areas of RPE cell death. (F) Wet AMD as demonstrated by choroidal neovascularisation (CNV) into the retina, ultimately leading to photo receptor cell death. (Armento, Ueffing and Clark, 2021). Ganglion cell layer (GCL), Inner nuclear layer (INL), Outer nuclear layer (ONL), Retinal pigment epithelium (RPE), Bruch's membrane (BM), Choriocapillaris (CC), and Choroid (CH).

1.1.4. Risk Factors for AMD

AMD is a complex, multifactorial disease caused by a combination of risk factors which function together to define an individual's predisposition to AMD. These include ageing, race, environmental and lifestyle risk factors, and genetic predisposition. Advancing age is considered the major non-modifiable risk factor for developing AMD (Klein, Klein and Linton, 1992; Mitchell *et al.*, 1995; Vingerling *et al.*, 1995), due to several physiological changes that occur within the eye, as outlined in section 1.1.2, which make the aged retina more susceptible to both internal and external stresses. In addition to ageing, ethnicity and gender are also significant non-modifiable risk factors, with Europeans (Wong *et al.*, 2014) and white (Friedman *et al.*, 1999) females (Age-Related Eye Disease Study Research Group, 2000) the most suspectable to developing severe late AMD. Eye colour can also contribute, with AMD being more prevalent in individuals with blue or hazel irises compared to those with brown irises (Frank *et al.*, 2000).

Of the modifiable risk factors, smoking status is the most important environmental risk factor (Age-Related Eye Disease Study Research Group, 2000). In one study, current smokers had a 3.6-fold increased risk for developing late-stage AMD, and former smokers a 3.2-fold increased risk, compared to those who had never smoked (Delcourt *et al.*, 1998). Both types of late AMD were also associated with smoking, with an Odds Ratio (OR) of 3.43 for GA and 2.49 for CNV (Khan *et al.*, 2006). It is hypothesised that smoking increases the risk for AMD due to an increase in oxidative stress and inflammation in the macular, which leads to mitochondria deoxyribose nucleic acid (DNA) damage inducing RPE degeneration, contributing to the build-up of drusen (Wang *et al.*, 2009; Woodell and Rohrer, 2014).

Other lifestyle related factors that contribute to an increase AMD risk include obesity, high trans-fat intake and poor cardiovascular health (Cho *et al.*, 2001; Milton *et al.*, 2005; Chong *et al.*, 2009). Cardiovascular disease risk factors such as hypertension, and high dietary cholesterol are particularly associated with wet AMD (OR = 4.4), whereas dry AMD demonstrated no association with these risk factors in one study (Hyman *et al.*, 2000). Due to these associations, it is clear that an individual's diet can have a noticeable impact on an AMD risk. It has been shown that a diet that contains a larger proportion of fruits, vegetables, legumes, and fish oils, compared to red meat, and processed foods is particularly beneficial in reducing the risk of developing AMD (Kang and Kim, 2019); with an adherence to a 'Mediterranean diet' associated with a 41% reduced risk for the incidence of advanced

AMD (Merle *et al.*, 2019). Improving diet through antioxidant and/or zinc supplementation, is currently one of the only options for slowing the progression of dry AMD. The AREDS 2 formulation without zinc, showed an odds ratio reduction to 0.76, in patients with late AMD, and a reduction to 0.66 when used in combination with zinc supplementation (Kassoff *et al.*, 2001). Taken together, this highlights that implementing positive lifestyle changes may provide the first course of action for reducing a patients AMD risk.

The first evidence for a genetic contribution to AMD originated from twin and familial studies (Klein, Mauldin and Stoumbos, 1994; Meyers, Greene and Gutman, 1995; Seddon, Ajani and Mitchell, 1997; Klaver *et al.*, 1998; Hammond *et al.*, 2002). Monozygotic twins demonstrated a disease concordance of 37-100% (Klein, Mauldin and Stoumbos, 1994; Meyers, Greene and Gutman, 1995; Hammond *et al.*, 2002), whereas dizygotic twins ranged from 19-42% (Meyers, Greene and Gutman, 1995; Hammond *et al.*, 2002). Providing further support for a genetic link to AMD was the familial aggregation studies, which identified a higher prevalence among first-degree relatives (OR = 2.4) (Seddon, Ajani and Mitchell, 1997), in addition to an increased rate of disease progression (Klaver *et al.*, 1998).

Following the technological advancements that enabled the analysis of whole genomes, this greatly accelerated the discovery of new genetic associations with AMD. In 2005, landmark studies associated a common single nucleotide polymorphism (SNP), p.Tyr402His (rs1061170), in the *CFH* gene on chromosome 1 with AMD (Edwards *et al.*, 2005; Hageman *et al.*, 2005; Haines *et al.*, 2005; Klein *et al.*, 2005). Further investigations into the *CFH* gene and the surrounding locus, identified that possession of the heterozygous Y402H mutation could increase the risk of developing AMD by 2.7-fold, and may account for 50% of the attributable risk for AMD (Edwards *et al.*, 2005).

Shortly after the identification of the *CFH* locus, a second genome-wide significant signal was identified on 10q26 (Rivera *et al.*, 2005), a region which harbours the genes: Pleckstrin Homology Domain Containing A1 (*PLEKHA1*), Age-related maculopathy susceptibility protein 2 (*ARMS2*) and high temperature requirement A serine peptidase 1 (*Htra1*) (Iyengar *et al.*, 2004; Rivera *et al.*, 2005; Dewan *et al.*, 2006; Kortvely *et al.*, 2010). Polymorphisms in the *CFH* and the *PLEKHA1/ARMS2/Htra1* genes were identified as a major risk factor for AMD, particularly in individuals with homozygous risk alleles in both loci (OR = 57.6) (Rivera *et al.*, 2005).

Subsequent genome wide association studies (GWAS) have identified both common and rare genetic variants associated with AMD across 34 discrete loci (Fritsche *et al.*, 2016). The locations of these polymorphisms implicate the involvement of the complement system (complement factors (CF) H, I and B (*CFH, CFI, CFB*) and complement components (C) 3 and 9 (*C3, C9*)), extracellular matrix remodelling (Recombinant human fusion protein 3 (*TMP3*), Collagen type VIII alpha 1 chain (*COL8A1*), Age-related maculopathy susceptibility protein 2 (*ARMS2*)), cholesterol metabolism (Apolipoprotein E (*APOE*), ATP-binding cassette transporter 1 (*ABCA1*), Cholesteryl ester transfer protein (*CETP*)), and other undefined pathways (RhoGAP Rho GTPase Activating Protein 21 (*ARHGAP21*) and Beta-1,3-glucosyltransferase (*B3GALTL*)) (Yu *et al.*, 2011; Fritsche *et al.*, 2013, 2016; Seddon *et al.*, 2013; Corominas *et al.*, 2018). Rare variants (Minor allele frequency (MAF) ≤ 1%) associated with AMD have been of particular interest due to their potentially larger effect on disease phenotype (Geerlings, de Jong and den Hollander, 2017). Rare genetic variants in three of the complement genes (*CFI*, *C3* and *C9*), have been associated with a significantly higher burden in AMD patients, compared to controls (OR = 3.6, 3.8 and 2.2 respectively) (Seddon *et al.*, 2013; Fritsche *et al.*, 2016).

Further strengthening of the link between complement and AMD was achieved through the sequencing of candidate genes in case-control studies and AMD families. Rare variants associated with AMD cases were identified in the genes *CFI*, *CFH*, *C3*, *C9*, and *CFB* (Gold *et al.*, 2006; Boon *et al.*, 2008; Fagerness *et al.*, 2009; van de Ven *et al.*, 2013; Zhan *et al.*, 2013; Duvvari *et al.*, 2014; Kavanagh *et al.*, 2015; Wagner *et al.*, 2016; Kremlitzka *et al.*, 2018), strongly implicating the alternative pathway of complement as a key component of AMD susceptibility and highlighted the role of the innate immune system in the pathogenesis of the disease.

1.2. The Complement System

The complement system is a key component of innate immunity, providing a first line of defence against infection by facilitating phagocytosis and lysis of pathogens (Johnston *et al.*, 1969). Complement also plays a key role in tissue homeostasis, flagging apoptotic cells and debris for removal (Mevorach *et al.*, 1998) and guiding immune complexes to the reticuloendothelial system for clearance (Brown *et al.*, 1983). The by-products of complement activation have a crucial role in the regulation of inflammation, recruiting immune cells to sites of infection or injury (Vandendriessche *et al.*, 2021), bridging the gap between innate and adaptive immunity (Dunkelberger and Song, 2010; Walport, 2001).

The complement system is a proteolytic cascade composed of over 30 proteins, which function both in the plasma and on cell surfaces (Walport, 2001). Complement is a highly intricate immune surveillance system, which can discriminate between healthy host tissue, cellular debris, apoptotic cells and pathogens, and modify its response accordingly (Ricklin *et al.*, 2010). The complement system can be activated through three major pathways: the classical pathway (CP), the lectin pathway (LP) and the alternative pathway (AP), each leading to a common terminal pathway (Merle, Church, *et al.*, 2015; Merle, Noe, *et al.*, 2015). Complement activation must be tightly regulated, with both inefficient and over stimulation of complement having a detrimental impact to the host due to an increased susceptibility to infections or non-infectious diseases.

1.2.1. The Classical Pathway and the Lectin Pathway

The CP is activated by the binding of the pattern recognition molecule (PRM), C1q (part of the C1 complement complex), to either the Fragment crystallisable region (Fc) portion of immunoglobulin (Ig) G (IgG) or IgM immune-complexes, or to surface-bound pentraxins such as C-reactive protein (CRP) or pentraxin 3, on the surface of foreign or host cells (Kishore *et al.*, 2004). Once C1q binds to a target surface, a conformational change occurs in the C1 complex, inducing the auto-activation of the proteases C1r, and C1s. The C1 complex, is a Ca^{2+} dependant macromolecular complex (Roumenina *et al.*, 2005) comprised of C1q and the proenzyme tetramer C1r2C1s2. Upon activation, C1r cleaves and activates C1s, facilitating the subsequent cleavage of C4 into C4a and C4b, and C2 into C2a and C2b. The hydrolysis of C4 by C1s, exposes a reactive thioester in the C4b molecule which leads to covalent deposition of C4b on to surfaces in the immediate vicinity of the activation site (opsonisation). C2 binds to C4b, and is cleaved by C1s, leading to the generation of the C3 convertase, C4bC2b (formerly C4b2a), which is capable of cleaving C3 and initiating amplification of the AP and downstream effector functions (Kerr, 1980).

The LP functions in an analogous way to the CP but is instead activated by the binding of the PRMs; the collectins (mannose-binding lectin (MBL), collectin-10 and collectin-11) and the ficolins (ficolin-1, 2 and 3, formally, M, L, and H), to carbohydrate and fibrinogen-like domains, respectively (Garred *et al.*, 2016). Each PRM assembles with the MBL-associated serine proteases (MASPs), MASP-1, MASP-2 and MASP-3, in a similar Ca-dependent manner as C1r and C1s in the C1 complex. Where the CP and the LP differ, is that the majority of MBL molecules are associated with only one of the MASP homodimers, and therefore require the action of adjacent complexes for their activation. Once the MBL complex is bound to a target, MASP-1 activates MASP-2, cleaving both C4 and C2, to generate the C3 convertase, C4bC2b. In contrast to C1r of the CP, MASP-1 can also cleave C2, supplementing the MBLP response through increased C3 convertase formation (Chen and Wallis, 2004; Dobó *et al.*, 2009).

Both the CP and the LP converge at the production of the C3 convertase, C4bC2b, which cleaves C3 into the anaphylatoxin C3a (Cochrane and Müller-Eberhard, 1968; Klos *et al.*, 2009), and the opsonin C3b. When C3 is cleaved into C3b, a reactive thioester domain is uncovered, initiating the covalent binding of the molecule to hydroxyl and amino groups, typically on cell surfaces, in a process known as opsonisation. In the presence of excess C3b, the thioester will instead bind to the α' chain of C4b (Takata *et al.*, 1987), rather than to a target surface, initiating the formation of the trimeric C5 convertase, C4bC2bC3b (Kinoshita *et al.*, 1988). The formation of the C5 convertase initiates the cleavage of C5 into the anaphylatoxin C5a (Cochrane and Müller-Eberhard, 1968; Klos *et al.*, 2009), and the terminal pathway initiator, C5b. C5b production starts the generation of the terminal complement complex (TCC) (C5b-9), and eventually results in the assembly of the membrane attack complex (MAC) (Bubeck, 2014).

Assembly of the MAC occurs in a sequential process whereby, C5b recruits C6 to form the C5b-C6 complex, which binds reversibly to target surfaces, and acts as the molecular foundation for the MAC formation. C7 then binds to C5b-C6, generating C5b-7, and is then partially integrated into the phospholipid membrane bilayer through the association of C8. This allows C9 to insert into the lipid bilayer, which initiates polymerisation of up to 18 C9 molecules (C5b-9), resulting in the formation of the MAC, a stable pore (110Å diameter) (Menny *et al.*, 2018). The MAC is the central effector molecule of the complement system and is responsible for the lysis and direct cell killing of both host cells and pathogens (Morgan, 1992). In unnucleated cells, formation of the MAC induces cells lysis through a rapid increase in Ca^{2+} ion concentration, resulting in lysis through osmotic stress. In contrast, nucleated cells modulate the influx of Ca^{2+} ions through ion pumps, however this process is very demanding, leading to profound ATP depletion and a loss of mitochondrial membrane potential, and results in cell necrosis (Papadimitriou *et al.*, 1991). Due to the destructive potential of the terminal pathway, host cell surfaces are protected by the membrane glycoprotein, cluster of differentiation (CD) 59 (CD59), which regulates the TCC by binding to C5b-9 preventing C9 polymerisation (Davies *et al.*, 1989).

1.2.3. The Alternative Pathway

The AP is mechanistically distinct from the CP and LP and is responsible for driving three overlapping processes: opsonisation, inflammation, and cell lysis. The AP is in a constant state of low-level activation, known as 'tick-over' (Bexborn *et al.*, 2008; Pangburn *et al.*, 1981), where C3 is spontaneously hydrolysed, exposing the thioester domain and forming C3(H_2O), a molecule analogous to C3b. In the hydrolysed form, C3(H_2O) recruits the plasma proteases, factor B (FB) and factor D (FD). FB binds to the C3(H_2O) molecule and is cleaved by FD, in a Mg^{2+}-dependant manner (Lesavre and Müller-Eberhard, 1978). Cleavage of FB into Ba and Bb, generates the enzymatic complex, C3(H_2O)Bb, the initial fluid phase C3 convertase of the AP. The C3(H_2O)Bb complex is able to cleave C3 into C3a and C3b, mirroring the function of the CP and LP C3 convertase. C3b is deposited onto surfaces in the vicinity and associates with FB, which in turn is then activated by FD, to generate the major AP C3 convertase, C3bBb. The C3bBb is a short-lived complex, with a half-life of ~90s (Pangburn and Müller-Eberhard, 1986), and requires stabilisation through the binding of properdin (P), to ensure efficient host defence (Fearon and Austen, 1975; Medicus *et al.*, 1976). C3bBb cleaves C3 into C3a and C3b, a process which enables host defence through both the generation of anaphylatoxins (via C3a) and opsonisation (via C3b).

At the heart of the AP, is the amplification loop, which is brought about through a cycle of C3 cleavage and convertase assembly, facilitating rapid exponential C3b deposition once triggered (Lachmann, 2009). Through exponential C3b deposition, the amplification loop facilitates the formation of the C5 convertase, C3bBbC3b. Cleavage of C5 by C3bBbC3b results in the main source of C5b for formation of the TCC and the MAC, in addition to C5a, a potent neutrophil chemoattractant. Further to the role of recruiting pro-inflammatory cells to the site of complement activity, C5a stimulates neutrophils to release properdin from their granules, exacerbating complement activation and amplification through the AP (Camous *et al.*, 2011; Cortes *et al.*, 2012).

Since both the CP and LP feed into the amplification loop through the generation of C3b, it is clear to see how the AP can supplement the action of both the CP and LP, and exemplifies how the AP may account for 80-90% of total complement activation (Harboe *et al.*, 2009; Harboe and Mollnes, 2008) (Figure 1-2). As a consequence of this, the action of the AP is tightly regulated through a number of complement inhibitory proteins. These proteins are responsible for confining complement activation on the appropriate targets and preventing errant complement activation on healthy host cells (Zipfel and Skerka, 2009).

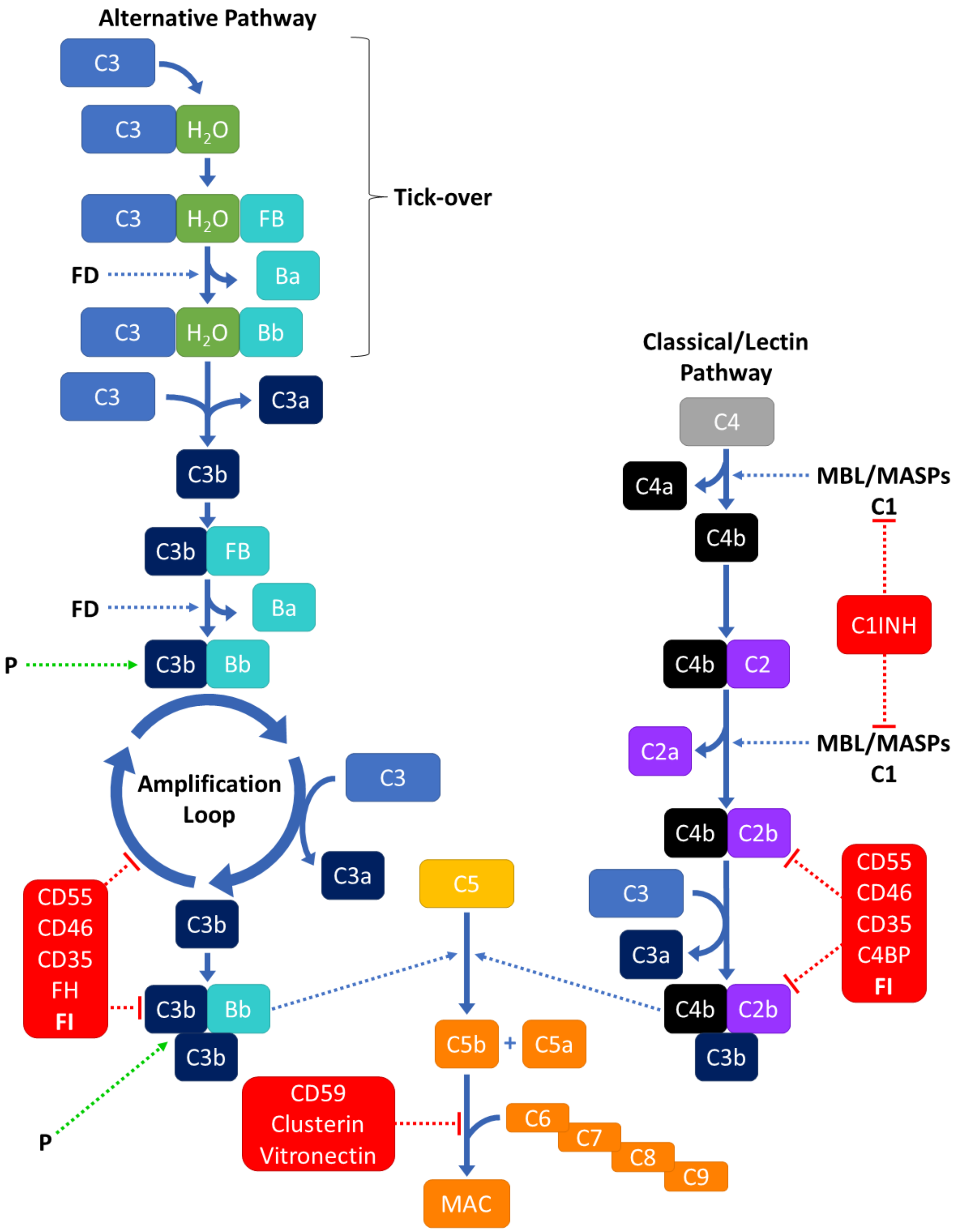

Figure 1-2 Activation and control of the complement cascade (adapted from Harris *et al.*, 2018).

Tick-over occurs when the thioester in native C3 undergoes spontaneous hydrolysis, resulting in a conformational change which generates a C3b-like protein (C3(H_2O)). C3(H_2O) then binds Factor B (FB) and is subsequently activated by Factor D (FD) to form the C3 convertase C3(H_2O)Bb. The C3 convertase then cleaves the first C3 molecule generating nascent C3b which is capable of covalently attaching to surfaces and initiating the alternative pathway of complement. Once C3b is deposited on a target surface, FB binds and is cleaved by FD to form the primary C3-cleaving enzyme, C3bBb. This enzyme then cleaves further C3 to C3a and C3b, initiating the amplification loop, facilitating more C3 cleavage. C3b then either acts as an opsonin by binding to surfaces or it binds to the C3 convertase to form the C5 convertase, C3bBbC3b. The formation of both the C3 and the C5 convertase can be stabilised by properdin (P). Activation of the classical and lectin pathways results in the covalent binding of C4b to target surfaces. C4b then binds C2 and is activated by C1r/s or mannose-binding lectin-associated serine proteases (MASPs) to form the C3 convertase, C4bC2b. C4bC2b can then cleave C3 to generate more C3b for the formation of the C5 convertase, C4bC2bC3b. Cleavage of C5 initiates the terminal pathway through the production of the pro-inflammatory chemoattractant C5a, and the terminal pathway initiator C5b. C5b binds C6, forming C5b-C6 which triggers the sequential process that results in the formation of the membrane attack complex (MAC), a transmembrane pore made from C5b-C6, C7, C8 and multiple molecules of C9. The complement cascade is controlled by the complement regulators highlighted in red. This can either occur at the initiation level with C1 esterase inhibitor (C1INH), or at the level of C3b and the convertases with CD55, CD46, CD35, Factor H (FH), Factor I (FI) and C4-binding protein (C4BP), or at the terminal level through CD59, Clusterin or Vitronectin. (Harris *et al.*, 2018).

1.2.4. Regulation of Complement Activation

Complement is regulated by several fluid-phase and membrane bound regulators, two of the most important of these inhibitors are the serine protease Factor I (FI) and its cofactor, Factor H (FH). Complement regulation occurs predominately at three points within the cascade. The first point affects CP and LP activation, the second, the assembly and the enzymatic activity of the convertases, and the third, the assembly of the MAC. The first point of control begins with activation of the CP and LP. Activation of the CP is primarily controlled by the activity of C1 esterase inhibitor (C1-INH), a serine protease inhibitor which covalently binds to activated C1r and C1s, inhibiting their activity and causing their dissociation away from the C1 complex. C1-INH also plays an inhibitory role in the LP, by inactivating both MASP-1 and 2. Additional CP and LP control is achieved by the ECM proteoglycans decorin and biglycan, which bind to the collagen-like regions of C1q and MBL respectively, preventing activation of these pathways (Groeneveld *et al.*, 2005).

Complement activation is largely driven by the production of the molecules C3b and C4b, and therefore the degradation of these molecules is key for preventing bystander cell damage. FI mediated cleavage of C3b and C4b, results in the generation of the inactive molecules iC3b, C3dg and C4d which prevents the formation of active convertases by degrading their substrates. To prevent non-specific regulation of complement activity by FI, FI mediated cleavage is modulated by the presence of cofactors. FH and FH-like protein 1 (FHL-1) are required for C3b, C4 binding protein (C4BP) is required for C4b, and membrane cofactor protein (MCP; CD46) and complement receptor 1 (CR1; CD35) facilitate both (Nilsson *et al.*, 2011). Many of the cofactor proteins also function to regulate C3 convertase formation through decay-accelerating activity (DAA), shortening the half-life of preformed convertases through destabilisation, limiting their ability to participate in further complement activation. Proteins which possess DAA for the CP and LP convertase include decay-accelerating factor (DAF; CD55), CR1 and C4BP, and the AP inhibitors with DAA are DAF, FH and CR1 (Morgan and Meri, 1994).

The final point of complement control is at the level of the MAC. Inhibition of MAC formation is achieved either through the membrane-bound CD59, or through the fluid-phase inhibitors vitronectin and clusterin. CD59 has two inhibitory functions, where it binds to C8 in the C5b-8 complex, preventing incorporation of C9, and through the blockade of C9 polymerisation. Whereas both vitronectin and clusterin function through the prevention of C5b-9 insertion into the phospholipid bilayer (Meri *et al.*, 1990; Tschopp and French, 1994).

Regulation of the anaphylatoxins generated by the cleavage of C3 and C5, is also critical. The anaphylatoxins are potent proinflammatory molecules which bind to the receptors, C3aR and C5aR, found on a variety of immune cell types, initiating numerous downstream processes e.g., chemotaxis, migration, and phagocytosis (Hugli and Müller-Eberhard, 1978). The activity of the anaphylatoxins is controlled by the carboxypeptidases -N, B and R, which cleave the N-terminal arginine of C3a and C5a, converting the molecule into the desarginated form, which leads to impaired signalling through their cognate receptors (Klos *et al.*, 2009).

It is clear that tight regulation of complement activation is required to maintain tissue homeostasis and prevent undesirable inflammation and damage to the host. Despite the numerous complement inhibitors and fail-safes within the system, uncontrolled complement regulation can still occur, resulting in severe and life-threatening diseases. Of particular interest for this project, is the implication that over-activation of the AP is a key driver in the pathogenesis of a number of systemic and organ specific diseases, including age-related macular degeneration, atypical haemolytic uremic syndrome (aHUS) and the C3 glomerulopathies; membranoproliferative glomerulonephritis (MPGN), C3 glomerulonephritis (C3G), and dense deposit disease (DDD) (Zipfel *et al.*, 2006), in addition to systemic lupus erythematosus (SLE) and rheumatoid arthritis (RA) (Thurman and Holers, 2006).

Much of the uncontrolled regulation of complement is brought about through mutations in the complement genes, which translate to proteins which exhibit either a loss, or gain of function. In this thesis, the role of rare genetic variants in the *CFI* gene and their functional consequences on AP regulation will be further examined. Genetic variants in the *CFI* gene are more frequently identified in patients with AMD, aHUS, and the C3 glomerulopathies, however in many cases their causative role is yet to be established and are therefore considered as variants of unknown significance (de Jong *et al.*, 2020; Kavanagh and Anderson, 2012; Osborne *et al.*, 2018). Whilst complete deficiencies of FI result in severe, recurrent pyogenic infections (Streptococcus pneumoniae, Haemophilus influenzae, Neisseria meningitidis) through uncontrolled AP activation and C3 consumption (Alba-Domínguez *et al.*, 2012), haploinsufficiency has also been implicated in both AMD and aHUS (Fremeaux-Bacchi *et al.*, 2004; Kavanagh *et al.*, 2015; Gleeson *et al.*, 2016)).

1.2.5. Complement Factor I

1.2.5.1. *Historical Background*

FI was first described by Lachmann and Muller-Eberhard in 1968 as the Conglutinogen-Activating Factor (KAF), based upon its ability to facilitate the agglutination of activated erythrocytes by bovine conglutinin, through an interaction with surface bound C3b (Lachmann and Müller-Eberhard, 1968). Following its initial assignment as KAF, FI was later known as an inactivator of complement, as demonstrated through its role in C3 degradation (Ruddy and Austen, 1969) and as a result of its depletion causing spontaneous activation of the AP (Nicol and Lachmann, 1973). Upon the identification of these additional properties, FI began to be known interchangeably as the C3 inactivator (C3INA) (Ruddy and Austen, 1969). In the 1970s, further investigations into C3INA demonstrated that this molecule exerted its inhibitory function through the cleavage of the alpha chain of the C3b and C4b (Pangburn, Schreiber and Muller-Eberhard, 1977), leading to the names C3b inactivator, C4b inactivator or C3b/C4b inactivator, in addition to highlighting its key role in the regulation of all three pathways of complement.

1.2.5.2. *The CFI Gene*

Human *CFI* is a 63 kb gene, responsible for coding the complement inhibitor FI, an 88kDa serum glycoprotein. *CFI* is located on the long arm of chromosome 4 at position 4q25 (Goldbergers *et al.*, 1987; Shiang *et al.*, 1989) and consists of 12 introns and 13 exons, with a genomic organisation which correlates to the modular structure of the protein (Vyse *et al.*, 1994). The minimal promoter region of the *CFI* gene lies, between −46 and +160, relative to the transcription start point. Transcription of *CFI* is controlled by an initiator element (Inr) promotor, which binds ribonucleic acid (RNA) polymerase II in the absence of a TATA-box; and is acutely regulated through the presence of inflammatory cytokines such as tumour necrosis factor (TNF) (α) TNF-α and Interleukin (IL) 6 (IL-6) (Minta *et al.*, 1998; Minta, Fung and Paramaswara, 1998). Inr-dependant transcription is also modulated by a CTGAA repeat region located immediately upstream of the Inr at −9 to −4, and downstream of the Inr at +101 to +106. This region is proposed to be responsible for assembly of the transcription machinery onto the Inr promotor, facilitating efficient transcription, with mutations in the region decrease *CFI* promoter activity by 40–50% relative to the wild-type (Paramaswara and Minta, 1999).

1.2.5.3. *The FI Protein*

FI is a heterodimeric protein, consisting of a 50 kDa heavy chain and a 38 kDa catalytic light chain, covalently linked by a disulphide bridge (Fearon, 1977; Goldberger *et al.*, 1984). The heavy chain of FI (Lys19–Ile335) consists of the FI membrane attack complex domain (FIMAC), a scavenger receptor cysteine-rich domain (SRCR), two low-density lipoprotein receptor class A (LDLRA1 and LDLRA2) domains, and a divergent segment (D segment) which has an unknown function (Minta *et al.*, 1996). The light chain of FI (Ile340–Val583) contains the serine protease (SP) domain, formed by the catalytic triad of His380, Asp429 and Ser525, and is responsible for the cleavage activity of FI (Catterall *et al.*, 1987; Perkins and Smith, 1993; Tsiftsoglou *et al.*, 2005).

1.2.5.4. *FI Synthesis*

Systemic production of FI primarily occurs in the liver by hepatocytes (Goldberger *et al.*, 1984; Morris *et al.*, 1982), but many other cells also exhibit the ability to produce FI locally, including monocytes (Whaley, 1980), fibroblasts (Vyse *et al.*, 1996), keratinocytes (Timár *et al.*, 2007), human umbilical vein endothelial cells (HUVEC) (Julen *et al.*, 1992) and importantly for this project the RPE (Dreismann *et al.*, 2021; Radeke *et al.*, 2015). FI is an acute phase protein, with an average serum concentration of approximately 29.3 µg/mL (Kavanagh *et al.*, 2015). FI is first translated as a linear, single chain polypeptide precursor, prePro-I (Catterall *et al.*, 1987; Goldberger *et al.*, 1987). PrePro-I then undergoes further intracellular processing, through N-linked glycosylation and cleavage of the 18-residue signal peptide, generating Pro-I. Pro-I is then proteolytically cleaved by Furin, a serine endoprotease, at the ^{336}RRKR^{339} linker located between the heavy and light chain, producing mature FI (Figure 1-3) (Goldberger *et al.*, 1984; Wong *et al.*, 1995). The mature form of FI is heavily N-glycosylated (25-27% w/w), with both the heavy and light chains carrying three N-linked oligosaccharides each (Tsiftsoglou *et al.*, 2006).

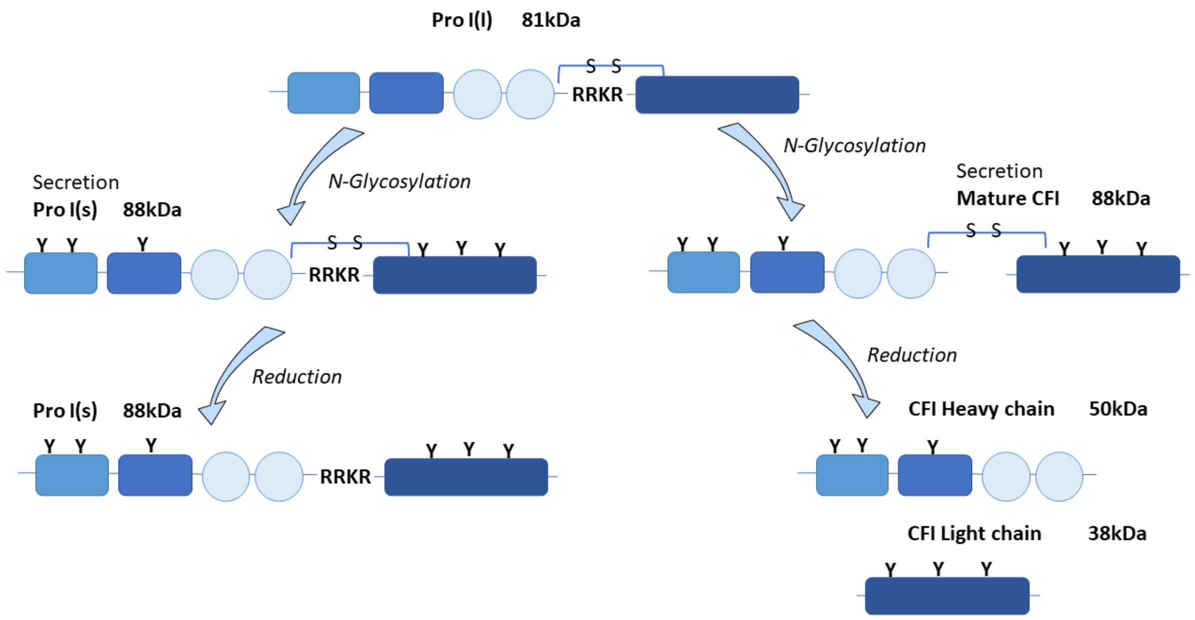

Figure 1-3 Two routes of Factor I synthesis (adapted from Kavanagh *et al.*, 2008).
FI is synthesised as a single polypeptide chain precursor (Pro-I(i)). Upon translocation to the endoplasmic reticulum, pro-I undergoes post-translational cleavage at the RRKR linker and N-glycosylation of both the light and heavy chains. In mammalian cells transfected with recombinant *CFI*, not all of the Pro-I undergoes cleavage of the RRKR linker peptide. This results in secretion of an N-glycosylated Pro-I and mature disulfide-linked FI consisting of a 50 kDa heavy chain and a 38 kDa light chain. The incomplete cleavage of the Pro-I form is thought to be due to the high expression of the protein that saturates the cleaving ability of the cells. (Kavanagh *et al.*, 2008) Complement Factor I (*CFI*), Intracellular (i), Secreted (s).

1.2.5.5. *FI Function and Trimolecular Complex Formation*

FI has no endogenous inhibitor, and circulates in an inactive zymogen-like form, until a transient complex is formed between the cofactors and their substrates (Sim and Tsiftsoglou, 2004). In plasma, FI has a highly disordered serine protease domain, whereby many of the activation loops crucial for the formation of the active-site triad and the oxyanion hole are in a proteolytically incompetent state, prior to rearrangement upon substrate-cofactor binding. In this disordered state, the SP domain is still functional as demonstrated by the cleavage of synthetic aminomethyl coumarin (AMC) peptide substrates, albeit with a much lower cleavage rate (Tsiftsoglou and Sim, 2004).

The process of FI activation consists of three stages: 1) The cofactor binds to the substrate producing a stable platform onto which FI can dock; 2) The heavy chain rotates 11°, allowing allosteric activation of the SP light chain; 3) The active site forms around the substrate in an ordered manner for initiation of the primary cleavage event (Roversi *et al.*, 2011) (Figure 1-4). FI is recruited to sites of complement activation by the cofactors, a protein family of regulators of complement activity (RCA). FI cleavage specificity is determined by the cofactor present. FH is required for C3b, C4BP is required for C4b, and MCP and CR1 are required for both (Zipfel and Skerka, 2009). Through the action of the different cofactors, FI is able to perform a regulatory role in all three pathways of complement activation, both at cell surfaces (FH, MCP and CR1) and in the fluid-phase (FH and C4BP) (Masaki *et al.*, 1992). Following the formation of the cofactor-substrate complex, FI binds and subsequently degrades C4b or C3b, by cleaving them up to two or three times, respectively. Cleavage of C4b results in the generation of iC4b, after one cleavage, and C4c and C4d after two cleavages. For C3b, two cleavages are required to produce the first inactive molecule, iC3b, followed by a further cleavage which generates C3dg and C3c, which only occurs in the presence of CR1 (Xue *et al.*, 2017).

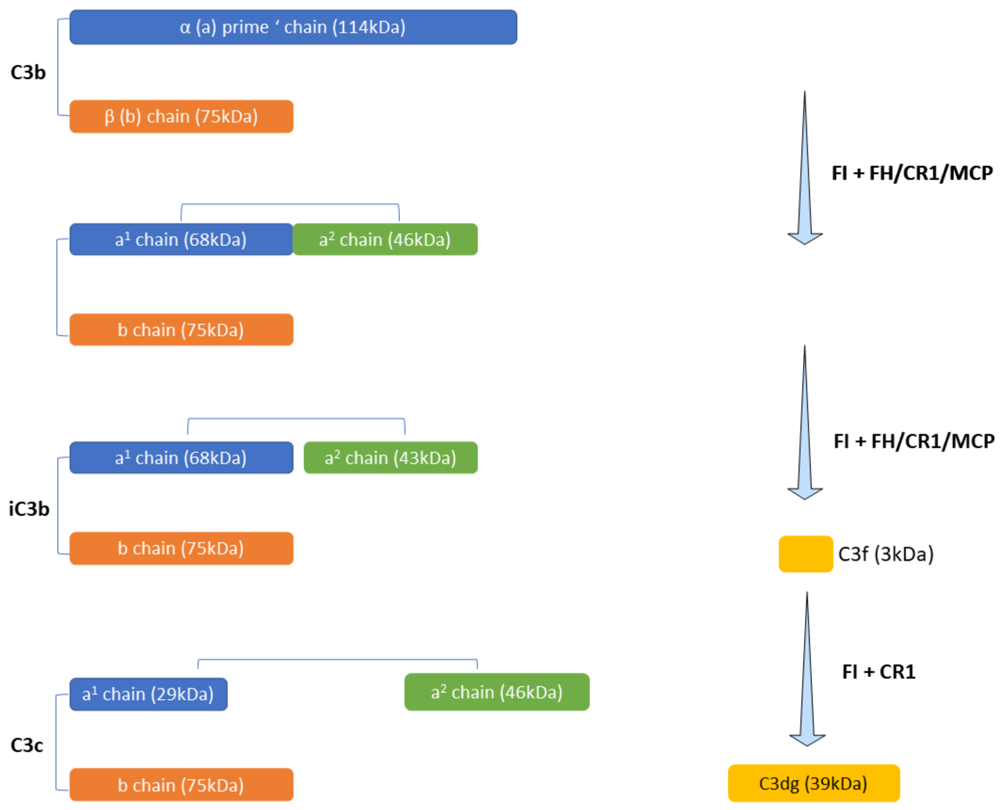

Figure 1-4 Cofactor mediated proteolytic cleavage of C3b by FI (adapted from Thurman *et al.*, 2013).
The three cleavage sites of FI on C3b and the subsequent breakdown products when in the presence of different cofactor proteins. C3dg is further degraded by trypsin (not shown). (Thurman *et al.*, 2013).

Insights into this sequential cleavage process and the role of the AP cofactors were obtained through the crystallisation of the AP trimolecular complex (TMC), C3b:FH:FI (Xue *et al.*, 2017). As mentioned above, the initiation of FI activity starts with the formation of the

C3b:FH complex facilitating the docking of FI in a niche between the C-terminal C3b (CTC) domain and the complement control protein (CCP) 1-3 (CCP1–3) domains of FH. Upon binding of FI, the CTC domain rotates 34° enabling an interaction with the FI membrane attack complex domain (FIMAC) domain in the heavy chain of FI, which acts to stabilise the complex, and exposes the complement C1r/C1s, Uegf, Bmp1 (CUB) domain of C3b to the catalytic triad located in the SP of the light chain. Following the formation of the TMC, the catalytic sequence transpires as follows: the first proteolytic cleavage occurs at Arg1303-Ser1304 inducing local flexibility which enables a minor rearrangement of the CUB domain, positioning the second scissile bond at Arg1320-Ser1321 into the active site, and once cleaved, results in the generation of iC3b. Unfolding of the CUB domain after the second cleavage, results in a major conformational change through the extension of a flexible peptide chain between macroglobulin (MG) 7 and the thioester domain (TED), in addition to the release of C3f. Extension of the peptide chain facilitates the docking of the third bond, Arg954-Glu955, into the catalytic site for cleavage, resulting in the generation of C3dg and C3c. This third and final cleavage of C3b can only occur in the presence of CR1, due to a lack of requirement for TED domain binding through CR1 CCPs 15-17 (Forneris *et al.*, 2016). FH and MCP, however, can only facilitate the cleavage of C3b as far as iC3b, since the TED and MG1 domains of C3b are both relied upon for FH CCP4 and MCP binding, and following the unfolding of CUB and dislodging of TED, as in iC3b, these two domains can no longer participate in cofactor binding (Xue *et al.*, 2017).

Through the cofactor mediated proteolysis of C3b, FI both facilitates host protection and determines cellular fate (Figure 1-5). When C3b binds to healthy host surfaces, the surface bound regulators MCP and CR1 facilitate the binding and activation of FI, resulting in C3b cleavage to iC3b. Generation of iC3b prevents the formation of C3 convertase on these host surfaces due to the disruption of the CUB domain, the FB binding site (Janssen *et al.*, 2009), halting the amplification loop of the AP. Whereas on invading microbes and apoptotic host cells, which either lack or have insufficient RCAs, AP activation occurs leading to rapid opsonisation. Depending on the complement regulator present, a variety of opsonins are formed, which in turn define the fate of the cell and the immune response that is raised. For example, cleavage of C3b to C3dg in the presence of CR1, leads to an increased antibody response through binding to complement receptor type 2 (CR2) to C3dg on B cells (Janssen *et al.*, 2006).

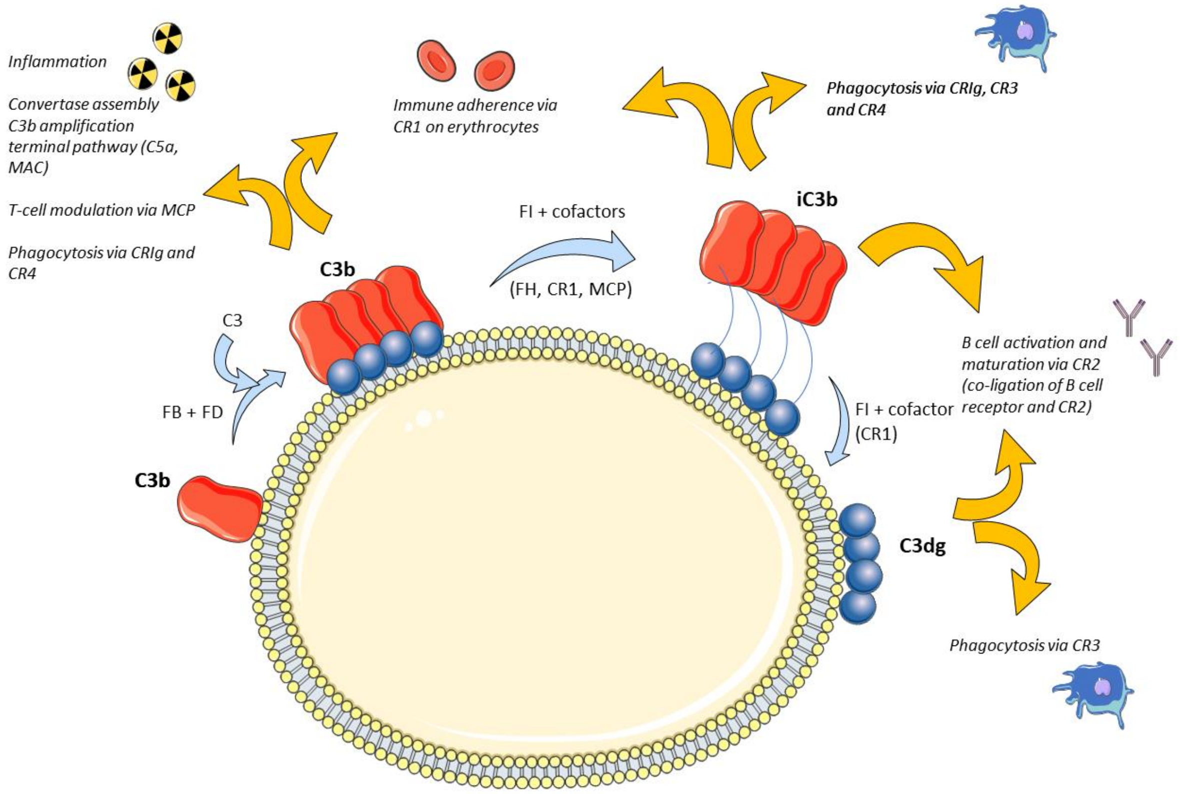

Figure 1-5 Overview of regulator dependent C3b proteolysis by FI in protection against over-activation of the complement cascade and signalling adaptive immune responses (adapted from Xue *et al.*, 2017).
Opsonisation and cofactor mediated cleavage of C3b by FI on a cell surface. Downstream interaction demonstrated through the signalling of adaptive immune responses. (Xue *et al.*, 2017)

1.2.5.6. *Genetic Variants of CFI in disease*

Genetic variants of *CFI* can be categorised into two subclasses: Type 1 and Type 2 (Kavanagh *et al.*, 2008, 2015). Type 1 variants are characterised by a quantitative deficiency of FI, in the serum or plasma, due to a lack of expression or impaired cellular secretion. Type 2 variants, however, lead to normal levels of FI in the plasma, but with functional defects resulting in impaired complement regulation.

Type 1 *CFI* variants are associated with aHUS (Kavanagh *et al.*, 2008), MPGN (Leroy *et al.*, 2011) and AMD (Hallam *et al.*, 2020; Kavanagh *et al.*, 2015), and typically occur as the result of heterozygous *CFI* mutations (Fremeaux-Bacchi *et al.*, 2004). In these instances, the haploinsufficiency is usually a consequence of the introduction of a premature stop codon (Nilsson *et al.*, 2009), or due to endoplasmic reticulum retention as identified by co-localisation with protein disulphide isomerase and an increased susceptibility to endoglycosidase H digestion (Bienaime *et al.*, 2010).

Complete FI deficiency (CFID) is also associated with Type 1 variants and arises due to homozygous or compound heterozygous mutations in the *CFI* gene. CFID results in the systemic consumption of C3 due to uninhibited AP activation (Nilsson *et al.*, 2009). As a consequence of this consumption, patients with CFID are more susceptible to recurrent pyogenic infections (Du Clos and Mold, 2008), and an increased incidence of SLE (Amadei *et al.*, 2001).

Type 2 variants are more likely to impact complement regulation through a dysfunction in FI binding to the substrate-cofactor complex, or through an impaired ability to cleave either C3b or C4b following the formation of the TMC. Since Type 2 variants are secreted, they require a functional assessment for their characterisation. This is typically achieved through serum C3b degradation assays (Geerlings *et al.*, 2017), and fluid-phase and cell surface cofactor assays (Kavanagh *et al.*, 2008), however a quantitative assessment of iC3b may also provide a surrogate for impaired FI function (Java *et al.*, 2020).

Many of these variants associated with aHUS, C3G, MPGN, DDD and AMD have been recorded in the Database of Complement Gene Variants (https://www.complement-db.org/home.php), by Osborne *et al.* (Osborne *et al.*, 2018). In aHUS, most genetic variants are heterozygous with 4-8% of cases attributed to variants in *CFI* (Noris and Remuzzi, 2015). Rare variants in *CFI* are associated with AMD (Fritsche *et al.*, 2016), particularly those which result in low FI levels (Kavanagh *et al.*, 2015; Hallam *et al.*, 2020). In C3G however, rare variants of *CFI* were not significantly associated with the disease, however pathogenic variants are found at a low frequency (Osborne *et al.*, 2018; Rodriguez *et al.*, 2014). Whilst this database is not exhaustive, it is clear that genetic variants in *CFI* are linked to a variety of diseases, with many of these variants shown to play a role in the disease pathology through functional assessments.

1.3. Complement in AMD

1.3.1. General Evidence

The first evidence for the role of complement in AMD was through the identification of the complement components C1q, C3c and C3d in the subretinal membranes of patients with AMD (Baudouin *et al.*, 1992). This finding was supported in the following year, through the staining of complement components in the outer collagenous zone of the BM, adjacent to the choriocapillaris, in donor eyes that contained hard drusen (van der Schaft *et al.*, 1993). In the ensuing years, many of the complement components and regulators were identified in drusen, a pathological hallmark of AMD (Anderson *et al.*, 2010; Crabb *et al.*, 2002; Gold *et al.*, 2006; Hageman *et al.*, 2005; Johnson *et al.*, 2001; Mullins *et al.*, 2000), leading to the model that local inflammation accompanied by complement activation may contribute to the pathogenesis of AMD (Hageman *et al.*, 2001; Johnson *et al.*, 2001).

1.3.2. Genetic Evidence for Complement in AMD

Although the initial investigations into the association between complement and AMD focused on the deposition of complement proteins in or around drusen, a major breakthrough occurred in 2005, when several genetic studies identified a significant association between AMD and a single *CFH* polymorphism (Edwards *et al.*, 2005; Hageman *et al.*, 2005; Haines *et al.*, 2005; Klein *et al.*, 2005). Each of these studies converged on the SNP rs1061170, which causes a substitution of a histidine at position 402 instead of a tyrosine in the FH protein, and confers a 2.27-fold higher risk of late AMD (Sofat *et al.*, 2012). Subsequent functional studies have elucidated that the Y402H variant reduces binding to CRP, heparin, and RPE cells, but maintains fluid-phase cofactor activity (Skerka *et al.*, 2007). The Y402H variant was also shown to affect FHL-1, a differential splice product of FH, which functions as the main complement regulator within the BM (Clark *et al.*, 2014; Skerka *et al.*, 2007).

Following these seminal findings, the genetic link between AMD and the complement system was further expanded through the identification of genetic variants in *CFB* and *C2*. In 2006, Gold *et al.* identified four variants significantly associated with AMD. The two common polymorphisms L9H and R32Q in *CFB* were in nearly complete linkage disequilibrium (LD) with the two *C2* variants E318D and rs547154, and were associated with a lower risk of AMD (OR = 0.45 and 0.36, respectively) (Gold *et al.*, 2006). Further studies into the R32Q mutation in FB have demonstrated that this mutation influences C3 convertase formation, with the Q32 variant forming the convertase less efficiently than the WT (Heurich *et al.*, 2011; Montes *et al.*, 2009). This may provide a causative link with the observed reduction in disease burden through LD, due to a dampening of the AP amplification loop associated with this variant.

Later in 2007, two studies identified a single SNP in *C3* (rs2230199) that was significantly associated with AMD in two distinct cohorts (Maller *et al.*, 2007; Yates *et al.*, 2007). The SNP results in a nonsynonymous substitution, whereby the arginine at position 102 (80 with the leader sequence removed) is mutated to a glycine, resulting in the generation of two allotypes; C3S (slow, R102) and C3F (fast, G102), as named by their different electrophoretic motility. The OR for AMD in C3S/F heterozygotes and C3F/F homozygotes was 1.7 and 2.6, respectively, when compared to the WT (S/S) (Yates *et al.*, 2007). The increased risk associated with C3F was later confirmed through functional studies, which identified that FH had a reduced binding affinity for C3F, compared to C3S, resulting in decreased FI cofactor activity, and enhanced AP activation (Heurich *et al.*, 2011).

In addition to the variants identified in *CFB*, *C2* and *C3*, a common protective haplotype was identified near the *CFH* gene on chromosome 1q23 and resulted in a deletion of the CFH related genes *CFHR1* and *CFHR3* (Hughes *et al.*, 2006). Further investigations into this haplotype identified CFHR1 as an inhibitor of C5 convertase activity (Heinen *et al.*, 2009) and CFHR3 as a cofactor for FI-mediated inactivation of C3b (Fritsche *et al.*, 2010). It was therefore proposed that CFHR1 and CFHR3 compete with FH for C3b binding, and in their absence, FH binding to C3b dominates. This may be beneficial in the retina as FH exhibits decay accelerating activity, an ability which both CFHR1 and CFHR3 lack, in addition to its role as a cofactor, and therefore enhances local complement regulation at an earlier stage within the alternative pathway (Fritsche *et al.*, 2010).

The identification of these initial variants reinforced the hypothesis that AMD was indeed associated with the complement system, particularly through the AP. In 2008, a SNP (rs2511989) in the *SERPING1* gene (Serpin (serine protease inhibitor) Family G Member 1), a C1 inhibitor, was identified as exhibiting a significant association with AMD (Ennis *et al.*, 2008). The identification of this protective variant suggested a potential role for the CP in the pathogenesis of AMD, however subsequent studies were unable to replicate this association (Allikmets *et al.*, 2009; Park *et al.*, 2009).

Following a meta-analysis of genome-wide linkage studies in AMD, seven chromosomal regions (1q, 2p, 3p, 4q, 10q, 12q and 16q) were identified as putative candidate regions for susceptibility genes (Fisher *et al.*, 2005). In 2009, a case-control association study was performed based upon these regions of interest, and led to the identification of 12 SNPs within and nearby the *CFI* gene that were significantly associated with AMD. The rs10033900 SNP was the most significantly associated SNP with advanced AMD (OR = 0.7056; $P = 6.46\times10^{-8}$) and is located 2781 bp upstream of the 3′ untranslated region of *CFI* (Fagerness *et al.*, 2009). Later, two other nominally associated SNPs not genotyped by Fagerness *et al.*

were identified in the *CFI* region (Ennis *et al.*, 2010), further implicating genomic variation in the *CFI* gene with AMD susceptibility. Within the same year, the rs10033900 SNP was also identified within a Japanese cohort (OR = 0.68), proving support for the initial association between rs10033900 and AMD (Kondo *et al.*, 2010). In addition, another of the SNPs identified by Fagerness *et al.* was also reported by Chen *et al.* (2010) and provided confirmation of the significant association between rs2285714 and AMD (OR = 1.31; P = 3.4×10^{-7}) (Chen *et al.*, 2010).

In 2011 a rare, high-risk *CFH* haplotype resulting in an R1210C substitution was identified. Genotyping for the R1210C in 2,423 AMD cases and 1,122 controls, demonstrated a high degree of penetrance (P = 7.0×10^{-6}), and earlier onset of disease (65 years vs 71 years, P = 2.3×10^{-6}) (Raychaudhuri *et al.*, 2011). Previously, this variant had also been associated with aHUS (Martinez-Barricarte *et al.*, 2008), where it was shown to compromise C-terminal function, resulting in reduced binding to C3b and heparin (Manuelian *et al.*, 2003).

The first genetic link between the terminal complement pathway and AMD, was in 2012 when a common, nonsense *C9* polymorphism (R95X) was shown to be protective against wet AMD (CNV) in a Japanese cohort (OR = 0.2). The authors also noted that intraocular injection of an anti-C9 antibody led to a decrease in laser-induced CNV and intraocular vascular endothelial growth factor (VEGF) levels in mice, suggesting that lower C9 levels were protective against wet AMD, implicating a role for TCC/MAC formation the disease pathogenesis (Nishiguchi *et al.*, 2012). Also in the same year, a GWAS comparing the prevalence of variants in patients with dry AMD against those with wet AMD, identified a significant association with variants in *CFH*, *CFB*, *C3*, *CFI* and *C2* with advanced AMD, however none of these variants were significantly correlated with either form of the late stage of the disease (Sobrin *et al.*, 2012).

In 2013 there were a surge of publications associating a host of rare (minor allele frequency (MAF) <1%)) genetic variants of complement genes with AMD. A GWAS performed by the AMD Gene Consortium consisting of 18 international research groups, identified 19 loci with a significant association with AMD (P < 5×10^{-8}), and consisted of the previously reported complement genes: *CFH*, *C2-CFB*, *C3*, and *CFI* in addition to seven newly associated loci. Through a separate analysis of neovascularization and geographic atrophy cases, risk alleles within *CFH* were also preferentially associated with an increased risk of dry AMD (OR(wet)=2.34, OR(dry)=2.80) (Fritsche *et al.*, 2013).

A further rare, highly penetrant missense mutation in *CFI* was reported by van de Ven *et al.* (2013) encoding a p.Gly119Arg substitution, and conferred a high risk for AMD (OR = 22.2; P = 3.79×10^{-6}). Functional studies into this mutant identified that plasma and sera containing this variant exhibited reduced C3b degradation, both in the fluid-phase and on the cell surface (van de Ven *et al.*, 2013). Strengthening the association between rare missense *CFI* variants and AMD, was Seddon *et al.* (2013) who demonstrated that 7.8% of AMD cases compared to 2.3% of controls were carriers of rare missense *CFI* variants (OR = 3.57; P = 2×10^{-8}). Whilst there was no statistical association with a single *CFI* variant, likely due to their rarity, there was a greater burden of disease associated with rare variants that affected the catalytic light chain of FI (OR = 4.85), compared to the heavy chain (OR = 2.63). An addition 5 risk and 15 protective variants were also identified in the genes for *CFH*, *CFHR2*, *CFHR5*, *C3* and *C9*. Four of these variants were within or near *CFH* and included the previously reported R1210C. Separate to the *CFH* risk loci, two significantly associated risk variants were identified in *C3* (OR = 9; P = $1.5\text{x}10^{-5}$) and C9 (OR = 2.2; P = 0.01) respectively. The *C3* variant resulted in a p.Lys155Gln substitution, and caused a significant reduction in FI mediated cleavage, in addition to a reduced binding affinity for FH binding. Whilst at the time there was no functional data for the impact of the *C9* risk variant (p.Pro167Ser), this variant has now been associated with both higher (Kremlitzka *et al.*, 2018) and lower (McMahon *et al.*, 2021) circulating C9 levels, in addition to increase polymerisation in the TCC (Kremlitzka *et al.*, 2018; McMahon *et al.*, 2021). The *C3* variant (K155Q) identified by Seddon *et al.* (2013), was also reported in an independent Icelandic cohort, resulting in a combined OR of 3.65 (P = $1.6\text{x}10^{-10}$) (Helgason *et al.*, 2013). K155Q was also identified in a separate American cohort (OR = 2.91; P = $2.8\text{x}10^{-5}$), along with the previously reported *CFH* variants, R1210C (OR = 23.1; P = $2.9\text{x}10^{-6}$) and H402Y (OR = 0.56; P = $1.01\text{x}10^{-43}$) (Zhan *et al.*, 2013).

In 2015, Kavanagh *et al.* performed targeted sequencing of the *CFI* gene, followed by an assessment of serum FI levels. In 2266 individuals with, and 1400 without AMD, 71 different non-synonymous *CFI* variants were identified in 231 individuals (Kavanagh *et al.*, 2015). Rare genetic variants of *CFI* were strongly associated with disease (P = $1.1\text{x}10^{-8}$), and often resulted in lower FI levels. Low FI levels were significantly associated with an increased risk for advanced AMD, particularly in individuals with a rare *CFI* variant (OR = 13.6; P = $1.6\text{x}10^{-4}$). This study also identified eight very rare *CFI* variants that were more common within this population (counts ≥ 5), and three of these were nominally associated with AMD; p.P553S (OR = 2.69, P = 0.027), p.R406H (OR = 0.10, P = 0.015) and p.A240G (OR = 7.43, P = 0.023) (Table 3-1). Through the identification of the association between low systemic FI levels and AMD, these results indicated that low serum FI may provide a biomarker for those susceptible to AMD. This also suggested that individuals with low FI levels may benefit from a complement inhibitory therapy, such as FI supplementation (Kavanagh *et al.*, 2015). In addition to the rare variants in *CFI* identified by Kavanagh *et al.*, a further *CFI* variant p.V412M was also identified in 2015 in two Tunisian Jewish families with AMD (Pras *et al.*, 2015). This variant has also now been identified within another Jewish cohort, potentially implicating an association with ethnicity (Shoshany *et al.*, 2019).

Also, in the same year, Lay *et al.* investigated the effects of complotypes (Harris *et al.*, 2012) on FI mediated cleavage of C3b in healthy individuals. The complotypes were determined by the composition of the three common polymorphisms, *C3* p.R102G, and *CFH* p.V62I and p.Y402H. In individuals either homozygous or heterozygous for the risk alleles, there was a reduction in FI activity, as determined by the amount of iC3b formed and the rate at which iC3b was converted to C3dg. To rescue this effect, the authors supplemented with exogenous FI, and demonstrated that FI activity could be restored. This data provided evidence in support of the hypothesis that FI supplementation may provide a possible therapeutic aid for the downregulation AP amplification in diseases such as AMD (Lay *et al.*, 2015).

In 2016, Fritsche *et al.* expanded their work from 2013 by systematically examining common and rare variants of AMD within the International AMD Genomics Consortium (IAMDGC). Fifty-two common and rare variants were identified across 34 distinct loci that were independently associated with a higher risk of AMD ($P < 5x10^{-8}$). These loci included the previously identified complement genes: *CFH*, *CFI*, *C9*, *CFB*, *C2* and *C3*, reinforcing the evidence for a causal relationship between variants in complement genes and AMD. Most of the associated variants identified were common, however all seven of the rare variants (MAF < 1%) associated with genome wide significances were located in, or near complement genes. These included the four previously described nonsynonymous variants; *CFH* p.R1210C, *CFI* p.G119R, *C9* p.P167S and *C3* p.K155Q, in addition to three newly identified *CFH* SNPs, rs148553336, rs191281603 and rs35292876. Rare genetic variants in both *CFH* and *CFI* were associated with an increased burden (OR = 2.94 and OR = 2.95, respectively), and together with the previously identified individual variants *CFH* p.R1210C and *CFI* p.G119R, led to the conclusion that there is a causal role for both FH and FI in AMD aetiology (Fritsche *et al.*, 2016).

Confirming the finding that rare variants in *CFI*, *C9* and *C3* are significantly associated with AMD, the same rare variants (*CFI* p.G119R, *C9* p.P167S and *C3* p.K155Q) identified by Fritsche *et al.* were also found in the European Genetic Database (EUGENDA) cohort by Saksens *et al.* (2016). Carriers of these variants also demonstrated an earlier onset of disease and were typically found in patients with dry AMD, compared to wet AMD (P = 0.04), suggesting that genetic testing could enable earlier identification of the disease in patients and could also direct clinical treatment (Saksens *et al.*, 2016). Providing support to the notion of genetic testing for an earlier identification of disease, Wagner *et al.* (2016) also reported that carriers of the rare *CFH* variants R127H, R175P and C192F were associated with an earlier onset of disease (average age 59.2 vs 69.6) (Wagner *et al.*, 2016).

Following on from the work by Saksens *et al.* (2016) in the EUGENDA cohort, six new rare genetic variants (*CFH* p.S193L, *CFH* p.R175Q, *CFI* p.P553S, *CFI* p.L131R, *C9* p.R118W, and *C3* p.R161TW) exhibited an increased prevalence in families with AMD (OR = 2.04). Further analysis of the identified FI variants determined that G119R and L131R were associated with decreased serum FI levels, and that G119R, L131R and P553S had a reduced ability to degrade C3b in serum. This further strengthened the hypothesis that both Type 1 and Type 2 FI variants can lead to decreased C3b cleavage resulting in AP overactivation and therefore lead to a higher risk for developing AMD (Geerlings *et al.*, 2017).

In a continuation of the functional assessment of rare genetic variants of *CFI*, Tan *et al.* (2017) utilised an *in vivo* assay of retinal vascularisation in zebrafish embryos to provide a surrogate marker of FI function. Prior to the functional analysis they identified three novel variants (M532V, E305X, and D249E) in addition to seventeen others which had been previously identified (Tan *et al.*, 2017), 9 of which were previously identified in Kavanagh *et al.* (Kavanagh *et al.*, 2015) This assay demonstrated some concordance with the FI serum levels identified in Kavanagh *et al.* (2015), with variants that were associated with low levels demonstrating hypoactivity in the zebrafish functional assay (Tan *et al.*, 2017).

Later in 2018, Geerlings *et al.* sought to identify a genotype-phenotype correlation between low-frequency genetic variants in the *CFH*, *CFI*, and *C3* genes and the diseases, aHUS/C3G and AMD (Geerlings *et al.*, 2018). Of these three genes, *CFH* contained the largest number of unique rare variants, followed by *C3* and *CFI*. A substantial number of rare variants were identified in both aHUS/C3G and AMD (40%), with only 26% of variants specific to AMD. Rare variants located within SCR3, SCR5, and SCR7 domains of FH, the SRCR and the SP domain of FI, and the MG3 domain of C3 occurred with a significantly higher frequency in those with AMD (Geerlings *et al.*, 2018). This provided support for previous findings which demonstrated that variants which affect the N-terminus of FH are more likely to result in altered DAA or cofactor activity (Yu *et al.*, 2014), and that variants which affect the light chain of FI are significantly associated with an increased disease burden (Seddon *et al.*, 2013).

In 2020, Hallam *et al.* recapitulated the finding from Kavanagh *et al.* (2015), that rare genetic variants in *CFI* which result in low FI levels are a significant risk factor for AMD (OR = 10.6) in a Southampton cohort. Low serum FI levels were also significantly associated with early AMD in individuals without a *CFI* variant (OR = 2.6; P = 0.01) (Hallam *et al.*, 2020), further providing support for FI supplementation as an AMD therapeutic, even in individuals without a *CFI* mutation.

Another assessment of FI levels associated with *CFI* variants, was performed by de Jong *et al.* using samples from the EUGENDA cohort (de Jong *et al.*, 2020). FI levels were measured both in plasma, and *in vitro* in the supernatants of HEK293T cells expressing recombinant FI. Significantly reduced FI levels were observed for carriers with the previously reported Type 1 variants G119A, L113R and G188A, and the r.658_773del variant. Two mutations, P64L and R474X, were below the lower limit of normal, and two, V152M and I357M, were clustered near the lower limit. Overall, four definite Type 1 mutations were identified, five plausible, and the remainder were either Type 2, or variants of uncertain significance. For the recombinant expressions, 54% of the rare *CFI* variants caused significantly reduced expression compared to the recombinant WT control. Variants affecting the CD5 and LDLR1A domains of FI, resulted in the lowest median expression. The recombinant protein expression demonstrated moderate, significant, correlation with the FI level in plasma, (R^2 = 0.5396; P < 0.0001), indicating that recombinant protein expression may provide a surrogate marker for plasma FI levels. Recombinant protein expression could therefore aid in the identification of Type 1 and 2 *CFI* variants, as FI level are not affected by acute phase protein fluctuations *in vitro* (de Jong *et al.*, 2020).

Overall, there is strong and comprehensive genetic (and functional) evidence linking both rare and common variants of the complement system to AMD. Two of the genes specifically associated with an increased burden in the disease are *CFH*, and *CFI*, which is of particular interest in this project. The majority of the genetic evidence implicates the AP of complement, however variants affecting the terminal complement pathway may also confer a greater susceptibility to the disease. Ultimately, based upon the genetic evidence, it is reasonable to hypothesise that uncontrolled overactivation of the AP of complement plays a significant role in the pathogenesis of AMD, and that by designing therapeutics which target this pathway may provide a promising aid in the treatment of AMD.

1.3.3. Rare Genetic Variants of CFI in AMD

At the time of writing this thesis, there were 148 rare *CFI* variants identified within the literature associated with either functional or quantitative data (Figure 1-6). Despite an abundance of rare *CFI* variants demonstrating associations with disease, many of these are still uncharacterised. Whilst the location of the variant can offer an indication as to whether a variant may be pathogenic (Light chain OR = 4.85, Heavy chain OR = 2.63), functional studies are still required to provide any certainty (Seddon *et al.*, 2013). Serum FI levels can provide a biomarker for dysfunctional rare variants of *CFI*; however, some uncertainty may still surround these findings as FI is an acute phase protein which can lead to fluctuations in the circulating level (Kavanagh *et al.*, 2015). As a result, functional studies are therefore key for the distinguishing between Type 1 and Type 2 variants pathogenic variants.

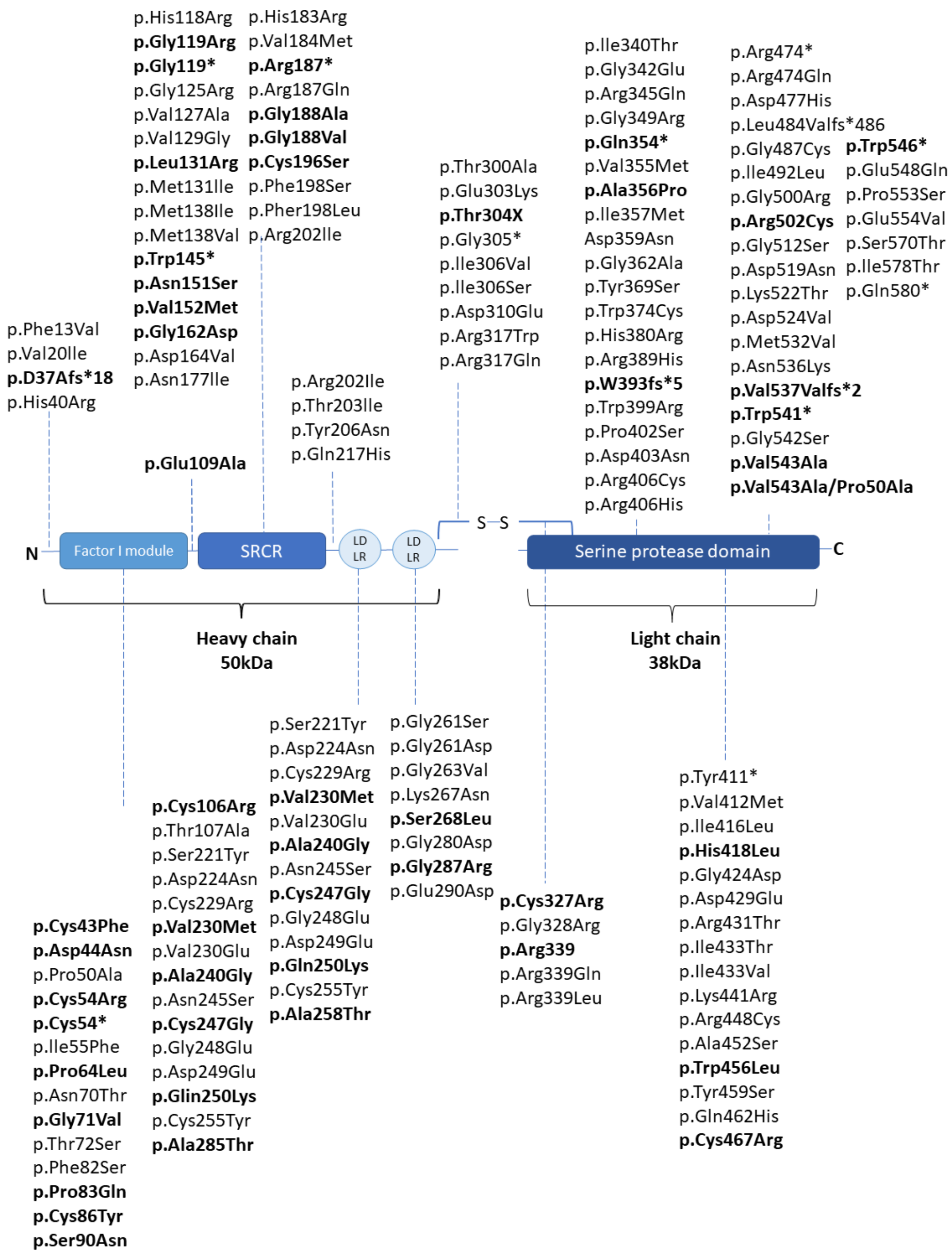

Figure 1-6 All rare *CFI* variants in the literature with functional or quantitative data and the location within FI (adapted and updated from Dr. T Hallam Thesis, National Renal Complement Therapeutics Centre).

A schematic of the protein domains of complement factor I from the N (left) to C (right) terminus is displayed. Variants highlighted in bold are associated with low serum levels. Scavenger receptor cysteine rich (SRCR), Low density lipoprotein receptor (LDLR)

1.3.4. Role of Complement of AMD in Pathogenesis

Whilst the role of complement in the pathogenesis of AMD is not fully understood, through the aforementioned genetic studies, functional data, and previous identification of complement components in and around drusen deposits, several mechanisms have been suggested for the underlying role of complement activation in AMD.

1.3.4.1. Alternative Pathway Activation

A mixture of both systemic and local complement activation is thought to drive the pathogenesis of AMD. Many complement activation products have shown elevated systemic levels in AMD patients, with consecutive stages of the disease demonstrating increasing levels of complement activation (Heesterbeek *et al.*, 2020; Reynolds *et al.*, 2009). An increase in local complement activation has also been identified in donor macular tissue, demonstrating significantly higher levels of C3, C3b, iC3b and TCC in individuals homozygous for the risk CFH-to-F13B diplotype. Significantly higher levels of TCC were identified in the BM and the choriocapillaris (Keenan *et al.*, 2015).

Adding further support for local activation in AMD, increased MAC deposition was also identified in hard drusen and in the RPE in some cases of advanced AMD (Mullins *et al.*, 2014). Transcriptome analysis of the neural retina, RPE cells and choroid isolates have indicated that cells within the human RPE-choroid complex express a virtually complete set of transcripts for both CP and AP components and regulatory molecules (Anderson *et al.*, 2010). Using single-cell RNA sequencing in mice retinal cells, evidence was provided for cell-type specific complement expression. The glial cells of the retina are the major providers of complement activators (C3, C4 and FB); the RPE mainly express FH and TCC, and *CFI* and *CFP* transcripts were most abundant in the neuronal cells (Pauly *et al.*, 2019). In a separate study in humans, four AP genes and one CP/LP gene (*C3*>*CFH*>>*CFI*=*CFB*>*C2*), were expressed at a much higher level in the RPE-choroid complex. Of these genes only *CFI* exhibited regional differential expression, with higher expression in the macular RPE, compared to the neural retina or the peripheral retina (Li *et al.*, 2014). Through the generation of humanised mouse models of CNV, this has illustrated that activation of C3 and MAC deposition are central to the pathogenesis of wet AMD (Cashman *et al.*, 2011; Ramo *et al.*, 2008).

1.3.4.2. Complement in the Extracellular Matrix

As demonstrated by Clark *et al.* (2017) most of the complement proteins are unable to diffuse through the BM, with the exception of FHL-1, FD and C5a, creating two semi-independent compartments with respect to complement activation and regulation (Clark *et al.*, 2017). Both with age and the development of AMD, the permeability of the BM is further reduced as a result of ECM thickening and drusen deposition (Pauleikhoff *et al.*, 1990). The reduction in permeability has a significant impact on the accumulation of complement activation products and cellular debris within the macular, resulting in increased inflammation (Handa *et al.*, 1999). Within the ECM, the only blood borne FI cofactors that are able to modulate C3b deposition are FH and FHL-1, which anchor to the ECM through the binding of sulphated glycosaminoglycans (GAGs) such as heparan sulphate proteoglycans (HSPG) (Clark *et al.*, 2014). With age, the proportion of HSPG in the BM decreases, and potentially leads to reduced protection against C3b deposition through the loss of FH and FHL-1 binding sites (Keenan *et al.*, 2014). The Y402H mutation commonly associated with AMD also affects both of these regulatory molecules by decreasing the binding affinity to polyanions such as heparin (Ormsby *et al.*, 2008), which may explain the increased incidence of AMD with age in individuals that are homozygous for this variant (Klein *et al.*, 2005). With the accumulation of drusen in advanced AMD, the permeability to FHL-1 is reduced, resulting in increased AP activation within the macular, as the passage of FD remains unhindered (Clark *et al.*, 2017). This may also lead to increased destabilisation of the RPE cells, through an increased susceptibility for oxidative stress-induced death in the absence of FHL-1 (Choudhury *et al.*, 2021).

In vitro drusen deposition is also correlated with increased expression of complement proteins including C3 and C5 (Johnson *et al.*, 2011), and has been supported by the culture of human-induced pluripotent stem cells (iPSC)-derived RPE from AMD patients which produced significantly increased complement and inflammatory factors compared to non-AMD donors (Saini *et al.*, 2017).

1.3.4.3. Complement and Inflammation

AMD is characterised by chronic inflammation within the eye which provides a strong link between complement activation and AMD pathology. Complement activation results in the production of the anaphylatoxins C3a and C5a, which aid in the recruitment and activation of immune cells via C3aR and C5aR. The anaphylatoxins stimulate inflammation by inducing a respiratory burst in macrophages, eosinophils, and neutrophils, and can induce histamine production by basophils and mast cells. They also act as chemo-attractants, with neutrophils and mast cells responding to C3a, and basophils, macrophages, lymphocytes and neutrophils to C5a (Merle, Noe, *et al.*, 2015).

The immune cells that are considered to be involved with AMD are resident retinal microglia cells in addition to circulating lymphocytes and monocytes/macrophages and mast cells (Behnke *et al.*, 2020; Ogura *et al.*, 2020). The pro-inflammatory immune changes observed with AMD was observed when RPE cells were treated with complement containing serum, which led to an increase in secretion and expression of IL-6, IL-8, and monocyte chemoattractant protein-1 (MCP-1), in addition to TNF-α, intercellular adhesion molecule-1 (ICAM-1) and vascular cell adhesion molecule-1 (VCAM-1), in a concentration dependant manner (Lueck *et al.*, 2015). Complement activation in the outer retina has also been associated with the recruitment of monocytes and phagocytosis of C3b-osponised photoreceptor outer segments (POS) (Katschke *et al.*, 2018).

1.3.4.4. Complement, Oxidative Stress and Energy Metabolism

Oxidative stress has long been hypothesised to play a substantive role in the development of AMD. The retina has one of the highest energy demands within the body, and any disruption in the supply of metabolites or oxygen often leads to increased oxidative stress which can result in cell death (Bill and Sperber, 1990; Liu and Prokosch, 2021; Werkmeister *et al.*, 2015). Of the cells of the retina, the RPE experiences a high level of oxidative stress due to its exposure to high-energy light, and its role in the phagocytosis of oxidised POS, both of which result in the generation of reactive oxygen species (ROS) (Datta *et al.*, 2017). To mimic this environment *in vitro*, RPE cells are exposed to H_2O_2, which results in oxidative stress. In 2009, Thurman *et al.* demonstrated that the exposure of H_2O_2 to ARPE-19 cells led to reduced surface expression of the complement regulators DAF, MCP and CD59, and increased complement activation upon the addition of human serum (Thurman *et al.*, 2009). Endogenous complement production has also been observed following oxidative stress (Trakkides *et al.*, 2019). Exposure to H_2O_2 caused increased expression of the complement receptors CR3 and C5aR in ARPE-19, signalling C3 cleavage and C5 activation. There was also an accumulation of C3, FH, and properdin intracellularly, with younger cells demonstrating greater secretion of C3 and FH than older cells. Due to the upregulation of intracellular complement components, this may indicate that complement is involved in RPE homeostasis following oxidative stress (Trakkides *et al.*, 2019).

As smoking is a major risk factor for AMD, cigarette smoke extract (CSE) has also been used to induce a high oxidative stress environment for RPE cells. Exposure to CSE triggered the production and release of C3 from the RPE cells, leading to activation of the AP (Kunchithapautham *et al.*, 2014). Taken together, these studies indicate that oxidative stress results in decreased expression of complement regulators, which in turn causes uncontrolled AP amplification, exacerbating AMD progression.

RPE cells are enriched with mitochondria, due to their high metabolic activity, and as a result contribute a major source of ROS within the RPE (Datta *et al.*, 2017). Transmission electron microscopy has shown that the mitochondria of RPE cells in AMD eyes undergo morphological changes resulting in disrupted cristae and ruptured membranes, in addition to a reduction in number (Feher *et al.*, 2006). Linking the mitochondrial dysfunction associated with AMD to complement are the results from the CFH knockout mice. Within these mice, the mitochondria of the RPE cells become abnormally large and reduced in number, resulting in reduced mitochondrial DNA levels and a decline in adenosine triphosphate (ATP) production (Sivapathasuntharam *et al.*, 2019), mirroring the changes that are observed with AMD.

1.3.4.5. Complement and Lipid Accumulation

Accumulation of lipids plays a fundamental role in AMD pathogenesis, as increased lipid deposition within the BM is known to occur at an early stage in disease progression, and that lipids are a major component of drusen, the pathological hallmark of AMD (Curcio *et al.*, 2009). In a metabolomic study by the EYE-RISK Consortium, 60 metabolites were shown to be significantly associated with AMD, including increased levels of high-density lipoproteins and decreased levels of low-density lipoproteins. Of the 60 significant metabolites identified, 57 of them were significantly associated with systemic complement activation, as determined by the C3 to C3d ratio, irrespective of AMD status (Acar *et al.*, 2020).

Further evidence for the overlap between lipid metabolism and complement, was provided by Toomey *et al.* using a heterozygous *CFH* knockout mouse model and a high fat, cholesterol-enriched diet (Toomey *et al.*, 2015). In the aged heterozygous mice, the high fat diet caused the mice to develop the characteristic signs of early AMD including ocular complement dysregulation, increased sub-RPE deposit formation and significantly impaired scotopic visual function; however, these changes did not occur in the homozygous mice. FH was shown to compete with lipoproteins for the HSPG binding sites within the BM, and with decreased FH in the heterozygous mice, this led to lipoprotein accumulation in the BM, triggering basal linear deposit formation. Since no basal deposits were formed in the homozygous mice, as a result of C3 consumption, this indicated that dysregulated complement was responsible for the basal deposit formation, which eventually result in RPE damage, and AMD (Toomey *et al.*, 2015).

The impact of impaired FH function on lipid accumulation was further supported by patient iPSC-derived RPE cells carrying the *CFH* Y402H SNP. The iPSC RPE derived from the high risk (H402) patients, showed an accumulation of lipid droplets, deposition of “drusen”-like deposits and increased inflammation and cellular stress (Hallam *et al.*, 2017), demonstrating a key interaction between complement activation, lipid accumulation and AMD.

1.3.4.6. AMD Therapies

Current AMD therapeutics have typically focused on wet AMD, targeting CNV through intravitreal anti-VEGF therapies. The VEGFR-1 and 2 receptors are located on the endothelial cells of the choriocapillaris, and when stimulated by VEGF-A, initiate angiogenesis and vascular permeability within the choroid (Ferrara *et al.*, 2003). VEGF-A upregulation within the retina is induced by a hypoxic environment, generated as a consequence of many of the physiological changes that occur during the pathogenesis of AMD (1.11.4.1.4). By targeting VEGF, this can result in decreased CNV leakage and CNV regression, resulting in an improvement in visual acuity (Hussain *et al.*, 2005; Iglicki *et al.*, 2021; Maguire *et al.*, 2016; Moshfeghi *et al.*, 2006). Although these are promising advancement in the field of AMD treatment, neovascular AMD only accounts of 10-15% of the overall prevalence of AMD (Cheung and Eaton, 2013).

Treatment for dry AMD currently remains limited to dietary supplementation (Age-Related Eye Disease Study Research Group, 1999, 2001), however there are a plethora of targets are being investigated in clinical trials which hope to improve patient outcomes in both forms of the disease. These include antioxidative drugs, anti-inflammatory drugs and complement inhibitors, amongst others (Table 1-1). Some of these studies have had promising results however it is critical to continue research in this area to address the current unmet need.

Table 1-1 Current treatments in phase I-III clinical development for dry and wet AMD (excluding terminated trials and drugs with discontinued development)

Drug Target/Name	Wet or Dry AMD	Clinical Trial ID	Trial Phase	Route of Administration	Company on Trial Record	Product description
Antioxidative						
AREDS	Dry	NCT00000145	III	Oral	Bausch & Lomb Incorporated	Vitamin E, vitamin C, beta-carotene, cupric acid, and zinc oxide
AREDS2	Dry	NCT00345176	III	Oral	National Eye Institute	Vitamin E, vitamin C, beta-carotene, cupric acid, zinc oxide with lutein and zeaxanthin or DHA and EPA
OT-551	Dry	NCT00306488	II	Topical	Othera Pharmaceuticals	Small molecule with anti-inflammatory and antioxidant effects
Reduction of toxic by-products						
GSK933776	Dry	NCT01342926	II	Intravenous	GlaxoSmithKline	An anti-amyloid β monoclonal antibody
Visual cycle modulators						
ACU-4429	Dry	NCT01802866	IIb/III	Oral	Kubota Vision Inc.	Emixustat hydrochloride
ALK-001	Dry	NCT03845582	III	Oral	Alkeus Pharmaceuticals Inc.	Modified form of vitamin A, with a deuterium isotope replacement at carbon 20
Fenretinide	Dry	NCT00429936	II	Oral	Sirion Therapeutics Inc.	Synthetic derivative of vitamin A that binds to the serum retinol-binding protein, allowing a rapid elimination of fenretinide–retinol-binding protein complex through urine

Anti-inflammatory						
AKST4290	Wet	NCT03558061, NCT03558074	II	Oral	Alkahest Inc.	CCR3 inhibitor that blocks the action of eotaxin, an immunomodulatory protein that increases as humans age and with specific age-related diseases
AL-39324	Wet	NCT00992563	II	Intravitreal	Alcon Research	Small molecule, receptor tyrosine kinase inhibitor
hI-con1	Wet	NCT01485588, NCT02358889, NCT03452527	II	Intravitreal	Iconic Therapeutics Inc.	Antibody-like molecule targeted against tissue factor, composed of two human Factor VII
RBM-007	Wet	NCT04200248, NCT04640272, NCT03633084	II	Intravitreal	Ribomic USA Inc	Anti-fibroblast growth factor 2 aptamer
Risuteganib	Dry	NCT03626636	II	Intravitreal	Bausch Health	Anti-integrin peptide that targets the multiple integrin heterodimers
Sirolimus	Dry	NCT00766649	I/II	Subconjunctival	National Eye Institute	A mammalian target of rapamycin inhibitor and immunosuppressive agent
Squalamine Lactate	Wet	NCT01678963, NCT02727881	II	Ocular	OHR Pharmaceutical Inc	Inhibits angiogenesis. The drug is taken up into activated endothelial cells through caveolae. Subsequently, the drug binds to and "chaperones" calmodulin to an intracellular membrane compartment and blocks angiogenesis at several levels

Tandospirone	Dry	NCT00890097	III	Ocular	Alcon Laboratories UK Ltd	A 5-HT1A receptor partial agonist
Complement inhibitors						
Avacinaptad pegol	Dry	NCT02686658	II/III	Intravitreal	IVERIC bio Inc.	An anti-C5 aptamer designed to decrease the activation of inflammasomes and the formation of MAC
Eculizumab	Dry	NCT00935883	II	Intravenous	Alexion Pharmaceuticals	An IgG antibody involved in the inhibition of C5
GEM103	Wet/Dry	NCT04684394, NCT04643886	II	Intravitreal	Gemini Therapeutics Inc.	Recombinant complement regulator and is a full-length and human, recombinant FH
HMR59	Dry	NCT04358471	II	Intravitreal	Hemera Biosciences	Increases the ability of retina cells to make a soluble form of CD59 called sCD59. The soluble CD59 circulates within the retina to block complement from further damaging the retina.
IONIS-FB-Lrx	Dry	NCT03446144, NCT03815825	II	Subcutaneous	Ionis Pharmaceuticals Inc.	Ligand-conjugated investigational antisense medicine designed to reduce the production of complement factor B
Pegcetacoplan	Dry	NCT03525600	III	Intravitreal	Apellis Pharmaceuticals, Inc.	Inhibits C3

Tesidolumab	Wet/Dry	NCT01527500, NCT01535950	II	Intravitreal	Novartis Pharmaceuticals	Anti-C5 monoclonal antibody
Neuroprotection						
Brimonidine tartrate	Dry	NCT00658619	II	Intravitreal	Allergan	An alpha2-adrenergic receptor agonist that has been established as an intraocular pressure-lowering agent
Cilliary nerve trophic factor	Dry	NCT00447954	II	Intravitreal	Neurotech Pharmaceuticals	Ciliary neurotrophic factor
Gene therapy						
AAVCAGsCD59	Dry	NCT03144999	I	Intravitreal	Janssen Research & Development LLC	Acts as a membrane-bound inhibitor that reduces MAC formation
AVA-101 (rAAV.sFlt-1)	Wet	NCT01494805	i/II	Subretinal	Adverum Biotechnologies Inc.	Comprised of the adeno-associated viral (AAV) 2 vector, which contains a gene encoding sFlt-1, a naturally occurring anti-VEGF protein
GT005	Dry	NCT03846193	I/II	Subretinal	Gyroscope Therapeutics	Designed to regulate complement activation and the formation of MAC. Consists of a recombinant non-replicating AAV vector encoding *CFI*, as a means to downregulate the alternative pathway.

RGX-314	Wet	NCT03066258, NCT04832724, NCT03633084	II	Intravitreal	Ribomic USA Inc	One-time subretinal treatment that includes the NAV AAV8 vector containing a gene encoding for a monoclonal antibody fragment. The expressed protein is designed to neutralise VEGF activity
Cell-based therapies						
AdipoCell	Dry	NCT02024269	N/a	Intravitreal	Bioheart Inc.	Adipose stem cell derived from the patient's adipose or fat for subsequent processing to isolate the stem cells.
CPCB-RPE1	Dry	NCT02590692	I/IIa	Subretinal	Regenerative Patch Technologies LLC	Polarised monolayer of human embryonic stem cell derived retinal pigment epithelial (RPE) cells
MAP09-hRPE	Dry	NCT01344993	I/II	Subretinal	Astellas Pharma Inc	RPE cells derived from human embryonic stem cells
OpRegen	Dry	NCT02286089	I/II	Subretinal	Lineage Cell Therapeutics Inc.	Single injection of human RPE cells derived from an established pluripotent cell line
Palucorcel	Dry	NCT01226628	I/II	Subretinal	Janssen Research & Development LLC	Human umbilical cord tissue derived cell compound that has been previously shown to reduce functional deterioration
PF-05206388	Wet	NCT01691261	I	Intraocular	Moorfield's Hospital & UCL	RPE replacement
RPESC-RPE-4W	Dry	NCT04627428	I/II	Submacular	Luxa Biotechnology	Human RPE

Mitochondrial Enhancer						
Elamipretide	Dry	NCT03891875	I	Subcutaneous	Stealth BioTherapeutics Inc.	Cardiolipin-protective compound that protects the structure of the mitochondrial cristae and promotes oxidative phosphorylation
VEGF Targeted						
Abicipar pegol	Wet	NCT02462486, NCT03539549, NCT02462928	III	Intravitreal	Allergan Ltd	DARPin directed to bind all VEGF-A isoforms; it has a higher affinity and a longer intraocular half-life than ranibizumab
Aflibercept	Wet	NCT04423718, NCT04126317	III	Intravitreal	Bayer	A VEGF inhibitor
AXT107	Wet	NCT04746963	I/II	Intravitreal	AsclepiX Therapeutics Inc	Inhibits VEGF-A and VEGF-C and activates Tie2
Brolucizumab	Wet	NCT02307682, NCT02434328, NCT01849692, NCT03930641, NCT04005352, NCT04239027, NCT04597632	III	Intravitreal	Alcon Research	Monoclonal antibody that inhibits VEGF-A
Conbercept	Wet	NCT03630952, NCT03577899	III	Intravitreal	Chengdu Kanghong Biotech Co. Ltd.	Recombinant human VEGF receptor-Fc fusion protein. Inhibits VEGF-A,B and C and placental growth factor

Faricimab	Wet	NCT03823300, NCT03823287, NCT03038880, NCT04777201	III	Intravitreal	Hoffmann-La Roche	Bispecific antibody designed for the eye. It targets two distinct pathways – via angiopoietin-2 and VEGF-A
KSI-301	Wet	NCT04964089, NCT04049266	III	Intravitreal	Kodiak Sciences Inc	Anti-VEGF biologic designed to rapidly inhibit VEGF and provide extended durability of action
ONS-5010	Wet	NCT04516278, NCT03834753	III	Intravitreal	Outlook Therapeutics Inc.	Investigational Ophthalmic Formulation of Bevacizumab-vikg
OPT-302	Wet/Dry	NCT04757636/ NCT03345082 NCT04757610	III	Intravitreal	Opthea Limited	VEGF-C/D 'trap'
PAN-90806	Wet	NCT03479372	I/II	Ocular	PanOptica	Once-daily topical anti-VEGF eye drop
Ranibizumab	Wet	NCT03677934, NCT03683251, NCT02510794, NCT04657289, NCT04853251	III	Intravitreal	Hoffmann-La Roche	Inhibits the biologic activity of human VEGF
SCT510A	Wet	NCT04564937	I/II	Intravitreal	Sinocelltech Ltd.	Intravitreal recombinant humanized anti-VEGF monoclonal antibody

Sunitinib Malate	Wet	NCT03953079	II	Intravitreal	Graybug Vision	Small-molecule inhibitor of multiple receptor tyrosine kinases including vascular endothelial growth factor receptors, platelet-derived growth factor receptors and the KIT receptor.
Vorolanib	Wet	NCT02348359	II	Intravitreal	Tyrogenex Inc	Orally available small molecule dual inhibitor targeting human VEGFRs and platelet-derived growth factor receptors

1.4. Summary

It is clear that unregulated complement activation driven by a range of compounding genetic and environmental risk factors, plays a significant role in the progression of AMD. The components of the alternative and terminal pathways of complement have been implicitly implicated in the disease, both through genetic studies and functional assessments. Rare and common genetic variants in *CFI* are significantly associated with increased AMD susceptibility, with rare variants carrying a particularly increased burden. Whilst serum antigenic FI levels can provide a biomarker for FI dysfunction, the functional consequences of many individual rare *CFI* variants remain unclear. By developing new assays for functional characterisation, we will not only improve our understanding of the impact of these rare genetic variants, but also provide further evidence to elucidate their role in the pathogenesis of AMD. Through the successful characterisation of Type 1 and Type 2 variants, this may facilitate a more personalised approach to AMD treatment in individuals experiencing complement dysregulation, either through regulator supplementation or complement blockade. Additionally correct classification of complement variants may also improve patient stratification within clinical trials for the development of new therapies for AMD. Ultimately, by improving our knowledge of the impact of rare genetic variants in *CFI*, this may pave the way improved patient outcomes in AMD, by identifying the individuals who would most benefit from FI supplementation or through therapeutics targeting the AP of complement.

1.5. Hypothesis and Aims

The primary aim of this project was to functionally characterise rare genetic variants of *CFI* that confer a susceptibility to AMD, with a focus on the functional assessment of Type 2 FI variants that are not associated with low FI levels. Furthermore, I aimed to establish a method for the purification of recombinant FI, without Pro-I contamination, to enable accurate quantification of FI activity. I also aimed to develop an antibody against the FI precursor, Pro-I, in order to determine its functional activity. Ultimately, I aimed to provide a comprehensive functional evaluation of Type 2 *CFI* variants, utilising a number of established and new methods for characterisation, in order to further understand the mechanism that these variants may play in the role of AMD pathogenesis through complement dysregulation.

Overall, it was hypothesised that:

- Rare genetic variants of *CFI* that are associated with AMD lead to complement overactivation as a consequence of quantitative or functional deficiencies.
- *CFI* variants associated with normal FI serum levels will lead to different degrees of abrogated function in C3b-FH binding and/or C3b degradation in the presence of a variety of cofactors.
- The precursor to FI, Pro-I, is a secreted but functionally inactive protein.
- Using either hybridomas or phage display, an antibody could be developed against Pro-I, without FI cross-reactivity.
- The use of an internal ribosomal entry site could be used to facilitate bicistronic expression of both Furin and *CFI*, resulting in a fully processed, functionally active recombinant FI protein.
- By incorporating an inactivating mutation within the serine protease catalytic triad, real-time binding of proteins within the AP regulatory TMC (C3b:FH:FI) could be assessed using SPR.

Chapter 2. Materials and Methods

2.1. Purification of Serum Factor I

2.1.1. OX-21 Production Using Hybridomas

B cell hybridomas expressing OX-21, a monoclonal antibody against human FI, were defrosted from liquid nitrogen stocks at in a 37°C water bath for 1-2 minutes before the gradual addition of 10 mL pre-warmed media containing Roswell Park Memorial Institute media (RPMI) 1640, 10% Ultra Low IgG foetal bovine serum (FBS) and 2 mM L-Glutamine. The cells were washed by centrifugation at 100 g for 3 minutes before seeding at a density of $5x10^5$ cells per mL into a T25 ($25cm^2$) (Grenier) tissue culture flask and incubated at 37^oC with 5% CO_2. Cells were routinely passaged once a density of $5x10^5$ – $1x10^6$ cells per mL was reached; this was typically after three days. Each culture was scaled up, by splitting every 3-5 days until a 5-day culture of cells in a T175 flask yielded $1x10^6$ cells per mL. At this point, the spent media was collected and centrifuged at 300 g for five minutes to isolate the cell pellet from the supernatant. The pellets harvested from two T175 flasks were resuspended in 20 mL of media and used to inoculate 400 mL total media in a magnetic spinner flask (Grenier). Each flask was set to agitate at 100 RPM at 37^oC with 5% CO_2 for ten days.

2.1.2. Purification of OX-21 by Protein G

After ten days, the culture media from the spinner flasks was decanted into 500 mL Sorvall centrifuge tubes (ThermoFisher) and spun at 6000 g for 20 minutes. The supernatant was then filtered through a 0.22 µM Durapore Polyvinylidene Fluoride (PVDF) membrane (Merck) and loaded onto a 5 mL HiTrap Protein G HP column (General Electric (GE), Boston, MA, USA) at 1 mL/min using an ÄKTA Start (GE).

To elute the bound OX-21, the protein G column was first equilibrated with 5 column volumes (CV) of phosphate buffered saline (PBS) (buffer A) before running 100% buffer B (0.1 M Glycine (pH 2.7)) over the column. 1 mL fractions were collected and the protein containing fractions were identified by a large peak in absorbance, at a fixed wavelength of 280 nm, as measured by the ÄKTA spectrophotometer. Next, 200 µL of 1 M Tris (pH 9) and 360 µL NaCl (1 M) was added to each fraction to neutralise the pH and limit any protein disruption. The peak fractions were combined buffer exchanged into PBS using a Protein desalting-10 (PD-10) column (GE healthcare, 17085101). The final concentration was determined by a NanoDrop One^c Spectrophotometer (Thermo Scientific) prior to storage in 1 mg aliquots at -20°C. Concentrations were calculated with the Beer-Lambert law using the molar extinction coefficient of 210,000 $M^{-1}cm^{-1}$ for a mouse IgG, and a percent extinction coefficient (Ɛ) of 1.37 at 280 nm for a 0.1% (1 mg/mL) IgG solution.

$$\text{Concentration (mg/ mL)} = \frac{\text{Absorbance at 280 nm}}{\text{0.1\% Percent solution extinction coefficient}}$$

2.1.3. Production of an OX-21 Column for FI Purification

A 1 mL N-hydroxysuccinimide (NHS) activated HiTrap column (GE) was coupled with 4 mg of OX-21 as per the manufacturer's operation instructions (71-7006-00 AX). In brief, the column was washed with 3 x 2 mL ice cold HCl (1 mM) at 1 mL/min using a 10 mL syringe connected to the top of the column via a HiTrap Luer connector (GE). 1 mL of OX-21 (4 mg/mL) which had previously been buffer exchanged into coupling buffer (0.2 M $NaHCO_3$, 0.5 M NaCl, pH 8.3), was injected onto the column. The column was then sealed and incubated at room temperature (RT) for 30 minutes. Following coupling, the column was washed and deactivated using alternate 3 x 2 mL washes with either Buffer A (0.5 M ethanolamine, 0.5 M NaCl, pH 8.3) or Buffer B (0.1 M sodium acetate, 0.5 M NaCl, pH 4). Once Buffer A had been injected over the column twice, the column was then incubated again at RT for 15 minutes, before the final three 3 x 2 mL washes with buffers B and A. Finally, the column adjusted to a neutral pH by the addition of 2 mL PBS with 0.02% sodium azide and stored at 4°C.

To determine the coupling efficiency of OX-21 to the column, three column volumes of coupling buffer were washed through the column post-coupling, and the flow-through collected. 0.5 mL of the flow-through was separated using a PD-10 desalting column (GE Healthcare, 17085101) and the absorbance measured at 280 nm. The following formula was used to calculate the coupling efficiency:

Loaded coupling solution: $A = A_{280} \times V$

Where:

A_{280} = Absorbance of coupling solution at 280 nm

V = Loaded volume of coupling solution

Amount not coupled: $B = \frac{A_{280} \times 1.5 \times V}{0.5}$

Where:

A_{280} = Absorbance of coupling solution at 280 nm after PD-10 run

1.5 = Volume collected from PD-10

V = Volume post coupling wash

0.5 = Volume loaded on PD-10

$$\text{Coupling efficiency } (\%) = \frac{(A - B)}{A} \times 100$$

2.1.4. Citrated Plasma Preparation

Non-sterile mixed pool human plasma (TCS biosciences, PR100-500) was clotted in Sorvall centrifuge tubes (ThermoFisher) by the addition of $CaCl_2$ (25 mM) and $MgCl_2$ (2 mM) and incubated at 37°C water bath for at least 90 minutes. Once the plasma solution had congealed, it was centrifuged at 7000 g for 60 minutes at 37°C using a JA10 rotor. The supernatant was then filtered using a 0.22 µm pore Stericup filter (Millipore, SCGPU05RE) and mixed 1:1 with mixing buffer (20 mM Ethylenediaminetetraacetic acid (EDTA), 300 mM NaCl, PBS).

2.1.5. Purification of FI by OX-21 Affinity Chromatography

FI purification was performed using an ÄKTA Start protein purification system (GE). First the system was primed with the elution buffer (0.1 M Glycine, pH 2.7) and the running buffer (10 mM EDTA, 300 mM NaCl, PBS) before the OX-21 column was attached. Prior to loading the supernatant, the column was blank eluted by applying 4 CV of running buffer before 4 CV of elution buffer. This process was repeated until the increase in UV observed was less than 15 mAU. The prepared plasma was then loaded onto the column at 0.5 mL/min overnight at 4°C. Once loading was complete, the column was washed with 5 CV running buffer to remove any unbound protein. The bound FI was then eluted into 1 mL fractions containing 200 µL 1 M Tris (pH 9.0) and 360 µL NaCl (1 M) using 100% elution buffer. Elution buffer was flowed through the column until the UV returned to ~0 mAU, at this point, running buffer was applied to the column until the UV and conductivity stabilised. The column was stored in PBS with 0.02% sodium azide at 4°C.

The purified FI was run on a 10-20% Sodium dodecyl sulphate-polyacrylamide gel electrophoresis (SDS PAGE) gel, either before or after buffer exchange, and imaged using Coomassie staining or Western Blotting to confirm protein identity.

2.1.6. Protein Polishing by Size-Exclusion Chromatography (SEC)

To remove low and high molecular weight impurities from the affinity purified FI, gel filtration was performed using a HiLoad 16/600 Superdex 200 pg size exclusion column (GE Healthcare, 28989335) connected to an ÄKTA prime in a 4°C cabinet. The column was equilibrated overnight in PBS before loading 4 mL FI via a 10 mL Superloop (GE Healthcare, 18-1113-81). The sample was run through the system at 1 mL/min and the flow-through collected into 1 mL fractions. The fractions were then analysed by SDS-PAGE and Western Blot to assess purity. Concentrations were determined using a NanoDrop One^{c} to measure the absorbance at 280 nm. For FI, the molar extinction coefficient was calculated as 125,840 $M^{-1}cm^{-1}$ using the ProtParam tool by ExPASy (Gasteiger *et al.*, 2005), and a percent extinction coefficient (Ɛ) of 1.43 at 280 nm for a 0.1% (1 mg/mL) solution.

$$\text{Concentration (mg/ mL)} = \frac{\text{Absorbance at 280 nm}}{\text{0.1\% Percent solution extinction coefficient}}$$

2.2. Analysis of Purified Proteins by SDS PAGE and Western Blotting

2.2.1. SDS PAGE

In most instances, purified samples were run on Novex WedgeWell™ 10-20% Tris-Glycine Gels (ThermoFisher) under either non-reducing or reducing conditions. Generally, protein samples were diluted in PBS in 0.6 mL Eppendorfs (Corning) to give 1 µg protein per well, and a total volume of 15 µL. 5 µL of 4X LaemmLi Sample Buffer either non-reducing (without β Mercaptoethanol (2ME)) or reducing (with 2ME (355 mM)) was then added to each sample. The prepared protein samples were then boiled for 5 minutes at 95°C and cooled slightly before loading into the individual lanes of a 10-20% gradient gel. To provide an indicator of protein size, 4 µL PageRuler™ Plus Pre-stained Protein Ladder (ThermoFisher) was also loaded onto each gel. Electrophoresis was performed in an XCell SureLockTM Electrophoresis Cell (ThermoFisher) filled with ~800 mL SDS running buffer (3.03 g Tris-base, 14.41 g Glycine, 1 g SDS per 1 L of water) at 200 V for 60 minutes or until the dye-front had run off the bottom of the gel.

2.2.2. Coomassie Staining

Following electrophoresis, gels were washed briefly with H_2O, and incubated at RT with either 1% Coomassie Brilliant Blue™ R-250 (ThermoFisher, diluted in 10% (v/v) acetic acid, 40% (v/v) methanol and 50% (v/v) water) for 60 minutes, or InstantBlue Coomassie Protein

Stain (Sigma) for 15 minutes on a rocker. Depending on the stain used, the gels were then washed in either H_2O for 60 minutes for the InstantBlue or de-stain solution (10% (v/v) acetic acid, 40% (v/v) methanol and 50% (v/v) water) for the Brilliant Blue.

2.2.3. Western Blotting

Proteins were transferred from an SDS PAGE gel to a Protran^{TM} Nitrocellulose Western blotting membrane (Amersham Biosciences, Amersham, UK) by Western Blotting. Gels were transferred at 100 V, 400 mA for 75 minutes in transfer buffer (12 mM Tris base, 96 mM Glycine, pH 8.3, 20% methanol) at 4°C. The membrane was washed three times in PBS with 0.1% Tween 20 (PBS-T) and then blocked for one hour at RT or overnight at 4°C in 5% milk powder (Marvel) in PBS-T. Following blocking, the membrane was incubated in 5% milk powder in PBS-T containing the primary antibody (Table 2-1) for one hour at RT. The membrane was then washed three times in PBS-T, before incubation with the secondary antibody (Table 2-1) in 5% milk powder in PBS-T for one hour at RT. Finally, the membrane was washed three times in PBS-T before the application of the chemiluminescent substrate, Clarity Western enhanced chemiluminescence (ECL) (Bio-Rad, Hercules, California, USA). To image the blot, a LI-COR Fc imaging system (LI-COR Biosciences, Lincoln, Nebraska, USA) was used.

2.2.4. Antibodies Used in Western Blotting

Table 2-1 Antibodies and conditions used for the detection of Factor I and Pro-I by Western Blotting

Protein Target	FI	FI	Pro-I
Size	88 kDa	88 kDa	90 kDa
Reduced or non-reduced	Both	Non-reduced	Reduced
Primary Antibody	Polyclonal Sheep anti-human FI (Ab8843, Abcam)	Monoclonal Mouse anti-human FI (OX-21, in-house)	Polyclonal Sheep anti-human FI (Ab8843, Abcam)
Concentration	1 µg/mL	2 µg/mL	1 µg/mL
Secondary Antibody	Donkey anti-Sheep horseradish peroxidase (HRP) (Ab97125, Abcam)	HRP-conjugated AffiniPure Donkey Anti-mouse IgG Ab (H+L) (Jackson ImmunoResearch)	Donkey anti-Sheep HRP (Ab97125, Abcam)
Concentration	1:3000	1:2000	1:3000

2.3. Production of Recombinant FI in CHO Cells

2.3.1. Polyhistitine Tagged CFI Vector for the Production of FI

The pDEF-*CFI* construct used for mutagenesis and future recombinant protein production was provided by Professor David Kavanagh. The construct consists of a pDR2 EF-1α expression system with an inserted histidine tagged mammalian *CFI* sequence.

2.3.2. Small Scale Extraction of Vector cDNA

From a glycerol stock, *E. coli* possessing the vector were streaked onto Luria Bertani (LB) agar (Fisher scientific, BP9724) plates containing with 50 µg/mL ampicillin and left to grow overnight at 37°C. A single colony was inoculated into 5 mL Miller's LB broth (Merk, L3522) with 100 µg/mL Ampicillin and incubated at 37°C for 16 hours with shaking at 225 RPM.

The bacterial cells were then harvested by centrifugation at 3600 g for 20 minutes at 4°C. To extract the DNA, a Qiagen QIAprep Spin Miniprep kit (Qiagen Inc., Hilden, Germany) was used according to the manufacturer's instructions. Briefly, the bacterial pellet was first resuspended in 250 µL of Buffer P1 containing 100 µg/mL RNase A. The resuspended contents were transferred to a microcentrifuge tube before the addition of 250 µL Buffer P2 and were mixed by inverting six times. 350 µL of Buffer N3 was then added to stop lysis, and the suspension centrifuged for ten minutes at 17,900 g. The supernatant was then applied to a QIAprep spin column before centrifugation at 21,000 g for 60 seconds. The spin column was washed with 500 µL Buffer PB and 750 µL Buffer PE with a 60 second centrifugation step after each wash. Finally, the DNA was eluted by the addition of 50 µL dH_2O, incubation for one minute, and centrifugation for one minute.

The purified plasmid DNA was then quantified using a NanoDrop One^c and stored at -20°C prior to sequencing.

2.3.3. Determining Plasmid DNA Concentration

To calculate the DNA concentration of a sample, a NanoDrop One^c was used to measure the absorbance at 260 nm. Using the Beer-Lambert law, and the mass extinction coefficient for dsDNA (50 ng-cm/µL), the concentration of DNA within a sample was then calculated. The absorbance at 280 nm was also measured to provide an 260/280 ratio. The 260/280 ratio is used as an indicator for sample purity, with a ratio of ~1.8 being accepted as pure for DNA, due to the absence of residual phenol, guanidine or other reagents used within the extraction process.

2.3.4. Site Directed Mutagenesis for Introduction of Stop Codon

1 µL of pDEF-*CFI* DNA (50 ng/µL) was added to a reaction mixture of 1.25 µL 10 pmol forward and reverse mutagenesis primer, 5 µL 10x reaction buffer, 1 µL dNTP mix and made up to 49 µL with dH_2O. Lastly, 1 µL *PfuUltra* HF DNA polymerase (2.5 U/µL) before the reaction mixture was placed into a Bio-Rad Thermal Cycler T100. The polymerase chain reaction (PCR) was programmed to run for 30 seconds at 95°C, and then the following for 16 cycles: 30 seconds at 94°C, one minute at 55°C and seven minutes at 68°C. To finish, the reaction was held at 4°C. Amplification products were then checked on a 1% agarose gel. Following temperature cycling, the generated PCR product was treated with 1 µL of *Dpn* I restriction enzyme (R0176, New England BioLabs) and incubated at 37°C for one hour to digest the parental DNA.

2.3.5. Agarose Gel Electrophoresis

A 1% agarose gel was prepared with 50 mL 1X TAE (40 mM Tris, 20 mM Acetic acid, 1 mM EDTA), 0.5 g UltraPure™ Agarose (Invitrogen, 16500500) and 2 µL Ethidium Bromide (Sigma-Aldrich, E1510). DNA was diluted to a concentration of 10 ng/µL. 5 µL of DNA was then added to 1 µL of blue/orange 6X loading dye (Promega, G1881) and loaded onto the agarose gel along with 6 µL HyperLadder 1Kb (Bioline, BIO33053). Gels were run in 1X TAE at 100 V for one hour using PowerPac Basics (Bio-Rad. 300 V, 400 mA). DNA bands were then visualised using a LI-COR Fc imaging system (LI-COR Biosciences, Lincoln, Nebraska, USA).

2.3.6. Transformation of the Modified CFI Vector into E. coli

Transformations were performed using a QuikChange II Site-Directed Mutagenesis Kit (Agilent, 200523). 1 µL of the *Dpn* I-treated pDEF-*CFI* DNA (5 and 50 ng/µL) was added to 50 µL of thawed XL1-Blue Supercompetent Cells (Agilent, 200236) and incubated on ice for 30 minutes. The mixture was then heat-shocked for 45 seconds at 42°C before incubating on ice for two minutes. 500 µL of SOC media (Sigma-Aldrich, S1797) (prewarmed to 37°C) was then added to the competent cells, and the mixture incubated in a shaking incubator at 37°C, 225 RPM for one hour. Either 450 µL or 50 µL of transformed cells were then inoculated into LB agar plates containing 50 µg/mL Ampicillin. After 16 hours growth at 37°C, successfully transformed clones were selected for miniprep and sequencing by inoculating into 5 mL Miller's LB broth with 100 µg/mL Ampicillin.

2.3.7. Sanger Sequencing

20 µL of plasmid DNA (80-100 ng/µL) and 20 µL of sequencing primers (10 pmol/µL) (forward and reverse) were sent to GATC Biotech for sequencing. Sequencing data was reviewed using Sequencher (Gene Codes Corporation, Version 5.0).

2.3.8. Cryopreservation of Modified Clones (Glycerol Stocks)

Single clones or 50 µL overnight LB cultures were inoculated into 5 mL Miller's LB broth containing 100 µg/mL Ampicillin and were incubated 37°C for 16 hours whilst shaking at 225 RPM. The bacterial cells were harvested by centrifugation at 3600 g for 20 minutes. The pellet was resuspended by vortexing and the cells preserved in 15% glycerol by mixing 500 µL of the concentrated cell culture with 500 µL of 30% glycerol in dH_2O. Transformed colonies were then stored in liquid nitrogen.

2.3.9. Large Scale Extraction of CFI Vector cDNA

Clones containing the correctly mutated pDEF-*CFI* DNA were picked and cultured in 5 mL Miller's LB broth containing 100 µg/mL Ampicillin for eight hours at 37°C with vigorous shaking. 200 µL of the initial culture was then added to 100 mL Miller's LB broth containing 100 µg/mL Ampicillin for 16 hours. Cultures were incubated at 37°C with shaking at 225 RPM. Cells were pelleted by centrifugation at 3600 g for 20 minutes at 4°C. The resulting supernatant was discarded, and the plasmid DNA extracted from the cell pellet using a QIAprep Spin Maxiprep Kit (Qiagen). First, the cells were resuspended in 10 mL Buffer P1 containing 100 µg/mL RNase A by vortexing. To this, 10 mL of Buffer P2 was then added and inverted six times, before incubating at RT for 5 minutes to lyse the cells. 10 mL of chilled Buffer P3 was then added and incubated on ice for 20 minutes before the lysate was transferred to a QIAfilter Cartridge and incubated for 10 minutes. The lysate was then filtered through the QIAfilter Cartridge and collected in a QIAGEN-tip equilibrated with 10mL of Buffer QBT. The QIAGEN-tip was then washed with 2 x 30 mL of Buffer QC. The DNA was then eluted with 15 mL Buffer QF and collected. To precipitate the DNA, 10.5 mL of isopropanol was added to the eluted DNA, and immediately mixed and centrifuged at 3600 g for one hour at 4°C. The supernatant was decanted, and the DNA pellet washed in 5 mL 70% ethanol before centrifugation at 3600 g for 20 minutes. The ethanol was then decanted and the DNA pellet air dried prior to resuspension in 500 µL of dH_2O. The purified plasmid DNA was then quantified using a NanoDrop One[c]. Sanger sequencing was performed to confirm fidelity before storage at -20°C.

2.3.10. Transfection of pDEF-CFI Vector into CHO Cell Cultures

Chinese hamster ovarian (CHO) cells (ThermoFisher) were defrosted at 37°C for 1 minute and added to 10 mL prewarmed CHO cell media (Dulbecco's Modified Eagle Medium (DMEM) F12 (Lonza) supplemented with 10% FBS, 1% Penicillin-Streptomycin-Glutamine (100X) (ThermoFisher)). The cells were washed twice in CHO media by centrifugation at 200 g for 5 minutes. Cells were then counted and seeded at a density of $5x10^5$ cells per mL in a T25 ($25cm^2$) cell culture flask (Grenier), in 5 mL of media. The cells were incubated at 37°C with 5% CO_2 until 80% confluent. To passage the cells, the supernatant was decanted, and the cells washed twice with Dulbecco's phosphate-buffered saline (DPBS) (Lonza) before the addition of 2 mL 1X Trypsin (ThermoFisher) diluted in DPBS. Once the trypsin was added, the cells were incubated for 5 minutes at 37°C until the cells detached. The cells were then resuspended in CHO media and pelleted by centrifugation at 300 g for 5 minutes. The supernatant was decanted, and the pellet resuspended in 5 mL CHO media before counting using a haemocytometer. The cells were then seeded at 100,000 cells per well in a 12-well plate (Corning, CELLSTAR™ Flat Bottom Cell Culture Plates), in 2 mL of CHO media, 24 hours prior to transfection.

Once the cells had reached 50-70% confluency, 2 µg, 4 µg or 0 µg of wild-type pDEF-*CFI* DNA was mixed with 4 µL, 8 µL or 4 µL JetPEI reagent, respectively, in a total volume of 100 µL 150 mM NaCl solution. The DNA mixture was then incubated at RT for 30 minutes before being added dropwise to the cells, with each DNA concentration performed in duplicated. The 0 µg DNA wells were used to provide a negative control. Following transfection, the plates were incubated at 37°C for 72 hours, with a media change after three hours to remove the toxic JetPEI.

After 72 hours incubation, supernatant was collected and a dot blot or a FI enzyme-linked immunosorbent assay (ELISA) performed to ensure successful transfection had occurred. At this stage, the cells were then incubated in selection media, containing either 600 or 800 µg/mL Hygromycin B (ForMedium™, Hunstanton, UK). The selection media was changed every 72 hours until the cells in the negative control wells had died, and the transfected wells had reached confluency. Once confluent, the supernatant was collected and a FI ELISA was performed to determine FI expression.

2.3.11. FI ELISA for Screening of Recombinant FI Expression

96 well-plates (Maxisorp, ThermoFisher) were coated with 2 mg/mL of the polyclonal antibody sheep anti-human FI (ab8843, Abcam) in a coat buffer (16% 0.2 M Sodium Carbonate, 35% 0.2 M Sodium Bicarbonate in H_2O, pH 9.6) and incubated overnight at 4°C. The plates were then washed three times using a Wellwash Microplate Washer (Thermo Fisher Scientific, 5165040) with PBS-T (0.1% Tween 20) before the addition of 150 µL blocking buffer solution (1% bovine serum albumin (BSA) (Sigma, A7906) in PBS-T) to each well. The plates were then incubated in blocking buffer at RT for one hour, before another three washes with PBS-T. 50 µL of both sample and standard were added to the plate in triplicate. The FI standard (A138, CompTech) was serially diluted 1 in 2 across the plate from 1 mg/mL in CHO media. Sample supernatant was either added neat or diluted 1 in 2 in CHO media. The plates were then incubated for one hour at RT before an additional three washes in PBS-T. Next, 50 µL of the monoclonal antibody OX-21 (1 µg/mL in blocking buffer) was added to the wells and incubated for one hour at RT, before washing three times in PBS-T. 50 µL per well of the tertiary antibody HRP-conjugated donkey anti-mouse secondary Ab (715-035-150JIR, Stratech) (1 in 2000 in blocking buffer) was added and the plate incubated for 30 minutes at RT. A final wash (3x PBS-T) was performed before the addition of 100 µL tetramethylbenzidine (TMB) solution to each well. The plate was incubated on a plate shaker at room temperature for 5-15 minutes before quenching the reaction using 100 µL 1 M sulphuric acid. The absorbance 450 nm was immediately measured using a Labtech LT-4500 MTP Microplate reader (Tecan). To determine the concentration of FI within a sample, the concentration was interpolated from the standard curve using GraphPad Prism 9.4.1. The standard curve was generated using the four-parameter logistic regression model to produce a log(concentration)-response curve.

2.3.12. Cryopreservation of Mammalian Cells

If FI was present in the collected supernatant, the best expressing wells were scaled up to T25 then T75 (75 cm^2) flasks, passaging with 1% trypsin. To prepare the cells for cryopreservation, trypsin was used to remove the adherent cells from the flask before centrifugation at 300 g for 5 minutes. The cells were then resuspended in 1 mL CHO media containing 10% Dimethyl sulfoxide (DMSO) and transferred into Nalgene™ General Long-Term Storage Cryogenic Tubes (ThermoFisher) and frozen at -80°C for 24 hours using a Mr.

Frosty™ freezing container. The cells were then transferred to liquid nitrogen for long term storage.

2.3.13. FI Production Using CHO

Cells were continuously scaled up, using 1% trypsin to remove adhered cells, from T25, to T75 and finally T175 (175 cm^2) flasks, with splitting in fresh selection media at least once per week. Once the cells were steadily growing, the cell pellets from two T175 flasks was utilised to inoculate a 1.5 L roller bottle containing 200 mL CHO selection media (600 µg/mL hygromycin). Roller bottles were left to equilibrate for a minimum of 4 hours by incubating 37°C and 5% CO_2 with loosened lids. After equilibration, the bottles were transferred to an electronic roller shelf left gently rolling (1 RPM) for 10 days at 37°C. After 10 days, the spent media was collected and an addition 200 mL of fresh media was added to each flask, before further incubation at 37°C for 4 days. All supernatants were collected and stored at -80°C before FI purification.

2.3.14. Furin Supplementation for Full Processing of FI

Prior to Furin cleavage, recombinant CHO FI was buffer exchanged into 1X cleavage buffer (100 mM 4-(2-hydroxyethyl)-1-piperazineethanesulfonic acid (HEPES), pH 5.2, 0.5% Triton X-100, and 1 mM $CaCl_2$) using a PD-10 desalting column (GE Healthcare). 31.2 µL of buffer exchanged FI and mixed with either 2 µL Furin (R&D Systems) or 2 µL PBS and made up to a final volume of 50 µL with 1X cleavage buffer. The cleavage reaction mixture was then incubated at 37°C for 16 hours, and the resulting products ran on SDS PAGE and assessed by Western Blotting. The reaction mixture containing FI only was used as a negative control.

2.4. Mouse Monoclonal Antibody Production

2.4.1. Mouse Immunisation

Generation of a mouse monoclonal antibody against the RRKR linker was carried out under the animal project licence number PD86B3678. As a brief overview of the process, mice were immunised with either a Keyhole limpet hemocyanin (KLH) conjugated RRKR peptide or recombinant FI according to a schedule. Antibody titres were monitored by ELISA using tail bleeds before harvesting the spleens. The splenocytes were then fused with mouse myeloma (Sp2/0) cells and grown in selective media. A combination of RRKR peptide and recombinant FI was used to screen for antibody producing hybridomas. Expressing cells were diluted until monoclonality and stable monoclonal hybridomas were then scaled up to spinner flasks before the supernatant was harvested for antibody purification.

2.4.2. Immunisation RKRR Peptide

To produce monoclonal antibodies specific to the RRKR region of Pro-I, mice were immunised with the custom peptides KLH-GVKNRMHIRRKRIVGGKRAQ and GVKNRMHIRRKRIVGGKRAQ-KLH (ThermoScientific). These peptides share 60% sequence homology with the mouse *CFI* protein within the covered region (Appendix 1), and through conjugation to KLH they can be used to elicit an immune response. Mice were immunised with the peptides according to the licensed study plan 379. For the peptide-based immunisation, the following schedule was utilised for 4 C57Bl/6 mice (Table 2-2).

Table 2-2 Mouse immunisation schedule using RRKR peptide.

Day	Activity
0	Tail bleed (50 µL) + immunisation in the flank with 0.1 mg of RRKR peptide antigen in Complete Freund's Adjuvant (Sigma, F5881) via subcutaneous (SC) route; 2 sites = 50 µL each
14	Immunisation in the flank with 0.1 mg of RRKR peptide antigen in Incomplete Freund's Adjuvant (IFA) (Sigma, F5506) via SC route; 2 sites = 50 µL each
28	Tail bleed (50 µl) + 0.1 mg of RRKR peptide antigen in IFA via SC route; 2 sites = 50 µL each
42	Tail bleed (50 µL) + 0.1 mg of RRKR peptide antigen in IFA, SC as above
70	Boost with 0.1 mg of RRKR peptide antigen in 200 µL saline intraperitoneal (IP)
72	Boost with 0.1 mg of RRKR peptide antigen in 100 µL of saline intravenous (IV)
74	Terminal exsanguination and collection of spleen for fusion

2.4.3. Immunisation RKRR Peptide and CHO FI

To facilitate the generation of a monoclonal antibody against Pro-I, a combination of both the RRKR peptides and recombinant CHO produced FI were utilised. Purified CHO FI consists of a mixture of mature FI and Pro-I, with both species present in a ratio of 60:40, respectively. Four C57bl/6 - Wild type by genotype, C3D1115N heterozygous mice were used for this study (590), following the immunisation schedule outlined below (Table 2-3).

Table 2-3 Mouse immunisation schedule using RRKR peptide and recombinant (CHO) FI.

Day	Activity
-2	Tail bleed (50 µL)
0	Tail bleed (50 µL) + immunisation in the flank with 0.1 mg of a mixture of RRKR peptide and recombinant CHO FI in Complete Freund's Adjuvant (Sigma, F5881) via SC route; 2 sites = 50 µl each
14	Immunisation in the flank with 0.1 mg of a mixture of RRKR peptide and recombinant CHO FI in Incomplete Freund's Adjuvant (IFA) (Sigma, F5506) via SC route; 2 sites = 50 µL each
28	Tail bleed (50 µL) + 0.1 mg of recombinant CHO FI in Incomplete Freunds Adjuvant (IFA) via SC route; 2 sites = 50 µLeach
42	Tail bleed (50 µL) + 0.1 mg of recombinant CHO FI in IFA, SC as above
70	Boost with 0.1 mg of a mixture of RRKR peptide and recombinant CHO FI in 200 µL saline intraperitoneal (IP)
72	Boost with 0.1 mg of a mixture of RRKR peptide and recombinant CHO FI in 100 µL of saline intravenous (IV)
74	Terminal exsanguination and collection of spleen for fusion

2.4.4. ELISA for Tracking Antibody Titre in Tail Bleeds

Medisorp ELISA plates (Thermo Fisher Scientific, 467320) were coated with 50 µL per well of 1 µg/mL RRKR peptide (unconjugated to KLH) in coat buffer (0.2 M Sodium Carbonate, 0.2 M Sodium Bicarbonate) and incubated overnight at 4°C. Plates were washed three times using a Wellwash Microplate Washer (Thermo Fisher Scientific, 5165040) with PBS-T (0.1% Tween 20) and blocked for one hour with 200 µL per well with 1% BSA in PBS-T at RT. In triplicate, serum samples were diluted 1 in 200 and 1 in 2000 in 1% BSA-PBS-T. Again, the plates were washed three times, before 50 µL of sample was added to wells in triplicate. The plates were incubated for one hour at RT and washed three times before the addition of 50 µL of detection antibody (HRP-conjugated AffiniPure Donkey Anti-mouse IgG Ab (H+L) (Jackson ImmunoResearch)) diluted 1 in2000 in PBS-T. The plate was then incubated at RT for one hour before another three washes. 100 µL per well of TMB (Leinco Technologies, T118) was applied to the plate, and incubated on a shaker for 10 minutes. 10% sulphuric acid was added 100 µL per well to stop the reaction. The absorbance at 450 nm was measured with a reference of 660 nm by a LT-4500 Microplate Absorbance Reader (Labtech). For analysis, the background was subtracted using the results from the 1% BSA-PBS-T only wells. The replicates were then averaged, and the pre-immunisation result subtracted from the subsequent tail bleed results.

2.4.5. Macrophage Preparation

A wild-type C57Bl/6 mouse was euthanised by cervical dislocation and macrophage cells were collected by lavage of the peritoneal cavity with 10 mL of B cell media (500 mL RPMI 1640, 10% Ultra Low IgG FBS, 5 mL L-Glutamine, 5 mL Kanamycin, 5 mL MEM Non-essential amino acids, 5 mL Sodium Pyruvate and 2.5 mL 2ME. Cells were pelleted by centrifuging at 300 g for 5 minutes at 4°C and then washed twice in un-supplemented RPMI 1640. The cell pellet was then re-suspended in 100 mL RPMI 1640 (Sigma) supplemented with 15% FBS (Labtech, FBS-SA), 1% Penicillin-Streptomycin (Sigma, G1146), 50 µM 2ME and 1:50 hypoxanthine aminopterin thymidine (HAT) (Gibco, 21060-017). The cell suspension was then plated out according to need and plates incubated at 37°C, in 5% CO_2.

2.4.6. Cell Counting

An Improved Neubauer 1 in 400 square mm haemocytometer (Weber Scientific, 3048- 11) was prepared with a coverslip. The cells to be counted were harvested. 10 µL of the cell suspension was mixed with 40 µL of trypan blue by pipetting up and down. 10 µL of the mix was pipetted into the top or bottom chamber. The haemocytometer was placed under a light microscope. Dead cells were stained blue. The live cells were counted in the four outer quadrants of the grid, and the average was taken. The average is then multiplied by five to account for the dilution factor, and then by 10000 to obtain the number of cells per mL.

2.4.7. Splenocyte Harvest and Sp2/0 Fusion

The day before the spleens were due to be harvested, cultured Sp2/0-Ag14 (ECACC, 85072401) murine myeloma cells were split to ensure they would be in the log phase of cell growth. Peritoneal macrophages were also collected from two mice per mouse spleen to be harvested and prepared as above (section 2.4.5). The macrophages were plated out at 100 µL per well in ten flat bottom 96-well plates for each fusion. These were incubated overnight at 37°C with 5% CO_2.

The immunised mice were euthanised by cervical dislocation and doused in 70% ethanol. The spleens were harvested, removing all connective tissue and fat, and put into 5 mL sterile PBS on ice. In sterile conditions, extract splenocytes by crushing the spleens between two sterilised and air-dried glass slides. The pulp was then passed through subsequently smaller gauged needles (19G to 22G to 25G) by syringe to create a single cell suspension in ice cold RPMI. The suspension was left to settle for five minutes. The upper portion of the suspension, containing the splenocyte, was transferred to a fresh container.

Splenocytes and Sp2/0-Ag14 were washed separately three times in ice-cold un-supplemented RPMI 1640, by centrifuging at 400 g for 5 min at 4°C; vigorously resuspending the pellet between each wash. After the final wash, the pellets of the splenocytes and the Sp2/0-Ag14 were combined in a ratio of 2:1 and resuspended in warm un-supplemented RPMI 1640. The suspension was then transferred to a 50 mL falcon tube, and centrifuged at 400 g for five minutes, before decanting the supernatant. The cell pellet was gently broken up by flicking and whilst agitating the tube, add 1.5 mL pre-warmed polyethylene glycol (PEG) 1500 (Roche, 10783641001) dropwise over one minute. The suspension was then incubated for 30 seconds before the dropwise addition of 20 mL warm un-supplemented RPMI 1640 whilst agitating and rotating the tube. An additional 30 mL of warm RPMI was added before centrifugation at 300 g for five minutes. The supernatant was then discarded, and the pellet gently resuspended in 100 mL RPMI 1640 supplemented with 15% FBS (Labtech, FBS-SA), 1% Penicillin-Streptomycin (Sigma, G1146), 1% MEM Non-essential amino acids, 50 µM 2ME and 1:50 HAT (Gibco, 21060-017).

100 µL was plated out into each well of the ten prepared plates containing macrophages. Plates were incubated at 37°C, CO_2 5%. After seven days 100 µL of fresh supplemented RPMI 1640 was added to each well.

2.4.8. ELISA for Screening of Antibody Producing Hybridomas

Medisorp ELISA plates (Thermo Fisher Scientific, 467320) were coated with 50 µL per well of either 1 µg/mL RRKR peptide (unconjugated to KLH) or 1 µg/mL recombinant CHO produced FI in carbonate coat buffer. The plates were incubated overnight at 4°C. Plates were washed three times using a Wellwash Microplate Washer with 0.1% PBS-T and blocked for one hour with 200 µL per well 1%BSA in PBS-T at RT. Plates were washed three times and incubated at RT for one hour with 50 µL of supernatant from each fusion well. Two wells contained media only to provide a background control. Plates were washed three times, and incubated for one hour at RT with 50 µL HRP-conjugated AffiniPure Donkey Anti-mouse IgG Ab (H+L) diluted 1 in 2000 in PBS-T. The plates were washed three times and incubated for ten minutes at RT with 50 µL per well of TMB. To stop the reaction 50 µL per well of 10%

sulphuric acid was added. The absorbance at 450 nm was measured with a reference 660 nm by a LT-4500 Microplate Absorbance Reader. Following background subtraction, positive hybridoma cells were identified and taken forward.

2.4.9. Hybridoma Limiting Dilution

The day before diluting out hybridomas, macrophage coated plates were prepared as before (section 2.4.5). Two flat-bottom 96-well plates were coated with 100 µL macrophage suspension in each well, per hybridoma well to be diluted. The cells from the wells which produced a positive response on the ELISA (section 2.4.8) were resuspended in 200 µL of supplemented RPMI 1640 containing 15% FBS, 1% Penicillin-Streptomycin, 1% MEM Non-essential amino acids, 50 µM 2ME and 1:50 HAT, and counted using a haemocytometer. Cells were then resuspended at 100 cells per 100 µL. 200 µL of the cell suspension was then pipetted into wells of columns 1-3 and serial dilutions were performed across two plates, to achieve a dilution of approximately one cell per well. Plates were incubated at 37°C with 5% CO_2 for ten days until colonies in the section with one cell per well or less were visible. These colonies were then screened again as per section 2.4.8 and the process of dilution repeated until all hybridoma colonies expressed positive results, indicating monoclonality.

2.4.10. Clonal Expansion of Expressing Hybridomas

Once a monoclonal hybridoma was identified, it was transferred to a 24-well plate pre-coated with macrophages in supplemented RPMI 1640 containing 15% FBS, 1% Penicillin-Streptomycin, 1% MEM Non-essential amino acids, 50 µM 2ME and 1:50 HAT for seven days. Once confluent, the hybridoma was then transferred to a T25 flask and incubated at 37°C with 5% CO_2 for a further week. At this point, the media was exchanged for media supplemented with HT 1 in 50 (hypoxanthine thymidine) (Gibco, 41065-012), and incubated for one week. Then hybridomas were transferred into media without HT for a week. Finally, the 15% FBS was substituted for 10% low IgG FBS and the cells grown for 1 week. Once established in low IgG FBS, the hybridomas were scaled up into a T75 and then a T175 flask. The final step was to transfer hybridomas into a magnetic spinner flask containing 500 mL 10% low IgG FBS B cell media and to incubate at 37°C with 5% CO_2 for ten days before harvesting. Collected supernatant was then stored at -80°C.

2.4.11. Determination of antibody isotype

An IsoStrip™ Mouse Monoclonal Antibody Isotyping Kit (Roche, 11493027001) was used according to the Manufacturer's instructions. The supernatant was first diluted 1 in 10 in 1%

BSA PBS, and 150 µL was pipetted into the development tube. The solution was incubated at RT for 30 seconds before agitation to resuspend the blue powder. An isotyping strip was placed into the tube and left to develop for 5-10 minutes. The blue bands observed indicate the antibody isotype and the class of light chain.

2.4.12. Antibody Purification

Once the antibody isotype was determined as outlined in section 2.4.11, the collected supernatant was prepared for purification. Supernatant was first defrosted in a water bath at 37°C, prior to centrifugation at 3600 g for 20 minutes, and filtered using a 0.22 µm pore Stericup filter (Millipore, SCGPU05RE).

2.4.13. Protein G

To purify IgG antibodies, a 5 mL Protein G column (GE Healthcare, 17040501) was used. The column was attached to an ÄKTA Start protein purification system and washed with 4 CV of 0.2 M PBS pH 7.2 to prepare for sample loading. 500 mL of prepared supernatant was then loaded onto the column at 0.5 mL/min overnight at 4°C. The column was then washed with 4 CV of 0.2 M sodium phosphate pH 7.2, prior to elution with 0.1 M glycine pH 2.7. 1 mL fractions were collected and 200 µL 1 M Tris pH 9 was added to neutralise the pH of eluted solution.

2.4.14. Protein L

To purify antibodies with kappa light chains, a 1 mL Protein L column (GE Healthcare, GE29-0486-65) was used. Prior to loading, the column was washed with 4 CV of 0.2 M PBS. 500 mL of antibody containing supernatant was then loaded onto the column at 0.5 mL/min overnight at 4°C. The following day, 4 CV of 0.2 M sodium phosphate pH 7.2 was flowed over the column before elution with 0.1 M glycine pH 2.7. 1 mL fractions were collected and 200 µL 1 M Tris pH 9 was added to neutralise the pH of eluted solution.

2.4.15. Antibody Assessment by Western Blotting

Assessment of the purified antibodies was achieved using Western Blotting as outlined in section 2.2.3. The generated antibodies were used to detect the presence of serum purified FI, recombinant CHO purified FI and later, recombinant and serum purified Pro-I, under both reducing and non-reducing conditions. Either 1 µg/mL of purified antibody or neat supernatant was used for protein detection, depending on the success of the purification.

The antibodies were then detected using HRP-conjugated AffiniPure Donkey Anti-Mouse IgG Ab (H+L) (Jackson ImmunoResearch) at 1 in 1000 dilution in PBS-T with 5% milk powder.

2.5. Production of Pro-I

2.5.1. Transient transfection of pDEF-CFI Vector in the Presence of a Chloromethyl Ketone Furin Convertase Inhibitor

To generate Pro-I, HEK293T cells were transfected with the pDEF-*CFI* vector following a variation of the protocol outlined in 2.3.10 in the presence of 75 µM Furin convertase inhibitor (chloromethylketone) (ALX-260-022-M001, Enzo Lifesciences). Briefly, prior to transfection HEK293T cells were seeded at 500,000 cells per well in a T25 cell culture flask, in 5 mL of HEK cell media (DMEM containing 10% FBS, 1% L-Glutamine, 1% Penicillin-Streptomycin) and grown until approximately 80% confluent at 37°C with 5% CO_2. On the day of transfection, the media was replaced four hours before the addition of the transfection reagents. JetPEI was used at a ratio of 1:2 (DNA:PEI), where 5 µg of pDEF-*CFI* plasmid DNA was incubated with 10 µL jetPEI reagent for 20 minutes at RT. Following the addition of the transfection mixture, 75 µM Furin convertase inhibitor was added to the cells.

On the following day, the media containing the inhibitor was replenished, and the cells were incubated for a further two days prior to harvest of the supernatant. The supernatant was centrifuged at 3600 g for 20 minutes to remove cells debris and stored at -80°C before purification.

2.5.2. Purification of Recombinant Pro-I by OX-21 Affinity Chromatography

Pro-I purification was performed by affinity chromatography with an OX-21 column, using an ÄKTA Start protein purification system (GE Healthcare, 29022094-ECOMINSSW) as outlined in section 2.1.5. First, the system was primed with running buffer PBS before attaching the OX-21 column. The supernatant was loaded onto the column, and any unbound protein removed using running buffer. The bound FI was then eluted with 0.1 M Glycine (pH 2.7) into 1 mL fractions. 1 M Tris-base (pH 9.0) was added to neutralise the pH, before buffer exchange into PBS using a PD-10 desalting column (GE Healthcare, 17085101). An anti-FI ELISA (section 2.3.11) was performed to ensure complete removal of Pro-I from the supernatant. The purified Pro-I protein was assessed by SDS PAGE stained with Coomassie and by Western Blotting (section 2.2.3), under both reducing and non-reducing conditions.

2.5.3. Purification of Pro-I by Ion-Exchange Chromatography

Due to the difference in isoelectric point between Pro-I and Factor I, 7.38 and 6.49 respectively, separation of the two species was attempted by ion-exchange chromatography. Before separation could be achieved, the purified FI (serum or recombinant) was collated and transferred to 3.5 kDa dialysis tubing (Thermo Scientific, 10005743), before dialysing overnight at 4°C with constant stirring. The protein was dialysed from PBS into either 20 mM Tris-HCL, pH 7 for Mono Q, or 50 mM Sodium phosphate monobasic, pH 6 for Mono S ion exchange chromatography. In each instance, a volume of dialysis buffer which was at least 200-fold greater than the sample volume was used. Following dialysis, the pH of the sample was checked to ensure that samples had been successfully exchanged into the appropriate buffer.

2.5.4. Mono Q

First the column (Mono Q 5/50 GL column (Sigma-Aldrich, GE17-5166-01)) was equilibrated with 5CV of the dialysis buffer (20 mM Tris-HCL, (Sigma-Aldrich, T1503) pH 7), before injecting 5.5 mL sample using a 10 mL Superloop. Once the sample was injected, the column was washed with 2 CV of buffer before eluting using a linear salt gradient. The percentage of the 1 M NaCl elution buffer was increased from 0-40%, for a duration of 35 CV. The eluted proteins were collected in a 96 deep well plate, and the resulting fractions run on SDS PAGE and stained with Coomassie Blue (section 2.2.2).

2.5.5. Mono S

Prior to loading the dialysed FI onto a Mono S 5/50 GL column (Sigma-Aldrich, GE17-5168-01), the column was first equilibrated with 5 CV of the dialysis buffer (50 mM Sodium phosphate monobasic, pH 6), before injection of the sample using a 10 mL Superloop. Once the sample was injected, the column was washed with 2 CV of buffer before eluting using a linear salt gradient. The percentage of the 1 M NaCl elution buffer was increased from 0-40%, for a duration of 35 CV. The eluted proteins were collected in a 96 deep well plate, and the resulting fractions run on SDS PAGE and stained with Coomassie Blue (section 2.2.2). The fractions attributed to each UV peak were collated and buffer exchanged into PBS using a PD-10 desalting column (Cytiva, 17085101) before freezing.

2.5.6. Pro-I Identification Using Mass Spectrometry

To confirm the identity of the purified Pro-I, the samples were sent to the BSRC Mass Spectrometry Facility at the University of St Andrews, where they were analysed on liquid chromatography (LC) tandem mass spectrometry (MS) (LC-MS/MS) following GluC and LysN digest by Dr Sally Shirran. The results were interpreted using the Mascot Server (www.matrixscience.com).

2.5.7. Cofactor Assay in the Fluid Phase for Pro-I

To determine the role that Pro-I may play as a serine protease enzyme within the AP regulatory TMC, its ability to break down C3b into iC3b was compared to that of WT FI in a fluid phase cofactor assay. Successful break down of C3b by FI is shown by the cleavage of C3b at Arg1303-04Ser (generating α2 46 kDa and α1 68 kDa) and Arg1320-21Ser (generating α2 43 kDa and releasing C3f).

To do this, 7.5 µL of either Pro-I or FI, at 10 ng/µL, was added to 1 µL of C3b (CompTech, A138, 1 µg/µL), and 2.5 µL of 200 ng/µL FH1-4 (in-house, Pichia recombinant). Each reaction mixture was made up to a total of 15 µL with PBS and incubated for 60 minutes at 37°C. After this time, 5 µL of 4X reducing sample buffer was added immediately to each test and control. The products were then visualised on a 10-20% SDS-PAGE gel using standard reducing conditions and Coomassie staining. Gel images were imported to ImageStudio Lite (Licor), and densitometry was performed before the data was imported to GraphPad Prism 9.4.1 for statistical analysis.

This was also repeated at time intervals of 5, 15, 30, 45, 60 and 90 minutes using FH as a cofactor. The reaction at each specified interval was quenched by the addition of Lamelli reducing buffer.

2.6. Custom Recombinant Monoclonal Antibody Generation

2.6.1. Human Combinatorial Antibody Libraries (HuCAL)

As an alternative approach for the generation of an antibody against Pro-I, Bio-Rad's custom recombinant monoclonal antibody generation service was used. This service centres around the HuCAL PLATINUM phage library and CysDisplay technologies to facilitate *in vitro* generation of highly specific antibodies. The HuCAL PLATINUM approach combines a 45 billion Fab format antibody library with the use of filamentous phage to provide an efficient display method for selecting high affinity binders. The HuCAL antibody generation process is outlined in Figure 2-1.

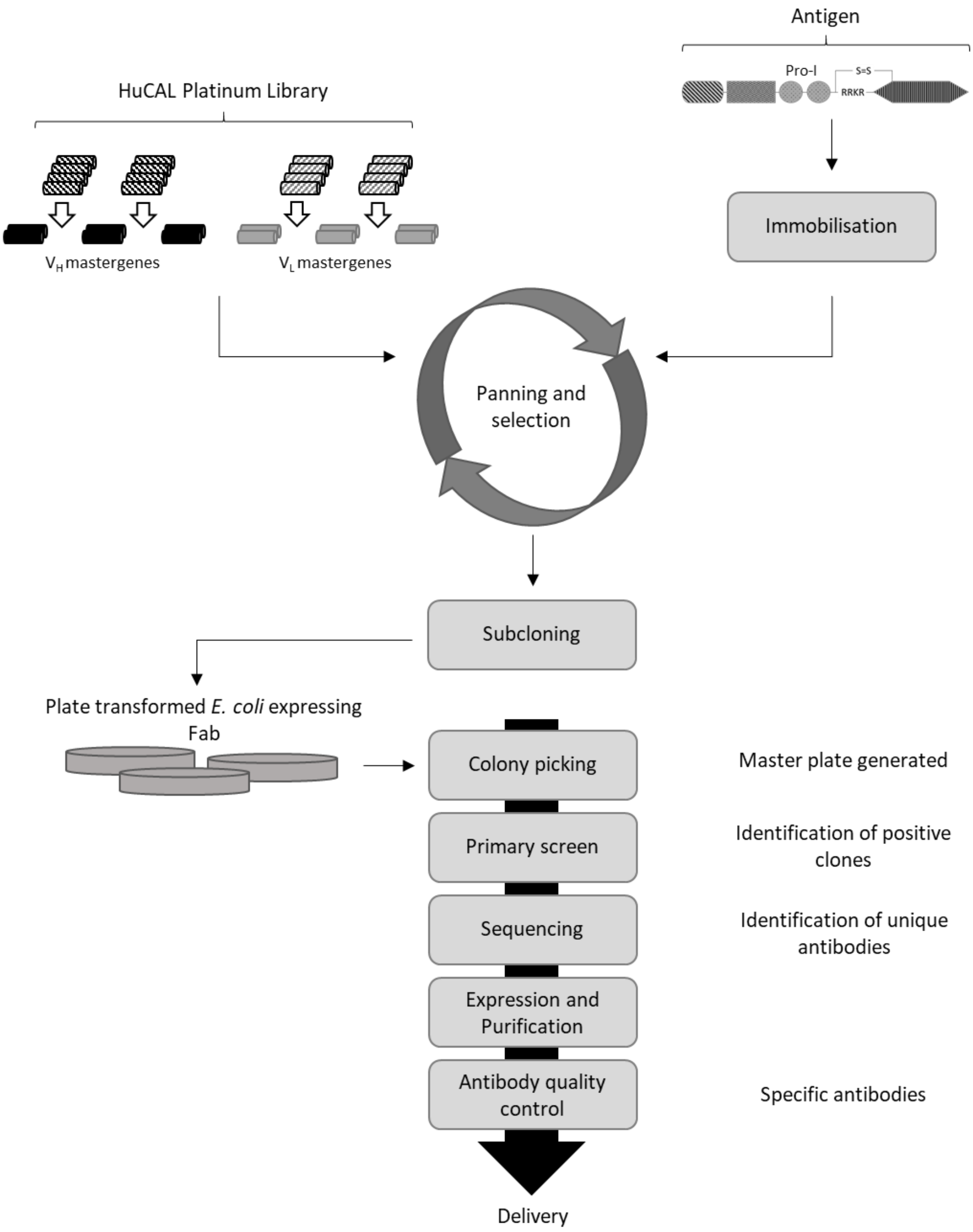

Figure 2-1 Summary of custom antibody generation process using HuCAL (Adapted from Bio-Rad https://www.bio-rad-antibodies.com/hucal-antibody-process-overview.htmL).

The antigen is supplied by the customer and adsorbed to polystyrene ELISA microtiter plates. The HuCAL library presented on phage is incubated with the immobilized antigen. Non-specific antibodies are removed by extensive washing and specific antibody phages are eluted by adding a reducing agent. Three rounds of panning are used with guided selection that can be employed to select highly specific antibodies from the library. After panning the phagemid DNA encoding the enriched antibody population is isolated as a pool and subcloned into a Fab expression vector. Colonies are picked and grown in a 384-well microtiter plate. Antibody expression is induced, and the culture is harvested and lysed to release the antibody molecules. Culture lysates are screened for specific antigen binding by indirect ELISA. Hits from the primary screening experiment are sequenced to identify unique antibodies. The Fab antibodies are expressed in *E. coli* and purified using affinity chromatography. Purified Fab antibodies are tested by ELISA for required specificity. Purity is assessed by SDS-PAGE and concentration is measured by UV absorbance at 280 nm.

2.7. Production of CFI Variants using CFI_IRES Vector

2.7.1. CFI_IRES Vector Design

To address the issue of FI and Pro-I co-production, a custom *CFI* expression vector was designed. The vector contains an internal ribosomal entry site (IRES) to facilitate the production of two proteins from a single bicistronic messenger RNA (mRNA) through cap-independent translation (Pelletier and Sonenberg, 1988). The IRES is positioned between the 3' end of human Furin complementary DNA (cDNA) hFURIN[X19094.1] and the 5' end of human full-length *CFI* cDNA h*CFI*[NM_00204.4]. The inclusion of an IRES element in this vector enabled the translation of both Furin and *CFI* from the same transcript, promoting the cleavage of FI from the Pro-I form into fully processed FI, by Furin. Furin was positioned upstream of the IRES element to ensure excess Furin relative to Factor I for Pro-I cleavage. The vector also contains human eukaryotic translation elongation factor 1 α1 (EF1A) to act as a strong promoter in addition to a Simian virus 40 (SV40) domain which enhances protein expression in mammalian cell lines with the large T antigen. Two antibiotic resistance genes (ampicillin and hygromycin) were also included to facilitate selection in *E. coli* and mammalian cell lines respectively. The vector was produced by VectorBuilder (www.vectorbuilder.com) and the vector ID was: VB171219-1127wqz. In total, the vector was just over 10kb in length.

2.7.2. Site Directed Mutagenesis of CFI within the IRES Vector

The WT *CFI* cDNA contained within the *CFI* IRES Vector was modified using the Stratagene QuickChangeTM II Mutagenesis kit (Stratagene, San Diego, CA, USA) to introduce the rare *CFI* variants R406H, K441R and P553S, in addition to the deactivating catalytic triad mutation, S525A. 1 µL of FI cDNA (50 ng/µL) was added to a reaction mixture of 1.25 µL 10 pmol forward and reverse mutagenesis primer, 5 µL 10X reaction buffer, 1 µL dNTP mix and lastly 1 µL Pfu Ultra DNA polymerase. These mixtures were made up in PCR tubes before being placed into a Bio-Rad Thermal Cycler T100. The PCR was programmed to run for 30 seconds at 95°C, and then the following for 16 cycles: 30 seconds at 95°C, one minute at 55°C and seven minutes at 68°C. After temperature cycling, the reaction was cooled to ≤37°C before the addition of 1 µL of *Dpn* I enzyme (10 U/µL) (R0176, New England Biolabs (NEB), Ipswich, MA, USA). The reaction mixtures were then incubated for one hour at 37°C to digest the parental supercoiled dsDNA.

Following SDM, the *Dpn*-1 treated DNA was used to transform NEB 5-alpha Competent *E. coli* using the heat-shock method described in 2.3.5. The transformed cells were plated onto ampicillin-treated agar plates and individual colonies were used to inoculate 5 mL Miller's LB broth prior to small scale cDNA extraction (2.3.6), which was then sequenced by Eurofins genomics using 2 µL of 10 pmol/mL sequencing primer and 15 µL of 50 µg/mL DNA. Sequences were reviewed using Sequencher (Gene Codes Corporation, Version 5.0) before large scale cDNA extraction and transfection (2.3.8).

2.7.3. Transfection of CFI_IRES Vector into CHO and HEK Cell Cultures

Either Chinese hamster ovarian (CHO) or HEK293T cells were plated at a density of 200,000 – 400,000 cells per well in a 6 well plate 24 hours prior to transfection. Once the cells had reached 50-70% confluency, 3 µg, 5 µg or 0 µg of variant or wild-type *CFI* IRES Vector cDNA was mixed with 6 µL, 10 µL or 6 µL JetPEI reagent, respectively, in a total volume of 200 µL 150 mM NaCl. The solution was incubated at RT for 25 minutes before being added drop-wise to the cells, with each DNA concentration performed in duplicate. The 0 µg cDNA wells were used to provide a negative control. Following the transfection procedure, the plates were incubated at 37°C for 72 hours, with a media change after three hours to remove the toxic JetPEI.

After 72 hours incubation, supernatant was collected and a FI ELISA performed to ensure successful transfection had occurred. At this stage, the cells were incubated in selection media, containing either 200 or 400 µg/mL Hygromycin B (ForMedium™, Hunstanton, UK) for the HEK293T, and 600 or 800 µg/mL Hygromycin B for the CHO cells. The selection media was changed every 72 hours until the cells in the negative control wells had died, and the transfected wells had reached confluency. Once confluent, the supernatant was collected again and an FI ELISA was performed to monitor FI expression.

2.7.4. Limiting Dilution and Clonal Selection of Transfected HEK Cell Cultures

To ensure monoclonality, a limiting dilution of the successfully transfected FI expressing cells was performed. First, a feeder layer of wild-type HEK293T cells were seeded at a density of 500 cells per well in a 96-well flat-bottomed tissue culture plate, for each of the transfected bulk cultures. The non-transfected cells were cultured at 37°C for 48 hours prior to the addition of the transfected cells. To determine the number of cells required for the limiting dilution, the cell supernatant was first removed before two washes with 2 mL DPBS. The washed cells were then incubated with 1 mL trypsin at 37°C for 5 minutes, until the cells had become unadhered. The unadhered cells were then resuspended in 2 mL media prior to counting using trypan blue staining and a haemocytometer. The cell suspension was then diluted to a density of four cells per µL, before transferring 200 cells per well to the first column of the feeder cell containing 96 well plate. The cells were then double diluted across the plate to enable the generation of monoclonal colonies. The diluted cells were incubated at 37°C for 96 hours before the growth media was exchanged for selection media containing 200 µg/mL hygromycin. Once the wells seeded with less than one transfected cell per well had reached confluency, these were scaled up into T75 flasks, prior to cryopreservation or further culture.

2.7.5. FI Production in HEK Cells

Cells were continuously scaled up, using 1% trypsin to remove adhered cells, from T25, to T75 and finally T175 flasks, with splitting in fresh selection media at least once per week. Once the cells were steadily growing, the cell pellets from two T175 flasks was utilised to inoculate one Millicell HY 5-layer flask, T-1000 culture flasks containing 250 mL selection media, for each variant and the wild-type FI. The multilayer flasks were incubated at 37°C and 5% CO_2 for one month, with splitting into fresh selection media every five days. All supernatant was collected and stored at -80°C before purification of the secreted FI.

2.7.6. Deglycosylation of FI using Peptide-N-Glycosidase F (PNGase F)

To assess differences in motility observed on SDS PAGE between plasma and recombinant FI, 2 µg of each glycoprotein was combined with 2 µL of GlycoBuffer 2 (10X) and made up to 20 µL total reaction volume with H_2O. To the glycoprotein solution, 2 µL PNGase F was added and the mixture incubated at 37°C for 24 hours. A negative deglycosylation control was also subjected to the same conditions, with the addition of 2 µL H_2O in place of PNGase F. The deglycoslated proteins and their controls were then analysed by SDS PAGE with Coomassie staining.

2.8. Functional Assessment of FI Variants

2.8.1. Cofactor Assays in the Fluid Phase for FI Variants

To detect differences in serine protease activity between the FI variants and WT FI, fluid phase cofactor assays were performed. These assays assess the breakdown of C3b into iC3b, in combination with a cofactor, to determine the function of FI within the regulatory alternative pathway TMC. FI activity was demonstrated by cleavage of C3b at Arg1303-04Ser (generating α2 46 kDa and α1 68 kDa) and Arg1320-21Ser (generating α2 43 kDa and releasing C3f), and at Arg954-55Glu (generating α1 29 kDa and C3dg 39 kDa), when using soluble CR1 (sCR1) as a cofactor.

For each FI protein tested, purified FI was added to 1 µL of C3b (CompTech, A138, 1 µg/µL), and 2.5 µL of 155 ng/µL full-length Factor H (FLFH) (CompTech, A137) or 200 ng/µL sCR1 (in-house, CHO recombinant) or 200 ng/µL FH1-4 (in-house, Pichia recombinant) or 200 ng/µL FHL-1 (in-house, CHO recombinant) or 200 ng/µL MCP (in-house, CHO recombinant). Each reaction mixture was made up to a total volume of 15 µL with PBS and incubated at 37°C. The amount of FI and the incubation duration depended on the cofactor used. 30 ng FI and a 15 minute incubation was utilised for FH1-4 and MCP, whereas FLFH, FHL-1 and sCR1 required 10 ng FI and a 15 minute incubation. At the end of the incubation, 5 µL of 4X reducing sample buffer was added immediately to each test and control (no cofactor), to quench the reaction. The products were then visualised on a 10-20% SDS-PAGE gel using reducing conditions and Coomassie staining. Gel images were captured using a Samsung Galaxy S9 camera and analysed by densitometry using ImageStudio Lite (Licor). The data was then imported to GraphPad Prism 9.4.1 for statistical analysis.

Regarding the cofactors utilised in these cofactor assays, all were produced using standard recombineering. FH CCP1-4 (FH1-4) was a gift from Dr Thomas Hallam and was produced in-house using *Pichia pastoris*. The FHL-1 was produced in-house using standard CHO cell culturing and was a gift from Professor Kevin Marchbank. The sCR1 was produced using CHO, was a gift to our lab from Professor Paul Morgan (Cardiff, UK) and was characterised in Watson *et al.* (Watson *et al.*, 2015).

2.8.2. Analysis of Cofactor Assays by Densitometry

To compare the activity between the FI variants and the WT, degradation of the C3b α'-chain was measured using densitometry. When comparing the break down products the C3b α'-chain was normalised to the beta chain, to act as a loading control. To minimise the effect of inter-assay differences between repeated measurements, the normalised result was given as the C3b α' chain /β chain ratio of a negative control (C3b and cofactor only).

2.8.3. Statistical Analysis

All statistical tests comparing mutant and WT FI protein were performed using GraphPad Prism 9.4.1. To compare the performance of each variant against the WT protein, an unpaired t test with a two-tailed p-value was used.

2.8.4. Real-Time SPR Analysis of FI Variants

2.8.4.1. Immobilisation of C3b onto a CM5 Sensor Chip using a BIAcore S200

A BIAcore S200 (General Electric (GE), Boston, MA, USA) was utilised to prepare the surface of a Carboxymethyl 5 (CM5) Sensor Chip (GE) for C3b immobilisation through amine coupling. The chip was first activated by flowing N-(3-dimethylaminopropyl)-N'-ethylcarbodimide hydrochloride (EDC) and N-hydroxysuccinimide (NHS) over the surface of the selected flow cells, to create a negatively charged chip surface. Once the surface is charged, proteins can then be immobilised through covalent binding when a low pH (4.5) buffer is used. Preparing the surface in this way enabled analysis of the interactions between chip-bound C3b and protein analytes through surface plasmon resonance (SPR).

For amine coupling, surface activation was achieved by flowing 260 µL EDC and 180 µL NHS over the two flow cells to be used in the experiment (one for C3b binding and one for the blank). Purified C3b (CompTech, A114) was then immobilised on a single flow cell of the CM5 chip by flowing 5 µg/mL protein diluted in 50 mM sodium acetate (pH 4.5) over the chip in multiple 20 second intervals at 20 µL/min, until ~1000 resonance units (RU) were reached. After the target amount of C3b had been bound to the surface, 1 M ethanolamine was used to block any remaining active sites on the surface, by a two minute injection at 20 µL/min. This methodology for amine coupling of C3b has been previously described by Harris *et al.* (2005) and is in accordance with the manufacturer's instructions (NHS/EDC kit, GE) (Harris *et al.*, 2005).

Alternatively, C3b was coupled to the chip surface via its thioester domain, in a physiological relevant manner. This process was achieved by first binding a small amount (~100 RU) of C3b by amine coupling, as described before, to generate a nidus for the formation of the AP C3 convertase. Next, FB and FD (CompTech, A135 and A136 at 500 nM and 60 nM, respectively) were injected for 60 seconds at 10 µL/min to build the AP C3 convertase (C3bBb) on the chip surface. C3 (0.1 mg/mL, serum purified by Dr Kate Smith-Jackson) was then injected for 90 seconds at 20 µL/min. The injected C3 is cleaved by the surface-bound C3 convertase to C3b.

The newly generated C3b is then covalently bound to the surface through the reactive thioester domain. Several subsequent cycles of convertase formation and C3 cleavage resulted in the immobilisation of ~1000 RU C3b onto the chip surface, in a physiologically relevant way.

2.8.4.2. On-Chip AP TMC Formation for Analysis of Pro-I and FI Variants

On-chip building of the AP TMC was performed on both amine coupled, and physiologically coupled C3b chip surfaces. As the incorporation of activate FI into the TMC would lead to the degradation of the surface-bound C3b, a deactivating catalytic triad mutation, S525A (Xue *et al.*, 2017), was incorporated to facilitate the analysis of TMC formation without C3b cleavage.

Before the TMC was generated, FH1-4, S525A FI, and the three inactivated variants were each injected separately to determine their affinity for the C3b surface. All proteins were used at a concentration of 125 nM, diluted in PBST+Mg^{2+} buffer (0.05% Tween 20 and 1 mM $MgCl_2$). Following this initial assessment, the TMC was then built by co-injecting FH1-4 and FI (Both at 125 nM) for 2 minutes at 30 µL/min, followed by a 500 second dissociation. These injections were all performed in PBST+Mg^{2+} buffer at 25°C. Before the generation of each subsequent TMC, the flow cells were regenerated using 10 mM sodium acetate and 1 mM NaCl for 40 seconds at 30 µL/min. On the amine coupled surface, the FI concentrations used ranged from 250 nM to 15.61 nM and were achieved by four 1 in 2 serial dilutions. On the physiologically coupled surface, the FI concentration ranged from 125 nM to 15.61 nM and was also achieved by 1 in 2 serial dilution. The data were collected at 40 Hz. A successful TMC build was demonstrated by a significant increase in RU on the C3b coupled flow cell, followed by a gradual decrease in RU upon completion of the injection. This increase and decrease in RU represented the formation and subsequent disassociation of FH and FI from the TMC.

The process for AP TMC building was also repeated using serum purified and recombinant Pro-I.

To determine the extent of C3b surface degradation, before and after AP TMC building, the AP C3 convertase was formed. The difference in RU before and after the TMC building was used to establish the amount of surface degradation. The AP C3 convertase was formed as before, using FB and FD (CompTech, A135 and A136 at 500 nM and 60 nM, respectively). To provide a positive control for surface degradation, both FH1-4 and active WT FI were co-injected at 125 nM to form an active TMC. In the absence of the S525A mutation, FI rapidly cleaved C3b to iC3b. Following the generation of the active TMC, the AP C3 convertase was formed and demonstrated a significant decrease in RU, indicating a loss of surface bound C3b.

All sensorgrams displayed in this thesis have been adjusted by subtracting the response obtained from the injection over the appropriate blank flow cell.

2.8.5. Amidolytic Assay Using the Flurogenic Subtrate Boc-Asp(OBzl)-Pro-Arg-AMC

Previous work by Tsiftsoglou and Sim demonstrated that FI can cleave synthetic substrates in the absence of a cofactor (Tsiftsoglou and Sim, 2004). To determine whether the introduction of the variants had an impact on the serine protease activity of FI, independent of a cofactor, the fluorogenic substrate Boc-Asp(OBzl)-Pro-Arg-AMC (DPR-AMC) was used. 25 µM (final concentration) of the DPR-AMC substrate was prepared in 50 µL of 25 mM HEPES, 0.5 mM EDTA, 146 mM NaCl, pH 8.2, and mixed with 0.25 µM (final concentration) of FI, in 200 µL of the same buffer, on a white microfluor plate (Corning). The amidolytic activity of FI was measured using a Spark multimode microplate reader (Tecan) by excitation at 355 nm and continuous monitoring of emission at 460 nm for 90 minutes at 37°C. To provide a negative control for activity, both the inactive WT FI (S525A) and WT FI which had been preincubated with 0.25 mM Pefabloc-SC (Roche) for one hour at 37°C, were used. FI activity was determined by the change in emission per minute at the linear portion of the emission curve (ΔOD).

2.8.6. C3b-Coated Sensitised Sheep Erythrocytes (EA-C3b) Cofactor Haemolysis Assay

FI activity was also assessed using a novel C3b-coated sensitised sheep erythrocytes (EA-C3b) cofactor haemolysis assay, developed within the Complement Therapeutics Group (Newcastle University).

2.8.6.1. Generation of C3b-Coated Sensitised Sheep Erythrocytes

2 mL Sheep erythrocytes in Alsever's solution (TCS Biosciences) were washed twice in 20 mL PBS by centrifugation at 800 g for 5 minutes, followed by resuspension. The cells were washed twice more in complement fixation diluent (CFD) (Oxoid). 200 µL of the cell pellet was diluted in 2 mL CFD, prior to the addition of 50 µL of anti-sheep RBC antibody (Amboceptor, Testline, UK). The cells were then incubated for 30 minutes at 37°C to

generate sensitised sheep erythrocytes (SEA). The SEA were then washed twice before resuspension in 10 mL CFD. 5 mL of the washed SEA was then incubated for 12 minutes at 37°C with 8% (v/v) FB and FH depleted normal human serum, containing 60 µL eculizumab, to deposit C3b onto the erythrocytes surface (E-C3b). EA-C3b were then washed twice in GVB (Gelatin veronal buffer; CFD with 0.1% Gelatin) and stored at 4°C overnight.

2.8.6.2. E-C3b Cofactor Haemolysis Assay

In a U-bottomed 96-well plate, 50 µL of EA-C3b were incubated with an equal volume of either FH (4 µg/mL; 24 nM final concentration in 100 µL per well) and variable FI, WT or the variants (4 µg/mL), for 10 minutes at 22°C with 400 RPM shaking. FI was serially diluted 1 in 2 in FH, leaving two columns for a no FI and FH, and a no FH control. After the incubation period, the cells were washed three times in 100 µL GVB by centrifuging at 800 g for 5 minutes.

To determine the FI activity for each variant and the WT, 50 µL of EA-C3b was incubated with an equal volume of CompTech FH (4 µg/mL; 24 nM) and a concentration range of FI (diluted from 40 µg/mL) for 10 minutes at 22°C, with constant shaking (400 RPM). After the incubation period, the cells were washed three times in 100 µL GVB by pelleting at 800 g for 5 minutes. To form the AP C3 convertase, EA-C3b were resuspended in 50 µL of FB (75 nM) and FD (16 nM) solution and incubated for ten minutes at 22°C with constant agitation (400 RPM). Wells were included with 1:1 mixture (100 µL total) of EA-C3b and GVB for a 0% control, and dH_2O for 100% lysis control. Finally, 50 µL of a 1 in 50 diluted Guinea Pig serum (Sigma-Aldrich, UK) in 40 mM EDTA-GVB was added to each test well to initiate lysis. The plate was then incubated at 37°C for 20 minutes. Cells were pelleted, and 90 µL of supernatant transferred to a flat-bottomed 96-well plate for the detection of haemoglobin release using a plate-reader (Labtech L4500) with the absorbance set at 412 nM and a reference of 660 nM.

Percentage lysis was determined from the Optical Densities (OD) as follows:

$$\text{Lysis (\%)} = 100 \times \left(\frac{\text{Sample OD - 0\% lysis control OD}}{\text{100\% lysis control OD - 0\% lysis control OD}}\right)$$

The percentage of lysis protection was then calculated using the following formula:

Lysis Protection (%) =

$$100 \times \left(\frac{\text{Average percentage lysis FH only - Percentage lysis sample}}{\text{Average percentage lysis FH only}} \right)$$

Chapter 3. Purification of Functionally Active Recombinant and Plasma Derived Factor I

3.1. Introduction

Various variants in the components of the alternative pathway have been implicated in a variety of diseases, however the role of the AP in the pathogenesis of AMD is still somewhat unclear. Many rare genetic variants in *CFI* have been identified in patients with AMD, and whilst individually they may not all reach a genome-wide significance in association (Kavanagh *et al.*, 2015), when taken together there is a significant increase in disease burden in those who carry rare missense *CFI* variants (Seddon *et al.*, 2013; van de Ven *et al.*, 2013; Fritsche *et al.*, 2016; Geerlings, de Jong and den Hollander, 2017). Loss of function variants have the greatest impact on increasing the risk of AMD (Seddon *et al.*, 2013), a finding which is also corroborated by the significant association between low systemic FI levels and AMD (Kavanagh *et al.*, 2015; Hallam *et al.*, 2020), further implicating the role of rare *CFI* genetic variants in the pathogenesis of AMD.

This chapter will outline the identification of three rare *CFI* variants from the literature for subsequent functional analysis. In addition, a method for the purification of functionally active FI from human plasma will be defined, prior to the generation of a functionally active recombinant FI. The methodology outlined here will be used to underpin the generation of the chosen rare *CFI* variants, facilitating their characterisation to aid understanding of the role that rare *CFI* variants play in the development of AMD.

3.2. Aims

- To review the literature and select three rare *CFI* for production
- To purify functionally active FI from plasma
- To produce functionally active recombinant FI

3.3. Results

3.3.1. Selection of CFI Variants for Characterisation

3.3.1.1. *CFI* Variants in the Literature

There are over 200 rare *CFI* variants reported within the literature, many of which were identified in patients with AMD (Fritsche *et al.*, 2013, 2016; Seddon *et al.*, 2013; Kavanagh *et al.*, 2015; Hallam *et al.*, 2020). *CFI* variants have also been identified in patients in numerous other diseases of complement dysregulation including aHUS, MPGN, C3G, Systemic lupus erythematosus and fulminant cerebral inflammation (Rodriguez *et al.*, 2014; Osborne *et al.*, 2018; Tseng *et al.*, 2018; Altmann *et al.*, 2020).

To determine which *CFI* variants should be chosen for functional analysis, a short-list was selected from the rare variants identified in Kavanagh *et al.* 2015 (Table 3-1). This table is composed of eight *CFI* variants that were present in predominately more cases than controls and appeared in greater than or equal to five individuals within the study population. Key for the stratification of Type 1 and Type 2 variants, there was also serum FI data available, which enabled the identification of two Type 1 variants, A240G and G119R. Since the association between low FI levels and AMD is well established, and the functional impact of rare genetic variants which do not result in low antigenic levels of FI (Type 2) remains unclear, these were therefore of interest in this project. The location of each variant was also considered as it has been shown that a greater disease burden is associated with variants which affect the catalytic light chain, compared to those located on the heavy chain (Seddon *et al.*, 2013; Geerlings *et al.*, 2018). In addition to their location within the FI protein, their 3D position within the AP TMC (Xue *et al.*, 2017) was also interrogated through the use of the molecular visualisation system PyMOL (Schrödinger and DeLano, 2020) (Figure 3-1).

Table 3-1 Variants significantly associated with AMD (from Kavanagh et al., 2015).

Variant	Domain	Odds Ratio (95% CI)	P-value	PolyPhen2 Prediction	Mean serum FI (µg/mL)	Range serum FI (µg/mL)	Percentage low serum FI (%)
p.A240G	LDLR 1	7.43	0.02	Probably damaging	23.4	10.5-40.0	80
p.G119R	SRCR	3.09	0.15	Probably damaging	26.1	22.0-28.1	100
p.P553S	SP	2.69	0.03	Benign	46.3	32.8-70.8	0
p.K441R	SP	1.43	0.35	Benign	41.7	23.6-56.6	11
p.G261D	LDLR 2	0.93	1.00	Benign	48.7	39.6-64.4	0
p.A300T	Linker 2	0.77	0.74	Benign	48.4	34.6-66.1	0
p.R202I	SRCR	0.35	0.07	Probably damaging	46.1	36.1-62.6	0
p.R406H	SP	0.10	0.02	Probably damaging	47.7	46.2-50.5	0

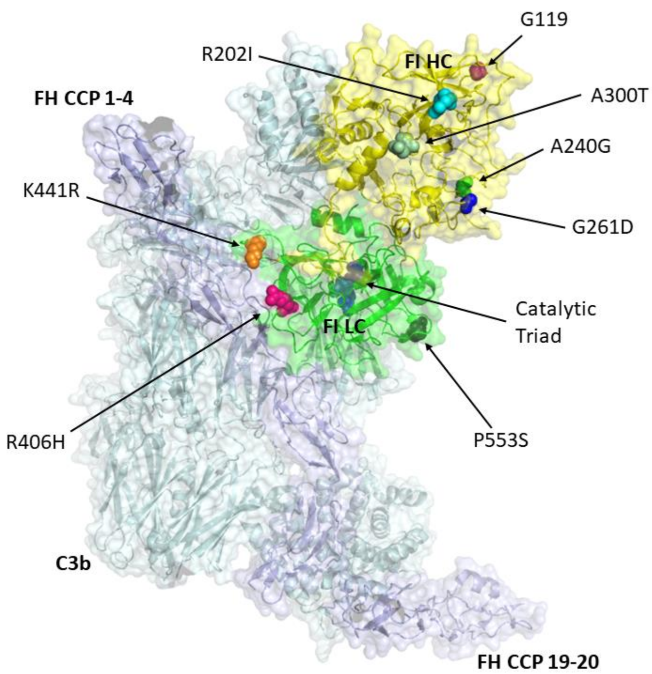

Figure 3-1 Variants associated with AMD from Kavanagh *et al.*, (2015) modelled on the Alternative Pathway regulatory trimolecular complex (FH:C3b:FI).

Locations of the identified rare genetic variants (Table 3-1) in a 3D visualisation of FI bound to FH and C3b in the TMC. FI light chain (green), FI heavy chain (yellow), FH (purple), C3b (pale cyan), amino acid with identified variation within the cohort (coloured spheres), catalytic triad (blue spheres). This graphic was produced using Pymol (V4.6) and the PDB 5O23 molecular structure described in Xue *et al.* (2017). (Xue *et al.*, 2017).

3.3.1.2. Structural Modelling and in silico Analysis

Following the criteria outlined in section 3.3.1.1, the initial eight variants considered were condensed to three: R406H, K441R and P553S. These variants were prioritised as they were associated with normal serum FI levels (Type 2); are located in the catalytic light chain of FI positioned near the serine protease domain (Figure 3-2); are in close proximity to FH and C3b binding domains (Figure 3-3). *In silico* analysis was also utilised to provide a predictor of the impact that these variants may have. The R406H mutation was predicted by Polymorphism Phenotyping v2 (PolyPhen-2) (Adzhubei *et al.*, 2010) to be possibly damaging, with a score of 0.933. Whereas both K441R and P553S were predicted to be benign, with scores of 0.001 and 0.284, respectively.

To further interrogate the impact of the chosen variants, the Combined Annotation-Dependent Depletion (CADD) scores were also determined (Rentzsch *et al.*, 2019). Each variant was scored using the position within the human genome build GRCh38/hg38 with CADD model version 1.5. R406H had a scaled score of 9.753, K441R was 0.061 and P553S was 14.11. Since there is no definitive cut off for deleteriousness, a score above ten is likely to be an indicator of a pathogenic variant; indicating that P553S is more likely to be pathogenic compared to K441R and R406H, providing a contrast to the PolyPhen-2 predictions. To further compare the variants, the OR was considered to determine whether a particular exposure (variant) was a risk factor for a particular outcome (AMD). In Geerlings *et al.* 2016 and Kavanagh *et al.* 2015, P553S had an OR of 3.7 and 2.69 respectively, and in Kavanagh *et al.* 2015, R406H had an OR of 0.10 and K441R of 1.43 (Kavanagh *et al.*, 2015; Geerlings *et al.*, 2017). As both P553S and K441R had an OR greater than one, exposure to these mutations was associated with higher odds of developing AMD. Interestingly, R406H had an OR less than 1, and was therefore associated with lower odds of developing AMD. The final consideration when choosing these variants was the impact of each amino acid substitution on the structure, molecular weight and the pK_a (where K_a is the acid dissociation constant), outlined in Table 3-2. A summary of the chosen variants is presented in Table 3-3.

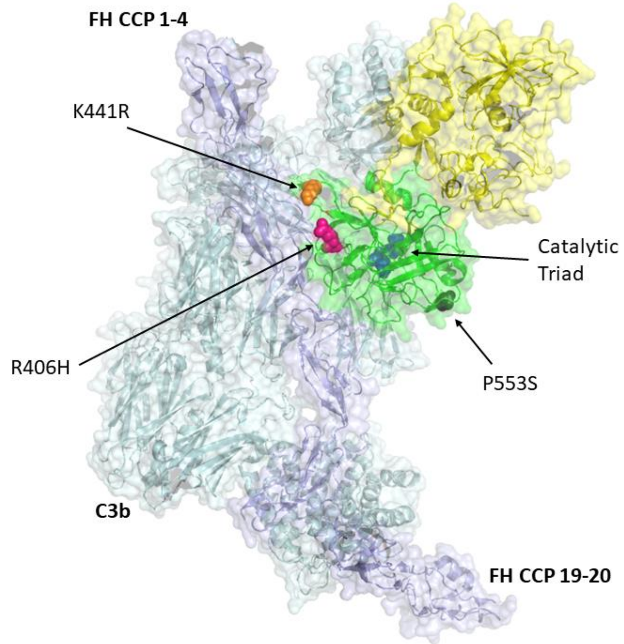

Figure 3-2 Figure 3-2 Variants selected for production, position within the Alternative Pathway regulatory trimolecular complex (FH:C3b:FI) (side on).

Structure of alternative pathway TMC. FH (purple), C3b (cyan) and Factor I (heavy chain yellow, and light chain, green). Position of the Lysine to Arginine change at p.K441R indicated in orange. Position of the Proline to Serine change at p.P553S in black. Position of Arginine to Histidine change at p.R406H in pink. Position of catalytic triad indicated in blue. This graphic was produced using Pymol (V4.6) and the PDB 5O23 molecular structure described in Xue *et al.* (2017). (Xue *et al.*, 2017).

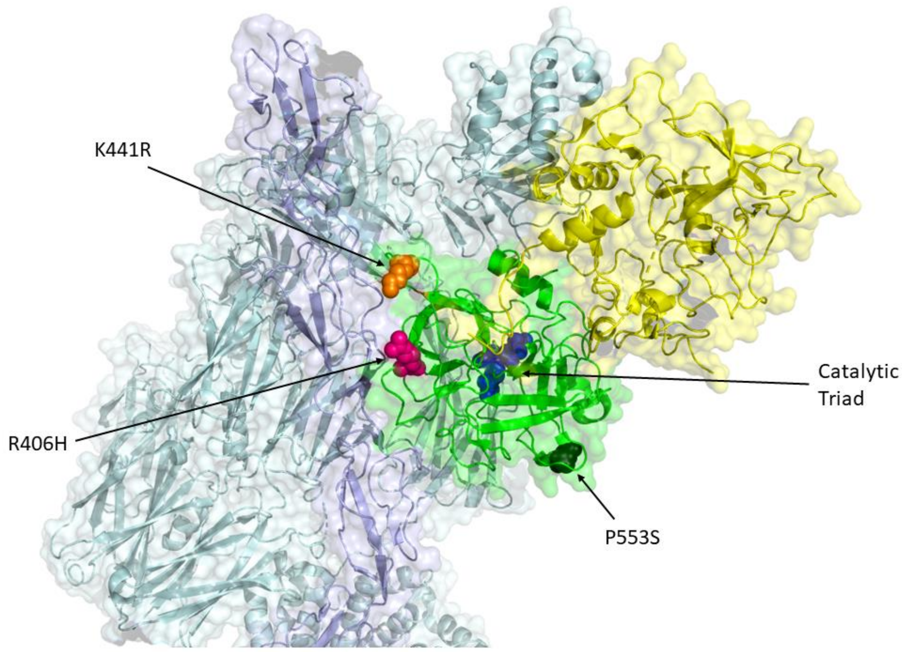

Figure 3-3 Variants selected for production, position within the AP TMC (top down).

Structure of alternative pathway TMC. FH (purple), C3b (cyan) and Factor I (heavy chain yellow, and light chain, green). Position of the Lysine to Arginine change at p.K441R indicated in orange. Position of the Proline to Serine change at p.P553S in black. Position of Arginine to Histidine change at p.R406H in pink. Position of catalytic triad indicated in blue. This graphic was produced using Pymol (V4.6) and the PDB 5O23 molecular structure described in Xue *et al.* (2017). (Xue *et al.*, 2017).

Table 3-2. Properties of the chosen AMD variants. Amino acids and their substitution properties. (https://international.neb.com/tools-and-resources/usage-guidelines/amino-acid-structures).

Amino Acid Change	**Structure**		**Residue Molecular Weight (Da)**		**pK_a of side chain**	
	Wild-Type	**Variant**	**Wild-Type**	**Variant**	**Wild-Type**	**Variant**
p.R406H	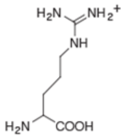	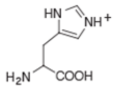	174.2	155.2	12.48	6.04
p.K441R	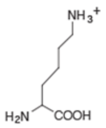	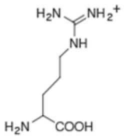	146.2	174.2	10.79	12.48
p.P553S	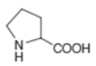	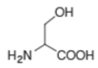	115.1	105.09	N/A	~16

Table 3-3 Summary of in silico analysis for selected CFI variants R406H, K441R and P553S

Variant	cDNA Change (NM_000204.3)	Genomic Position (GRCh38/hg38)	PolyPhen-2 Score	CADD Score	Known conditions	References
p.R406H	c.1217G>A	109746434	0.933	9.753	AMD, aHUS, C3G/ MPGN	Geerlings et al., 2018; Hallam et al., 2020; Kavanagh et al., 2015; Seddon et al., 2013; Tan et al., 2017; Fremeaux-Bacchi et al., 2004; Geerlings et al., 2018; Java et al., 2019; Kavanagh et al., 2008; Zhang et al., 2014
p.K441R	c.1322A>G	109746329	0.001	0.061	AMD, aHUS, C3G/ MPGN	Geerlings et al., 2018; Hallam et al., 2020; Kavanagh et al., 2015; Seddon et al., 2013; Tan et al., 2017; Shoshany et al., 2019; Bresin et al., 2013; Caycı et al., 2012; Fremeaux-Bacchi et al., 2004; Geerlings et al., 2018; Osborne et al., 2018
p.P553S	c.1657C>T	109740988	0.284	14.11	AMD, aHUS, C3G/ MPGN	Geerlings et al., 2018; Hallam et al., 2020; Kavanagh et al., 2015; Seddon et al., 2013; Tan et al., 2017; Bienaime et al., 2010; Bresin et al., 2013; Fang et al., 2008; Fremeaux-Bacchi et al., 2013; Java et al., 2019; Kavanagh et al., 2012; Osborne et al., 2018

3.3.2. FI Purification

To facilitate the functional analysis of the chosen rare FI variants, it was necessary to be able to purify pure and active FI from either plasma or tissue culture supernatant. The purification of homogenous FI from human serum was first described by Pangburn *et al.* in 1977 utilising a column generated by coupling goat anti-rabbit C3bINA antisera to cyanogen bromide-activated-Sepharose (Pangburn, Schreiber and Muller-Eberhard, 1977). Within the same year, Fearon also described the purification of FI from human plasma, albeit through the use of a multi-step process which separated proteins based upon their solubility in ammonium sulphate, charge, and size (Fearon, 1977). The process of purifying FI from human plasma was later improved by Crossley and Porter (1980), where they were able to increase the yield to 6 mg from 500 mL of plasma, an approximately 20% recovery of the total FI available (Crossley and Porter, 1980). Despite this improvement, the purification of FI still required multiple steps over several days.

In 1982 Hsiung *et al.* described a two-step purification method with an ~60% yield through the generation of the anti-FI monoclonal antibody, OX-21. By coupling OX-21 to Sepharose CL-4B beads, a specific affinity column was made, facilitating the purification of 16.7 mg of FI from 700 mL of human plasma, following gel filtration. The purified protein also retained enzymatic activity as demonstrated by the cleavage of both C3b and C4b in the presence of the appropriate cofactors (Hsiung *et al.*, 1982). Since this method was able to generate a good yield of active FI, with little contamination, the protocol outlined by Hsiung *et al.* (1982) was therefore adapted for use in this project.

3.3.2.1. Monoclonal Antibody Affinity Chromatography

3.3.2.1.1. OX-21 Production and Analysis

OX-21 is a mouse monoclonal antibody to human FI of the IgG_1 subclass (Hsiung *et al.*, 1982), which binds specifically to non-reduced FI (Nilsson *et al.*, 2010). For this project OX-21 was purified in-house from hybridomas (ECACC 91060417) for the generation of FI affinity columns and for use in ELISAs and Western Blots. Before the OX-21 could be utilised, it was first harvested from cell culture supernatant by passing over a HiTrap Protein G HP column. Figure 3-4 is a representative UV trace obtained when the column was eluted using 0.1 M Glycine, pH 2.7. Multiple runs were required to ensure complete depletion of the supernatant. From 1 L of supernatant, ~30 mg of antibody was purified.

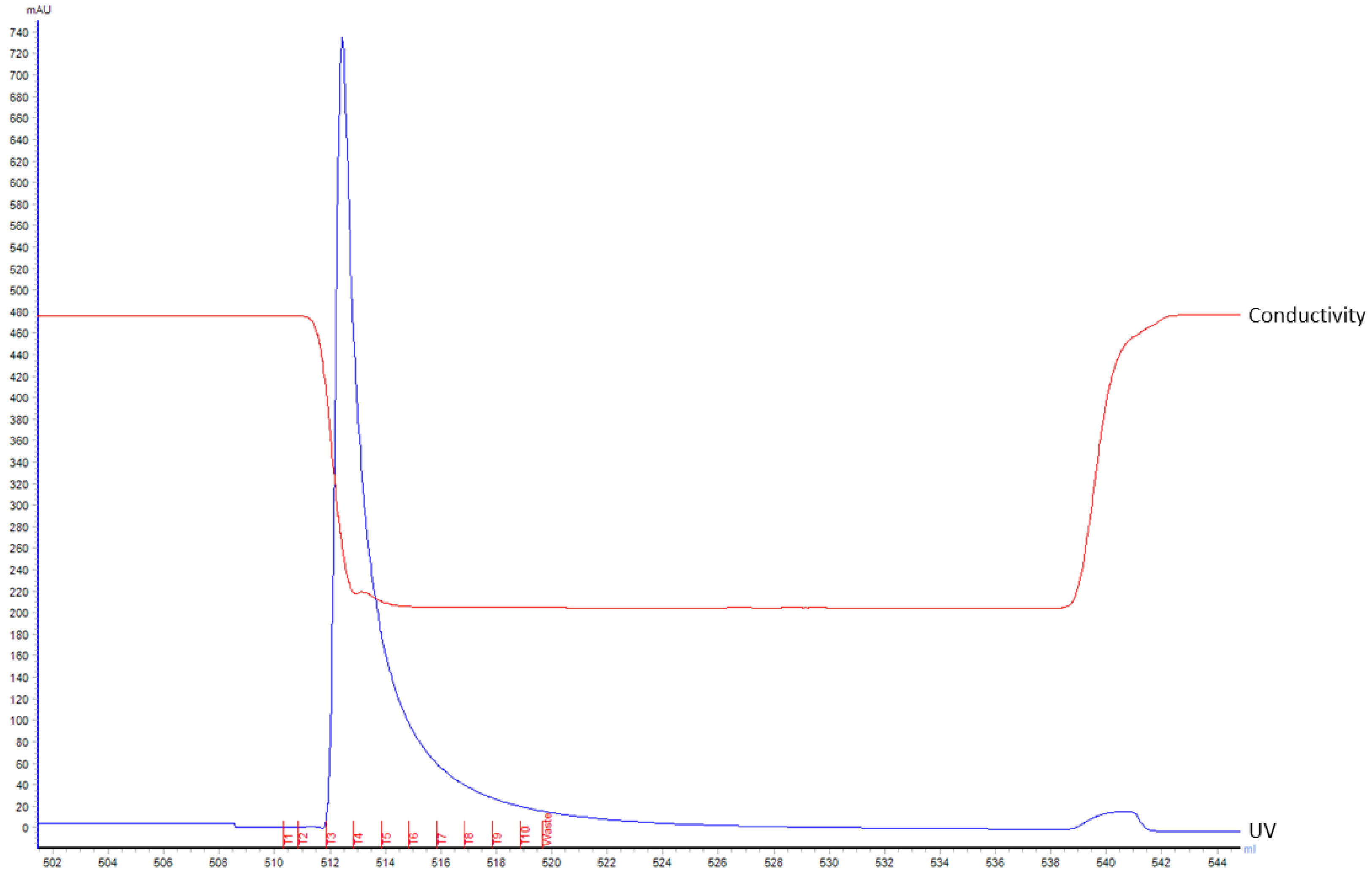

Figure 3-4 Purification of OX-21 from hybridoma supernatant using a Protein G affinity column.

OX21 was purified cell culture supernatant using the ÄKTA Start protein purification system with a 5 mL HiTrap Protein G HP Column. UV trace produced upon elution of with 0.1 M Glycine, pH 2.7.

The resulting OX-21 was then pooled and assessed by SDS PAGE stained with Coomassie (Figure 3-5A) and by Western Blot (Figure 3-5B). On both the SDS PAGE and the Western Blot, a single band was visualised at approximately 150 kDa under non-reducing conditions. Under reducing conditions, three bands were observed on both the gel and the blot. With a single band at ~50 kDa, and a doublet at ~20 kDa. The band at ~50 kDa was representative of IgG_1 heavy chain and the bands at ~20 kDa are indicative of the light chain.

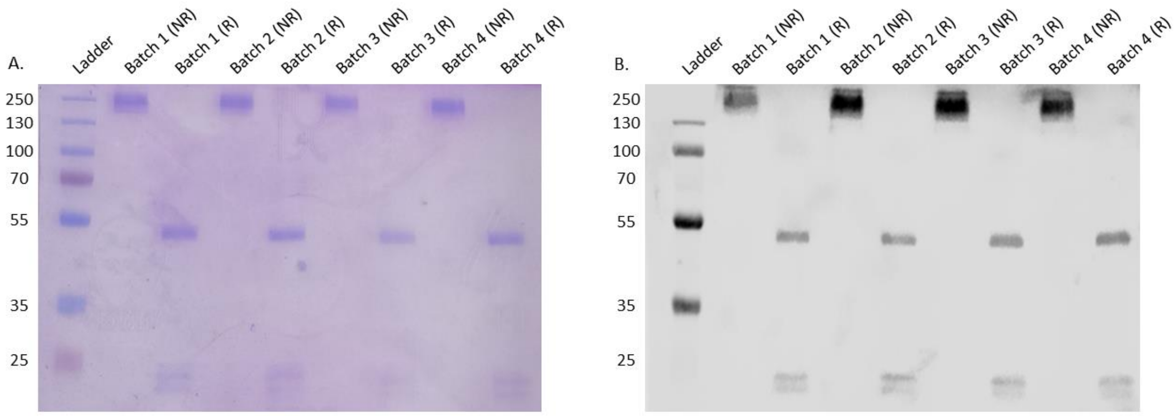

Figure 3-5 SDS PAGE and Western Blot of Protein-G purified OX-21.
OX-21 was purified cell culture supernatant using the ÄKTA Start protein purification system with a 5 mL HiTrap Protein G HP Column. (A) Results of SDS PAGE comparing subsequent runs of OX-21, under both reduced and non-reduced conditions with a PageRuler Prestained Protein ladder (10 – 250 kDa). (B) Western Blot comparing subsequent runs of OX-21, under both reduced and non-reduced conditions with a PageRuler Prestained Protein ladder. Detected using donkey anti-mouse IgG (H+L) HRPO diluted 1:500. Ladder size 10 – 250 kDa

To confirm that the purified antibody was indeed OX-21, its ability to bind FI had to be verified. A Western Blot was performed on Comptech FI under reducing and non-reducing conditions utilising the purified OX-21 as the detection antibody. The OX-21 demonstrated binding to non-reduced FI by the appearance of intense band at 88 kDa (Figure 3-6), however there was no detection of either the heavy or the light chain of FI under reducing conditions, which was consistent with previous findings (Nilsson *et al.*, 2010).

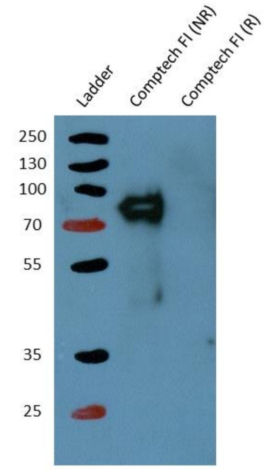

Figure 3-6 Western blot of Comptech FI under non-reducing and reducing conditions using OX-21.
A Western Blot was performed to determine whether purified OX21 bound to FI. Comptech FI was ran under reduced and non-reduced conditions. Purified OX21 diluted 1:1000 was used for the primary antibody, and donkey anti-mouse HRPO diluted 1:500 was used as the detection antibody. Ladder size 10 – 250 kDa.

3.3.2.1.2. Analysis of Light-Chain Doublet using PNGase F

Whilst OX-21 has been commonly used to purify FI from plasma, there is no evidence in the literature referring to the structure of the antibody itself. To determine whether the doublet at ~20 kDa was the result of differentially glycosylated light chains (Tachibana, Seki and Murakami, 1993; Zhang *et al.*, 2015), the purified OX-21 was deglycosylated using the enzyme PNGase F (Figure 3-7). Since treatment with PNGase F did not alter the appearance of the doublet, this confirmed that the difference in mass observed for these two light chains was not due to N-linked glycans. There was however a decrease in mass for the heavy chain, consistent with the removal of two N-linked glycans (~6 kDa) at position Asn297 in the C_H2 domain of the Fc region of the heavy chain (Zauner *et al.*, 2013). To determine whether O-linked glycans or glycation products were response for the doublet, a glycoprotein staining kit could have been used to stain the bands using with the periodic acid-Schiff method, however as the antibody was already proven to bind FI, further analysis of the doublet was not explored.

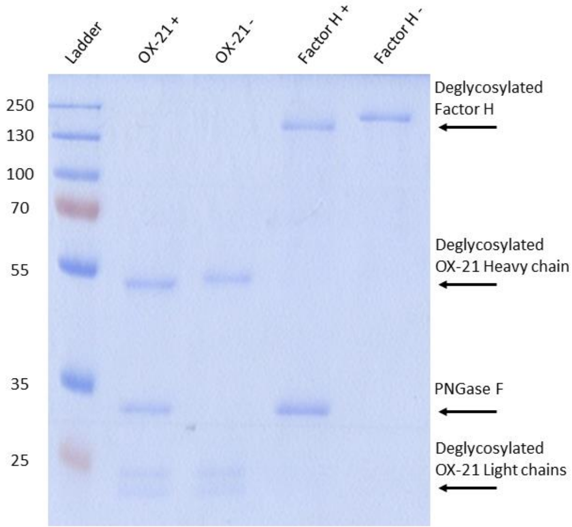

Figure 3-7 SDS PAGE of deglycosylated OX-21 and FH.
OX21 was deglycosylated using the Protein Deglycosylation Mix, according to manufacturer's instructions. Factor H was run as a positive control for deglycosylation. 2 µg of OX21 and FH were used per well. Samples run against a PageRuler Prestained Protein ladder (10 – 250 kDa). Control lanes contained no PNGase F.

3.3.3. FI Purification from Human Plasma

Following the purification of OX-21, an anti-human FI affinity column was generated by coupling 4 mg OX-21 to a 1 mL HiTrap NHS-activated HP column (98.7% coupling efficiency) (Methods 2.1.3). A protocol for the affinity purification of human FI from citrated plasma using an OX-21 column was developed by adapting the method outlined by Hsiung *et al.* (1982) (Methods 2.1.4-2.1.6). Figure 3-8 is representative of the UV trace obtained following elution with 0.1 M Glycine, pH 2.7. Multiple runs were required to completely deplete the FI from the plasma, and with each subsequent run, the peak UV decreased until the citrated plasma was completely deficient of FI. Typically, three runs were required to fully deplete 500 mL of plasma.

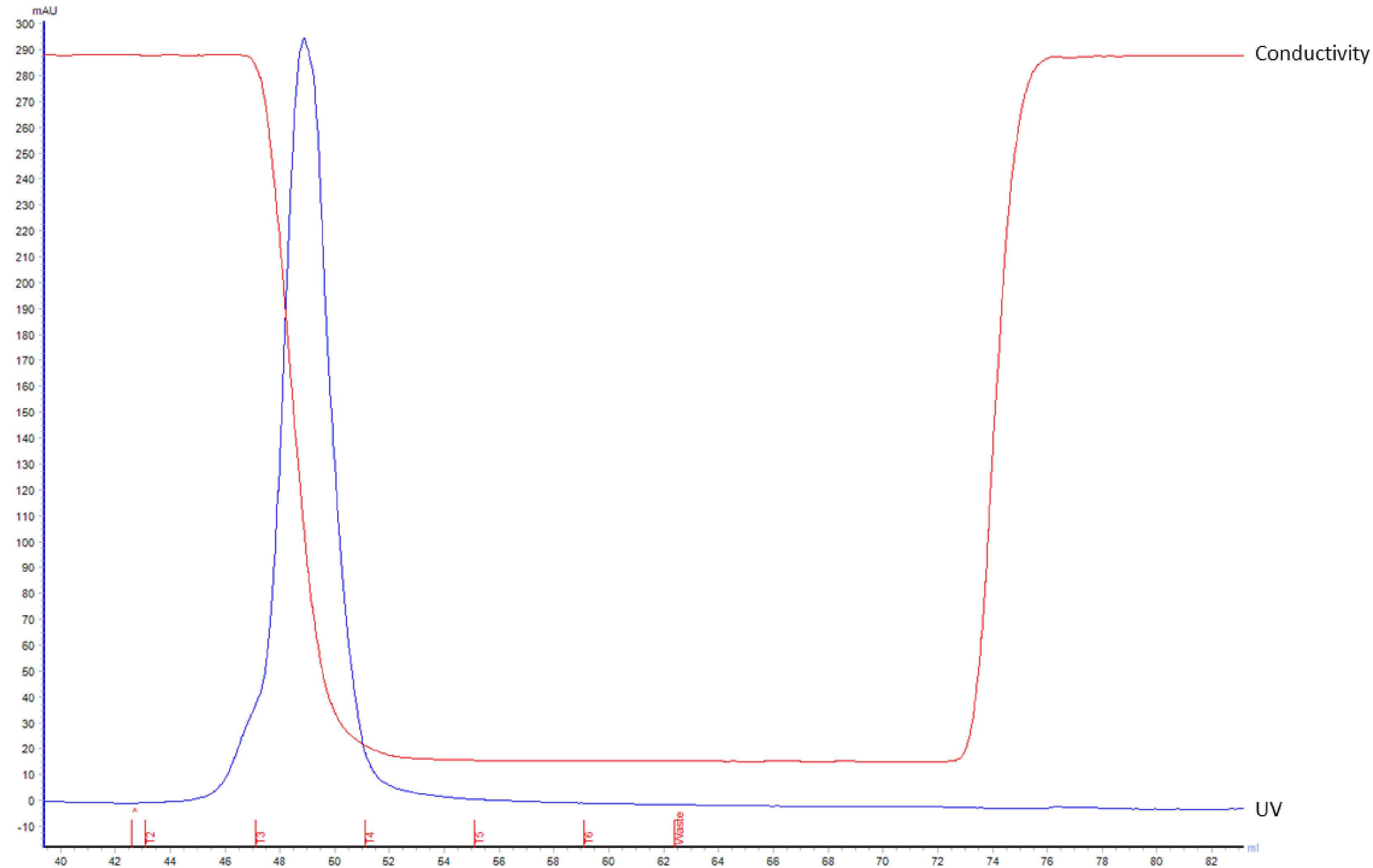

Figure 3-8 Plasma FI purification using OX-21 affinity chromatography.

Example UV trace obtained during Factor I elution with 0.1 M Glycine (pH 2.7) from an OX-21 column. In all instances the protein was collected in fractions T2, T3 and T4. Peak UV of 295 mAU. N = 7.

Following elution, the peak fractions from one run were pooled and analysed by SDS PAGE stained with Coomassie, under non-reducing and reducing conditions (Figure 3-9A). Under non-reducing conditions there was a main band seen at ~88 kDa and a minor band at ~250 kDa. Upon reduction, two major bands were observed at approximately 50 kDa and 38 kDa, likely corresponding to the heavy and light chains of FI, respectively. In addition, there were two minor bands seen at ~90 kDa and 25 kDa.

To confirm the identity of the purified protein, a Western Blot was also performed (Figure 3-9B) with a secondary only control (Figure 3-9C). Under non-reducing conditions a major band was seen at approximately 88 kDa for both Comptech and plasma purified FI; there was also a minor band at ~180 kDa for the plasma FI. The plasma purified FI was also visualised under reducing conditions, producing two major bands at ~50 kDa and 38 kDa, with a minor band at ~90 kDa. The major bands were in concordance with the results from the SDS PAGE and the Comptech non-reduced control, confirming the successful purification of human FI from plasma.

The presence of higher and lower molecular weight contaminants on both the SDS PAGE and the Western Blot highlighted the need for an additional polishing step. The contaminants at approximately 150 kDa and 25 kDa on the SDS PAGE, were likely due to contamination with human IgG, and on the Western, the band at ~180 kDa under non-reducing conditions was likely due to aggregated FI (dimer), whereas the band at ~90 kDa under reducing conditions was potentially due to the presence of Pro-I, a precursor to FI which has only previously been reported in recombinant preparations (Goldberger *et al.*, 1984; Wong *et al.*, 1995; Kavanagh *et al.*, 2008).

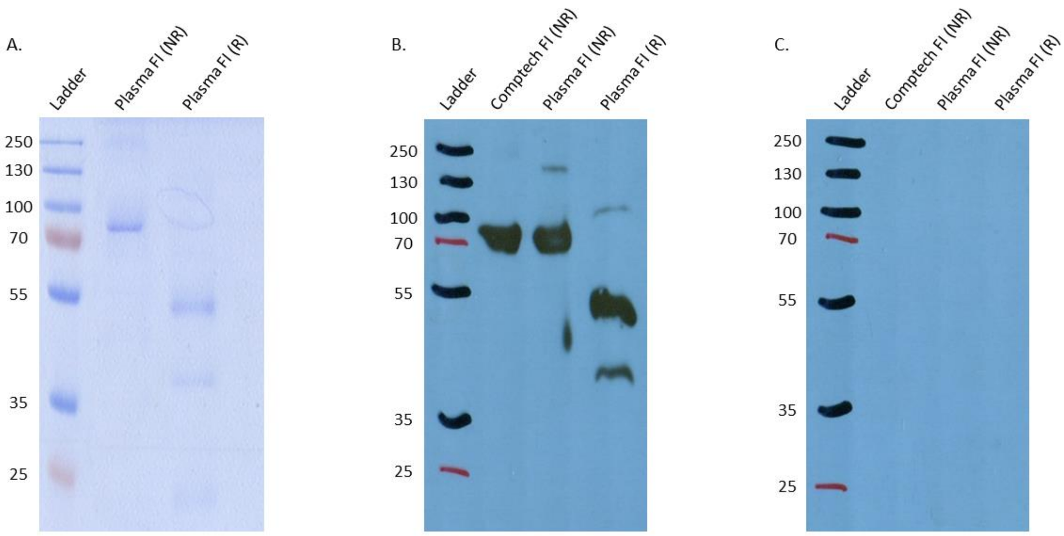

Figure 3-9 SDS PAGE and Western blot of OX-21 affinity purified plasma FI.
Plasma Factor I purified using affinity chromatography analysed using SDS PAGE and Western Blot. (A) SDS PAGE of pooled peak fractions under reducing and non-reducing conditions. The band at 88 kDa under non-reducing conditions represents FI. Under reducing condition, the band at 50 kDa indicate the FI heavy chain and the band at 38 kDa indicates the FI light chain (B) Western blots of pooled peak fractions. Reducing and non-reducing conditions. Comptech Factor I used as a positive control. Band at ~100 kDa under reducing conditions is indicative of Pro-I (C) Secondary only control. Primary antibody Sheep polyclonal to human FI (1 µg/mL), detected with Donkey anti-sheep diluted 1:3000.

3.3.3.1. Removal of contaminants through Size Exclusion Chromatography

Size Exclusion Chromatography (gel filtration) was used to polish the FI by separating contaminants from the desired protein. Five peaks were present on the resulting UV trace (Figure 3-10), with the larger molecular weight contaminants eluted first, followed by smaller weight contaminants. Since FI was the main species present in the sample, it was likely responsible for the largest peak. To confirm the identity of the species eluted between 1E3 and 1F3, an SDS PAGE and a Western Blot were performed (Figure 3-11). FI was identified as the main species in each fraction within this range, as determined by the presence of an ~88 kDa band on both the SDS PAGE and the blot. Fractions 1E3-1E6 contained a contaminant at ~180 kDa, and since it was detected by the anti-FI antibody on the blot, it was likely due to aggregated FI. The remaining fractions, 1E7-1F3, demonstrated no signs of contamination, therefore indicating that pure human FI could be obtained through a two-step process, combining affinity chromatography and gel filtration.

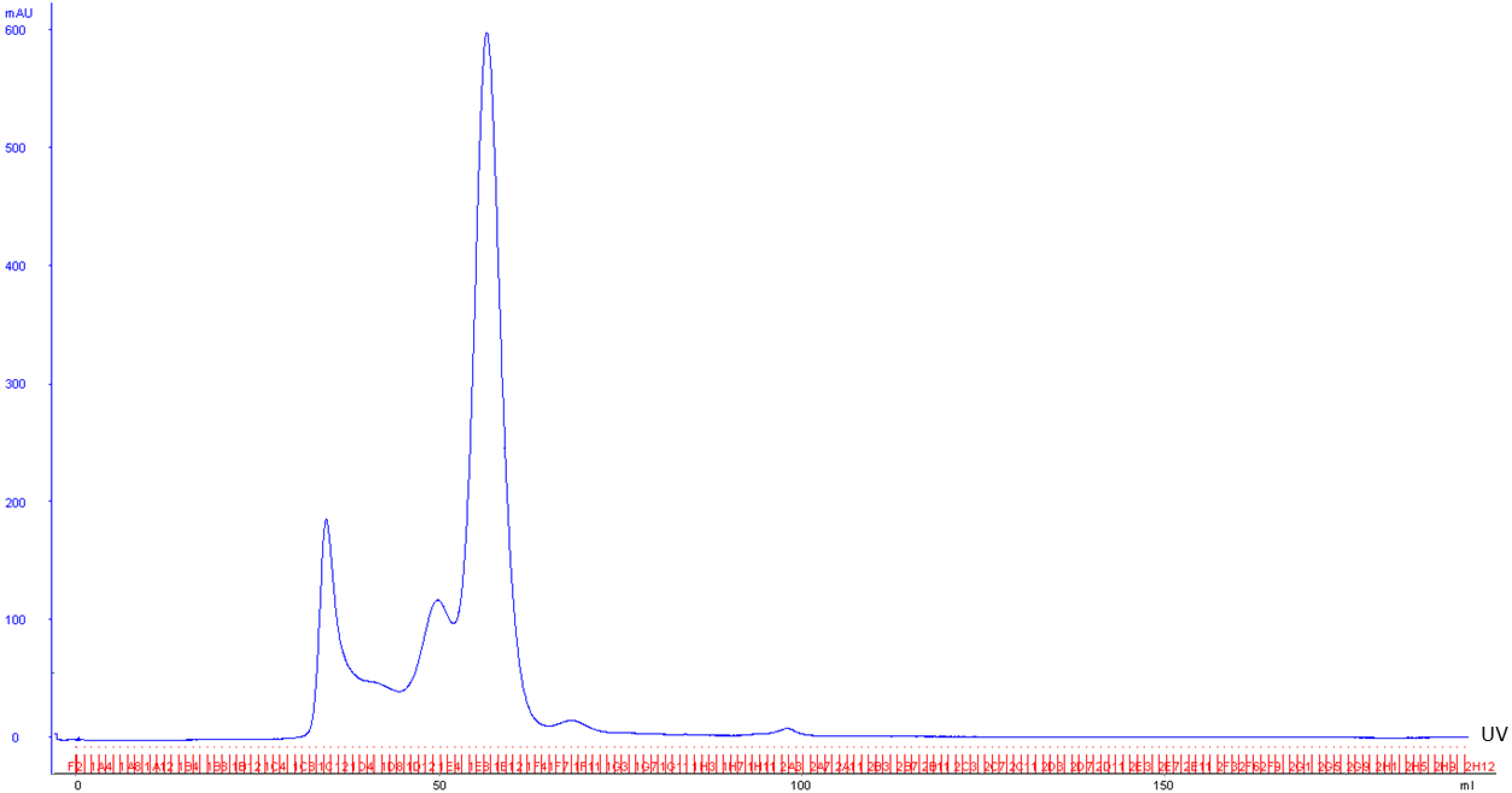

Figure 3-10 Chromatogram of the gel filtration of plasma FI.
A UV trace showing the six peaks seen during gel filtration following affinity chromatography of Factor I.

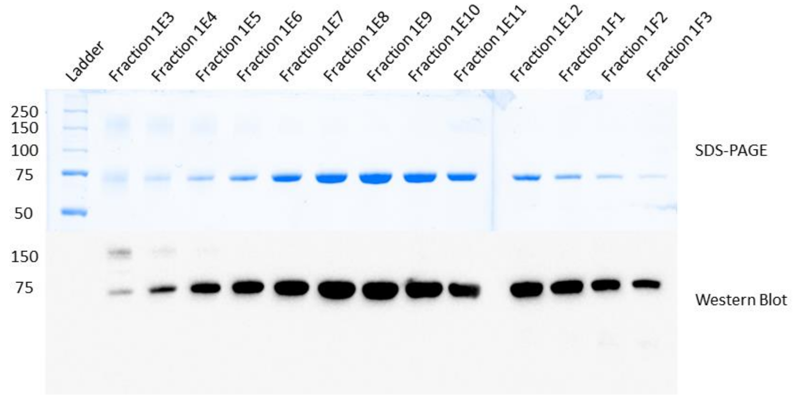

Figure 3-11 SDS PAGE and Western blot of gel filtration main peak.

SDS PAGE and Western Blot analysis of main peak from gel filtration. Run under non-reducing conditions. Fractions 1E3-1E6 show presence of aggregated FI. Fractions 1E7-1F3 show no signs of any contaminant. Western Blot primary antibody Sheep polyclonal to human FI (1 µg/mL), detected with Donkey anti-sheep diluted 1:3000.

3.3.4. Finalised Purification Method

Following the confirmation that gel filtration could be utilised to produce highly purified human FI, the remaining peak fractions (Figure 3-12) were collated and concentrated to 5 mL (Figure 3-13) before 'polishing' using size exclusion chromatography. As demonstrated in Figure 3-14, the UV trace obtained during gel filtration was very similar to that of the previous run (Figure 3-10), albeit with differing proportions of each contaminating species.

The main peak had a maximum UV of 1240 mAU and occurred between fractions 2C11 and 2E11. These fractions were confirmed as containing FI through the appearance of an approximately 88 kDa band on a non-reducing SDS PAGE (Figure 3-15). Fractions 2D8 – 2D11 were homogenous by SDS-PAGE. Fractions 2C12 – 2D7 exhibited a contaminant at ~250 kDa and fractions 2D12 – 2E11, produced an additional band at ~50 kDa on the SDS PAGE. The peak fraction, 2D8, was also ran under reduced conditions producing bands at 50 and 38 kDa, representative of the FI heavy and light chains, respectively. There was also a band at ~90 kDa, again suggesting the presence of Pro-I in human plasma.

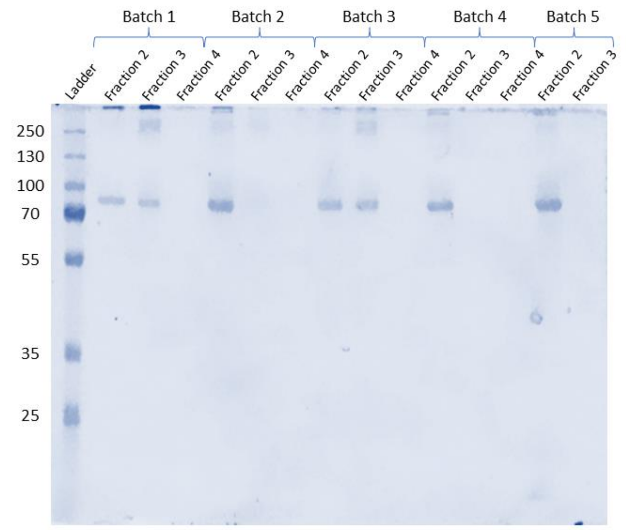

Figure 3-12 SDS PAGE of plasma FI purified using an OX-21 column.

SDS PAGE of OX-21 plasma purified FI run under non-reducing conditions, stained with Coomassie blue. The band at 88 kDa under non-reducing conditions represents FI.

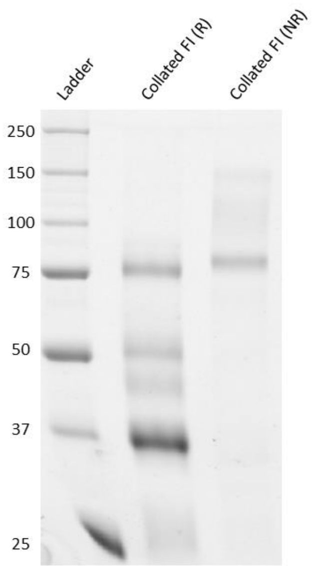

Figure 3-13 SDS PAGE of plasma purified FI stained with Coomassie. Collated Fractions.

SDS PAGE of OX-21 plasma purified FI run under non-reducing and reducing conditions, stained with Coomassie blue. The band at 88 kDa under non-reducing conditions represents FI. Under reducing condition, the band at 50 kDa indicate the FI heavy chain and the band at 38 kDa indicates the FI light chain. Band at ~90 kDa under reducing conditions is indicative of Pro-I.

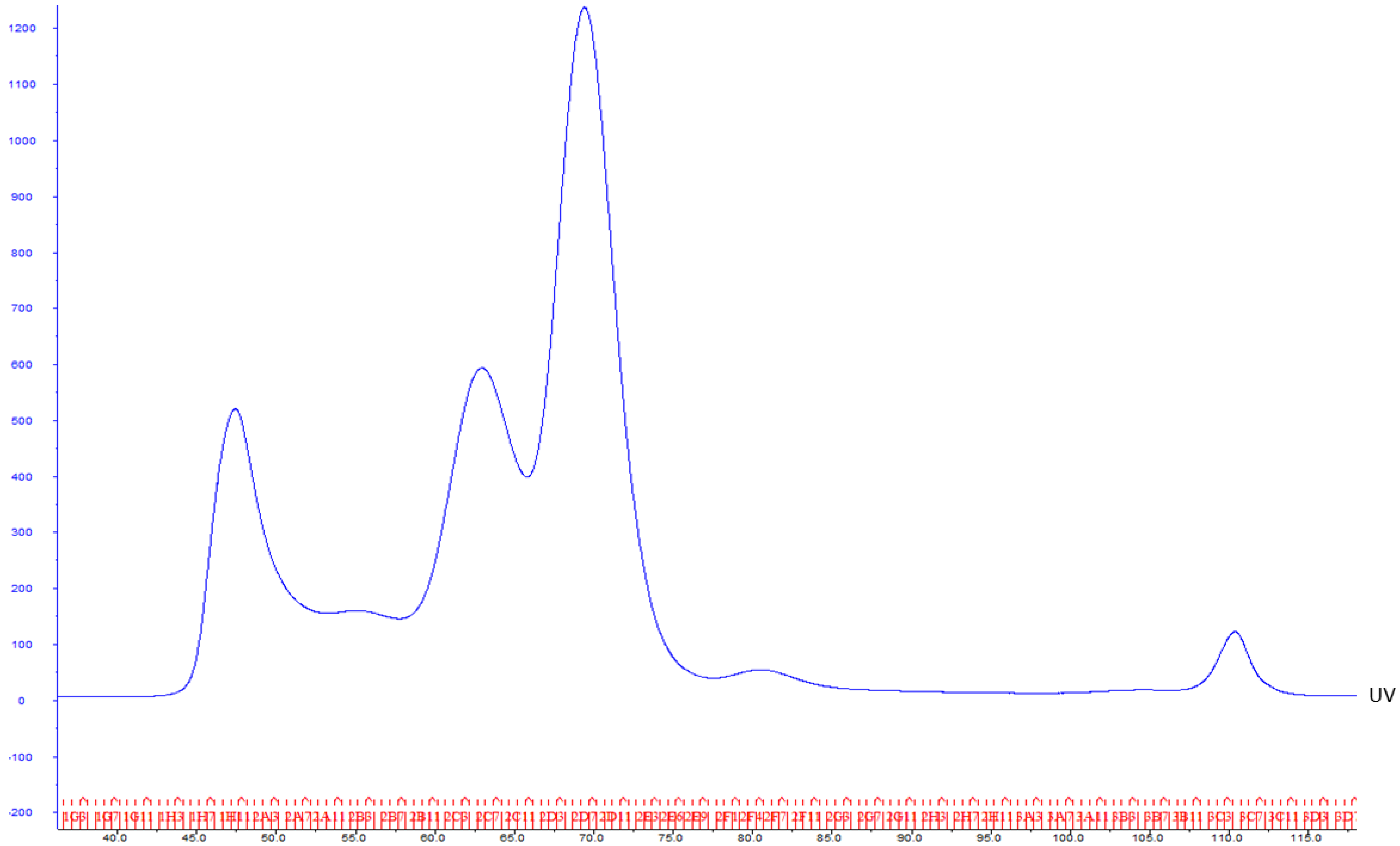

Figure 3-14 Chromatogram of collated plasma FI gel filtration.
A UV trace showing the six peaks seen during gel filtration following affinity chromatography of Factor I.

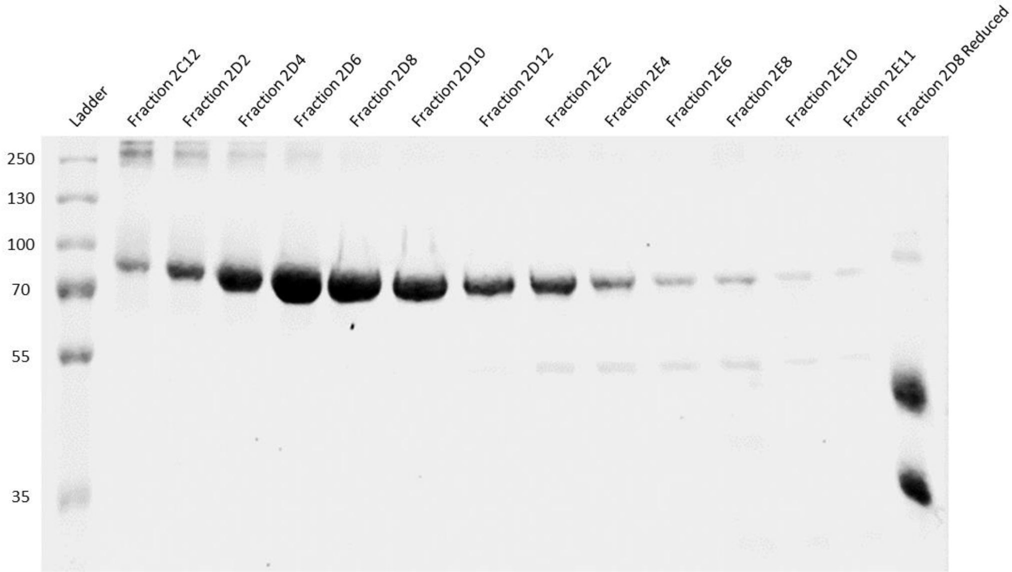

Figure 3-15 SDS PAGE stained with Coomassie of gel filtration peak fraction.
An SDS PAGE was run on the fractions collected at the main peak of figure 3-14. Fractions were run under non-reducing conditions unless stated otherwise. A single band at 88 kDa in fractions 2D10 – 2D12 was indicative of Factor I with no contaminants. The peak fraction 2D8 was also ran under reducing conditions and two bands were observed. The band at 50 kDa represents the heavy chain of Factor I, and the band at 38 kDa represents the light chain.

3.3.5. Analysis of Purified Human FI

The final FI product produced by combining fractions 2D8 – 2D11 was quantified by NanoDrop prior to analysis by SDS PAGE and Western Blot (Figure 3-16), and functional testing. On the SDS PAGE (Figure 3-16A) there was a single band at ~88 kDa in the non-reduced lane and two bands at approximately 50 kDa and 38 kDa in the reduced lane. The Western Blot (Figure 3-16B) also shows the same banding pattern, with one band at ~88 kDa in the non-reduced lane and two bands at 50 kDa and 38 kDa in the reduced lane. There were no bands present on the secondary-only control (Figure 3-16C), indicating that FI was the only species responsible for the bands observed on Figure 3-16B. From 1 L of plasma, 13.6 mg of FI was purified, with 4 mg of this being highly purified. Due to the absence of any contaminating species, utilising the protocol outlined in Methods 2.1.4-2.1.6, it was possible to obtain highly purified human FI from plasma.

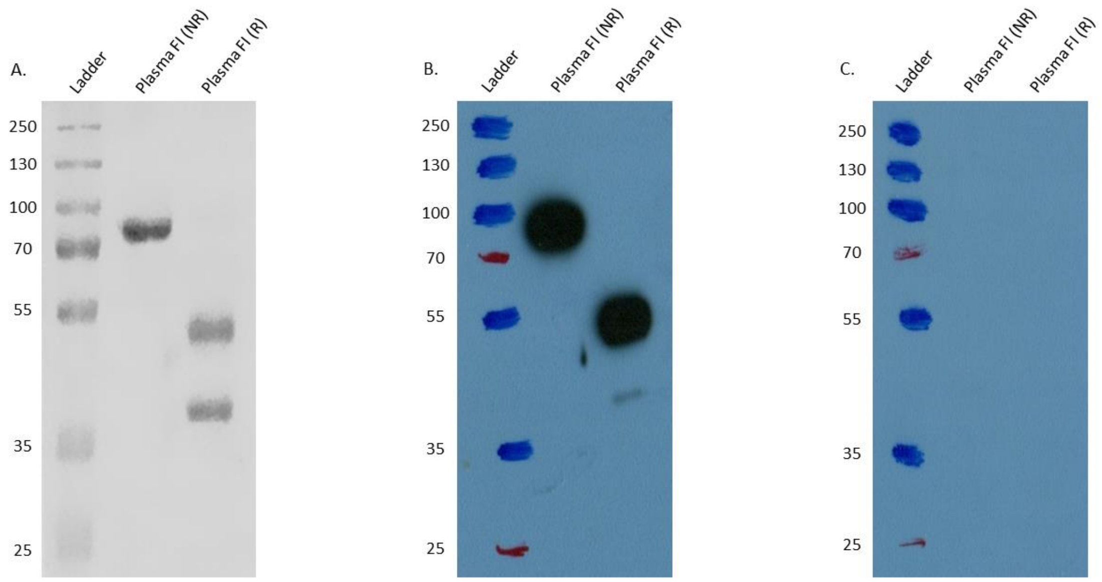

Figure 3-16 SDS PAGE and Western Blot analysis of pure plasma FI.

Once Factor I had been purified using gel filtration, fractions 2D8 – 2D11 were pooled to obtain the final sample. Samples were run on SDS PAGE and Western Blot. (A) SDS PAGE showing purified Factor I. In the non-reduced lane (NR) there is one band at 88 kDa and in the reduced lane (R) there are two bands at 50 kDa and 38 kDa. (B) Western Blot showing purified Factor I detected with a Sheep polyclonal anti-human Factor I (1 µg/mL) primary and a Donkey anti-sheep (1:3000) secondary. (C) Secondary only control. In the non-reduced lane (NR) there is one band at 88 kDa and in the reduced lane (R) there are two bands at 50 kDa and 38 kDa. No bands present in the secondary only control.

3.3.5.1. Plasma Purified FI Cofactor Activity

To determine whether the FI maintained its functionality following purification, a fluid-phase C3b cofactor activity assay was performed in the presence of full-length FH. The activity of the plasma purified FI was compared to that of Comptech FI, over a range of concentrations. In the presence of active FI and FH, C3b is cleaved to iC3b, through the degradation of the C3b α' chain (114 kDa) into the 68 kDa α1 and 46 kDa α2 chains. The α2 chain then undergoes a second cleavage by FI, releasing C3f (3 kDa) and forming iC3b. By resolving the breakdown products on an SDS PAGE gel (Figure 3-17), both the plasma FI and Comptech FI demonstrated the ability to cleave C3b, as determined by the generation of the cleavage products, α1 and the two α2 chains. To confirm that the plasma purified FI maintained a similar activity to the reference FI, densitometry was performed on the C3b α' chain, using the C3b β chain to normalise (Figure 3-18). At 50 ng FI, there was a slight discrepancy in activity between the Comptech FI and the plasma FI, with Comptech FI showing an increased activity, however, at the subsequent lower concentrations this discrepancy was resolved. Taken together, these results indicated that functionally active human FI had been successfully purified utilising the method outlined herein.

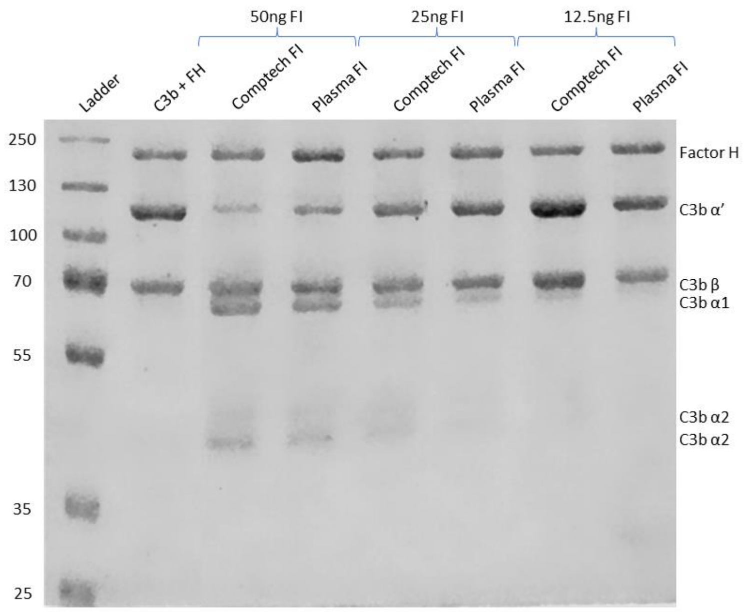

Figure 3-17 C3b cofactor assay comparison of plasma FI and Comptech FI C3b cleavage activity.

SDS PAGE showing proteolytic activity of Factor I across a range of concentrations (50 – 12.5 ng). Activity assessed by the ability of Factor I in combination with its cofactor Factor H, to cleave C3b to its inactive form iC3b. C3b cleavage was indicated by the appearance of α1 and the two α2 bands. All samples were ran under reducing conditions with a PageRuler Prestained Protein ladder (10 – 250 kDa). The purified Factor I was compared to that of Comptech FI which had already been shown to be active.

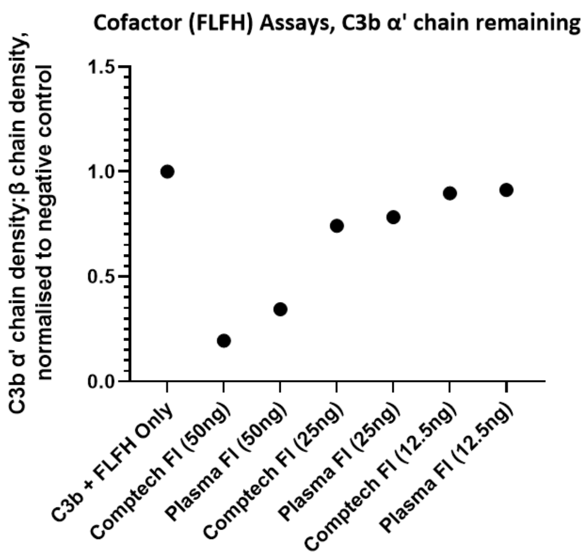

Figure 3-18 C3b α' chain degradation analysis of FLFH cofactor activity for plasma FI and Comptech FI.

Plotted is the density of C3b α' chain remaining (y-axis) after incubation with either Comptech or plasma purified FI with C3b and FH for 60 mins at 37°C during a fluid-phase cofactor assay. The density of the α' chain band was normalised to the density of the β chain band, before the resultant figure was normalised to a negative control containing no FI, giving a proportion of α' chain remaining compared to the no FI control.

3.3.6. Recombinant FI Production

Once a method to purify FI had been established, the production of recombinant FI was the next priority. Since access to patient plasma was not possible, and could contain a mixture of wild-type and mutant protein, recombinant protein had to be generated in order to perform a functional analysis of the variants of interest.

3.3.6.1. Polyhistidine Tag (His-tag) Removal

The eukaryotic expression vector pDR2EF1-α, modified with the insertion of polyhistidine tagged *CFI* (pDEF-*CFI*) was gift from Professor David Kavanagh. Using SDM, a stop codon was introduced to remove the histidine tag from the WT *CFI* sequence. The histidine tag was surplus to requirements as a result of the novel FI purification method outlined in this thesis and was therefore removed to prevent the any impact on FI structure or function. Removal of the histidine tag was achieved by changing the aspartic acid at position 584 to a stop codon through the mutation of two nucleotides (GAC → TAG). The pDEF-*CFI* DNA was amplified by PCR using the mutation primers (Appendix 2) and the product run on a 1% agarose gel (Figure 3-19A). The band at ~8000 bp indicated that amplification with all primer concentrations had been successful.

Following SDM, XL-1 blue supercompetent cells were transformed with the modified plasmid cDNA. A miniprep was performed to isolate the cDNA to confirm that the stop codon had been successfully incorporated using Sanger sequencing. The isolated DNA was visualised on a 1% agarose gel by the appearance of a single band at approximately 8000 bp, indicating that the plasmid was intact and of the expected size (Figure 3-19B). Sequencing of the plasmid by Eurofins Genomics using the primers described in appendix 3 confirmed that the TAG substitution had been incorporated in all pDEF-*CFI* clones and that there were no additional changes throughout the *CFI* insert (Figure 3-19C). Finally, a maxiprep was performed to amplify the pDEF-*CFI* plasmid cDNA prior to transfection into CHO cells for production of the recombinant protein.

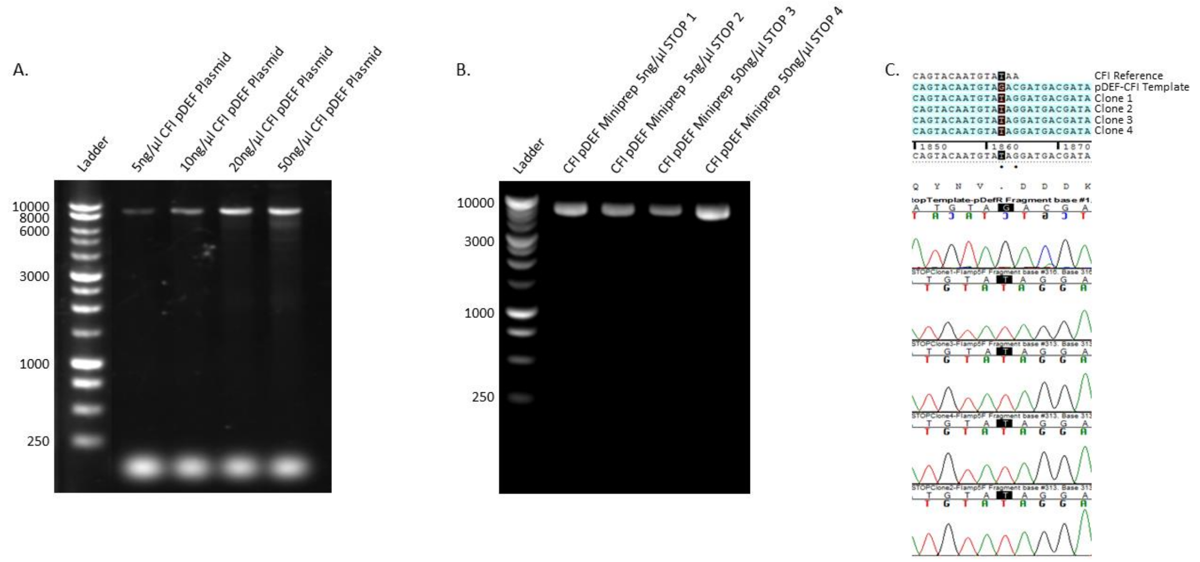

Figure 3-19 Site-directed mutagenesis of pDEF-*CFI* DNA for recombinant FI production.

(A) Gel electrophoresis of PCR product following amplification with mutagenesis primers of varying concentrations (5, 10, 20, 50 ng/µL). Samples run on a 1% agarose gel. (B) Gel electrophoresis of mutated plasmids isolated by miniprep. Samples run on a 1% agarose gel. (C) Sequencing chromatogram showing site of mutation in clones 1 – 4 generated using Miniprep 5ng/µL STOP 1 plasmid visualised in B. Template sequence; GAC, New sequence; TAG. UniProtKB – P05156 (CFAI_HUMAN) was used as the wild-type *CFI* reference sequence. Sequencing results visualised using Sequencher 5.0.

3.3.6.2. Recombinant WT FI Production

For recombinant production of WT FI protein, CHO cells were transfected with the pDEF-*CFI* plasmid and cultured in hygromycin containing media to select for successful incorporation of the *CFI* plasmid. After two weeks in the selection media, the cells were limiting diluted to identify monoclonal colonies of FI expressing cells. Once confluent, a Western Blot was used to confirm successful secretion of FI into the supernatant (Figure 3-20). All the colonies demonstrated successful FI production through the appearance of an ~88 kDa band under non-reduced conditions (Figure 3-20A) and a ~50 kDa band, indicative of the FI heavy chain, under reducing conditions (Figure 3-20B). In Figure 3-20A there was an additional band at approximately 250 kDa, which was later confirmed as bovine IgG from the culture media by the secondary only control (Figure 3-22A). There was also an additional band in Figure 3-20B at ~90 kDa, however, this was not present on the secondary only control (Figure 3-22B). Since the band at ~90 kDa was only present when using an anti-FI antibody, this indicated that the species responsible for this band was likely Pro-I, which is typically seen in recombinant preparations of FI (Goldberger *et al.*, 1984; Wong *et al.*, 1995; Kavanagh *et al.*, 2008).

To identify the highest expressing colony for expansion, an ELISA was performed. Expression levels in the CHO cell supernatant were typically in the range of 0.4-0.6 µg/mL (Figure 3-22). Colony 12E was identified as the highest expresser and was therefore scaled-up and cultured in roller bottles for recombinant FI production.

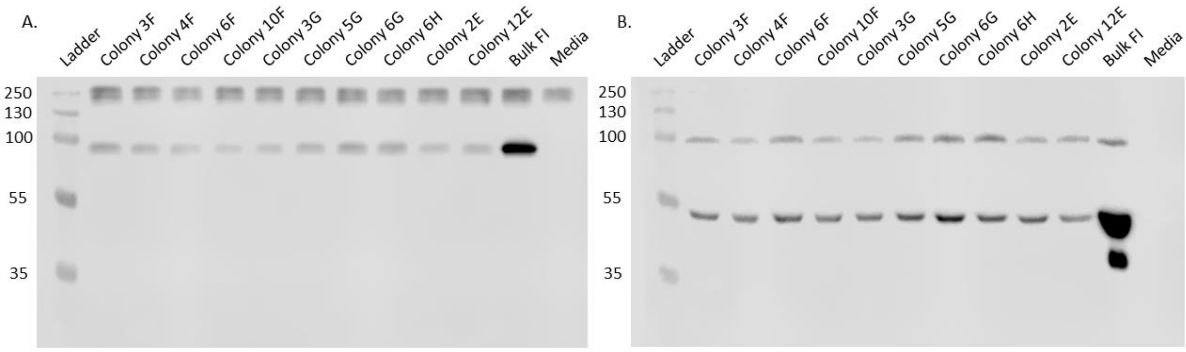

Figure 3-20 Western blot of stable transfection pDEF-*CFI* supernatant.
(A) Western blot of supernatant from stable pDEF-*CFI* transfected colonies run under non-reducing conditions. The band at 88 kDa under non-reducing conditions represents FI. (B) Western blot of supernatant from stable pDEF-*CFI* transfected colonies run under reducing conditions. Under reducing condition, the band at 50 kDa indicate the FI heavy chain and the band at ~90 kDa under reducing conditions is indicative of Pro-I. Detected with a Sheep polyclonal anti-human Factor I (1 µg/mL) primary and a Donkey anti-sheep (1:3000) secondary.

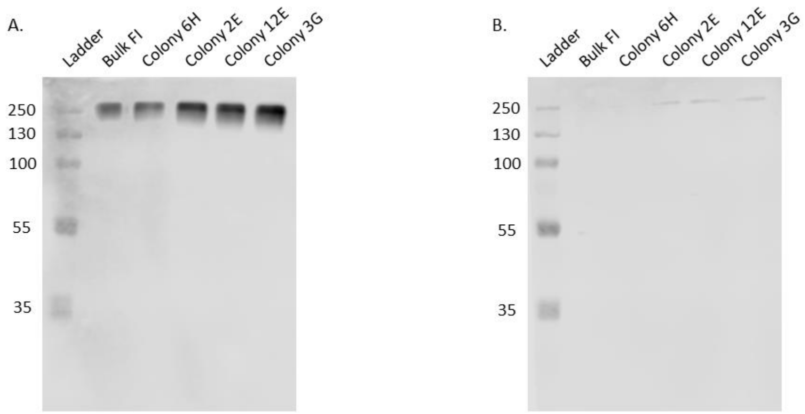

Figure 3-21 Western blot of selected stable transfection pDEF-*CFI* supernatant. Secondary only control.
(A) Western blot of supernatant from stable pDEF-*CFI* transfected colonies run under non-reducing conditions.
(B) Western blot of supernatant from stable pDEF-*CFI* transfected colonies run under reducing conditions. Detected with Donkey anti-sheep (1:3000) secondary.

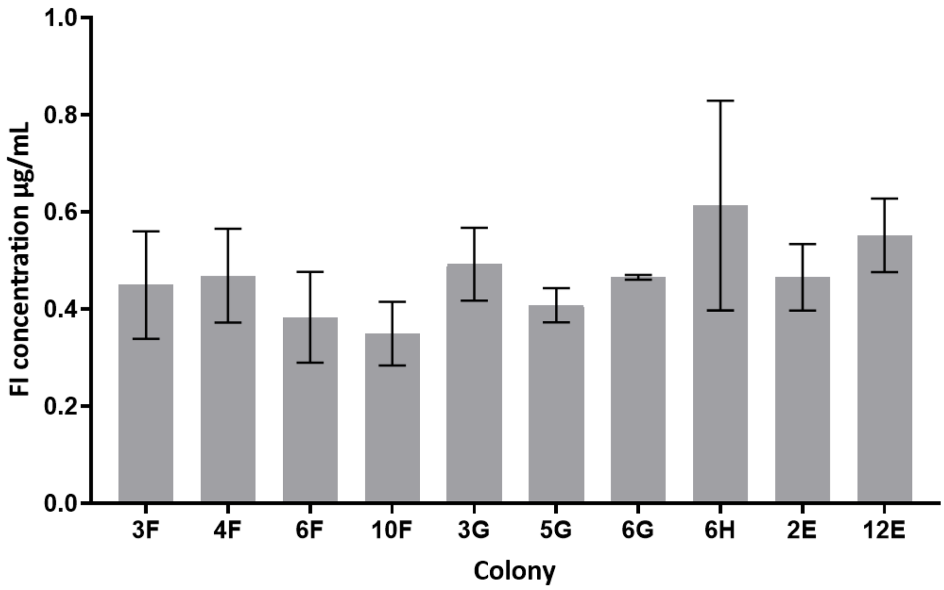

Figure 3-22 FI titre from the stable transfection of CHO cells with pDEF-*CFI* vector as determined by ELISA. ELISA for the detection of FI in CHO cell supernatant. Concentrations interpolated from Comptech FI standard curve. Error bars represent standard deviation.

3.3.7. Analysis of recombinant human FI

Recombinant FI was purified from the CHO cell supernatant by affinity chromatography using an OX-21 column, as developed for the purification of FI from plasma. From 1 L of CHO supernatant, 430 µg of recombinant FI was purified, a yield of ~70% the theoretical amount (Figure 3-23). A Western Blot was performed to confirm the identity of the purified protein (Figure 3-24). Under non-reducing conditions, a single band was present at ~88 kDa, consistent with intact FI, whereas under reducing conditions, two bands were observed at approximately 90 kDa and 50 kDa. The band at 50 kDa is attributed to the heavy chain of FI, and the band at 90 kDa was indicative of Pro-I. This demonstrated that recombinant FI could be successfully generated using the pDEF-*CFI* vector, albeit with some Pro-I contamination.

To ensure that the purified recombinant FI maintained its C3b cleavage ability, a fluid-phase cofactor assay was performed, and the breakdown products run on an SDS PAGE (Figure 3-25). After 5 minutes incubation, it was clear that the FI maintained its functional activity as indicated by the degradation of the C3b α’ chain, and the presence of the α1 and the two α2 chains. With prolonged incubation, the presence of the C3b α’ chain continued to decrease, demonstrating that the recombinant protein maintained its enzymatic activity.

To determine the extent of the C3b α’ chain cleavage, densitometry was performed (Figure 3-26). It was clear that the majority of the C3b α’ chain cleavage occurred in the first 5 minutes, with the amount of C3b α' chain remaining plateauing after ~30 minutes. These results confirmed that recombinant FI was functionally active and could therefore be used as a surrogate for assessment of plasma purified FI and for the characterisation of rare genetic variants of *CFI*.

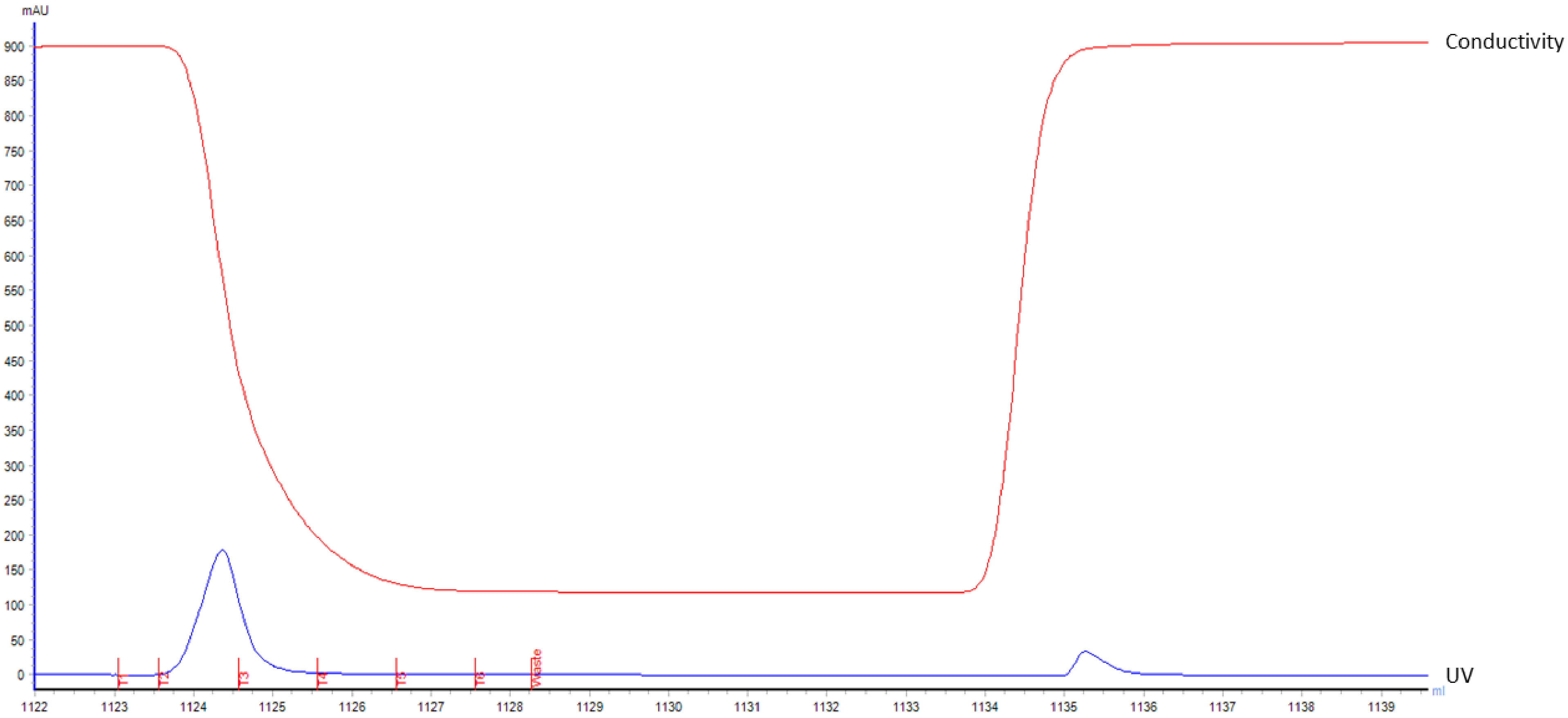

Figure 3-23 UV trace obtained during the purification of recombinant FI using the pDEF-*CFI* vector.
Example UV trace obtained during recombinant Factor I elution from supernatant with 0.1 M Glycine (pH 2.7) from an OX-21 column.

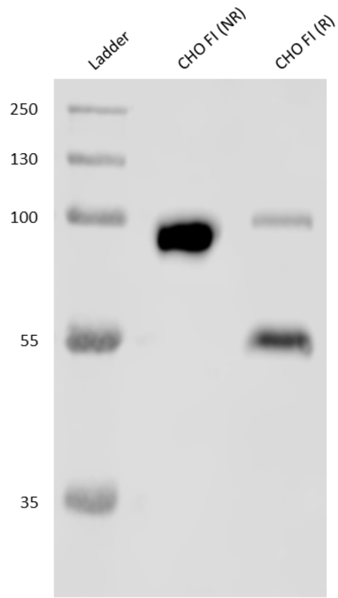

Figure 3-24 Western blot of recombinant FI purified by affinity chromatography using an OX-21 column.
Western Blot showing purified recombinant (CHO) produced Factor I detected with sheep polyclonal anti-human Factor I. In the non-reduced (NR) lane, there is one band at 88 kDa and in the reduced lane (R), there are two bands at 88 kDa and 50 kDa, for pro-I and the FI heavy chain respectively.

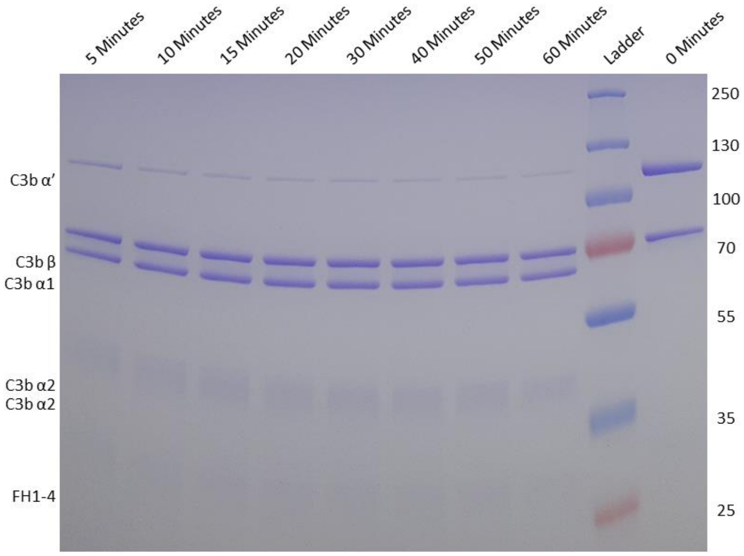

Figure 3-25 SDS PAGE visualisation of the fluid-phase cofactor (FH1-4) activity of recombinant (CHO) FI, over time.
SDS PAGE showing proteolytic activity of recombinant FI across a range of timepoints (5 – 60 minutes). Activity assessed by the ability of Factor I in combination with its cofactor FH1-4, to cleave C3b to its inactive form iC3b. C3b cleavage was indicated by the appearance of α1 and the two α2 bands. All samples were ran under reducing conditions with a PageRuler Prestained Protein ladder (10 – 250 kDa).

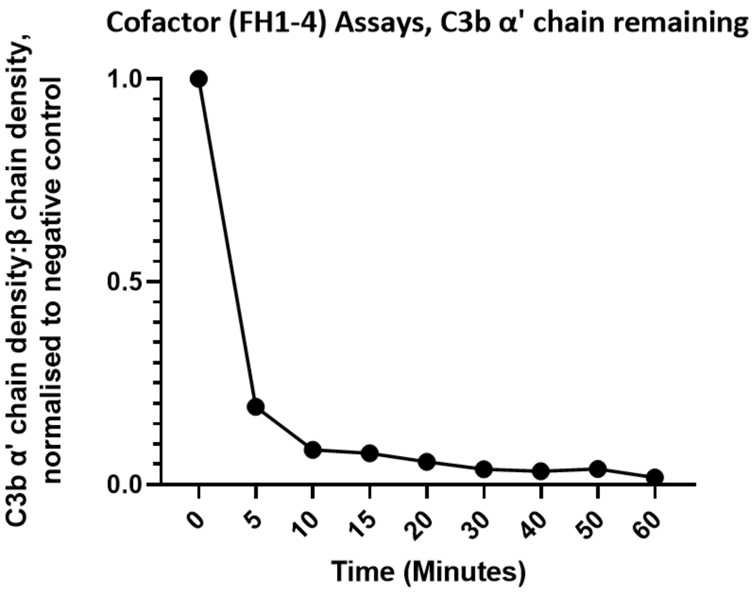

Figure 3-26 C3b α’ chain degradation analysis of the FH1-4 cofactor assay for recombinant (CHO) FI, over time.
Plotted is the density of C3b α’ chain remaining (y-axis) after incubation of recombinant purified FI with C3b and FH over a duration of 60 mins at 37°C during a fluid-phase cofactor assay. Each point represents the reaction at a different timepoint. The density of the α’ chain band was normalised to the density of the β chain band, before the resultant figure was normalised to a negative control containing no FI, giving a proportion of α’ chain remaining compared to the no FI control.

3.4. Discussion

3.4.1. CFI Variant Analysis

From the initial eight variants identified in Kavanagh *et al* (2015), three will be generated for further functional analysis. Of the chosen three, only R406H (R388H without the leader sequence) had undergone previous functional analysis before the start of this project. In this previous assessment, the R406H polymorphism performed comparably to WT with respect to both C3b and C4b degradation (Kavanagh *et al.*, 2008). Despite this finding, R406H was of interest for further interrogation due to its conflicting Polyphen-2 (possibly damaging) and CADD scores (benign), location within the TMC, and association with reduced disease burden (OR = 0.10) irrespective of a possible reduction in activity. The R406H change itself involves the substitution of a longer linear amino acid, to a ringed aromatic. Whilst both amino acids are classed as polar, the pK_a of Arginine is ~12, and is therefore always protonated at physiological pH, whereas the Histidine has a pK_a of ~6.5, and can therefore vary within the extracellular environment, shifting from protonated to neutral at a higher pH (Schönichen *et al.*, 2013). Due to this increase in pH sensing caused by the variant, this may lead to alterations in FI function at areas of high metabolic activity such as the retina (Yang *et al.*, 2005) or the kidney (Hamm, Nakhoul and Hering-Smith, 2015) as a result of protonation at a lower environmental pH leading to structural changes (Nordlund *et al.*, 2003). As demonstrated in Figures 3-2 and 3-3, the R406H mutation is located at the binding interface between FI and FH within the AP TMC, with a direct contact between residue R406 in FI, and E123 in FH (Xue *et al.*, 2017; Geerlings *et al.*, 2018). Since the arginine is directly involved in this interaction, it is hypothesised that the introduction of a histidine at this position will alter binding between FI and FH within the FH:C3b complex due to increased pH sensing, resulting in structural and charge changes that impact FI activity depending on the environmental pH.

In contrast to R406H, there were no prior studies assessing the functional significance of the rare variants P553S or K441R. From the *in silico* analysis, PolyPhen-2 predicted the impact of both variants to be benign, whereas the CADD score of the three selected variants identified P553S as the only one to be considered as deleterious. The P553S mutation involves changing a small nitrogen-containing ring (proline) for a small polar uncharged amino acid (serine). Whilst both amino acids are similar in size, they differ in conformation as proline is the only amino acid where the side chain is connected to the protein backbone at two positions. This conformation makes the amino acid structurally rigid and prevents the adoption of multiple conformations. Serine, on the other hand, is adaptable due to its small size and is typically well tolerated if switched for other small polar amino acids. Despite these fundamental differences in structure, serine may mimic proline through the formation of a hydrogen bond between the reactive hydroxyl group and the protein backbone (Betts and Russell, 2003), potentially reducing the impact of this mutation, which may account for the benign prediction by PolyPhen-2. Residue P553 is also neither involved with the substrate binding interface or the cofactor binding interface, but is instead located in the activation loop in close proximity to the catalytic triad (Geerlings *et al.*, 2018; Java *et al.*, 2019). Due to this proximity, it is therefore hypothesised that P553S mutation is deleterious through an alteration in the conformation of the activation loop which impacts substrate binding to the FI active site.

In silico analysis predicted the K441R mutation to be the least impactful, with a CADD score of 0.001 and a PolyPhen-2 classification of benign. With regards to the K441R amino acid change, a positively charged basic amino acid (lysine) is substituted for a positively charged basic amino acid (arginine). Whilst similar in pK_a, ~10.5 vs ~12.5, the guanidinium group of arginine enables an increase in the possible number of electrostatic interactions, compared to lysine, which can in turn generates more stable ionic interactions (Sokalingam *et al.*, 2012). As visualised on the AP TMC (Figure 3-2 and 3-3), the K441R mutation occurs at the FH binding interface, with residue K441 directly involved in FH binding through N136 (Xue *et al.*, 2017; Geerlings *et al.*, 2018). It is therefore hypothesised that this mutation may impact FI activity by modifying the enzyme-cofactor interaction through additional hydrogen bonding with FH. Additionally, an increase in binding affinity for FH may result in a reduction of free FH for decay of the C3 convertase through decay accelerating activity (Weiler *et al.*, 1976) which may also contribute to a reduction in complement regulation in individuals with this FI mutation.

Overall, the primary driver for the analysis of each of the selected variants was their recurrence in a variety of AMD patient cohorts. R406H, P553S and K441R were identified in 5 distinct cohorts (Seddon *et al.*, 2013; Kavanagh *et al.*, 2015; Tan *et al.*, 2017; Geerlings *et al.*, 2018; Hallam *et al.*, 2020), with K441R also identified in an additional cohort (Shoshany *et al.*, 2019). To add further support to the potential pathogenic role of these variants, they have also been identified in patients with other diseases of complement dysregulation such as aHUS and C3G/ MPGN. R406H was referenced in five papers (Fremeaux-Bacchi *et al.*, 2004; Kavanagh *et al.*, 2008; Zhang *et al.*, 2014; Geerlings *et al.*, 2018; Java *et al.*, 2019), P553S in seven (Fang *et al.*, 2008; Bienaime *et al.*, 2010; Kavanagh *et al.*, 2012; Bresin *et al.*, 2013; Fremeaux-Bacchi *et al.*, 2013; Osborne *et al.*, 2018; Java *et al.*, 2019), and K441R in five (Fremeaux-Bacchi *et al.*, 2004; Caycı *et al.*, 2012; Bresin *et al.*, 2013; Geerlings *et al.*, 2018; Osborne *et al.*, 2018). Due to the common identification of these variants in a variety of cohorts, this provided further weight to the selection of these individual variants for further functional analysis.

3.4.2. Plasma and recombinant FI purification

Through the adaptation of the method developed by Hsiung *et al.* (1982) a simplified method has been devised for the purification of both plasma and recombinant FI. By using an OX-21 column for affinity purification, FI can be purified from either plasma or cell culture supernatant via a two-step or one-step process, producing the protein in a conformationally correct and active form. Whilst the initial yield from human plasma was less than that reported by Hsiung (13.6 mg from 1 L vs 16.7 mg of FI from 700 mL), the resulting product was significantly more pure (Figure 3-16) with no evidence of a contaminating species at ~200 kDa (Hsiung *et al.*, 1982). The plasma purified FI also maintained a similar fluid-phase C3b cleavage activity as Comptech FI, which is generated using conventional techniques (Fearon, 1977; Crossley and Porter, 1980; Morgan, 2000), indicating that the more simplistic method of purification could be utilised without any detriment to downstream functional assessments.

Recombinant production of FI was first described by Wong *et al.* in 1995, where FI was expressed both transiently and stably in both monkey kidney cells (COS-1) and CHO-K1 cells, using a pMT2 expression vector. The recombinant protein was expressed as mixture of Pro-I and mature FI mirroring the results from this project (Figure 3-24). The proportion of Pro-I to FI, varied depending on the cell line used, with the COS-1 cells producing 90% Pro-I, and the CHO-K1 cells producing 50% (Wong *et al.*, 1995). The results shown here, indicate that the proportion of Pro-I to FI was 20% to 80%, respectively. As the function of Pro-I is yet to be established, it is typically cleaved through the use of additional Furin achieved through co-transfection (Wong *et al.*, 1995; Xue *et al.*, 2017; Java *et al.*, 2019), although this can lead to additional proteolysis at R315-R317 (Xue *et al.*, 2017). Efforts to either remove Pro-I or improve Pro-I cleavage will be outlined later in this thesis. The method for recombinant FI purification using an OX-21 affinity column is a novel approach in this project, as all previous iterations have utilised the use of polyhistidine tags for FI purification (Kavanagh *et al.*, 2008; Xue *et al.*, 2017; Java *et al.*, 2019). Whilst His-tag are typically believed not to interfere with the structure or function of the majority of proteins (Gräslund *et al.*, 2008), in some instances their presence can impact both function (Araújo *et al.*, 2000; Thielges *et al.*, 2011; Booth *et al.*, 2018) and structure (Carson *et al.*, 2007), and therefore should be excluded where possible.

3.5. Conclusion

Three rare genetic variants of *CFI* nominally associated with AMD have been identified for further functional analysis. Their selection was based upon occurrence in the literature, *in silico* analysis and structural modelling within the AP TMC. Each of the three variants are secreted and are typically reported within the normal range for serum FI (Kavanagh *et al.*, 2015; de Jong *et al.*, 2020; Hallam *et al.*, 2020). To facilitate the functional analysis of these selected variants, a method for FI purification was devised based upon the purification of FI from human plasma. Using an OX-21 affinity column and gel filtration, human FI was purified with high purity and functional activity comparable to that of FI purified by conventional methods. Recombinant FI was generated using a pDEF-*CFI* vector for expression in CHO cells. The vector was modified to remove an incorporated polyhistidine tag as an OX-21 column could be utilised for both plasma and recombinant FI purification. The purified protein showed no evidence of aggregation or degradation, with the expected Pro-I present as the only contaminant. The recombinant protein was functionally active and cleaved the α’ chain of C3b into both α1 and the two α2 chains in the presence of FH CCP1-4. Despite the confirmed cofactor activity of the recombinant FI, Pro-I contamination was still present. Prior to the functional analysis of the three selected variants, this issue of Pro-I contamination must be addressed as its presence may mask subtle differences in activity between R406H, K441R, P553S and WT FI, leading to their incorrect classification, which is key for elucidating the role they may play in the pathogenesis of AMD.

Chapter 4. Monoclonal Antibody Generation

4.1. Introduction

Previous evidence has suggested that Pro-I is an inactive form of FI, however this has never been proven (Kavanagh *et al.*, 2008; Wong *et al.*, 1995). Due to the similarities between Pro-I and FI, Pro-I may either act as another regulator of complement or could function as a complement activator by binding to the C3b-cofactor complex, preventing cofactor mediated cleavage. Since the functional role of Pro-I is currently unknown, the generation of an antibody against this precursor protein would not only be useful for the purification and subsequent functional assessment of Pro-I but would also facilitate easy removal of Pro-I contamination from recombinant preparations. Further, the generation of an antibody would enable the measurement of antigenic Pro-I levels in human serum, providing another tool for the analysis of AMD patients, as increased Pro-I could provide a surrogate marker for decreased AP regulation or mask the correct classification of Type 1 *CFI* variants.

Whilst there are numerous mechanisms for generating an antibody, the two most established methods are hybridoma generation and phage display. The production of stable monoclonal antibodies was first described by Köhler and Milstein in 1975 by fusing immortalised myeloma cells with activated B lymphocytes from the spleens of immunised mice, to generate antibody producing hybrid cells, known as hybridomas (Köhler and Milstein, 1975). Phage display on the other hand utilises the screening of synthetic antibody libraries generated using engineered bacteriophages, for the identification antibodies specific to the antigen of interest. Since the initial description of phase display by George P Smith in 1985 (Smith, 1985), this technology has evolved into the production of phages that are capable of displaying a plethora of antibody fragments (McCafferty *et al.*, 1990; Clackson *et al.*, 1991; Hoogenboom *et al.*, 1991) which are used to generate large immune libraries. Screening these libraries has enabled the identification of novel antibodies against antigens of interest that were previously impossible to target due to a lack of immunogenicity or accessibility.

This chapter will describe the attempt to generate an antibody against Pro-I. First, using mouse immunisation and hybridoma formation; and secondly through phage display using an optimised synthetic human combinatorial antibody library (HuCAL PLATINUM (Prassler *et* *al.*, 2011)). Also included is the production and purification of Pro-I, and the generation of an antibody against FI which demonstrates no Pro-I cross-reactivity.

4.2. Aims

- To generate a novel antibody against the precursor form of FI, Pro-I
- To generate a novel antibody against mature FI, without Pro-I cross-reactivity
- Develop a method for the production and purification of Pro-I

4.3. Results

4.3.1. Mouse Monoclonal Antibody Generation

4.3.1.1. Mouse Immunisation

Three mice were immunised with the custom peptides KLH-GVKNRMHIRRKRIVGGKRAQ and GVKNRMHIRRKRIVGGKRAQ-KLH (ThermoScientific) according to the schedule detailed in Methods 2.4.2. Antibody titre was assessed by tail bleed to ensure that there was an increasing immune response towards the peptide antigen (Figures 4-1 and 4-2). When recombinant (CHO) FI was used as an antigen, only mouse 633 demonstrated a notable response (Figure 4-1). As the OD at 450 nm readings were low when using CHO FI, the peptide GVKNRMHIRRKRIVGGKRAQ was also used as an antigen. Using the peptide, a positive signal was achieved for all mice at day 28 (Figure 4-2). Each mouse demonstrated a different response towards the antigen, with 633 and 634 responding more strongly than 638. As there was a trend for increasing antibody titres towards the peptide, the immunisation schedule was continued until day 74, when the mice were sacrificed. Following sacrifice, the serum obtained by cardiac puncture was used to compare the response against either the RRKR peptide or mature FI (Comptech) (Figure 4-3). All immunised serum demonstrated a response towards the peptide, with 633 producing the greatest signal. Both 633 and 638 demonstrated a significant response to the peptide compared to mature FI ($P = 3.2 \times 10^{-4}$ and $P = 2.6 \times 10^{-3}$, respectively), whereas 634 showed no difference. Interestingly, 633 also exhibited some cross-reactivity for mature FI.

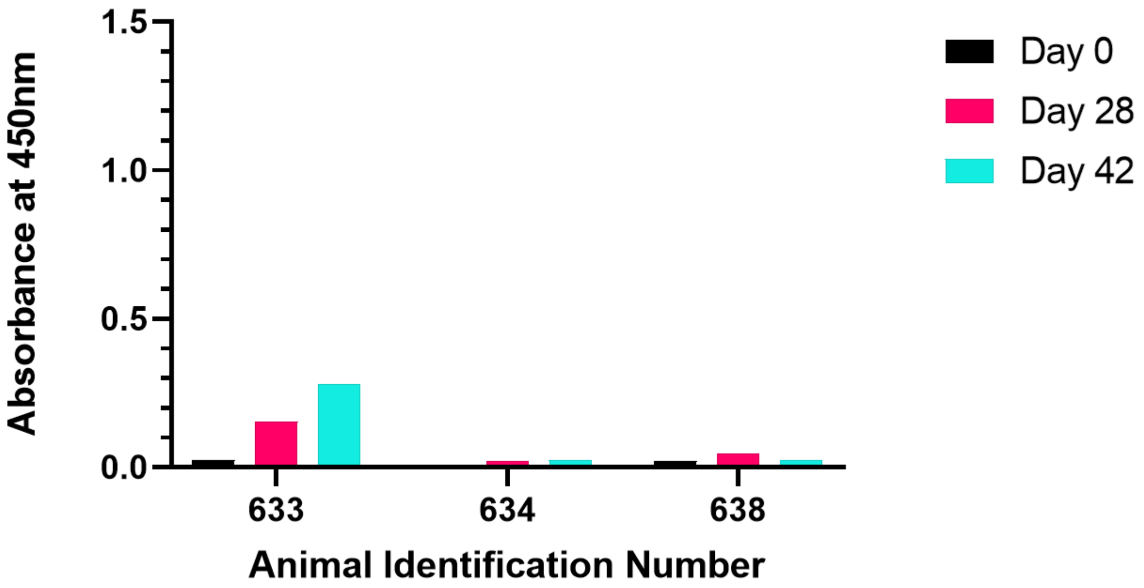

Figure 4-1 ELISA of mouse serum from peptide immunisation captured on recombinant FI.
Three mice (633, 634, 638) were immunised with the custom peptides KLH-GVKNRMHIRRKRIVGGKRAQ and GVKNRMHIRRKRIVGGKRAQ-KLH. Samples from tail bleeds from day 0, 28 and 42 were run on an ELISA, using recombinant (CHO) FI to coat (1 µg/mL).

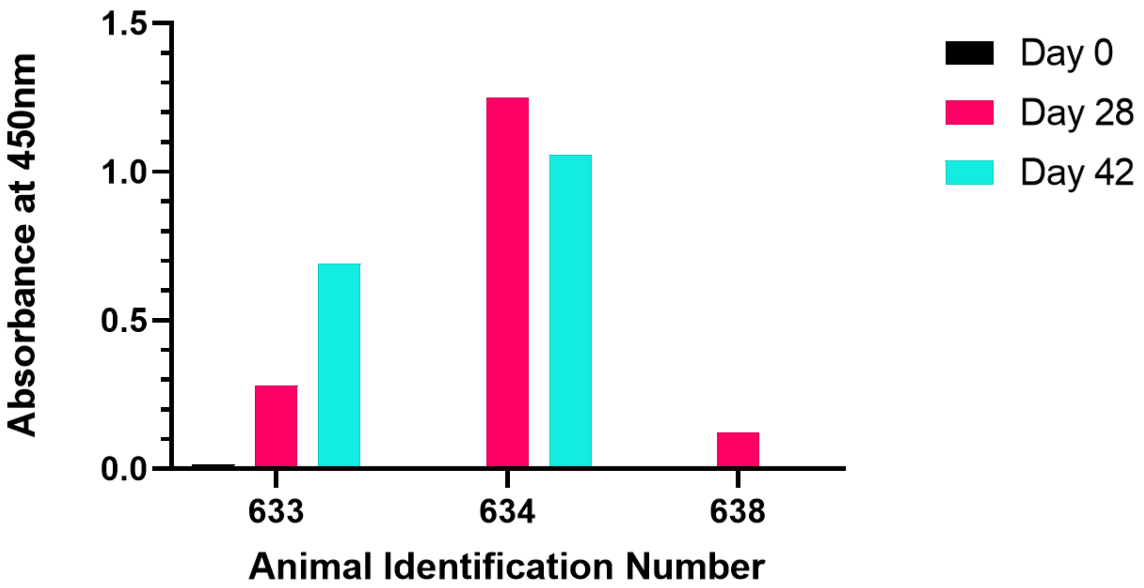

Figure 4-2 ELISA of mouse serum from peptide immunisation captured on peptide without KLH.
Three mice (633, 634, 638) were immunised with the custom peptides KLH-GVKNRMHIRRKRIVGGKRAQ and GVKNRMHIRRKRIVGGKRAQ-KLH. Samples from tail bleeds from day 0, 28 and 42 were run on an ELISA, using non-KLH conjugated peptide to coat (1 µg/mL).

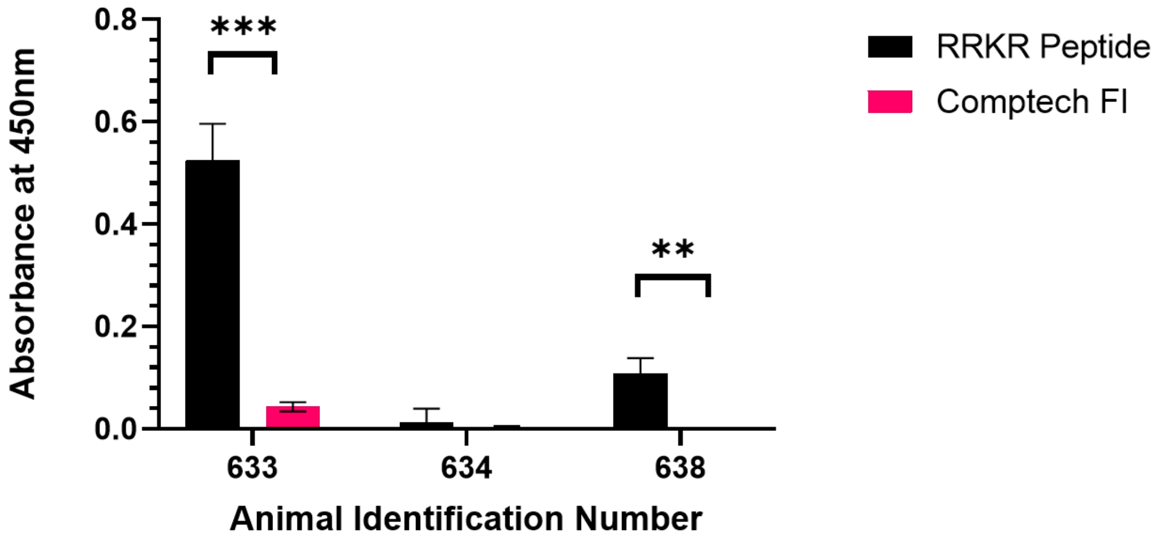

Figure 4-3 ELISA of cardiac puncture serum from peptide immunisation captured on peptide without KLH or recombinant FI coat.
ELISA of serum collected by cardiac puncture from three immunised mice (633, 634, 638) using unconjugated peptide and Comptech FI to compare response. Both capture coats were used at a concentration of 1 µg/mL. To compare the response on each coat an unpaired t test was used. 633 ($P < 0.01$) and 638 ($P < 0.05$).

4.3.1.2. Hybridoma Selection

Following completion of the immunisation schedule, the spleens from each mouse were harvested and the splenocytes isolated for fusion with Sp2/0 myeloma cells to produce hybridomas. After fusion, the cells were cultured for ten days and the supernatant screened for the expression of antibodies against the RRKR peptide (Figure 4-4). Only the fusion of 633 was able to generate viable hybridomas.

As the aim of the immunisation was to generate an antibody specific to the RRKR linker located in Pro-I, the hybridoma supernatant was also screened against mature FI (Comptech) and recombinant (CHO) FI, which contains a proportion of Pro-I (Figure 4-5). Over half of the hybridomas produced an antibody which detected both Comptech and CHO FI. No colony exhibited a response solely against CHO FI, indicating that it was unlikely that an antibody with the desired specificity to Pro-I had been generated. There were however seven colonies which produced a stronger signal on CHO FI compared to Comptech FI, and these where therefore scaled up.

Following expansion, only four colonies continued the expression of antibodies against either Comptech FI or the peptide (Figure 4-6). Of these colonies, only 5A2 and 2G8 continued to demonstrate a preference in binding to the peptide, whereas 1A3 and 2H8 produced a stronger response towards Comptech FI, and 5B2 lost expression completely.

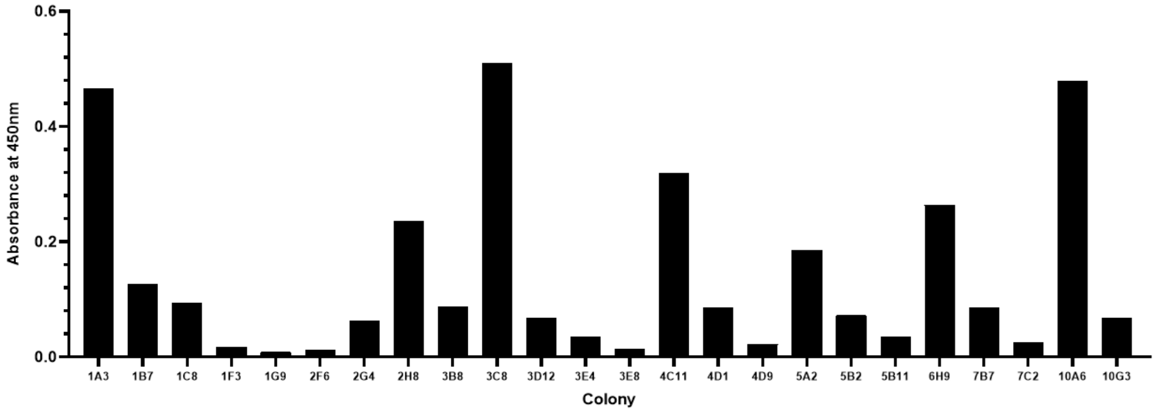

Figure 4-4 ELISA of hybridoma supernatant generated from the peptide immunisation approach captured on peptide without KLH.

ELISA showing hybridoma antibody response towards immunisation peptide without KLH.

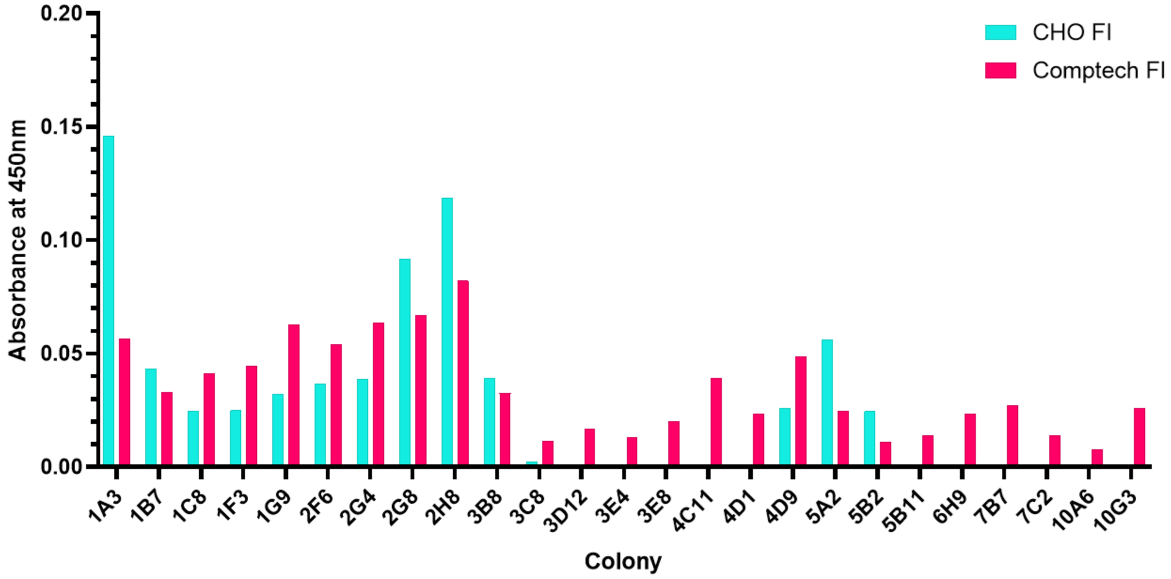

Figure 4-5 ELISA of hybridoma supernatant generated from the peptide immunisation approach captured on either recombinant (CHO) FI or Comptech FI.

Comparison of hybridoma antibody response to CHO FI and Comptech FI as assessed by ELISA. 1A3, 1B7, 2G8, 3B8, 5A2, 5B2, 2H8 colonies show a differential response towards recombinant FI.

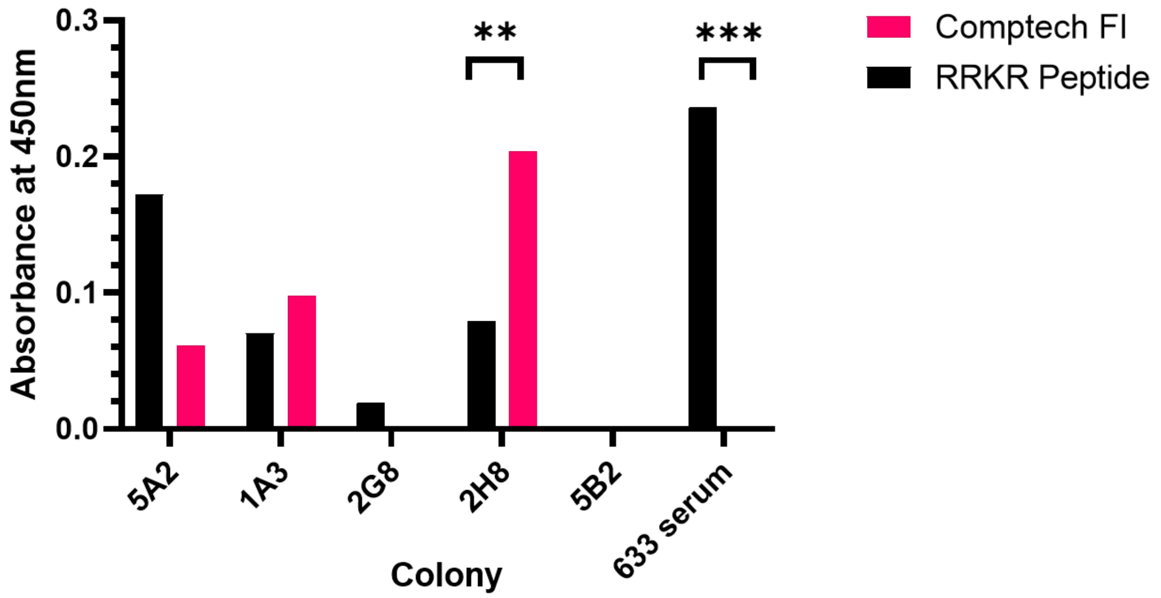

Figure 4-6 ELISA of hybridoma supernatant generated from the peptide immunisation approach captured on either Comptech FI or peptide without KLH.

Comparison of hybridoma antibody response towards unconjugated RRKR peptide and Comptech FI as assessed by ELISA. 5B2 shows no response to either RRKR peptide or FI. 2H8 shows significantly greater ($P < 0.05$) response towards Comptech FI compared to RRKR peptide. 2G8 exhibits a response to RRKR peptide but not Comptech FI. 1A3 shows a response towards both RRKR and Comptech FI. 5A2 shows a greater response towards RRKR peptide than Comptech FI. Immunised polysera from mouse 633 demonstrates a significant response towards the RRKR peptide ($P < 0.01$), and no response to Comptech FI. To compare the response on each coat an unpaired t test was used.

4.3.1.3. Functional Testing

To determine whether 5A2 supernatant could be used to detect the same RRKR region from the peptide in full length Pro-I, a Western Blot was performed. Under both non-reducing and reducing conditions, the supernatant from colony 5A2 was unable to detect the presence of either Pro-I or FI (Figure 4-7A). Due to the peptide specific response ($P = 1.4x10^{-4}$) observed on the ELISA when using the 633 polyclonal antiserum, a Western Blot was also performed. Interestingly, under non-reduced conditions a band at 88 kDa was detected, however under reducing conditions no bands were visualised (Figure 4-7B).

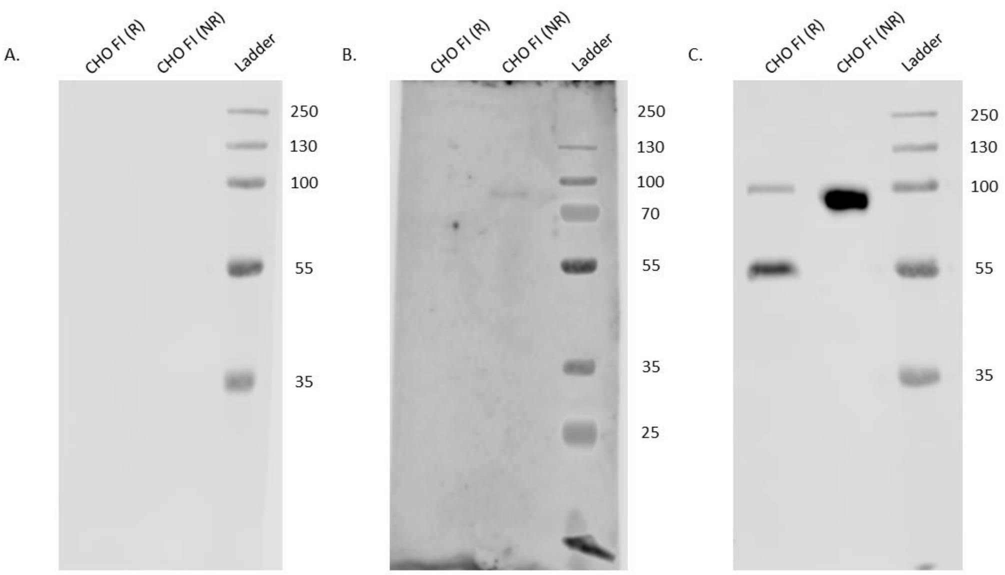

Figure 4-7 Western blot of recombinant (CHO) Factor I detected using either hybridoma supernatant, immunised polysera or sheep polyclonal anti-human FI.

(A) Western blot showing CHO produced FI detected with 5A2 supernatant. (B) Western blot showing CHO produced FI detected using immunised serum from mouse 638. A faint band is detected at 88 kDa under non-reduced conditions. (C) Western blot of CHO produced FI detected with sheep polyclonal anti-human Factor I. In the non-reduced lane, there is one band at 88 kDa, and in the reduced lane, there are two bands at 88 kDa and 50 kDa. Non-reducing conditions (NR), Reducing conditions (R).

4.3.2. Mouse Monoclonal Antibody Generation – Peptide and Recombinant Pro-I

To increase the likelihood of generating an antibody specific to Pro-I, a second group of mice were immunised. However, instead of solely using the KLH conjugated peptide, recombinant (CHO) FI was also included in the immunisation mixture. As recombinant FI is approximately 40% Pro-I, a combination of both the peptide and recombinant FI was utilised with the aim of providing both structural epitopes and sequence specific epitopes.

4.3.2.1. Mouse Immunisation

Four mice were immunised with 0.1 mg of the peptide-protein mixture as outlined in Methods 2.4.3. The antibody titre was regularly checked to monitor the immune response before further immunisation. For each mouse, the antibody titre continued to increase therefore the schedule was continued until the mice were sacrificed on day 74. The largest immune response towards the peptide antigen was seen in mouse 742, with 741 responding the least compared to its baseline (Figure 4-8).

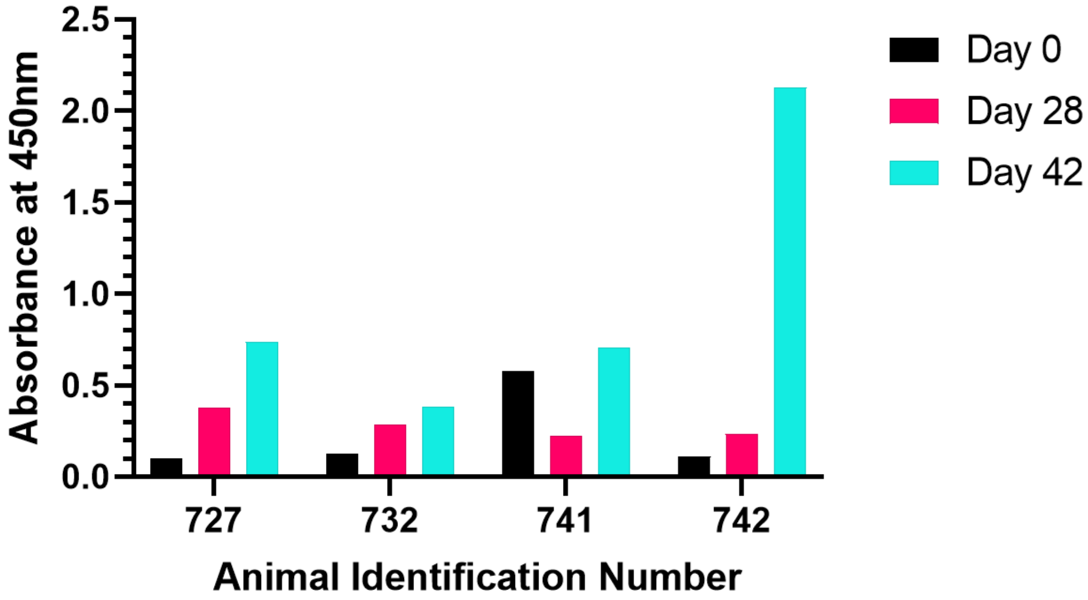

Figure 4-8 ELISA of mouse serum from peptide and recombinant FI immunisation captured on peptide without KLH.

Four mice (727, 732, 741, 742) were immunised with the custom peptides KLH-GVKNRMHIRRKRIVGGKRAQ and GVKNRMHIRRKRIVGGKRAQ-KLH, and recombinant (CHO) FI. Samples from tail bleeds from day 0, 28 and 42 were run on an ELISA, using non-KLH conjugated peptide to coat (1 µg/mL).

4.3.2.2. Hybridoma selection

After splenocyte harvest and Sp2/0 fusion, the generated hybridomas were screened for the presence of antibodies against the RRKR peptide. Figure 4-9 is representative of the response observed on the ELISA from the screening of a 96 well plate. In comparison to the previous attempt at hybridoma generation, the fusions from this round of immunisation produced substantially more positive colonies.

In order to select the hybridomas which produced an antibody specific to Pro-I, the colonies producing an absorbance at 450 nm greater than 0.4 were also screened on Comptech FI. Despite the large number of hybridomas that showed a response towards the peptide, only 1B2 exhibited the desired specificity (Figure 4-10). 1B2 was therefore diluted to monoclonality, whilst undergoing regular screening on both peptide and mature FI.

Interestingly, when diluting the 1B2 colony, in addition to a peptide specific clone D4, a clone demonstrating specificity for FI was also identified, 12E9 (Figure 4-11). This indicated that the initial 1B2 colony was polyclonal despite a lack of FI signal on the ELISA, highlighting the necessity of diluting the cells to monoclonality to obtain a monoclonal population with the desired specificity. With this in mind, both D4 and 12E9 were further diluted with the aim of reaching monoclonality. After two dilutions, a monoclonal population was established for 12E9 and for two D4 clones, D5 and D8 (Figures 4-12, 4-13 and 4-14).

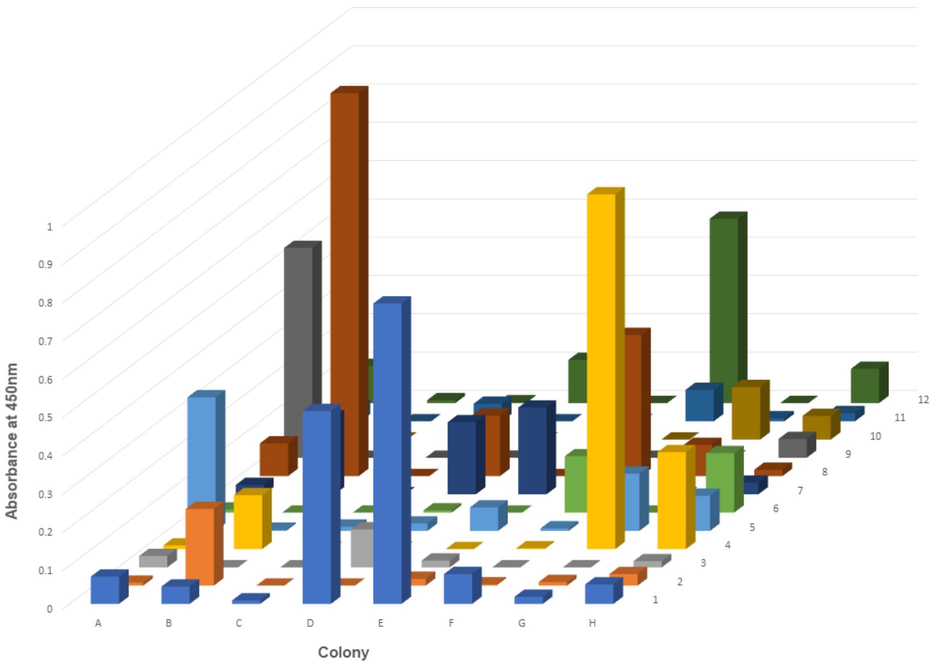

Figure 4-9 Representative hybridoma screening on peptide without KLH. Hybridomas generated from peptide and recombinant FI immunisation.

ELISA showing hybridoma antibody response towards immunisation peptide without KLH.

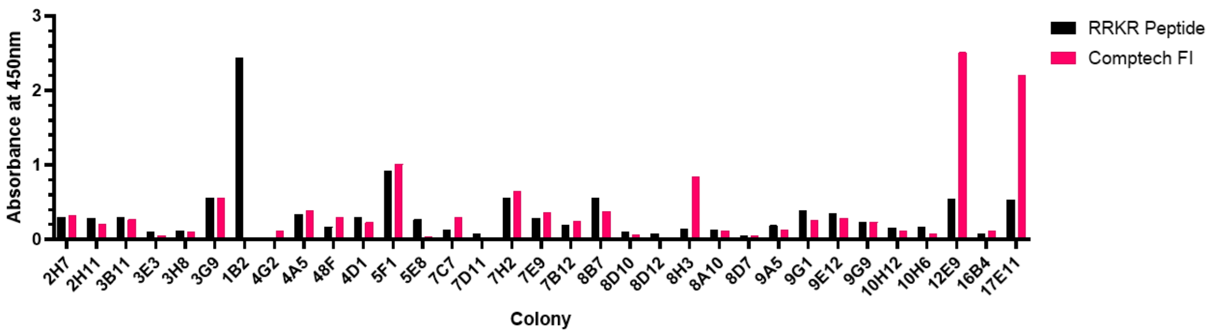

Figure 4-10 ELISA of hybridoma supernatant generated from peptide and recombinant FI immunisation approach captured on either Comptech FI or peptide without KLH.

Comparison of hybridoma antibody response towards unconjugated RRKR peptide and Comptech FI as assessed by ELISA.

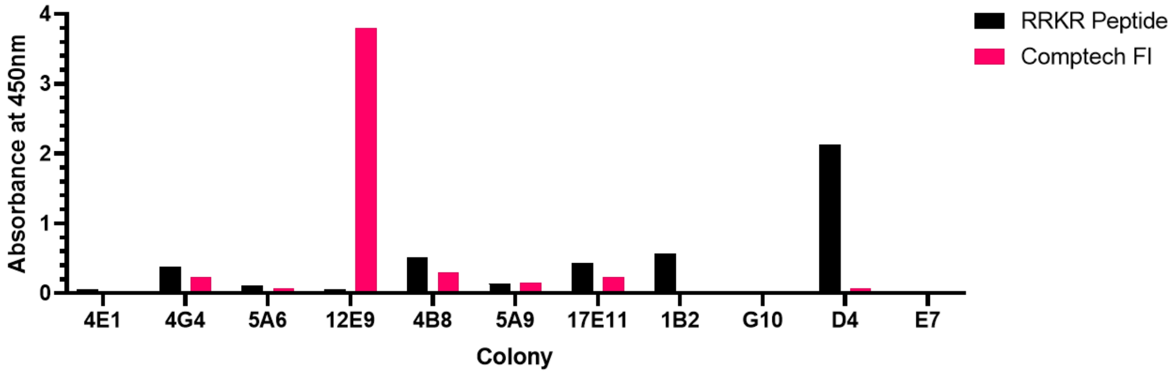

Figure 4-11 ELISA of selected hybridomas supernatant generated from peptide and recombinant FI immunisation approach captured on peptide without KLH or Comptech FI, following limiting dilution.
Comparison of hybridoma antibody response towards unconjugated RRKR peptide and Comptech FI as assessed by ELISA. Colonies 1B2 and D4 demonstrated selective binding for the RRKR peptide and colony 12E9 demonstrated selective binding towards Comptech FI.

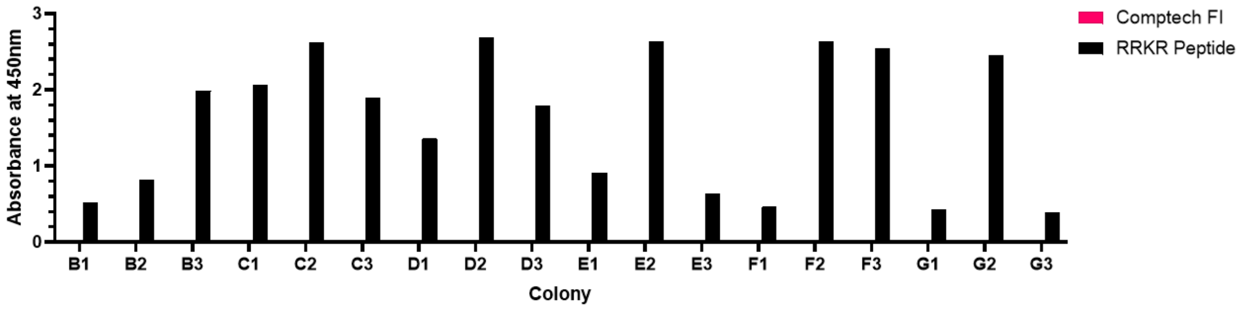

Figure 4-12 Representative ELISA of D5 supernatant to demonstrate monoclonality on peptide or Comptech FI.
Comparison of hybridoma antibody response towards unconjugated RRKR peptide and Comptech FI as assessed by ELISA.

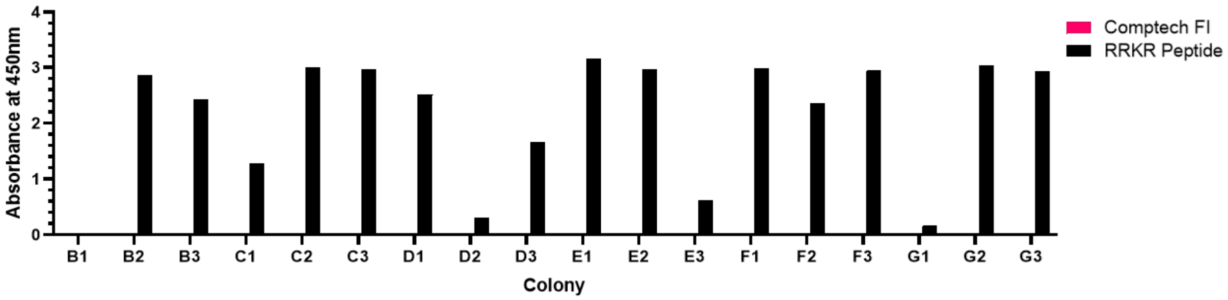

Figure 4-13 Representative ELISA of D8 supernatant to demonstrate monoclonality on peptide or Comptech FI.
Comparison of hybridoma antibody response towards unconjugated RRKR peptide and Comptech FI as assessed by ELISA.

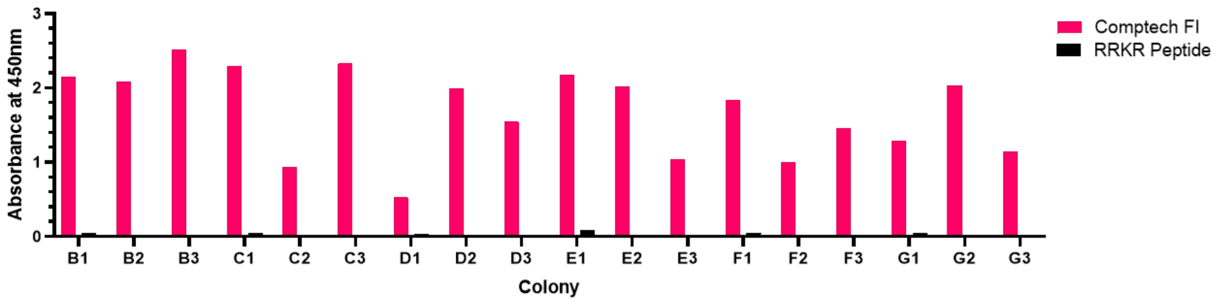

Figure 4-14 Representative ELISA of 12E9 supernatant to demonstrate monoclonality on peptide or Comptech FI.
Comparison of hybridoma antibody response towards unconjugated RRKR peptide and Comptech FI as assessed by ELISA.

4.3.2.3. Antibody Purification

Three hybridomas were selected for purification; D5-C10 and D8-G5 derived from the D4 colony, and 12E9-C11 from the 12E9 colony. These cells were sequentially cultured in flasks increasing in size, until they were transferred to a spinner flask. Prior to transfer, the supernatant was screened by ELISA on recombinant (CHO) FI, Comptech FI and the RRKR peptide (Figure 4-15).

Both D5-C10 and D8-G5 produced a positive signal on the RRKR peptide, with a negligible signal towards both the serum purified and recombinant FI. The lack of a response towards recombinant FI was somewhat surprising as the sample contained approximately 40% Pro-I (Figure 4-7C).

12E9-C11 on the other hand, produced a strong signal on both serum and recombinant FI, and a negligible signal on the peptide. As the response on both forms of FI was equal, this indicated that the targeted epitope was likely shared by both forms of FI, and not located in the region covered by the peptide.

Once the supernatant was harvested, an IsoStrip™ kit was used to determine the class, subclass and light-chain type of the antibodies produced by the hybridomas (Figure 4-16). 12E9-C11 was determined to be an IgG_3 with Kappa light chains. D8-G5 was also identified as an IgG_3 with Kappa light chains (Figure 4-16A). D5-C10 however, was characterised as an IgM with Kappa light chains (Figure 4-16B).

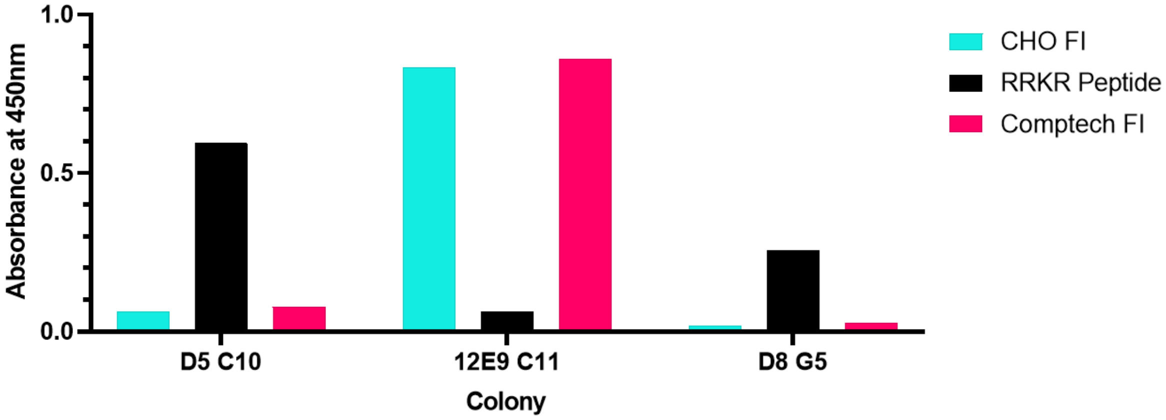

Figure 4-15 ELISA of hybridoma supernatant from T175 flasks on either recombinant (CHO) FI, peptide or Comptech FI.
Comparison of hybridoma antibody response towards unconjugated RRKR peptide, recombinant (CHO) FI and Comptech FI as assessed by ELISA.

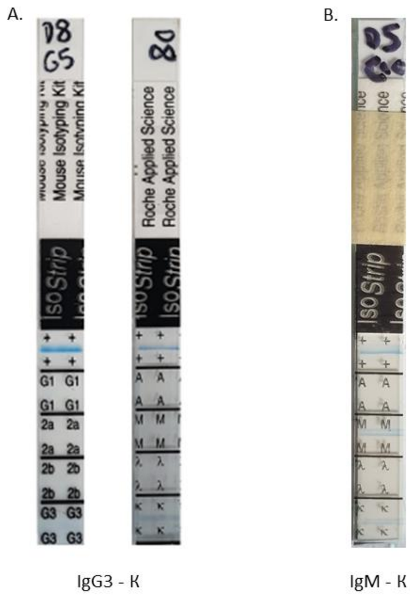

Figure 4-16 IsoStrip antibody characterisation of D8-G5 and D5-C10.
D8-G5 was identified as IgG_3 with Kappa light chains and D5-C10 identified as IgM with Kappa light chains.

4.3.2.3.1. 12E9-C11

The purification of 12E9-C11 was achieved using a Protein G column, yielding 20 mg of antibody from 500 mL of supernatant over multiple runs (Figure 4-17). The resulting antibody was then pooled and assessed by SDS PAGE stained with Coomassie and Western Blotting (Figure 4-18). On the SDS PAGE, a band greater than 250 kDa was visualised in the non-reduced sample, and two bands at approximately 55 and 25 kDa were visible after reduction. Whilst the band at >250 kDa is substantially larger than the predicted size of 170 kDa for an IgG_3 antibody, the bands at 55 and 25 kDa correspond with the expected size of the heavy and light chains, respectively (Figure 4-18A). When detected using an Anti-Mouse

IgG, under non-reducing conditions three bands were observed at ~110, 140 and >250 kDa, and under reducing conditions one band was identified at 55 kDa (Figure 4-18B). The bands at >250 kDa and 55 kDa, align with the results from the Coomassie stained gel, however the bands at ~110 and 140 kDa, indicate degradation or contamination with another subclass of IgG antibody.

To assess whether 12E9-C11 could be used in a Western Blot to specifically detect FI, both Pro-I (Results 4.3.3.1.1) and FI were run on an SDS PAGE gel (Figure 4-19). Under both reducing and non-reducing conditions, no bands for Pro-I were detected (Figure 4-19A). However, when using 12E9-C11 to detect FI, under non-reducing conditions a single band at ~88 kDa was present (Figure 4-19B) and absent on the secondary only control (Figure 4-19C). To determine whether 12E9-C11 was specific for recombinant FI, the antibody was also used to detect FI purified from human plasma (Figure 4-20). Under non-reducing conditions a faint band at approximately 88 kDa was detected in addition to two more bands at 110 and >250 kDa. Under reducing conditions, a single band at 50 kDa was observed when using 12E9-C11 (Figure 4-20B). This demonstrated that 12E9-C11 could also be used to detect human FI, as the bands at 88 and 50 kDa correspond to full length FI, and the FI heavy chain, respectively.

The findings from the Western Blots and the ELISA, indicate that 12E9-C11 is an antibody specific to FI, and can be used on both human and recombinant forms of the protein, under both reducing and non-reducing conditions.

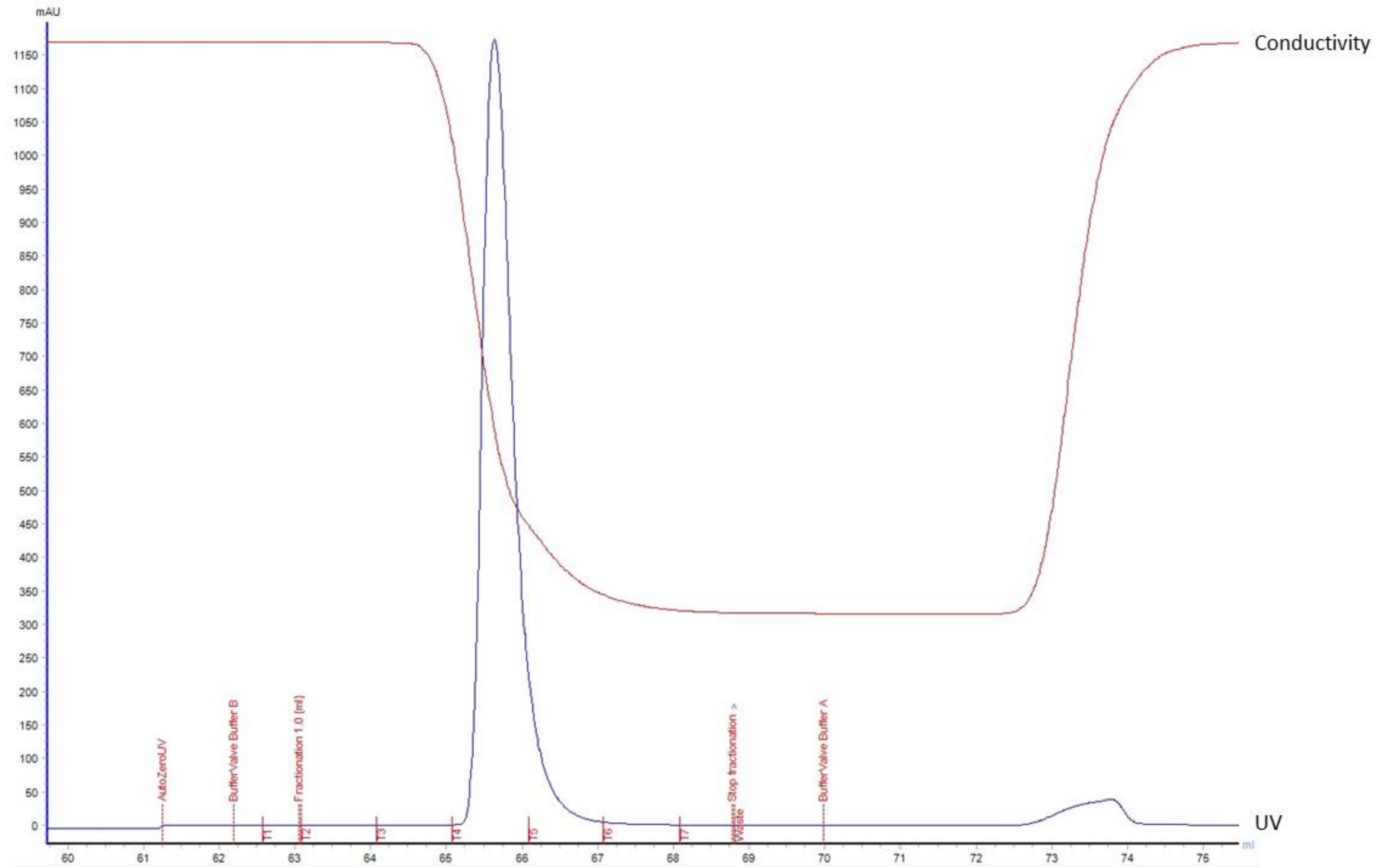

Figure 4-17 Chromatogram of 12E9-C11 purification using Protein G column.

12E9-C11 was purified from cell culture supernatant using the ÄKTA Start protein purification system with a 1 mL HiTrap Protein G HP Column. UV trace produced upon elution of with 0.1 M Glycine, pH 2.7.

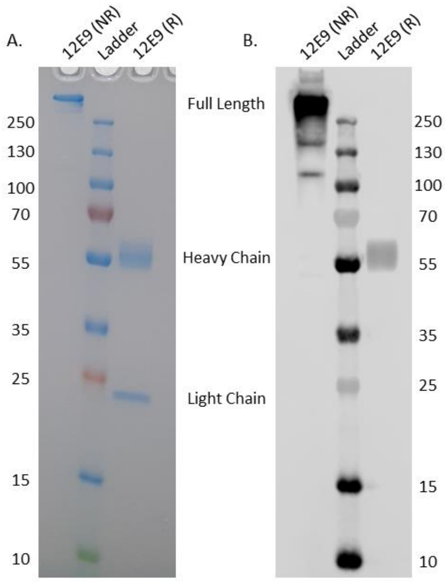

Figure 4-18 SDS PAGE and Western Blot of 12E9-C11.

Purified 12E9 was analysed by SDS PAGE stained with Coomassie Blue and by Western Blot. (A) 12E9 run under non-reduced (NR) and reduced (R) conditions on SDS PAGE. (B) 12E9 run under non-reduced (NR) and reduced (R) conditions detected by Western Blot, using 1 in 1000 dilution of Donkey anti-mouse IgG HRPO.

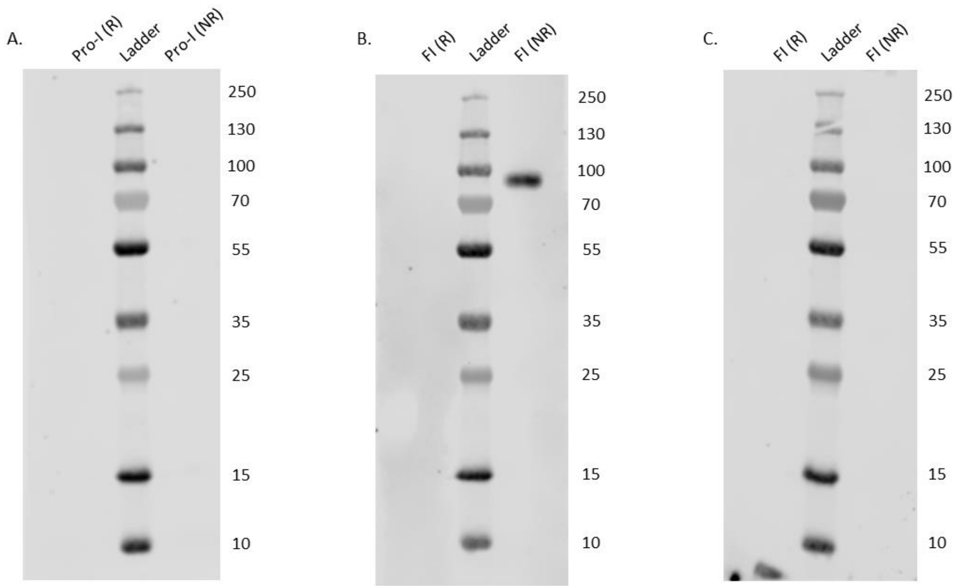

Figure 4-19 Western Blots of Pro-I and Comptech FI detected using 12E9-C11, with secondary only control.

Purified Pro-I and Comptech FI detected using 12E9-C11. (A) Purified Pro-I run under non-reduced (NR) and reduced (R) conditions detected with 12E9-C11 diluted 1 in 500 in 5% Milk-PBST. (B) Purified Comptech FI run under non-reduced (NR) and reduced (R) conditions detected with 12E9-C11 diluted 1 in 500 in 5% Milk-PBST. (C) Purified Comptech FI run under non-reduced (NR) and reduced (R) conditions detected with 1 in 1000 dilution of Donkey anti-mouse IgG HRPO in 5% Milk-PBST.

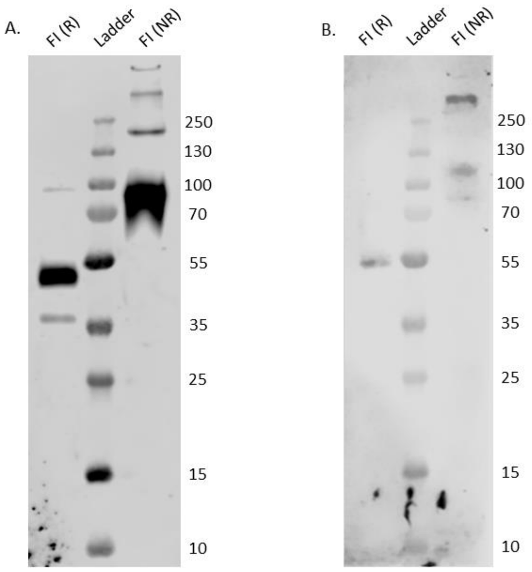

Figure 4-20 Western Blot of serum purified FI detected using either a sheep polyclonal antibody to human FI or 12E9-C11

Serum purified FI (pre-gel filtration) detected using either a sheep polyclonal antibody to human FI or 12E9-C11. (A) Serum purified FI run under non-reduced (NR) and reduced (R) conditions and detected with a sheep polyclonal to human FI diluted 1 in 2000 in 5% Milk-PBST. (B) Serum purified FI run under non-reduced (NR) and reduced (R) conditions detected with 12E9-C11 diluted 1 in 500 in 5% Milk-PBST, with a 1 in 1000 dilution of Donkey anti-mouse IgG HRPO in 5% Milk-PBST as the secondary antibody.

4.3.2.3.2. D8-G5

A Protein G column was also used to purify D8-G5 from the hybridoma supernatant, as it shares the same isotype as 12E9-C11. In contrast to the purification of 12E9-C11, a very low UV peak of 13.3mAU was observed for D8-G5 (Figure 4-21). As a low UV trace is indicative of low protein yield, the purified sample was also assessed by the NanoDrop; which was unable to accurately quantify the protein concentration as it was lower than 0.05 mg/mL.

Despite the low amount purified (48 µg), D8-G5 was used in a Western Blot to determine whether it could be used to detect Pro-I (Figure 4-22). Under both non-reducing and reducing conditions, the antibody was unable to detect Pro-I when used either as a purified protein (Figure 4-22B) or as a supernatant (Figure 4-22C) diluted 1 in 10 in 5% milk PBST.

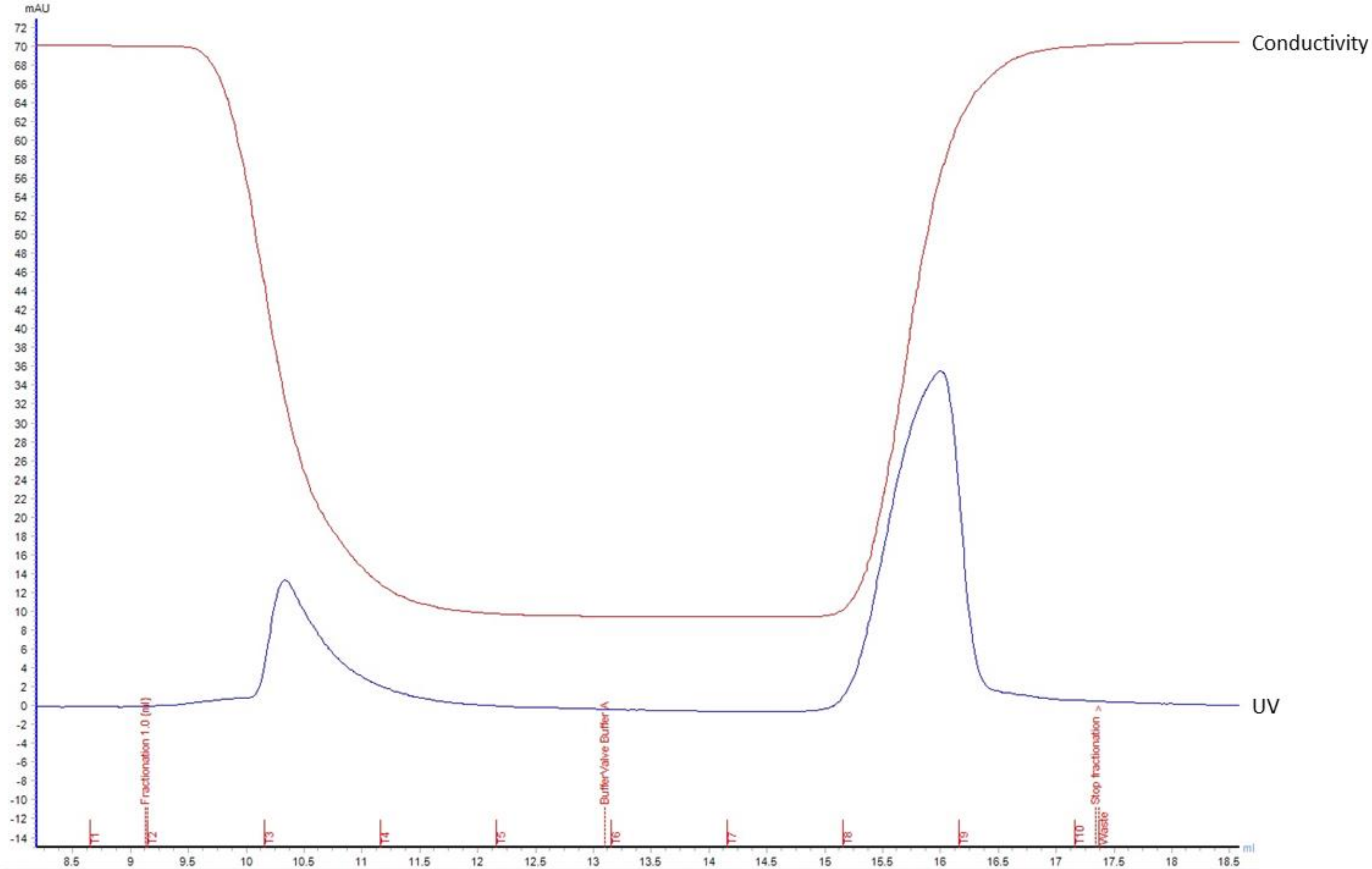

Figure 4-21 Chromatogram of D8-G5 purification using Protein G column.
D8-G5 was purified from cell culture supernatant using the ÄKTA Start protein purification system with a 1 mL HiTrap Protein G HP Column. UV trace produced upon elution of with 0.1 M Glycine, pH 2.7.

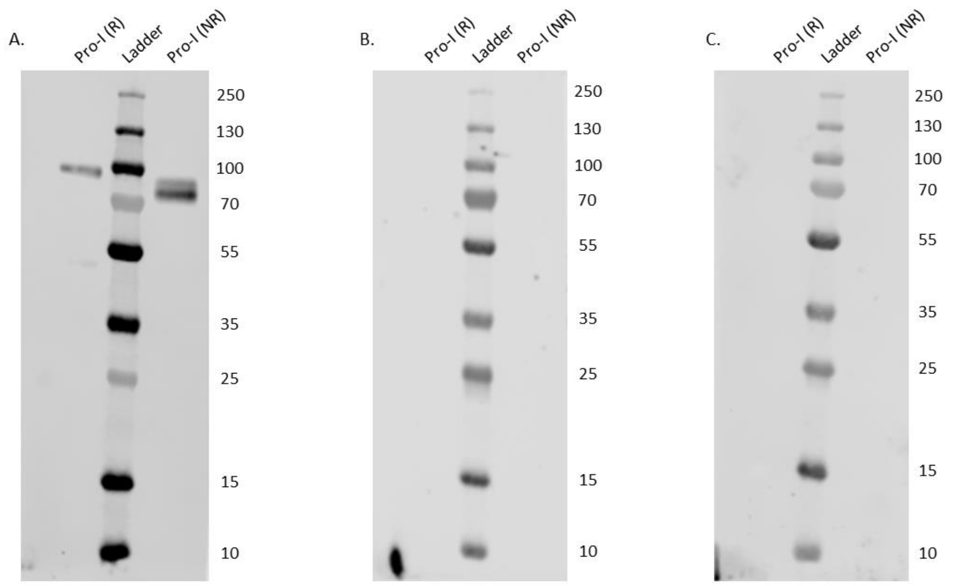

Figure 4-22 Western Blots of purified Pro-I detected using D8-G5 or sheep polyclonal anti-human Factor I.
Purified Pro-I detected using D8-G5. (A) Purified Pro-I run under non-reduced (NR) and reduced (R) conditions detected with sheep polyclonal anti-human Factor I. (B) Purified Pro-I run under non-reduced (NR) and reduced (R) conditions detected with purified D8-G5 diluted 1 in 100 in 5% Milk-PBST. (C) Purified Pro-I run under non-reduced (NR) and reduced (R) conditions detected with D8-G5 diluted 1 in 10 in 5% Milk-PBST.

4.3.2.3.3. D5-10

In contrast to the other two antibodies, D5-C10 is an IgM antibody which binds poorly to Protein G. The purification of this antibody was therefore achieved through the use of a Protein L column, as Protein L will bind mouse Kappa light chains.

It was found that 500 mL of supernatant generated a UV peak of 429.58 mAU, which resulted in a total protein yield of 1.3 mg (Figure 4-23). The purified antibody was assessed by SDS PAGE stained with Coomassie and by Western Blotting (Figure 4-24). On the SDS PAGE under non-reducing conditions there are 3 bands present at approximately 20, 45 and one at greater than 250 kDa, and under reducing conditions there are two bands present at approximately 75 and 23 kDa. The high molecular weight band located at the bottom of the loading well is consistent with non-reduced IgM in either the pentamer (~900 kDa) or hexamer (~1050 kDa) form (Keyt *et al.*, 2020), and the bands at ~20 and 45 kDa could be indicative of contaminants. The two bands present upon reduction are consistent with the expected sizes of the heavy µ chain and for the kappa light chain, respectively (Bornemann *et al.*, 1995). When visualised by Western Blot there is one high molecular weight band under non-reducing conditions and two bands at 75 and 52 kDa, under reducing conditions.

This confirms the high molecular weight band is intact IgM, the band at ~75 kDa is likely the μ heavy chain, and the band at 52 kDa is probably indicative of a small level of contaminating IgG heavy chain, not visible on the SDS PAGE.

To assess whether D5-C10 could be used to detect Pro-I in a Western Blot, both Pro-I and FI were run on an SDS PAGE gel (Figure 4-25). Under both non-reducing and reducing conditions, there was no evidence of D5-C10 binding to either Pro-I (Figure 4-25B, 4-25C) or FI (Figure 4-25D). Further support for the lack of binding was provided by an ELISA where there was no signal towards either FI or Pro-I (Figure 4-26).

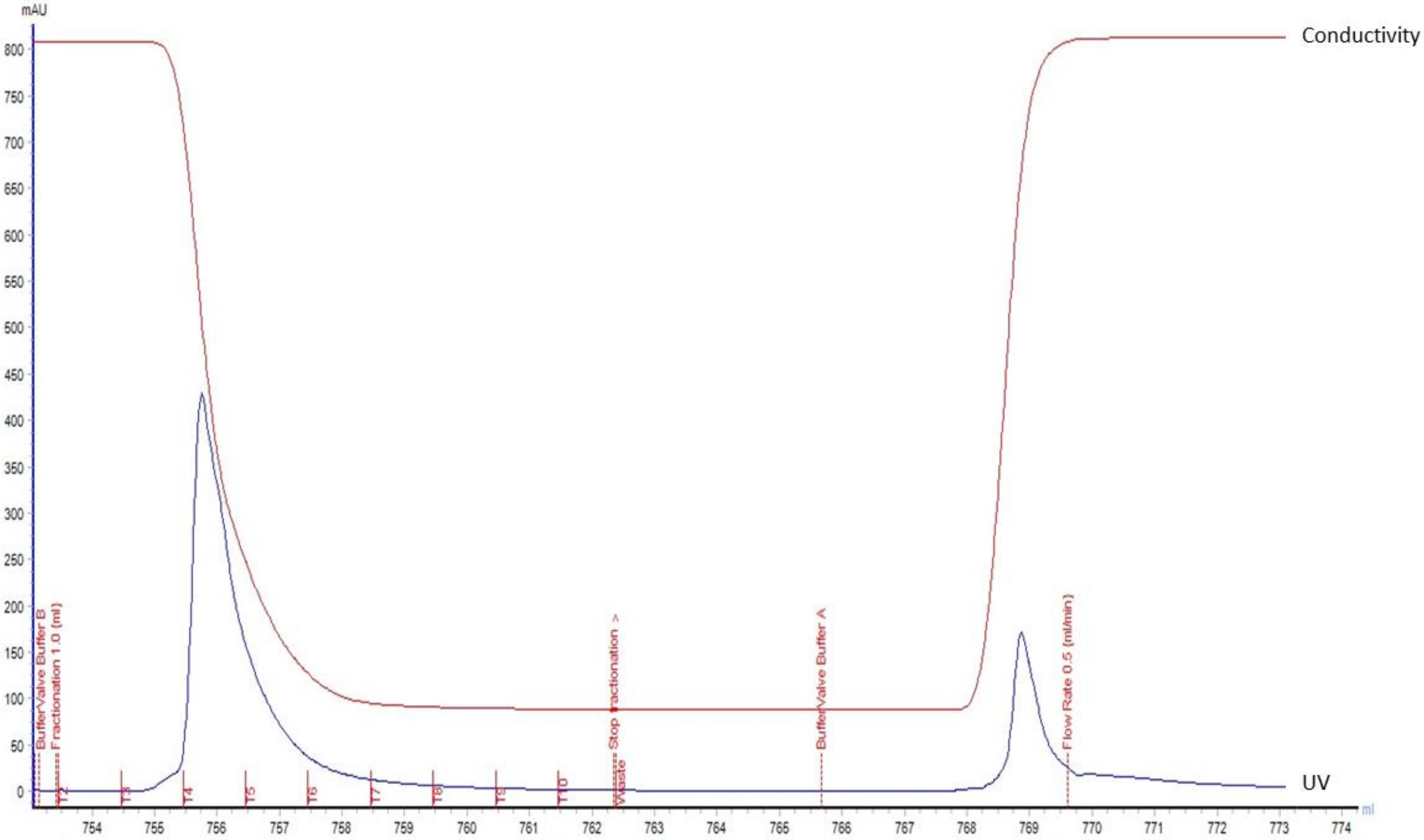

Figure 4-23 Chromatogram of D5-C10 purified using Protein L column

D5-C10 was purified from cell culture supernatant using the ÄKTA Start protein purification system with a 1 mL HiTrap Protein G HP Column. UV trace produced upon elution of with 0.1 M Glycine, pH 2.7.

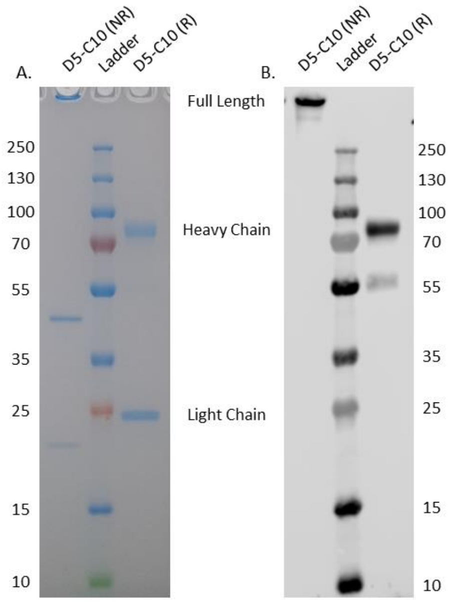

Figure 4-24 SDS PAGE and Western Blot of D5-C10.

Purified D5-C10 was analysed by SDS PAGE stained with Coomassie Blue and by Western Blot. (A) D5-C10 run under non-reduced (NR) and reduced (R) conditions on SDS PAGE. (B) D5-C10 run under non-reduced (NR) and reduced (R) conditions detected by Western Blot, using 1 in 1000 dilution of goat anti-human IgM HRPO.

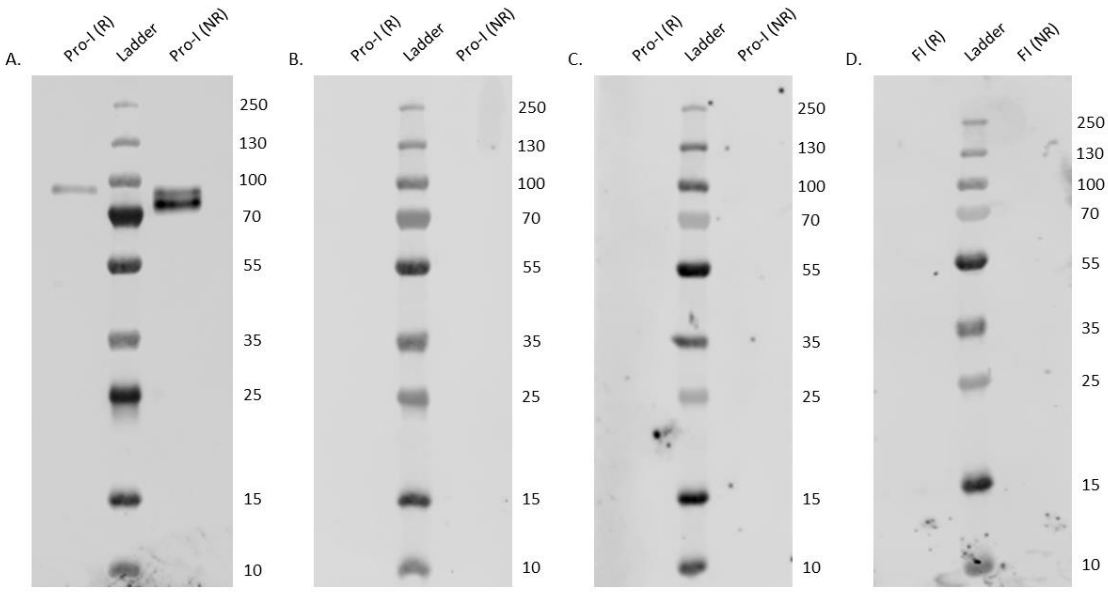

Figure 4-25 Western Blots of purified Pro-I or Comptech FI detected using D5-C10 or sheep polyclonal anti-human Factor I.

Purified Pro-I or Comptech FI was detected using D5-C10. (A) Purified Pro-I run under non-reduced (NR) and reduced (R) conditions detected with sheep polyclonal anti-human Factor I. (B) Purified Pro-I run under non-reduced (NR) and reduced (R) conditions detected with purified D5-C10 diluted 1 in 100 in 5% Milk-PBST with sheep anti-mouse IgG HRPO secondary. (C) Purified Pro-I run under non-reduced (NR) and reduced (R) conditions detected with D5-C10 diluted 1 in 10 in 5% Milk-PBST with goat anti-human IgM HRPO secondary. (D) Comptech run under non-reduced (NR) and reduced (R) conditions detected with D5-C10 diluted 1 in 10 in 5% Milk-PBST and goat anti-human IgM HRPO secondary.

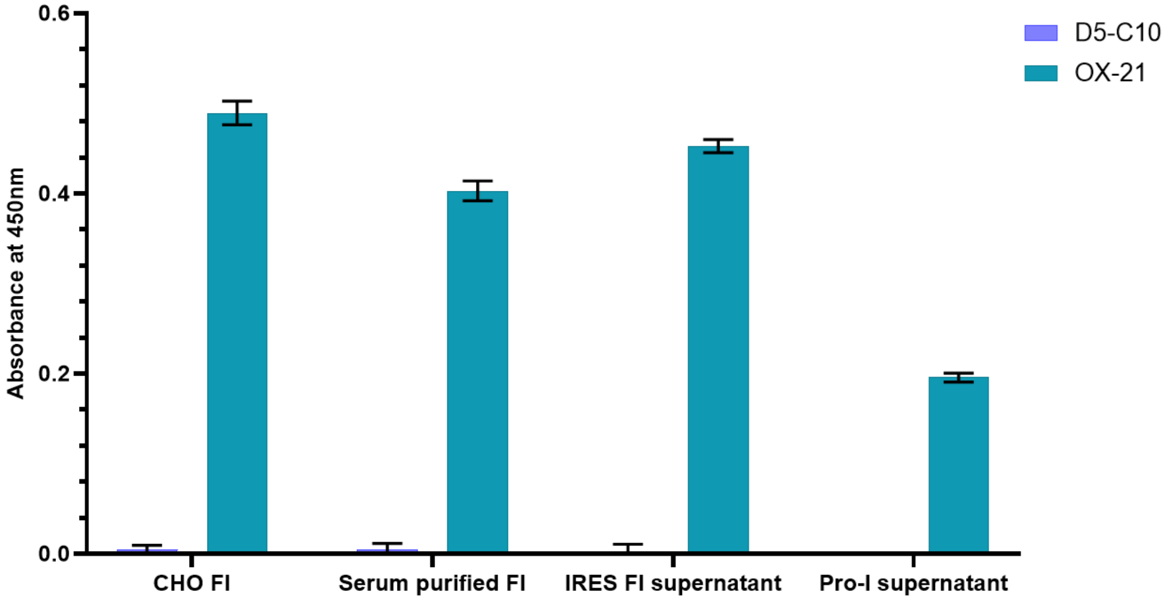

Figure 4-26 ELISA of recombinant (CHO) FI, serum purified FI, IRES FI supernatant or Pro-I supernatant detected using either D5-C10 or OX-21.

ELISA comparing the response of OX-21 or D5-C10 to recombinant (CHO) FI, serum purified FI, IRES FI supernatant or Pro-I supernatant. Error bars show the standard deviation.

4.3.3. Human Combinatorial Antibody Library

Despite the successful generation of an anti-FI antibody, an antibody against Pro-I remained elusive. To circumvent the random antibody specificity associated with *in vivo* antibody production, a more targeted *in vitro* approach was used. We employed the services of Bio-Rad to access their HuCAL PLATINUM system, a second-generation synthetic human Fab antibody library (Prassler *et al.*, 2011). The HuCAL PLATINUM library is constructed from variable heavy chain and variable light chain master genes which are used to reproduce the entire human antibody repertoire. In addition to mimicking naturally occurring antibody formats, six trinucleotide-randomised complementarity-determining regions are also included to provide novel synthetic formats. Using the HuCAL PLATINUM provides several advantages over mouse hybridoma formation, including shortened timelines, increased antibody diversity, optimised antibody design and the ability to target non-immunogenic antigens such as Pro-I (Alfaleh *et al.*, 2020).

Due to the sequence similarities between Pro-I and Factor I, a guided selection package was chosen. This method uses closely related antigens (CRA) to eliminate cross-reacting antibodies through the introduction of the CRAs during the panning process which act to provide a blocking agent. It is this aspect of the screening process which was particularly appealing as it facilitates the selection of antibodies specific to Pro-I only. In order to perform the guided antibody selection, the proteins; FI, the CRA, and Pro-I, the antigen, first had to be generated.

4.3.3.1. Production and Purification of Pro-I

In the first instance, a method for generating Pro-I had to be developed; something which has not been done before. Three methods were considered: one using a Furin inhibitor, one utilising a Furin deficient cell line, and the other using a chromatographic charge-based method.

4.3.3.1.1. Furin Inhibition

To inhibit the proteolytic conversion of Pro-I to FI by Furin, the peptidomimetic inhibitor Decanoyl-Arg-Val-Lys-Arg-Chloromethylketone (decanoyl-RVKR-CMK) was chosen (Henrich *et al.*, 2003; Remacle *et al.*, 2010). CHO cells were transfected with pDEF-*CFI* DNA in the presence of the inhibitor, and the supernatant collected after 96 hours. A concentration between 70-80 µM was used to ensure complete Furin inhibition. The resulting protein was purified from the supernatant using an OX-21 column. From 124 mL of supernatant a UV peak of 65 mAU was produced (Figure 4-27). The peak fractions were combined, buffer exchanged into PBS and concentrated to 500 µL using a 30,000 molecular weight cut-off Vivaspin 6 column. Initially a NanoDrop was used to determine the protein concentration as 55.5 µg/mL, using an extinction coefficient of 101280 $M^{-1}cm^{-1}$. The concentration was subsequently verified by ELISA.

To ascertain whether the purified protein was indeed Pro-I, a Western Blot was performed (Figure 4-28). Under non-reducing conditions, both the purified Pro-I and recombinant FI produced a single band at approximately 88 kDa. However, upon reduction Pro-I generated a single band at approximately 90 kDa, whereas recombinant FI generated two bands, at 90 and 50 kDa respectively. The 90 kDa band observed for both recombinant FI and Pro-I, confirmed the presence of unprocessed FI (Pro-I) in both samples. As there was no 50 kDa band seen in Pro-I upon reduction this indicated that the sample contained no FI contamination and provided compelling evidence that Furin inhibition can be used to generate Pro-I.

Despite the initial success of this method, the low yield and high cost of the inhibitor prevented the use of this method to generate the 0.3 mg of Pro-I required for use in the HuCAL system.

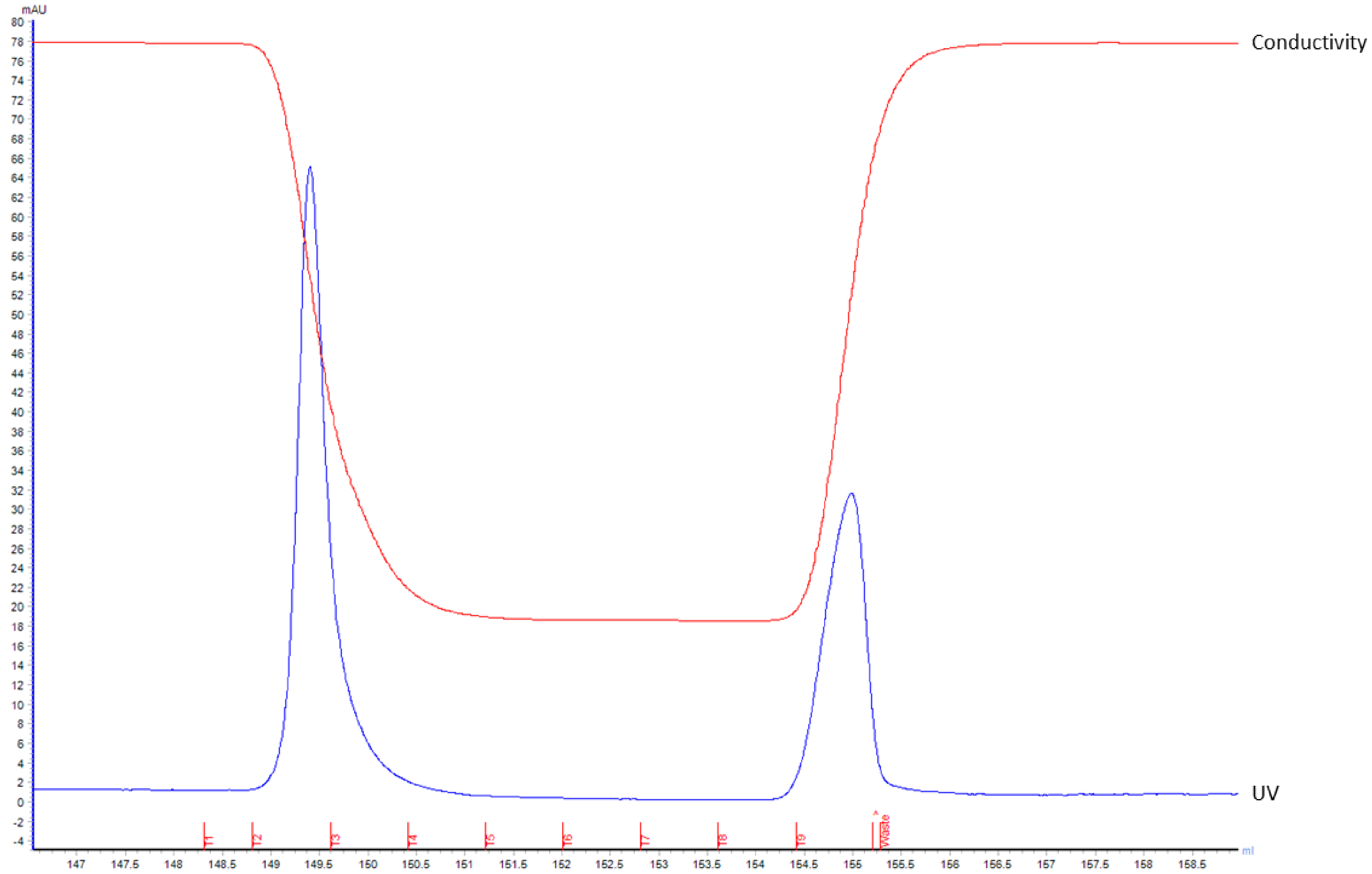

Figure 4-27 Chromatogram of Pro-I purification when using an CMK inhibitor.

Pro-I was purified from cell culture supernatant using the ÄKTA Start protein purification system with a 1 mL OX-21 Column. UV trace produced upon elution of with 0.1 M Glycine, pH 2.7.

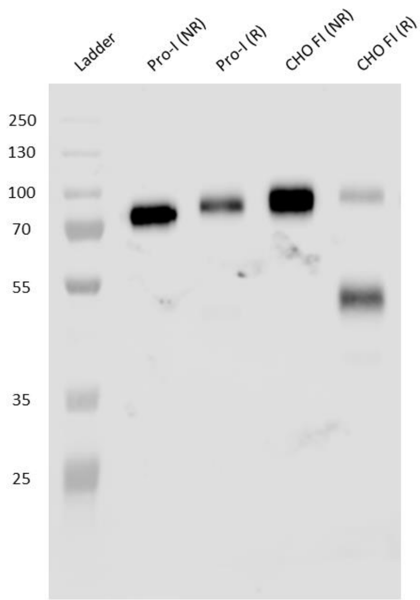

Figure 4-28 Western blot of purified Pro-I and recombinant (CHO) FI generated using an CMK inhibitor.
Western blot of purified Pro-I and recombinant (CHO) FI under non-reducing and reducing conditions. A band at ~90 kDa under both reducing and non-reducing conditions is indicative of Pro-I. Under reducing conditions, a band at 50 kDa is indicative of the FI heavy chain. Detected with sheep polyclonal anti-human Factor I. Non-reducing conditions (NR), Reducing conditions (R).

4.3.3.1.2. Furin Deficient Cell Line

There are several cells lines which have been developed to be Furin-deficient, including the two CHO-K1 derived CHO-FD11 (Gordon *et al.*, 1997) and RPE.40 (Moehring and Moehring, 1983), and the human colon carcinoma cell line, LoVo (Takahashi *et al.*, 1993, 1995). As both CHO-K1 derived cell lines required ethyl methane sulfonate mutagenesis and selection with Pseudomonas Exotoxin A (Gordon *et al.*, 1995), the commercially available LoVo cell line (ATCC® CCL-229™) was instead chosen. In LoVo cells, the Furin protease is inactivated through a frameshift mutation (429FS) within the homo B domain, with an additional mutation of tryptophan to arginine at position 547. Both of these mutant alleles inhibit RRXR processing (where X is any amino acid) by prevention of the autoproteolytic activation of Furin, leading to its retention in the endoplasmic reticulum (Takahashi *et al.*, 1995).

As many cancer types demonstrate increased gene expression particularly in complement regulators such as *CFI* (Roumenina *et al.*, 2019), the LoVo supernatant was first screened for FI and Pro-I expression by ELISA. After six days of culture, there was no significant difference between the supernatant collected from the LoVo cells and the media only control (Figure 4-29), indicating that there was no innate FI or Pro-I expression by this cell line.

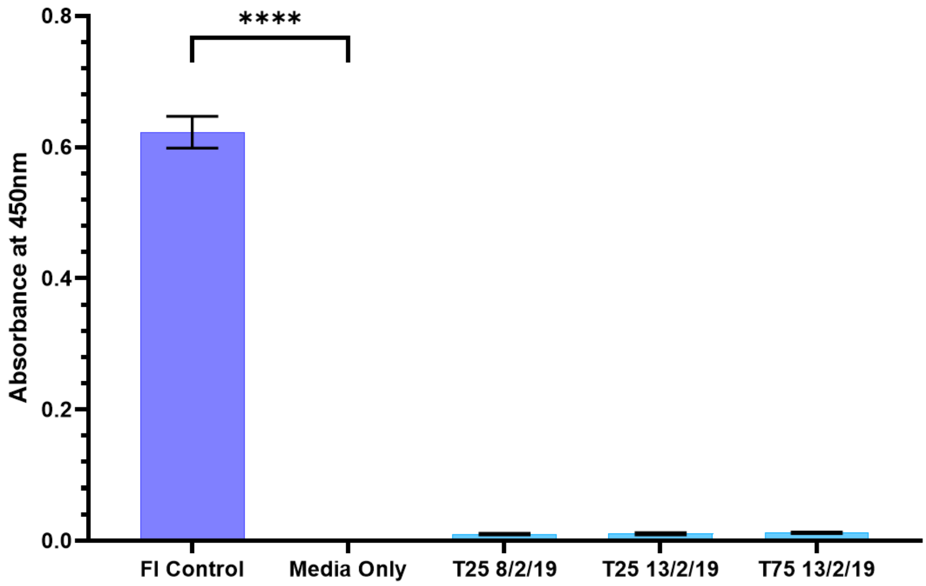

Figure 4-29 ELISA to determine FI production by LoVo cell supernatant.
FI ELISA of LoVo cell supernatant to determine innate FI production. An unpaired t test was used to compare between the FI control and media only. Error bars show the standard deviation.

Following confirmation that the LoVo cells did not secrete either FI or Pro-I, the cells were then transfected with the pDEF-*CFI* plasmid. At 72 hours post transfection, a FI ELISA was performed to determine the transient production of Pro-I (Figure 4-30). There was no significant difference between the transfected cells and the negative controls, indicating an unsuccessful incorporation of the plasmid DNA. These findings remained consistent when the transfection was repeated.

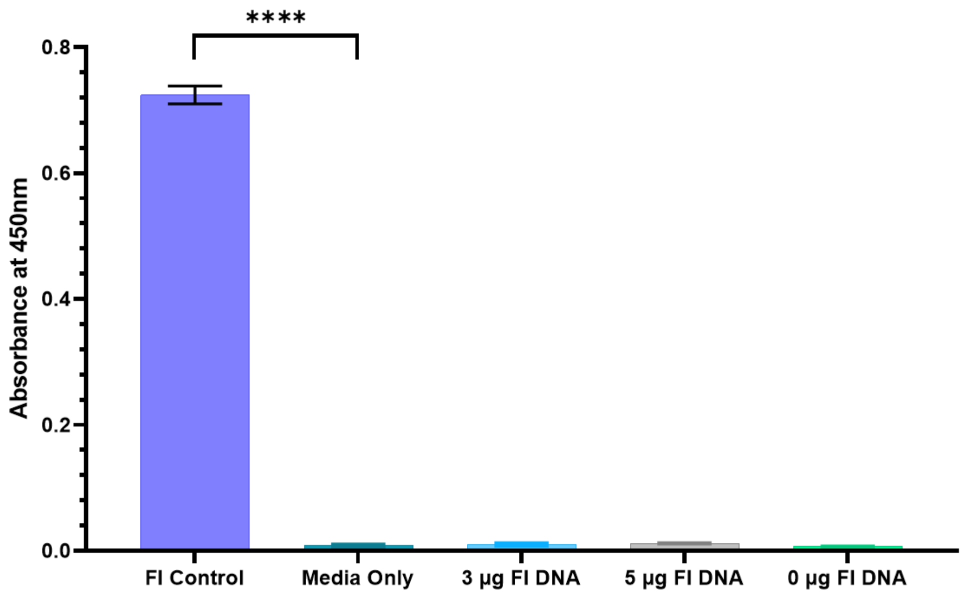

Figure 4-30 ELISA of LoVo cells supernatant following transfection with pDEF-*CFI*.
FI ELISA of LoVo cell supernatant following transfection with pDEF-*CFI*. An unpaired t test was used to compare between the FI control and media only. Error bars show the standard deviation.

4.3.3.1.3. Ion-exchange Chromatography

Regardless of the initial promising results achieved through the use of the Furin inhibitor, a method to generate sufficient Pro-I for the HuCAL and subsequent functional testing remained elusive. As demonstrated by Figure 4-28, recombinant (CHO) FI contains a mixture of both FI and Pro-I, providing an ideal starting point to determine whether these two proteins could be separated based on their biophysical characteristics.

When Furin cleaves Pro-I into FI, the cleavage event leads to the predicted removal of 4 basic ammino acids (RRKR) which in turn leads a difference in isoelectric point (pI) between the two proteins. Prior to removal of the RRKR linker, Pro-I has a theoretical pI of 7.38 and following cleavage the pI of FI decreases to 6.49. This difference in pI can therefore be targeted to facilitate the separation of these two species using ion-exchange chromatography.

4.3.3.1.3.1, Mono Q

Initially a Mono Q 5/50 GL anion exchange chromatography column was used to capture recombinant FI at pH 7 and in 20 mM Tris-HCl buffer. pH 7 was chosen as at this pH, FI would be negatively charged and would therefore bind to the column, whereas Pro-I would be positively charged and therefore be repelled. Following equilibration with the buffer and the recombinant FI, the bound protein was eluted using a 1 M sodium chloride gradient. A single peak of 15 mAU was observed when the conductivity measured 7.41 mS/cm (Figure 4-31).

To determine the identity of the purified species, the peak fractions were run on an SDS PAGE stained with Coomassie under reducing conditions (Figure 4-32). For all peak samples, there were three bands present at approximately 90, 50 and 38 kDa. The band at ~90 kDa is indicative of Pro-I, and the bands at 50 kDa and 38 kDa are representative of the heavy and light chains of FI, respectively. Due to the presence of both species in the purified fractions, this confirmed that Mono Q chromatography was unable to separate Pro-I from FI at this pH.

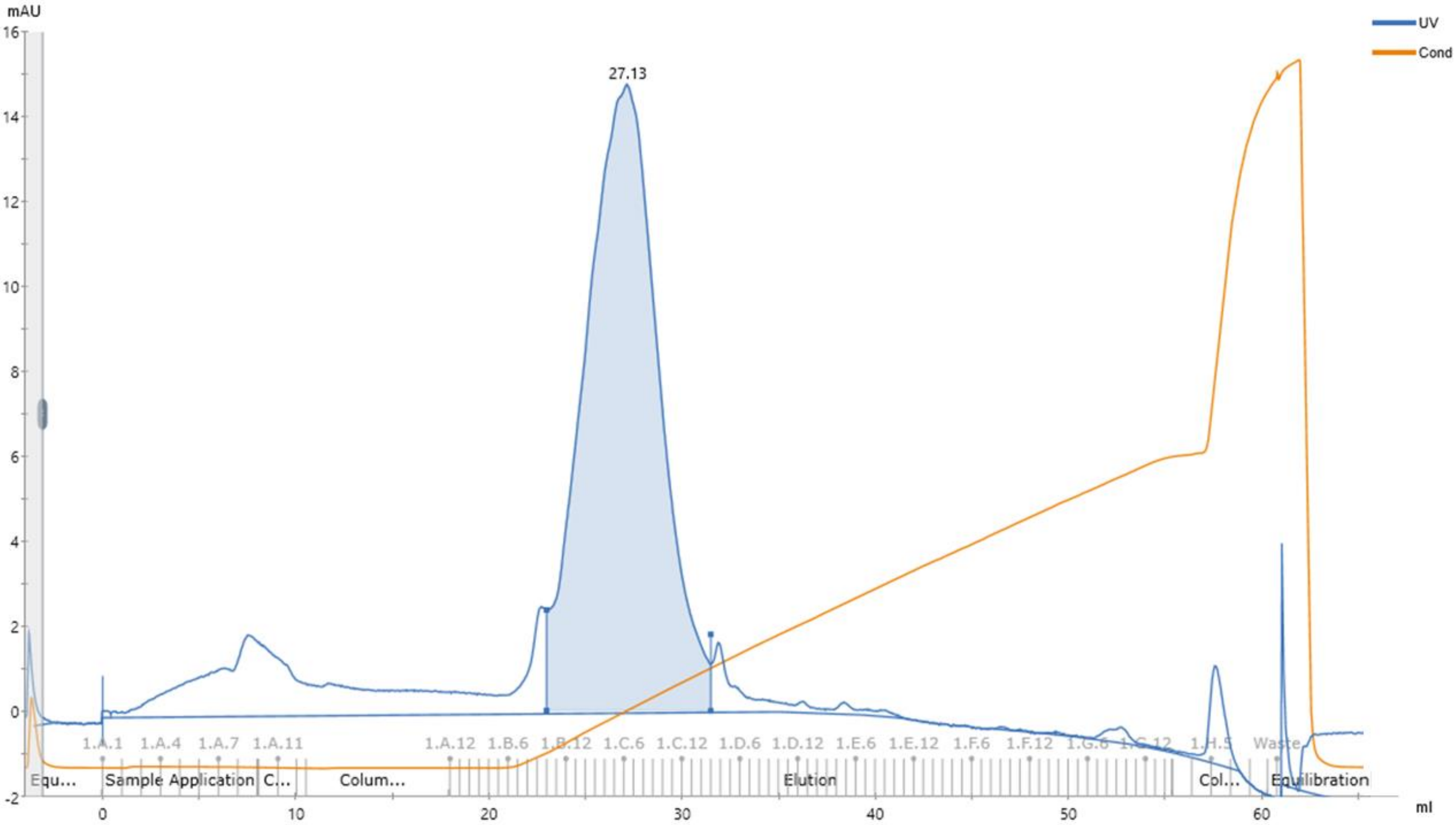

Figure 4-31 Mono Q purification of recombinant (CHO) FI at pH 7.

Chromogram of Mono Q ion-exchange chromatography purification of recombinant (CHO) FI at pH 7.

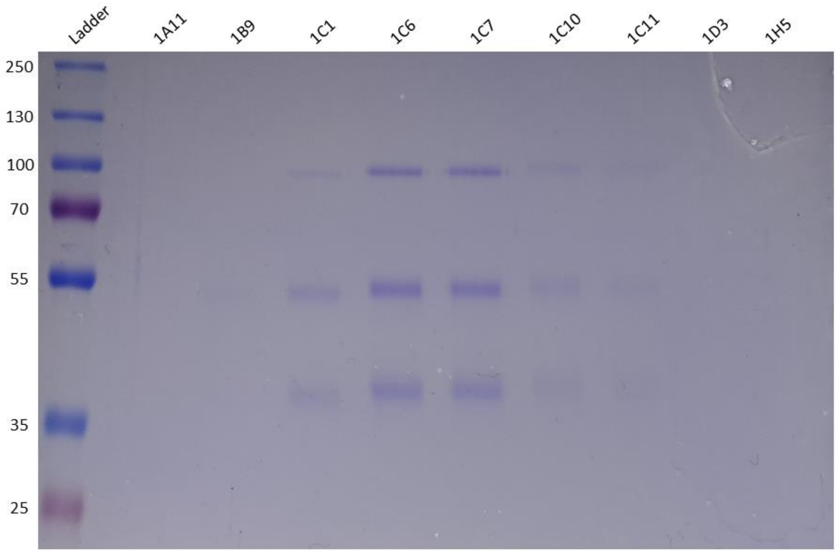

Figure 4-32 SDS PAGE of Mono Q purified recombinant (CHO) FI.
Reducing SDS PAGE of Mono Q peak fraction stained with Coomassie Blue.

4.3.3.1.3.2, Mono S

Due to the equivalent binding of both FI and Pro-I to the Mono Q column, a Mono S 5/50 GL cation exchange chromatography column was used as an alternative. As the Mono S column is negatively charged, a sodium phosphate buffer at pH 6 was used to alter the net charge of both Pro-I and FI to an overall positive charge, to ensure that both species would bind to the column. Following equilibration with the buffer and the recombinant FI, a 1 M NaCl gradient was applied to elute the bound proteins. Two UV peaks were observed, indicating that two species with different isoelectric points had been separated (Figure 4-33). The first peak eluted at a conductivity of 14.2 mS/cm and had a peak mAU of 10, and the second peak eluted at 22.47 mS/cm and had a peak of 3.2 mAU.

To determine the species responsible for the UV peaks, a reducing SDS PAGE was performed and stained with Coomassie (Figure 4-34A). The fractions attributed to the first peak (1C11-1D7) produced two bands at approximately 50 and 38 kDa, indicative of the FI heavy and light chains. The fractions collected from the second peak (1D11-1E8) however, produced one band at approximately 90 kDa, which was likely attributed to Pro-I. To confirm whether cation exchange chromatography was successful at the separation of Pro-I from FI, a Western Blot was also performed (Figure 4-34B). For the fractions attributed to FI, there was no evidence of Pro-I contamination. However, for the fractions attributed to Pro-I, whilst the Western Blot was able to provide confirmation of this species, it also highlighted the presence of a low-level contaminating band at approximately 50 kDa, in all fractions apart from 1E9. The band at ~50 kDa is consistent with the FI heavy chain, and therefore indicated some incomplete separation of Pro-I from FI. Using the densitometry software on ImageStudio, the Pro-I generated using this method was determined to have a purity of 93.7%, which was sufficient to provide the antigen for the HuCAL system.

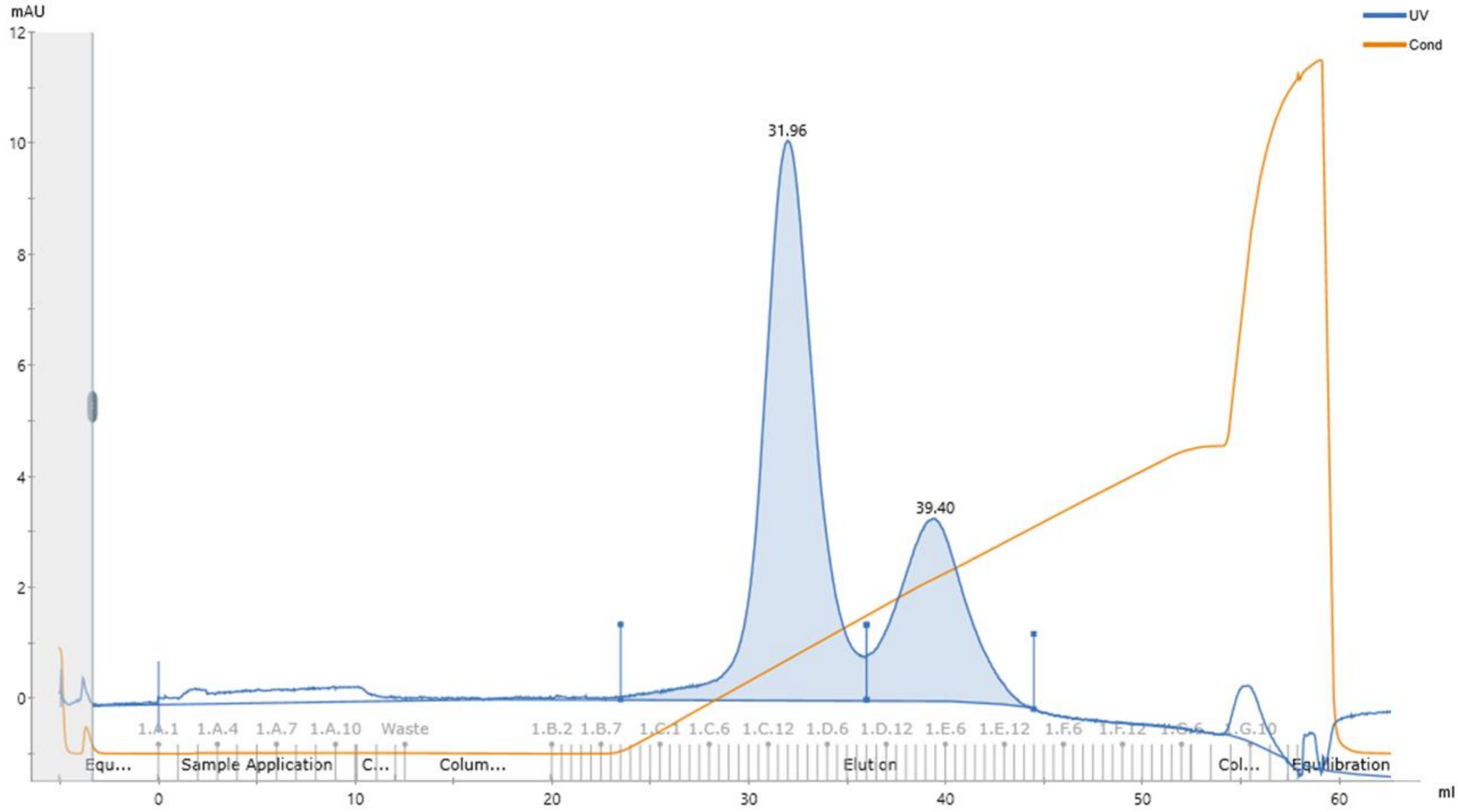

Figure 4-33. Mono S purified recombinant (CHO) FI at pH 6.
Chromogram of Mono S ion-exchange chromatography purification of recombinant (CHO) FI at pH 6.

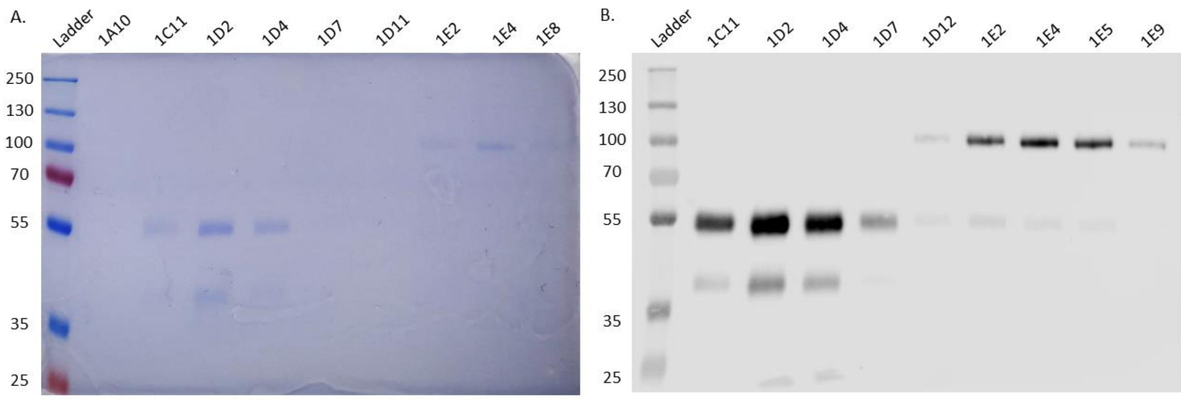

Figure 4-34 SDS PAGE and Western Blot of Mono S purified (CHO) FI under reducing conditions.
Reducing SDS PAGE and Western Blot of Mono S peak fractions. (A) Reducing SDS PAGE of peak fractions from Mono S purification of recombinant FI stained with Coomassie Blue. (B) Reducing Western Blot of peak fractions from Mono S purification of recombinant FI. Detected with sheep polyclonal anti-human Factor I.

To ascertain whether the separation of Pro-I from FI could be improved using more acidic conditions, the separation was repeated at pH 5.5. Following elution using a 1 M NaCl gradient, two UV peaks were again observed (Figure 4-35). The first peak had a maximum UV of 4.8 mAU at a conductivity of 18.19 mS/cm, and the second, a maximum of 1 mAU at 26.18 mS/cm. Despite binding to the column more tightly, the UV values obtained for each peak were much lower than those achieved at pH 6, indicating a reduction in the amount of protein bound to the column. This was also supported by a reduction in band intensity on the Coomassie stained SDS PAGE (Figure 4-36A). To determine the impact of the pH on the species separation, a Western Blot was also performed (Figure 4-36B). Again, the fractions from the first peak generated two bands at ~50 and 38 kDa, indicating the presence of FI, and the fractions from the second peak produced two bands at ~90 and 50 kDa, indicating Pro-I with FI contamination. Interestingly, when compared to the Pro-I purified at pH 6, the purity as determined by densitometry, was much lower at 76.4%.

Since performing the chromatography at pH 6 was able to generate both FI and Pro-I at the required level of purity, this method was therefore used for the larger scale production necessary to fulfil the protein requirements for use in the HuCAL system.

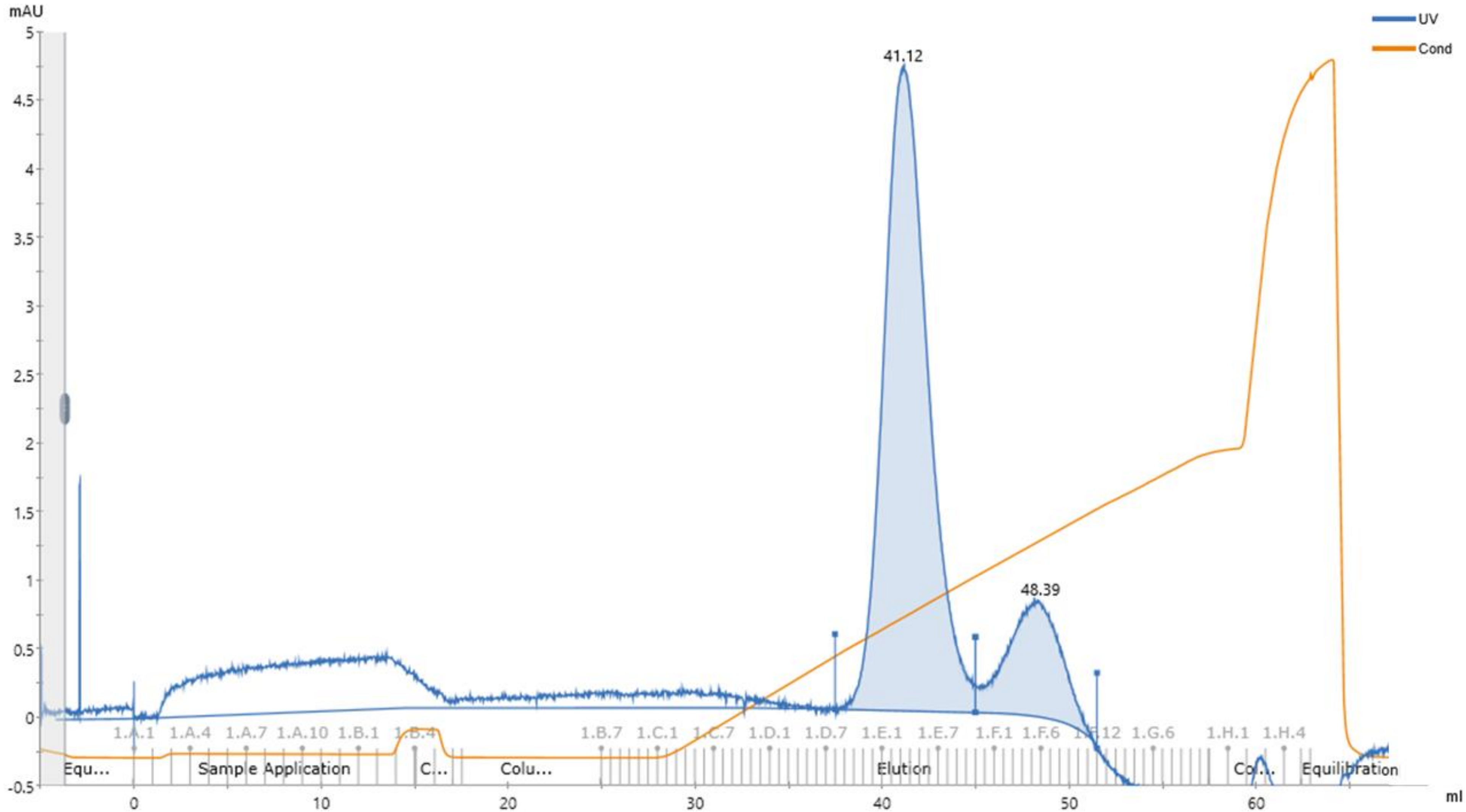

Figure 4-35 Mono S purification of recombinant (CHO) FI at pH. 5.5.

Chromogram of Mono S ion-exchange chromatography purification of recombinant (CHO) FI at pH 5.5.

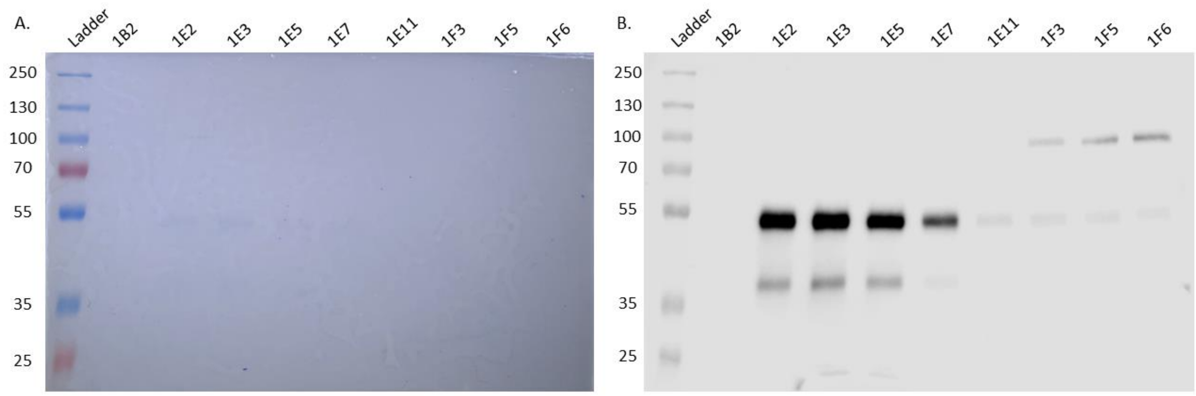

Figure 4-36 SDS PAGE and Western Blot of Mono S purified recombinant (CHO) FI under reducing conditions. Reducing SDS PAGE and Western Blot of Mono S peak fractions. (A) Reducing SDS PAGE of peak fractions from Mono S purification of recombinant FI stained with Coomassie Blue. (B) Reducing Western Blot of peak fractions from Mono S purification of recombinant FI. Detected with sheep polyclonal anti-human Factor I.

4.3.4. Pro-I Production for Bio-Rad

A total of 1.2 L of recombinant FI supernatant was loaded onto a 1 mL OX-21 column and the bound protein eluted with 0.1 M Glycine at pH 2.7. Three runs were required to deplete the supernatant of FI and a representative UV trace is shown in Figure 4-37. From 1.2 L of supernatant, 1.35 mg of recombinant FI was purified. The protein was then dialysed overnight in pH 6 sodium phosphate buffer, prior to loading onto the Mono-S column. After elution, two UV peaks were observed (Figure 4-38). The first peak of 11.5 mAU was generated at 14.16 mS/cm, and the second peak of 9 mAU was produced at a conductivity of 23.02 mS/cm. Interestingly, the relative UV absorbance attributed to the second peak was noticeably larger than the previous Mono S purification, indicating that a greater proportion of Pro-I had been purified. This finding was also supported by the reducing SDS PAGE and Western Blot analysis of the purified proteins (Figure 4-39). In addition to the increased proportion of Pro-I purified from the sample, the separation achieved had also noticeably improved. There was no evidence of cross-contamination in either protein species, apart from fraction F2, which exhibited minor heavy chain contamination. Both peak fractions were completely pure as confirmed by Coomassie staining and by Western Blot. Fractions F4 to G8 were collated and dialysed into PBS, before final assessment by SDS PAGE and Western Blot (Figure 4-40). From 1.35 mg of recombinant FI, 304.04 µg of Pro-I was purified, providing the desired amount of antigen for the HuCAL screening.

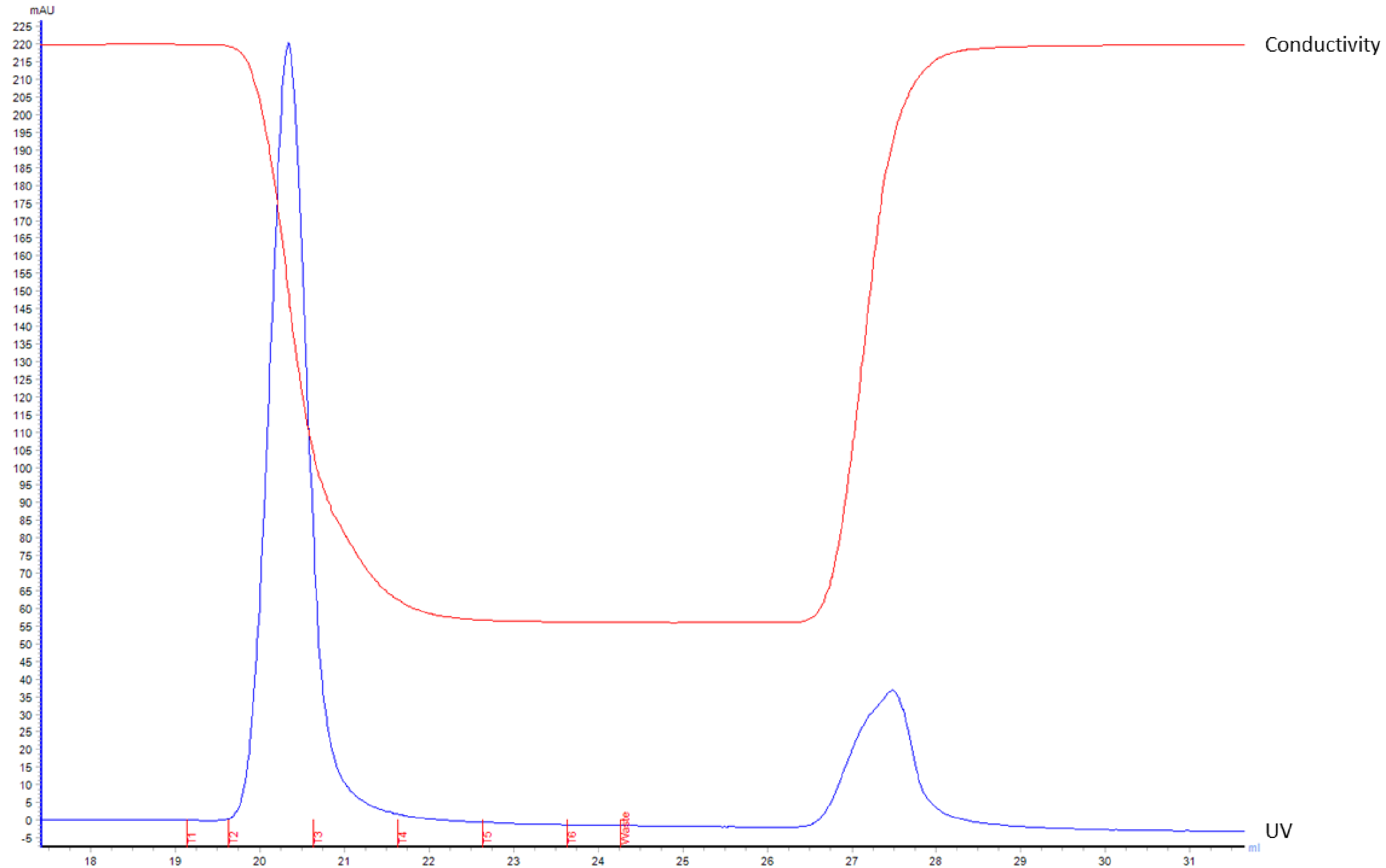

Figure 4-37 Chromatogram of recombinant (CHO) FI purification using an OX-21 column.

Recombinant FI was purified from cell culture supernatant using the ÄKTA Start protein purification system with a 1 mL OX-21 Column. UV trace produced upon elution of with 0.1 M Glycine, pH 2.7.

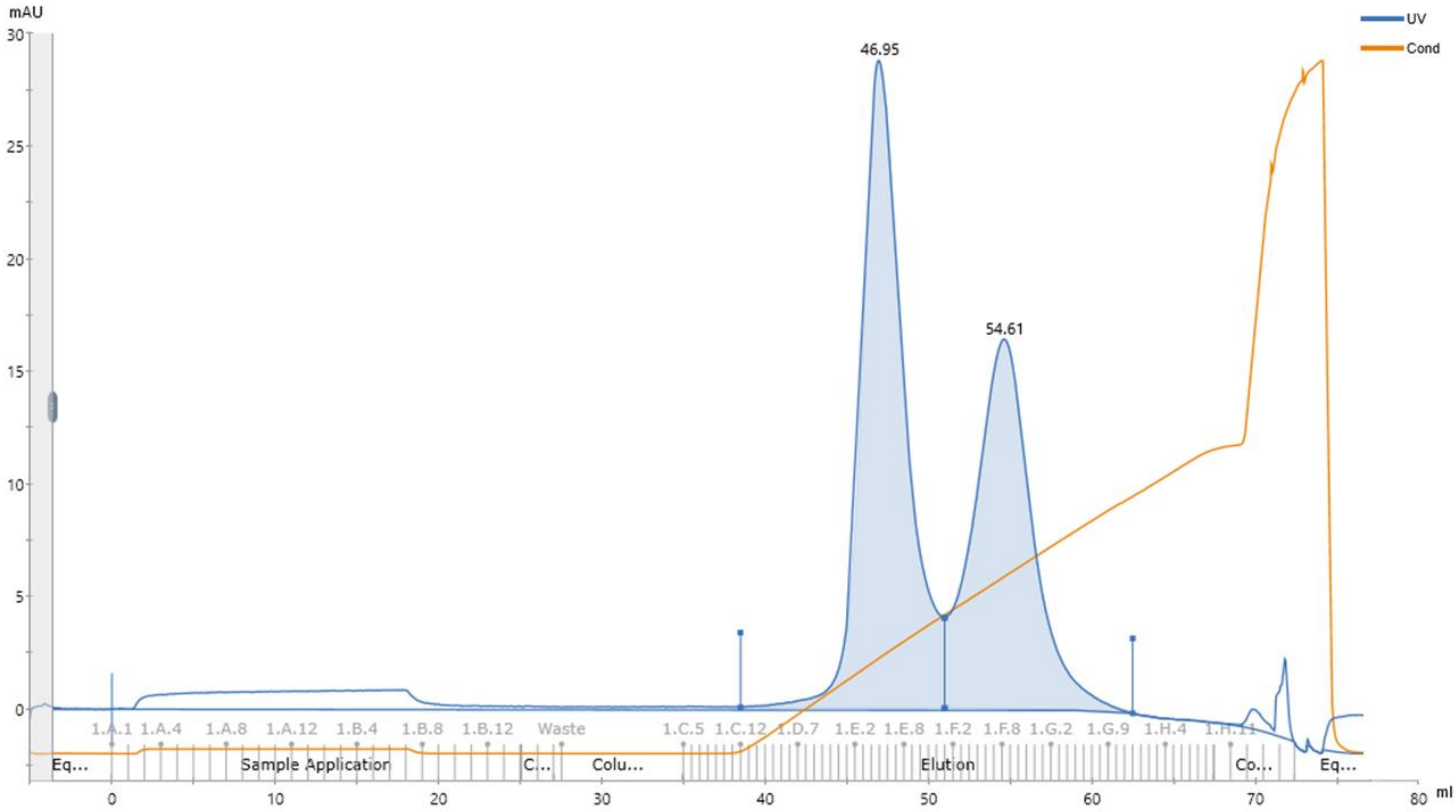

Figure 4-38 Mono S purification of recombinant (CHO) FI at pH 6. Production Run.
Chromogram of Mono S ion-exchange chromatography purification of recombinant (CHO) FI at pH 6.

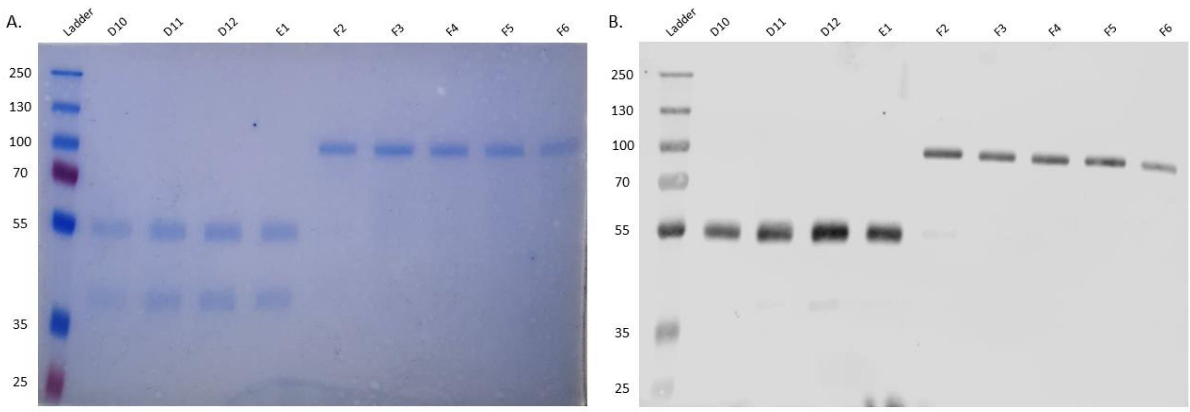

Figure 4-39 SDS PAGE and Western Blot of Mono S purified recombinant (CHO) FI under reducing conditions. Production Run.

Reducing SDS PAGE and Western Blot of Mono S peak fractions. (A) Reducing SDS PAGE of peak fractions from Mono S purification of recombinant FI stained with Coomassie Blue. (B) Reducing Western Blot of peak fractions from Mono S purification of recombinant FI. Detected with sheep polyclonal anti-human Factor I.

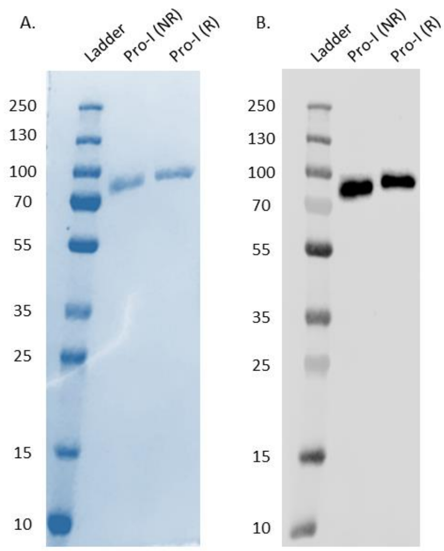

Figure 4-40 SDS PAGE and Western Blot of Pro-I.

Reducing and non-reducing SDS PAGE and Western Blot of purified Pro-I. (A) SDS PAGE of purified Pro-I stained with Coomassie Blue. (B) Western Blot of purified Pro-I. Detected with sheep polyclonal anti-human Factor I. Non-reducing conditions (NR), Reducing conditions (R).

4.3.4.1. Generation of the Closely Related Antigen

Human FI was chosen as the CRA over recombinant FI to ensure that the generated antibody could be used in human serum. Generation of the human FI, was performed as outlined in Chapter 3, using a combination of affinity chromatography with OX-21 and gel filtration (Figure 4-41). The peak fractions were run on SDS PAGE and Western Blot to confirm their identity and purity (Figure 4-42). Fractions B3 and B4 both exhibited a > 250 kDa contaminant under non-reducing conditions, and B3 also produced a contaminant band of approximately 110 kDa under reducing conditions. Fractions B5 and B6, however, showed no evidence of contamination. These two fractions were therefore collated, and 1.961 mg of purified serum FI was supplied to Bio-Rad for use as the CRA.

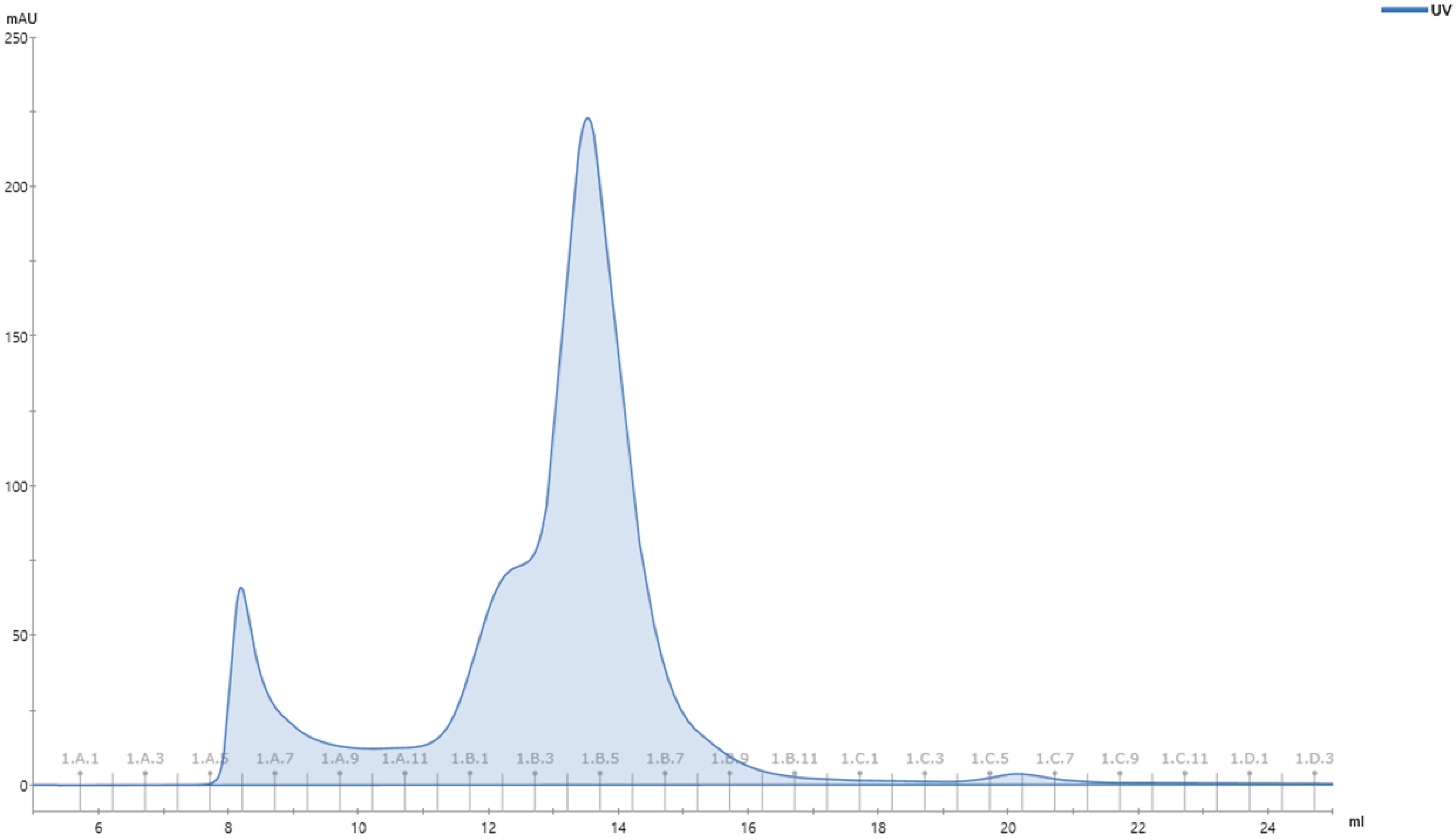

Figure 4-41 Chromatogram of plasma purified FI gel filtration.
A UV trace of the gel filtration of plasma purified FI. Three peaks observed. Main peak responsible for FI.

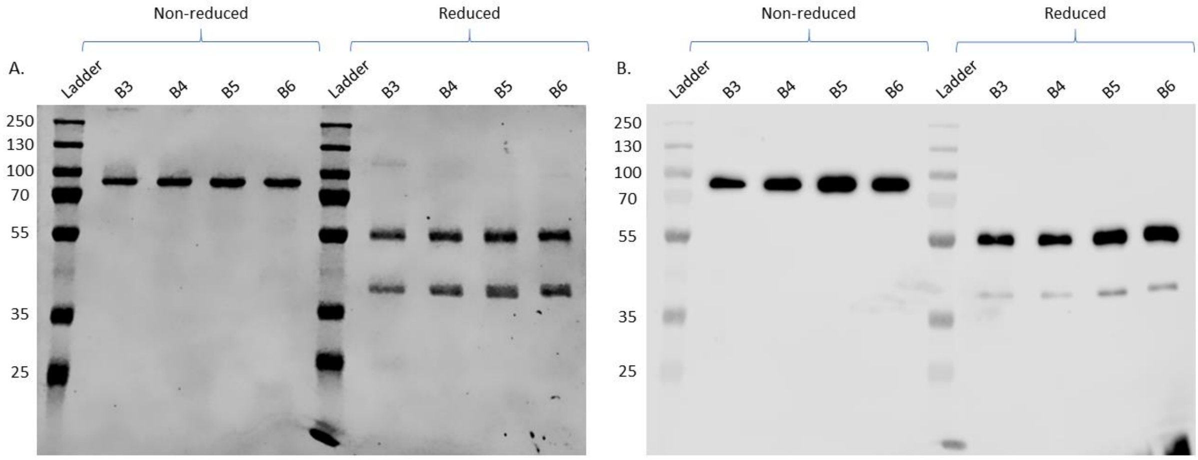

Figure 4-42 SDS PAGE and Western Blot of purified Pro-I

SDS PAGE and Western blot analysis of the main peak produced following the gel filtration of plasma purified FI. (A) SDS PAGE of FI peak fraction under reducing and non-reducing conditions, stained with Coomassie Blue. (B) Western Blot of FI peak fraction under reducing and non-reducing conditions. Detected with a sheep polyclonal anti-human Factor I (1 µg/mL) primary and a donkey anti-sheep (1:3000) secondary.

4.3.4.2. HuCAL Library Screening

The following results, Figures 4-43 to 4-45, were provided by Bio-Rad. To investigate whether the HuCAL library contained any Fab fragments which would bind to Pro-I specifically, an ELISA was performed using either Pro-I (antigen) or FI (CRA) as a coat. A response which was considered a positive result, was if the signal on the Pro-I plate was more than 5-fold the signal on the FI plate and the background (Lane 24, E-H). The signal obtained from each well was coloured according to the extent that the signal was increased above the background. Red indicated a signal between 2 and 5-fold above background. Yellow indicated a signal between 5 and 10-fold above background, and Green indicated a signal greater than 10-fold above background.

For the first batch of Pro-I generated (4.3.1.4), there were no clones which exhibited the desired signal criteria (Figure 4-43C). On the Pro-I coated plate, there were only 10 wells which had a signal 10-fold greater than the background (Figure 4-43A), in contrast, the FI coated plate predominately reached this signal intensity (Figure 4-43B). For each well on the Pro-I plate which produced a positive signal, the clone on the corresponding FI plate also generated a positive signal of either equal or greater intensity.

A.

	1	2	3	4	5	6	7	8	9	10	11	12	13	14	15	16	17	18	19	20	21	22	23	24
A	443	714	624	281	149	344	743	759	898	878	383	258	208	423	1033	522	462	1238	397	757	382	394	315	139
B	242	233	487	263	1265	247	1537	1032	243	275	307	294	494	453	421	468	262	393	467	753	286	412	832	145
C	1161	661	140	611	403	1147	177	135	272	390	250	185	291	704	4004	1110	688	613	213	567	368	959	205	29089
D	211	260	392	473	524	321	681	136	660	262	894	202	337	584	380	308	378	663	485	199	238	776	486	28711
E	297	397	6804	667	797	721	476	904	738	314	392	1089	497	1164	210	431	585	240	494	726	399	1270	500	227
F	621	240	697	857	382	538	2127	418	656	621	503	305	884	745	820	909	704	377	856	448	711	271	1151	169
G	148	384	160	1054	394	183	766	775	281	641	394	545	298	653	447	503	280	360	479	1182	217	169	448	166
H	2127	3051	624	835	530	1124	992	612	871	895	1129	354	2230	759	326	273	747	1270	443	149	686	687	163	147
I	197	1377	507	624	1356	2466	2394	1292	2544	844	142	678	1021	142	341	348	454	342	704	367	313	319	517	144
J	1156	599	592	961	455	1381	1372	1252	1159	311	1101	584	133	644	703	532	626	1122	664	1209	595	532	2147	284
K	392	292	338	1310	409	722	1479	522	161	388	179	413	516	581	645	455	687	780	465	290	178	497	545	139
L	192	253	287	678	454	877	304	433	376	230	370	159	256	156	345	536	294	214	592	604	569	439	509	150
M	360	268	213	201	446	309	158	222	161	231	790	368	395	194	388	395	331	175	278	559	236	913	220	129
N	179	195	254	194	333	314	173	274	265	249	135	164	235	416	362	147	346	181	616	327	234	186	392	145
O	140	168	210	125	168	179	206	191	206	246	290	333	268	290	375	307	256	318	214	273	355	475	337	126
P	161	169	214	145	174	134	229	212	408	178	199	154	300	211	257	121	161	245	531	218	406	239	125	145

B.

	1	2	3	4	5	6	7	8	9	10	11	12	13	14	15	16	17	18	19	20	21	22	23	24
A	3743	6205	8337	1616	158	2088	17349	13246	10376	22275	8850	10238	4318	9093	18395	11117	6712	17007	5137	10937	9586	10240	6060	136
B	4617	6725	9134	1840	10017	854	19813	18516	13761	17708	15735	22855	19333	18019	7621	15182	4769	11512	10271	21148	8532	9144	22108	147
C	7270	10811	147	5583	1988	4629	1877	260	12013	11480	16335	1109	8099	17026	3912	12526	15519	10881	9757	16544	15210	23622	310	29505
D	1177	2493	3219	3351	6261	1049	9915	224	29040	13013	18410	3387	13715	26511	16148	10005	13514	14740	14317	706	9417	26374	22184	24387
E	2368	8356	6514	12776	21026	21964	25159	5272	26129	6401	24066	21646	20106	27461	456	20479	20582	1124	24262	28972	18565	23475	19412	2830
F	23852	12804	22208	34703	22677	7442	35213	24625	38825	36539	37955	21114	30329	19372	26511	27132	23484	23433	20104	23377	36624	6895	23752	3154
G	257	17755	264	25087	21984	803	14582	29541	16979	32913	28749	12722	17903	22915	21431	18399	17075	20330	15974	24756	16525	723	30532	1654
H	31655	32864	22789	25117	26841	27649	23933	29006	34111	32572	19206	20741	27085	22904	17401	3136	22950	4563	20836	703	28188	24244	344	284
I	475	23690	18184	19349	29933	31028	33197	34391	30825	27225	284	24950	28870	35388	738	17721	19017	18812	23689	16127	13873	26919	29010	1335
J	25705	28232	19910	28069	20458	25038	35595	34569	3122	25980	29810	23159	32862	25977	27060	24939	22574	27588	27701	37380	27919	29265	33909	1654
K	26153	19267	576	29743	22029	25770	30954	32460	367	31062	305	14643	34485	24605	19186	18917	30019	31517	20756	18601	5547	23657	25213	2740
L	25270	29691	24052	28777	20932	31767	21325	24121	31594	20781	21086	1653	20987	1927	21778	21764	14701	12954	24572	22729	21239	18110	17762	3324
M	31222	31367	21254	15756	33757	35580	294	26176	326	28671	32657	22970	22013	14082	25377	18837	19575	9438	12051	19052	7636	21081	892	211
N	18342	25069	18597	19280	25662	21697	19274	25005	34249	25613	628	23128	15915	29414	20160	3135	20243	9707	5548	9124	8758	7587	15889	954
O	9191	11046	19364	2130	7369	16346	10256	21510	18654	29145	25435	26040	13369	13907	19615	8525	7402	5899	4270	4771	7411	15248	2520	339
P	4347	9294	19537	10046	11119	3614	10827	6860	18886	7313	4008	661	9854	720	10865	584	5988	7673	14655	8145	5390	6990	6996	5084

C.

	1	2	3	4	5	6	7	8	9	10	11	12	13	14	15	16	17	18	19	20	21	22	23	24
A	0	0	0	0	0	0	0	0	0	0	0	0	0	0	0	0	0	0	0	0	0	0	0	0
B	0	0	0	0	0	0	0	0	0	0	0	0	0	0	0	0	0	0	0	0	0	0	0	0
C	0	0	0	0	0	0	0	0	0	0	0	0	0	0	0	0	0	0	0	0	0	0	0	0
D	0	0	0	0	0	0	0	0	0	0	0	0	0	0	0	0	0	0	0	0	0	0	0	0
E	0	0	0	0	0	0	0	0	0	0	0	0	0	0	0	0	0	0	0	0	0	0	0	0
F	0	0	0	0	0	0	0	0	0	0	0	0	0	0	0	0	0	0	0	0	0	0	0	0
G	0	0	0	0	0	0	0	0	0	0	0	0	0	0	0	0	0	0	0	0	0	0	0	0
H	0	0	0	0	0	0	0	0	0	0	0	0	0	0	0	0	0	0	0	0	0	0	0	0
I	0	0	0	0	0	0	0	0	0	0	0	0	0	0	0	0	0	0	0	0	0	0	0	0
J	0	0	0	0	0	0	0	0	0	0	0	0	0	0	0	0	0	0	0	0	0	0	0	0
K	0	0	0	0	0	0	0	0	0	0	0	0	0	0	0	0	0	0	0	0	0	0	0	0
L	0	0	0	0	0	0	0	0	0	0	0	0	0	0	0	0	0	0	0	0	0	0	0	0
M	0	0	0	0	0	0	0	0	0	0	0	0	0	0	0	0	0	0	0	0	0	0	0	0
N	0	0	0	0	0	0	0	0	0	0	0	0	0	0	0	0	0	0	0	0	0	0	0	0
O	0	0	0	0	0	0	0	0	0	0	0	0	0	0	0	0	0	0	0	0	0	0	0	0
P	0	0	0	0	0	0	0	0	0	0	0	0	0	0	0	0	0	0	0	0	0	0	0	0

Figure 4-43 Screening results for Pro-I specific HuCAL Fab (Batch 1).

Screening results for Pro-I specific HuCAL Fab (Batch 1). Results from ELISA screening of crude *E. coli* lysate of expression culture containing HuCAL-Fab. A) ELISA result achieved when using Pro-I generated using Furin inhibitor chloro-methylketone to coat the plate. B) ELISA results achieved when using purified FI to coat the plate. C) Combined results of screening data on Figures A and B. 0 clones are positive on Pro-I (A) and negative on FI (B).

Due to the lack of clones exhibiting the desired response with the first batch of Pro-I, a second batch was also provided. For the second batch of Pro-I, the response on the Pro-I plate was much improved, with many of the clones demonstrating signals greater than 10-fold above the background (Figure 4-44A), and only 12.5% of clones being non-responders. The response from the FI coated plate was similar to that produced by the first batch (Figure 4-44B). Interestingly, there were a few instances where the signal on the Pro-I plate was more intense than on the FI plate e.g. A8. Unfortunately, none of the clones demonstrated the criteria required for a positive Pro-I specific result (Figure 4-44C).

A.

	1	2	3	4	5	6	7	8	9	10	11	12	13	14	15	16	17	18	19	20	21	22	23	24
A	20399	19410	2510	27654	28967	33618	214	20145	33160	25945	12174	11986	15463	15477	18401	13252	19807	7652	17201	22745	4626	6838	10199	229
B	577	248	17924	8211	536	12222	9784	7058	733	2779	14907	8267	9248	7967	14895	11343	5696	10384	14498	6289	9635	8914	19484	233
C	27710	15486	33145	27327	29930	29238	34234	19831	24253	29540	18876	17327	24027	558	2273	11129	18498	10197	630	14302	18018	1154	17797	20120
D	19295	25721	14847	15343	18760	6293	273	200	17540	30226	22211	7048	27663	14196	23088	20174	1820	20728	22742	15341	20430	27039	22451	25007
E	28018	23155	260	35666	24320	1433	32095	21499	26042	21545	7102	1199	21823	9443	21729	17499	8809	23024	24331	15733	214	1072	12082	646
F	313	11980	22155	12227	10715	15938	200	2587	3208	19001	10087	974	4615	12704	476	9166	6213	9020	8987	1917	4592	13394	16566	593
G	21170	20751	9719	21323	28267	19068	28091	21032	21124	26181	10714	7165	6637	14702	12929	14186	3113	6491	20186	4380	5800	12966	3575	645
H	8703	15027	19466	4290	8684	1170	2916	15991	5234	12233	1970	8729	13933	11465	10417	20753	10551	6652	13588	10305	8174	9393	10894	1326
I	340	14073	2384	10762	12406	17420	12600	17794	650	9506	2935	8868	7150	4444	1261	11205	3815	8332	9117	4275	3573	24970	11544	1444
J	18206	16230	16049	8202	469	14543	11934	14900	6334	11428	16685	14975	8068	1328	9211	19828	6936	7701	7195	1014	7582	7732	3914	275
K	535	9269	8552	7540	21601	14537	11200	16385	14747	11115	4067	4074	5666	5293	2911	9367	2175	410	1257	2040	17381	11954	639	210
L	246	14857	20558	3259	20180	26585	13123	921	28667	11223	27647	19768	20495	29459	750	13765	19755	838	3454	4280	6043	15110	9423	288
M	294	28047	10733	773	24233	30436	15010	13431	189	892	20181	22208	16343	25203	20913	20012	24297	21619	23901	18041	24256	3419	12654	248
N	28594	16822	25561	7574	27794	14613	10013	15886	29739	13158	28220	16802	395	24989	16222	25462	34482	20453	26856	1556	21960	23465	29009	364
O	31438	22992	19886	34068	33448	31844	37304	4954	544	23491	9832	14877	14437	19816	25493	21143	28375	24811	24542	23156	20540	18918	16949	643
P	17022	36202	25213	34189	36545	19516	613	20312	30818	29627	24853	498	871	468	26735	24465	1464	26315	27968	34255	26298	16323	36072	836

B.

	1	2	3	4	5	6	7	8	9	10	11	12	13	14	15	16	17	18	19	20	21	22	23	24
A	11002	11334	1668	11255	17797	16179	198	5463	14341	9391	11930	13865	14431	13372	13987	7653	15010	5726	9208	15348	4858	9830	12373	326
B	892	481	17159	8634	1202	13668	13742	8594	1667	5299	19646	12856	11887	10749	19381	16162	7934	13043	18672	8254	11668	9419	21942	236
C	24130	7637	22472	17322	26221	22714	24410	14836	18652	22509	13456	13566	25966	1071	1783	7554	13855	5607	577	10390	16898	1628	18431	19479
D	20152	30060	17260	31517	28553	12387	532	268	21048	34505	24542	8241	32737	20204	28102	23625	1172	26248	22965	13471	18037	24896	20220	24174
E	33646	26360	370	32996	19905	2708	30782	21708	19486	18785	8954	1222	27477	16150	27301	18396	3572	24466	22119	16083	322	1120	18642	655
F	552	24953	33994	20908	27481	28829	422	3754	8691	25443	24039	1278	18024	23397	573	26028	20240	22485	21616	1163	13244	18544	27754	840
G	25652	27061	21360	24298	29082	21013	29768	20603	22949	24654	21872	22497	18437	26989	18472	23063	2224	10569	26268	8081	13295	21439	11328	1197
H	21948	25239	33326	14335	17749	6168	14384	23258	14773	25100	7475	20456	27856	28896	21369	38542	30401	17594	21927	18499	13300	15940	15813	1343
I	472	35344	23747	29934	20840	31879	31930	28089	977	18519	10356	24312	26851	20524	1036	30054	19090	25964	23178	9527	2861	32722	26125	5078
J	29663	27337	29246	18905	1127	27500	21782	26542	17173	4355	25766	28144	26945	1305	22914	32162	18667	19822	22038	1006	21628	17530	10694	737
K	747	24098	27518	18028	33819	35584	21397	28967	30912	19634	11686	16386	20919	16682	8861	24420	1468	507	747	9354	20917	23514	670	281
L	567	26161	25033	8089	31226	31115	20541	982	34722	17075	28869	19820	25954	36273	1568	17823	21225	1360	12257	10549	14292	22824	11444	702
M	404	30811	17559	967	25470	31669	19351	12825	332	1055	23872	25970	24599	28032	18731	22138	22854	18711	24017	30114	24204	3026	14117	496
N	29741	18089	29548	9666	35909	20574	14317	29457	33821	17018	28738	13333	1209	29673	14105	29046	33980	25023	22684	1280	22189	24229	26526	503
O	28327	22182	21287	29322	27953	28937	35092	8767	639	19029	17489	22270	22933	30502	25013	18256	26770	26109	25895	23113	25738	23936	26325	1799
P	18635	35524	26696	35359	39462	20880	724	27800	35033	35394	34353	1134	1534	655	27600	26650	2055	30513	28830	34761	28208	18726	38711	1456

C.

	1	2	3	4	5	6	7	8	9	10	11	12	13	14	15	16	17	18	19	20	21	22	23	24
A	0	0	0	0	0	0	0	0	0	0	0	0	0	0	0	0	0	0	0	0	0	0	0	0
B	0	0	0	0	0	0	0	0	0	0	0	0	0	0	0	0	0	0	0	0	0	0	0	0
C	0	0	0	0	0	0	0	0	0	0	0	0	0	0	0	0	0	0	0	0	0	0	0	0
D	0	0	0	0	0	0	0	0	0	0	0	0	0	0	0	0	0	0	0	0	0	0	0	0
E	0	0	0	0	0	0	0	0	0	0	0	0	0	0	0	0	0	0	0	0	0	0	0	0
F	0	0	0	0	0	0	0	0	0	0	0	0	0	0	0	0	0	0	0	0	0	0	0	0
G	0	0	0	0	0	0	0	0	0	0	0	0	0	0	0	0	0	0	0	0	0	0	0	0
H	0	0	0	0	0	0	0	0	0	0	0	0	0	0	0	0	0	0	0	0	0	0	0	0
I	0	0	0	0	0	0	0	0	0	0	0	0	0	0	0	0	0	0	0	0	0	0	0	0
J	0	0	0	0	0	0	0	0	0	0	0	0	0	0	0	0	0	0	0	0	0	0	0	0
K	0	0	0	0	0	0	0	0	0	0	0	0	0	0	0	0	0	0	0	0	0	0	0	0
L	0	0	0	0	0	0	0	0	0	0	0	0	0	0	0	0	0	0	0	0	0	0	0	0
M	0	0	0	0	0	0	0	0	0	0	0	0	0	0	0	0	0	0	0	0	0	0	0	0
N	0	0	0	0	0	0	0	0	0	0	0	0	0	0	0	0	0	0	0	0	0	0	0	0
O	0	0	0	0	0	0	0	0	0	0	0	0	0	0	0	0	0	0	0	0	0	0	0	0
P	0	0	0	0	0	0	0	0	0	0	0	0	0	0	0	0	0	0	0	0	0	0	0	0

Figure 4-44 Screening results for Pro-I specific HuCAL Fab (Batch 2).

Screening results for Pro-I specific HuCAL Fab (Batch 2). Results from ELISA screening of crude *E. coli* lysate of expression culture containing HuCAL-Fab. A) ELISA result achieved when using Pro-I generated through Mono S separation to coat the plate. B) ELISA results achieved when using purified FI to coat the plate. C) Combined results of screening data on Figures A and B. 0 clones are positive on Pro-I (A) and negative on FI (B).

As a final attempt to identify a Pro-I specific HuCAL Fab, the ELISA was repeated using the proteins from the second batch, but instead of passively coating the plate, the Pro-I and the FI were instead biotinylated and immobilised using Streptavidin. On the Pro-I coated plate, there were only eight clones which reached the greater than 10-fold background signal intensity (Figure 4-45A). The number of clones with the optimum signal intensity on the FI coated plate (6), was also reduced in comparison to those achieved through passive coating (Figure 4-45B). Again, there were some clones which demonstrated the desired specific response towards Pro-I e.g B5 and B10, however, as the signal produced was only approximately two-fold greater on the Pro-I plate these also did not meet the required criteria for a Pro-I specific result (Figure 4-45C).

A.

	1	2	3	4	5	6	7	8	9	10	11	12	13	14	15	16	17	18	19	20	21	22	23	24
A	274	142	253	1283	141	557	211	742	351	207	293	217	1281	223	155	200	308	388	521	173	1258	271	1470	310
B	566	716	2094	158	2144	250	1248	1022	686	1333	143	252	349	555	889	332	913	3586	487	489	585	265	326	174
C	231	187	154	194	141	590	404	256	1951	266	4573	405	823	317	457	284	259	227	130	248	184	129	155	30183
D	173	949	169	650	1404	260	529	174	294	215	197	345	132	321	220	223	192	135	179	173	1470	362	817	32917
E	129	458	902	407	853	152	442	595	334	216	201	182	176	255	326	196	207	638	210	507	482	292	589	157
F	1278	139	980	267	176	1858	463	383	340	672	302	479	388	398	256	138	136	226	168	352	190	184	352	156
G	179	427	251	706	239	130	198	157	135	511	571	143	423	355	598	195	145	274	581	207	177	208	255	160
H	1107	250	152	750	1027	593	161	162	194	1516	235	204	158	366	621	419	998	241	181	713	146	181	327	164
I	414	451	158	158	206	145	631	156	613	689	606	521	403	162	219	409	232	279	268	153	191	173	156	175
J	216	266	836	155	967	140	219	318	231	196	730	137	522	445	182	158	150	781	763	383	156	523	189	177
K	2886	223	219	590	1067	4104	226	368	132	437	902	202	310	154	160	361	345	744	644	162	176	144	157	149
L	445	193	192	444	346	424	1332	575	147	224	235	214	325	477	1159	394	165	1065	188	390	840	1435	888	153
M	633	567	176	523	166	624	149	195	270	868	209	851	891	1066	950	864	1228	214	407	646	607	414	257	148
N	460	239	600	286	179	222	474	145	1365	143	1115	150	147	181	193	273	449	273	177	386	462	140	1445	164
O	140	322	611	511	666	639	236	199	234	244	309	709	210	140	148	241	628	476	147	326	1402	1364	187	141
P	166	204	135	561	849	393	766	878	250	386	450	179	134	544	192	1161	372	402	1510	221	1362	150	176	195

B.

	1	2	3	4	5	6	7	8	9	10	11	12	13	14	15	16	17	18	19	20	21	22	23	24
A	348	214	329	1145	215	544	291	802	470	369	348	288	769	223	211	227	310	410	445	225	1253	210	1101	215
B	695	597	2430	196	1806	271	1040	1709	586	741	179	272	336	520	767	268	894	3435	400	409	538	294	338	200
C	270	235	225	267	302	950	839	470	1095	201	2847	382	861	376	503	321	337	231	172	266	275	165	187	22508
D	233	1014	205	698	1074	235	365	213	287	200	217	285	190	373	267	265	252	176	201	203	1018	342	594	23771
E	212	422	1048	412	602	239	297	449	458	231	201	210	173	248	347	170	188	463	206	442	550	232	763	181
F	1084	167	1352	267	231	2827	622	700	458	960	253	400	264	241	279	170	173	252	184	336	211	194	373	200
G	225	510	354	803	249	189	205	280	171	548	628	191	306	254	485	197	179	274	577	201	195	180	313	180
H	983	286	215	822	642	865	184	675	267	1253	231	206	183	356	471	322	731	237	224	789	178	205	308	242
I	486	573	199	196	261	185	999	240	821	480	549	495	369	185	202	458	296	306	283	197	954	1328	219	182
J	287	302	615	194	1052	177	282	467	253	200	543	163	303	287	213	196	181	768	856	312	195	384	220	220
K	4060	290	181	750	1184	3186	224	546	192	399	1069	262	415	189	196	428	364	731	695	193	216	182	318	173
L	413	289	224	508	391	683	1478	548	922	306	258	270	372	532	1324	381	197	943	139	356	894	1164	647	179
M	718	565	221	591	189	941	210	281	299	801	244	728	1040	826	808	750	1011	248	350	614	497	411	246	171
N	550	289	612	382	217	316	408	193	1377	176	845	174	193	208	221	307	388	242	199	390	369	176	1507	202
O	189	373	749	696	1062	929	350	270	338	308	393	632	239	174	877	319	815	463	188	327	1103	979	192	181
P	212	272	187	689	1122	379	782	927	255	441	421	154	180	632	233	1232	415	402	1161	249	1045	186	196	228

C.

	1	2	3	4	5	6	7	8	9	10	11	12	13	14	15	16	17	18	19	20	21	22	23	24
A	0	0	0	0	0	0	0	0	0	0	0	0	0	0	0	0	0	0	0	0	0	0	0	0
B	0	0	0	0	0	0	0	0	0	0	0	0	0	0	0	0	0	0	0	0	0	0	0	0
C	0	0	0	0	0	0	0	0	0	0	0	0	0	0	0	0	0	0	0	0	0	0	0	0
D	0	0	0	0	0	0	0	0	0	0	0	0	0	0	0	0	0	0	0	0	0	0	0	0
E	0	0	0	0	0	0	0	0	0	0	0	0	0	0	0	0	0	0	0	0	0	0	0	0
F	0	0	0	0	0	0	0	0	0	0	0	0	0	0	0	0	0	0	0	0	0	0	0	0
G	0	0	0	0	0	0	0	0	0	0	0	0	0	0	0	0	0	0	0	0	0	0	0	0
H	0	0	0	0	0	0	0	0	0	0	0	0	0	0	0	0	0	0	0	0	0	0	0	0
I	0	0	0	0	0	0	0	0	0	0	0	0	0	0	0	0	0	0	0	0	0	0	0	0
J	0	0	0	0	0	0	0	0	0	0	0	0	0	0	0	0	0	0	0	0	0	0	0	0
K	0	0	0	0	0	0	0	0	0	0	0	0	0	0	0	0	0	0	0	0	0	0	0	0
L	0	0	0	0	0	0	0	0	0	0	0	0	0	0	0	0	0	0	0	0	0	0	0	0
M	0	0	0	0	0	0	0	0	0	0	0	0	0	0	0	0	0	0	0	0	0	0	0	0
N	0	0	0	0	0	0	0	0	0	0	0	0	0	0	0	0	0	0	0	0	0	0	0	0
O	0	0	0	0	0	0	0	0	0	0	0	0	0	0	0	0	0	0	0	0	0	0	0	0
P	0	0	0	0	0	0	0	0	0	0	0	0	0	0	0	0	0	0	0	0	0	0	0	0

Figure 4-45 Screening results for Pro-I specific HuCAL Fab (Batch 2 - Biotinylated).

Screening results for Pro-I specific HuCAL Fab (Batch 2 - Biotinylated). Results from ELISA screening of crude *E. coli* lysate of expression culture containing HuCAL-Fab on Streptavidin immobised antigens. A) ELISA result achieved when using Pro-I generated through Mono S separation to coat the plate. B) ELISA results achieved when using purified FI to coat the plate. C) Combined results of screening data on Figures A and B. 0 clones are positive on Pro-I (A) and negative on FI (B).

4.4. Discussion

4.4.1. Antibody Generation

Initially within this project, hybridoma generation through mouse immunisation was used to produce an anti-Pro-I antibody. Two approaches were considered for immunisation of the mice; the first was a peptide only approach, and the second, a combination of peptide and recombinant FI, used to provide epitopes against the full length Pro-I protein.

In both instances the peptide was conjugated to the carrier protein, keyhole limpet hemocyanin. KLH is a high molecular weight glycoprotein of marine origin which induces both cell-mediated and humoral responses in both animals and humans (Harris and Markl, 1999; Zhong *et al.*, 2016). Due to its potent immunogenicity, KLH was used to provide an immunostimulant against the RRKR containing peptide (Curtis *et al.*, 1970; Plitnick and Herzyk, 2010; Swaminathan *et al.*, 2014). To further enhance the immune response against the Pro-I antigens, the peptide and the recombinant protein were also prepared in Freund's complete adjuvant (FCA) and Freund's incomplete adjuvant (FIA), to induce a higher antibody titre (Leenaars and Hendriksen, 2005). These water-in-oil emulsions function through the formation “depot”, trapping the antigen so that it is slowly released into the system, enhancing antigen presentation and subsequent T- and B-cell responses (Awate, Babiuk and Mutwiri, 2013). By using an emulsified protein antigen the antibody response can persist for up to a year, due to increased antigen retention at the injection site, in comparison to an alternative adjuvant such as alum (Talmage and Dixon, 1953).

Despite the measures used to initiate a strong immune response towards the antigens of interest, both the peptide approach and the combination approach were unable to generate a strong immune response across all the mice. A potential reason for the reduced immune response, is the conservation of consensus residues within the Pro-I protein across species. Most of the insertions and deletions observed between murine and human factor I occur within the heavy chain, with the linking peptide chain (RRKR) in human Pro-I identical in mice. The area of greatest structural difference is in the aptly named divergent (D) segment, which consist of four subregions in mouse, and only two in humans (Minta *et al.*, 1996). Due to these morphological similarities this may make it harder to elicit an immune response, despite the inclusion of an immunostimulant and an adjuvant.

Utilising the fusion of immunised splenocytes with myeloma cells, numerous hybridomas were produced (Köhler and Milstein, 1975). From the peptide only immunisation, there were 24 hybridomas generated. Of these, only seven of these exhibited a differential response towards recombinant FI, and once scaled up, only 5A2 and 2G8 continued to demonstrate a preference in RRKR-peptide binding. As 2G8 demonstrated such a low signal on the ELISA (0.02 Abs), only 5A2 was used for the Western Blot however no signal was observed under either reducing or non-reducing conditions.

In contrast, the combination immunisation approach generated over 100 hybridomas which exhibited a positive response on the peptide. Despite the number of hybridomas generated, only colony 1B2 demonstrated the desired specificity towards the peptide. Once diluted to monoclonality, there were two RRKR-peptide responding hybridomas that were taken forward for further characterisation. These were D5-C10 and D8-G5. Although both hybridomas originated from the same initial colony, the antibodies produced had different isotypes, with D5-C10 being identified as IgM and D8-G5 being an IgG_3. Once purified by affinity chromatography, neither antibody however was able to detect Pro-I on either a Western Blot or by ELISA. In the case of D8-G5, this was likely due to the low protein yield obtained through Protein-G purification (< 0.05 mg). A major drawback of the method described by Köhler and Milstein is that an assortment of monoclonal antibodies are produced with very different structural and functional features. IgM antibodies are very large and exist as a pentamer, whereas the IgG antibodies monomeric and much smaller (Janeway *et al.*, 2001). Both antibodies also demonstrate differing affinities to their target antigens, with IgG binding very strongly as a result of affinity maturation, whereas IgM antibodies are typically exhibit lower affinities, particularly in monomeric interactions, as they predominately produced before somatic hypermutation (Eisen, 2014).

In addition to the two peptide-specific hybridomas selected, the hybridoma 12E9 was also chosen as it demonstrated specificity towards FI. Once diluted to monoclonality the clone 12E9-C11 was determined to be of isotype IgG_3 and was purified using a Protein G column. When used in a Western Blot, 12E9-C11 was able to detect both recombinant and serum FI, particularly under non-reducing conditions. There was no evidence of Pro-I cross-reactivity when using this antibody. 12E9-C11 is particularly interesting, as its specificity towards FI could facilitate its use in FI purification as either a primary purification antibody or for a polishing step, to separate FI from Pro-I. Unfortunately, due to time constraints this use of 12E9-C11 was unable to be explored further.

Following the unsuccessful attempt of generating an anti-Pro-I producing hybridoma, phage display was utilised to provide a 'targeted approach' using a CRA to select for antibodies demonstrating the desired specificity. Bio-Rad perform their antibody screening using the HuCAL PLATINUM antibody library, a synthetic library designed using master genes to reproduce the overall human antibody repertoire with regards to structure and amino acid diversity (Prassler *et al.*, 2011). After three rounds of panning, the phages isolated from each round were tested by ELISA to assess the enrichment of the binders towards Pro-I within the polyclonal pool. Following the identification of the clones which exhibited high enrichment, the individual phages are further screened by ELISA to determine the specificity for the antigen of interest compared to the CRA. Bio-Rad screened two batches of Pro-I by this method, yet no phages were identified which exhibited the desired specificity for Pro-I. To rule out whether the lack of specificity may have been due to an altered conformation of Pro-I when immobilised on a solid surface (Alfaleh *et al.*, 2020), the Pro-I was biotinylated and adsorbed to the ELISA plate by Streptavidin, however there were still no clones which had the desired specificity.

4.4.2. Pro-I Production and Purification

A key aim of this chapter was the production and purification of Pro-I, for use in the HuCAL system and for further functional analysis. Three different methods were explored to produce this precursor protein: Furin inhibition, use of a Furin deficient cell line and ion-exchange chromatography.

Furin inhibition was the first method explored. There are no natural protein inhibitors of Furin, however there are two classes of synthetic inhibitors available: the peptide-based inhibitors and the protein-based inhibitors. Of these, the most characterised are decanoyl-Arg-Val-Lys-Arg-chloromethylketone (dec-RVKR-cmk) (Henrich *et al.*, 2003; Remacle *et al.*, 2010) and α1-antitrypsin Portland (α1-PDX) (Benjannet *et al.*, 1997; Jean *et al.*, 1998). For this project dec-RVKR-cmk was chosen due to its high affinity (K_i ~2.0 nM), availability, and is often used as a reference molecule for Furin inhibition (Henrich *et al.*, 2003; Remacle *et al.*, 2010; Becker *et al.*, 2012). By transfecting CHO cells with pDEF-*CFI* DNA in the presence of the inhibitor, recombinant Pro-I was generated. Using the FI purification method outlined in Chapter 3, Pro-I was purified from supernatant using an OX-21 column and resulted in the production of Pro-I without FI contamination. This is the first instance in the literature for the generation and purification of this precursor species of FI. Despite this initial success, the low yield and high cost of the inhibitor meant that other methods for generating Pro-I were instead investigated.

To circumvent the requirement for the Furin inhibitor, Furin-deficient cell lines were then considered. The commercially available LoVo cell line (ATCC® CCL-229™) was chosen, due to its complete Furin inactivation by way of two mutations (Takahashi *et al.*, 1995), and the possibility of endogenous Pro-I production through increased complement regulator expression in colon carcinoma cells (Roumenina *et al.*, 2019). There was however no evidence of innate FI or Pro-I production as determined by ELISA, and following transfection with pDEF-*CFI* DNA there was no evidence of protein production indicating unsuccessful plasmid DNA incorporation. Plasmid incorporation could have been improved by using a transfection reagent specific for LoVo cells such as LoVo Cell Avalanche™ (EZ Biosystems) or LoVo Transfection Reagent (Altogen Biosystems), however this was not considered due to the success of the ion-exchange method, which was performed in parallel.

The final method for Pro-I production was based upon the difference in isoelectric point between Pro-I (7.38) and FI (6.49). The processing of Pro-I by Furin leads to the removal of the amino acid sequence, RRKR, which acts as a secondary linker between the heavy and light chains for FI. Both arginine and lysine are positively charged amino acids, and have high pKa values (R ~ 13.8 (Fitch *et al.*, 2015) and K ~ 10.5 (Harms *et al.*, 2008)); this linker is strongly basic at physiological pH, and therefore accounts for the difference in pI observed for the two species.

Separation of the two proteins was first attempted by ion exchange chromatography using a Mono Q column, packed with a strong anion exchange resin. At a protein's pI, the protein has no net charge and will not interact with a charged medium. However, at a pH above its pI, the protein will bind to an anion (positive) exchanger and, at a pH below its pI, a cation (negative) exchanger. Due to this, the recombinant FI was buffer exchanged into Tris-HCl at pH 7, however, when the bound proteins were eluted using a sodium chloride gradient there was only one peak observed, indicating poor selectivity (peak separation). As both species bound well to the Mono Q column despite a theoretical preference of FI binding, a Mono S column was then used instead. In contrast to Mono Q columns, Mono S columns are packed with a strong cation exchange resin and will therefore bind to proteins at a pH below their pI. Using a pH of 6, both FI and Pro-I bound to the column and when eluted with an increasing salt concentration two peaks were produced. When analysed by SDS PAGE and Western Blotting, the first peak was identified as FI and the second peak as Pro-I, indicating that at pH 6, FI had the lowest net charge of the two species and therefore was eluted with a lower ionic strength. Using this method, good separation was achieved for both species, however there was some indication of FI heavy chain contamination of the Pro-I when assessed by the more sensitive Western Blot, indicating that the selectivity could be improved to increase purity. A lower pH of 5.5 was used to see if this would lead to an improvement in selectivity, however both species bound more poorly to the column (lower peak UVs) and there was no noticeable increase in peak separation. As the factors which influence selectivity include pH, ionic strength and elution conditions, to improve the separation of the two species further pH values could be assessed, a step elution could be added, and a slower gradient elution could be used.

As IEX could be used to produce Pro-I with less than 30% FI contamination, this method was therefore used to produce the antigen for screening the HuCAL. Interestingly, the recombinant FI produced for the production run contained a greater proportion of Pro-I, indicating that the Pro-I expression may have overwhelmed the endogenous Furin in the transfected CHO cells (Cao *et al.*, 1996). Due to the increase in the amount of Pro-I, the fractions with the least amount of FI contamination could be selected whilst maintaining the desired amount of protein, leading to the production of a completely pure product as determined by SDS PAGE and Western Blot.

4.5. Conclusion

Unfortunately, within the time constraints of this project, development of an antibody against pro-I was unsuccessful. However, based on these results, there is the potential to develop an antibody in the future. Due to the development of a method for Pro-I production, pure Pro-I is now available for use during the immunisation process. In addition, the full-length Pro-I protein would also improve the screening ELISA, by allowing the identification of hybridomas that produce antibodies against conformational epitopes and those outside of the RRKR-peptide. By using the optimisations made during this project, this could pave the way for the development of a Pro-I antibody. Whilst the initial aim of generating a monoclonal antibody against Pro-I was unsuccessful; many important findings were generated along the way. A monoclonal antibody specific to FI was generated, a chromatographical method for separating Pro-I from recombinant FI has been established, and two methods for producing and purifying Pro-I were also developed.

Chapter 5. Functional Analysis of Complement Factor I Variants in AMD

5.1. Introduction

There are numerous rare genetic variants of *CFI* that have been identified in patients with AMD, and these are broadly categorised into two groups: Type 1 variants which lead to low serum FI levels, and Type 2 variants which are secreted at normal serum FI levels but reduced activity (Kavanagh *et al.*, 2015). Recently, a third group has also been proposed, and these are characterised by normal FI levels, and apparent normal degradation of C3b to iC3b, but with slightly reduced efficiency (Java *et al.*, 2020). In the case of the type 1 variants, the role that these mutations play in complement dysregulation is clear, as *CFI* haploinsufficiency results in reduced C3b degradation and therefore alternative pathway overactivation. However, for Type 2 and 3 variants, the role of these variants in the pathogenesis of AMD is not quite as clear and they must therefore be further examined through functional testing.

This chapter will demonstrate a robust assessment of the functional activity of three secreted *CFI* variants associated with AMD and normal FI levels. These mutations likely lead to different degrees of dysfunction, as attributed by their differing odds ratios, and therefore require multiple methods to assess their impact. As most previous analysis used recombinant protein with a mixture of fully processed FI and Pro-I, the functional impact of Pro-I will also be assessed. This chapter will also cover the development of a patented method for generating pure FI, without Pro-I contamination, and a new method for assessing the impact that mutant FI can have on the formation of the AP trimolecular complex.

5.2. Aims

- Determine the functional activity of Pro-I.
- Develop a method for producing fully processed FI in mammalian cells.
- Perform functional characterisation of the selected *CFI* variants.

5.3. Results

5.3.1. Functional Analysis of Pro-I

In Chapter 4, a method to produce pure Pro-I was developed. As Pro-I is present in all recombinant preparations of FI prepared in the absence of extracellular Furin, it was first critical to determine the function of this precursor form of FI. In addition to the functional assessment of recombinant Pro-I, there is also no definitive evidence for the presence of Pro-I in normal human serum, and therefore this was also investigated.

5.3.1.1.1. Recombinant Pro-I Purification

To generate Pro-I for functional testing, 1 L of recombinant FI supernatant was loaded onto a 1 mL OX-21 column and the bound protein eluted with 0.1 M Glycine at pH 2.7. Three runs were required for complete depletion from the supernatant, with Figure 5-1 providing a representative UV trace. Following affinity purification, the recombinant FI was dialysed into pH 6 sodium phosphate buffer and loaded onto a Mono-S column (Figure 5-2). As before two UV peaks were observed, occurring at conductivities of 14.47 mS/cm and 22.55 mS/cm respectively. The peak fraction attributed to FI (1F2) had a concentration of 0.151 mg/mL and the peak fraction for Pro-I (1G6) had a concentration of 0.056 mg/mL. When run on a reducing SDS PAGE gel stained with Coomassie, there was evidence of minor FI contamination in the peak Pro-I fraction, however this was completely removed by fraction 1G11 (Figure 5-3).

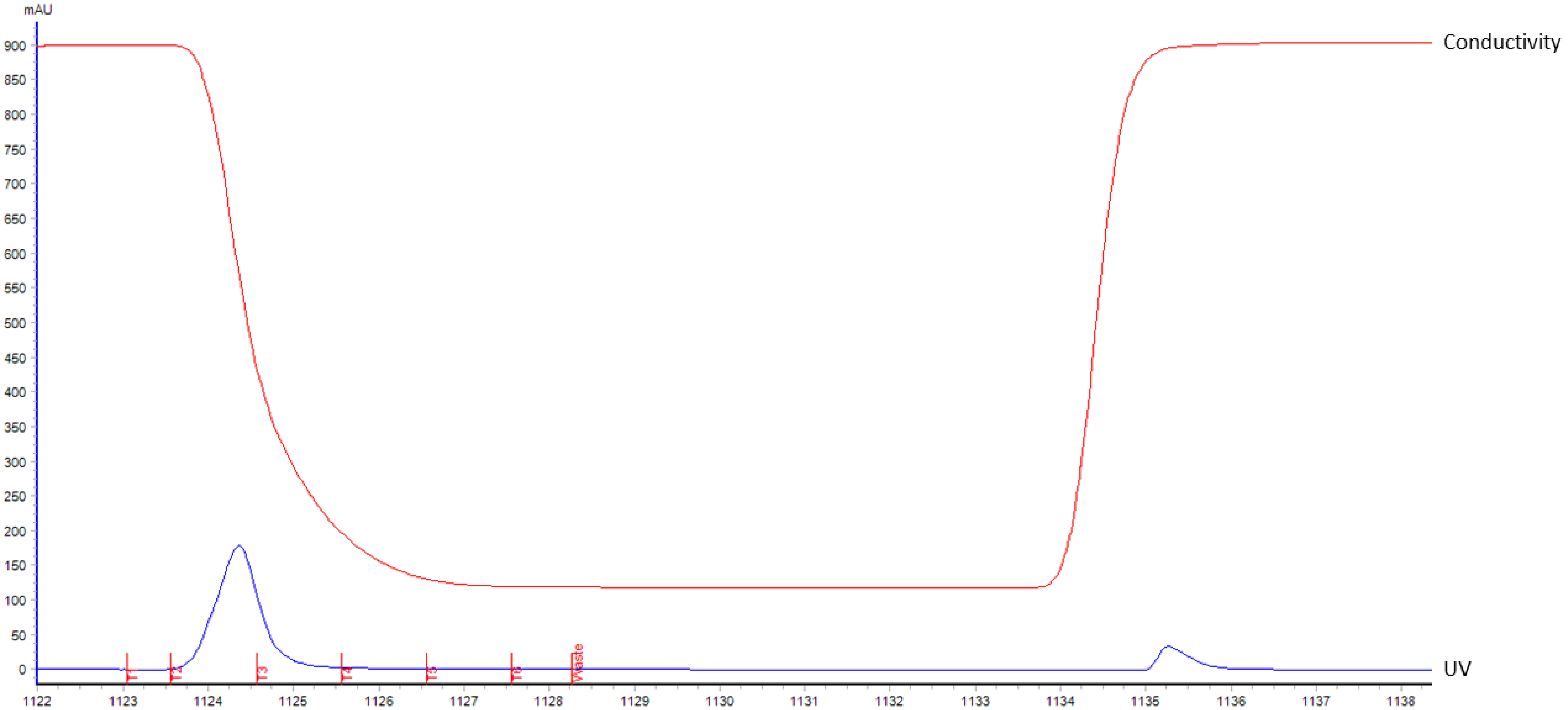

Figure 5-1 Recombinant (CHO) FI purification using OX21 affinity chromatography.

Recombinant FI was purified from cell culture supernatant using the ÄKTA Start protein purification system with a 1 mL OX-21 Column. UV trace produced upon elution of with 0.1 M Glycine, pH 2.7.

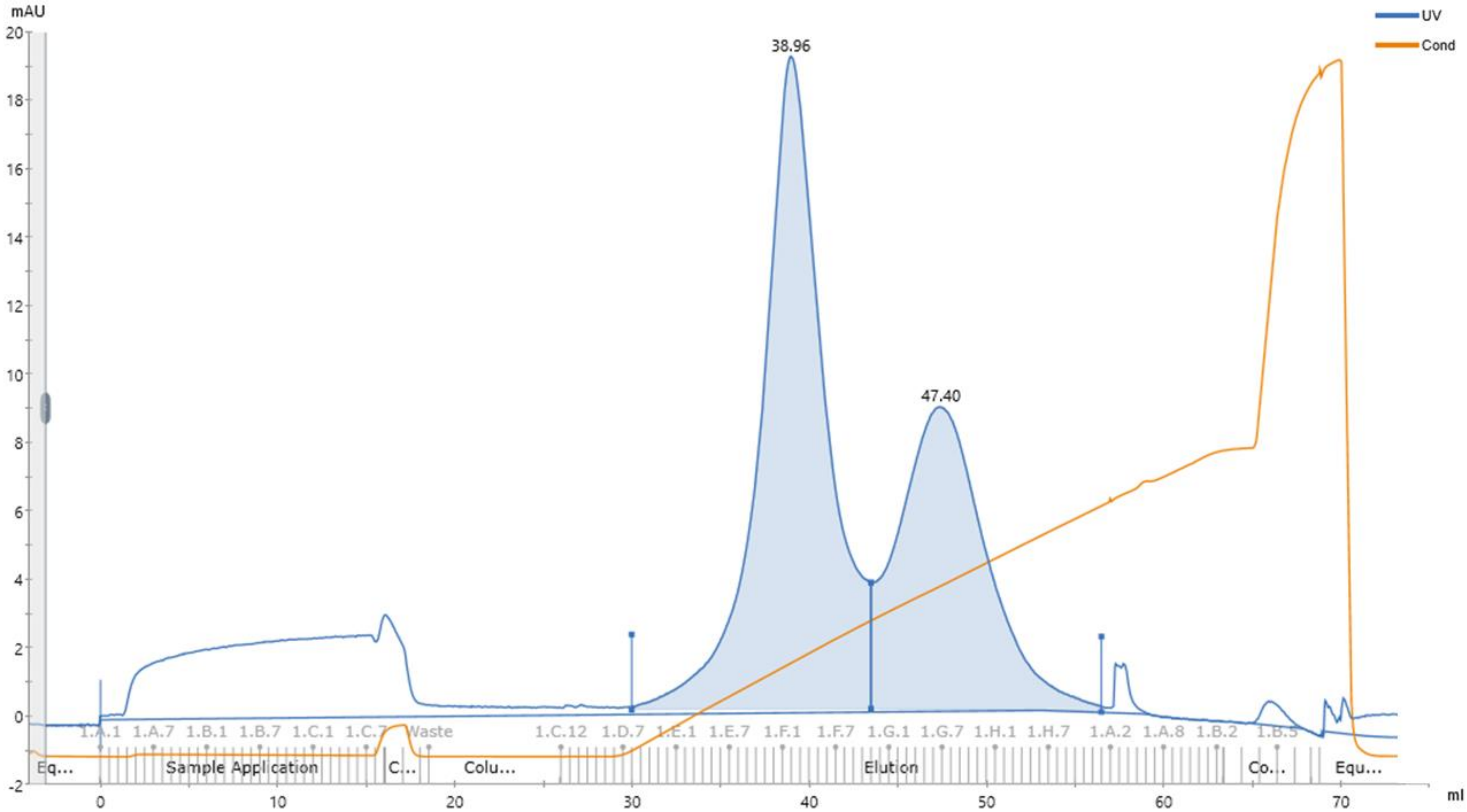

Figure 5-2 IEX chromatography of recombinant (CHO) FI using a Mono S column.
Chromogram of Mono S ion-exchange chromatography purification of recombinant (CHO) FI at pH 6.

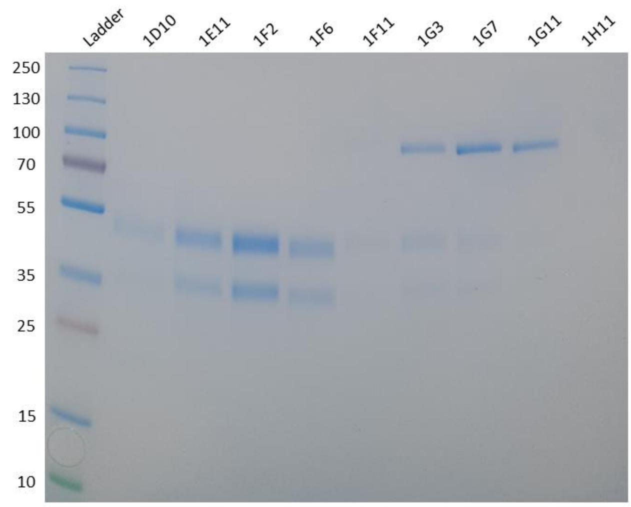

Figure 5-3 SDS PAGE of Mono S purified recombinant FI and Pro-I under reducing conditions.
Reducing SDS PAGE of peak fractions from Mono S purification of recombinant FI stained with Coomassie Blue.

5.3.1.1.2. Plasma Purified Pro-I

To determine whether Pro-I was also present in human serum, FI was purified from citrated plasma using an OX-21 column as described in Chapter 3. Figure 5-4 is representative of the UV trace obtained following elution with Glycine. Three runs were required to fully deplete the prepared plasma. Once purified, the protein collected from one run was collated and dialysed into pH 6 sodium phosphate buffer before loading onto the Mono-S column (Figure 5-5). Similarly, to the Mono S separation of recombinant FI, two distinct peaks were observed. The first peak had a maximum UV of 172 mAU and was eluted at a conductivity of 11.94 mS/cm, and the second peak had a maximum UV of 10 mAU and was eluted at 22.50 mS/cm. To confirm the species responsible for each peak, the peak fractions were analysed by a reducing SDS PAGE gel stained with Coomassie (Figure 5-6A), and by Western Blot (Figure 5-6B). On the SDS PAGE, the fractions attributed to the first peak (1D11-1E6), produced two main bands at 50 and 38 kDa, indicative of the FI heavy and light chains, with additional bands at 80 and 23 kDa. For the fractions from the second peak (1F4-1F9), three bands were present at 80, 90 and 100 kDa. The band at 90 kDa is indicative of Pro-I and the bands at 80 and 100 kDa indicate some contamination. The Western Blot confirmed that the two bands at 50 and 38 kDa were FI, and that the band at 90 kDa was Pro-I. None of the other bands identified on the SDS PAGE were detected by the Western Blot. These findings provide evidence for circulating Pro-I and demonstrate a method of its purification for further functional testing.

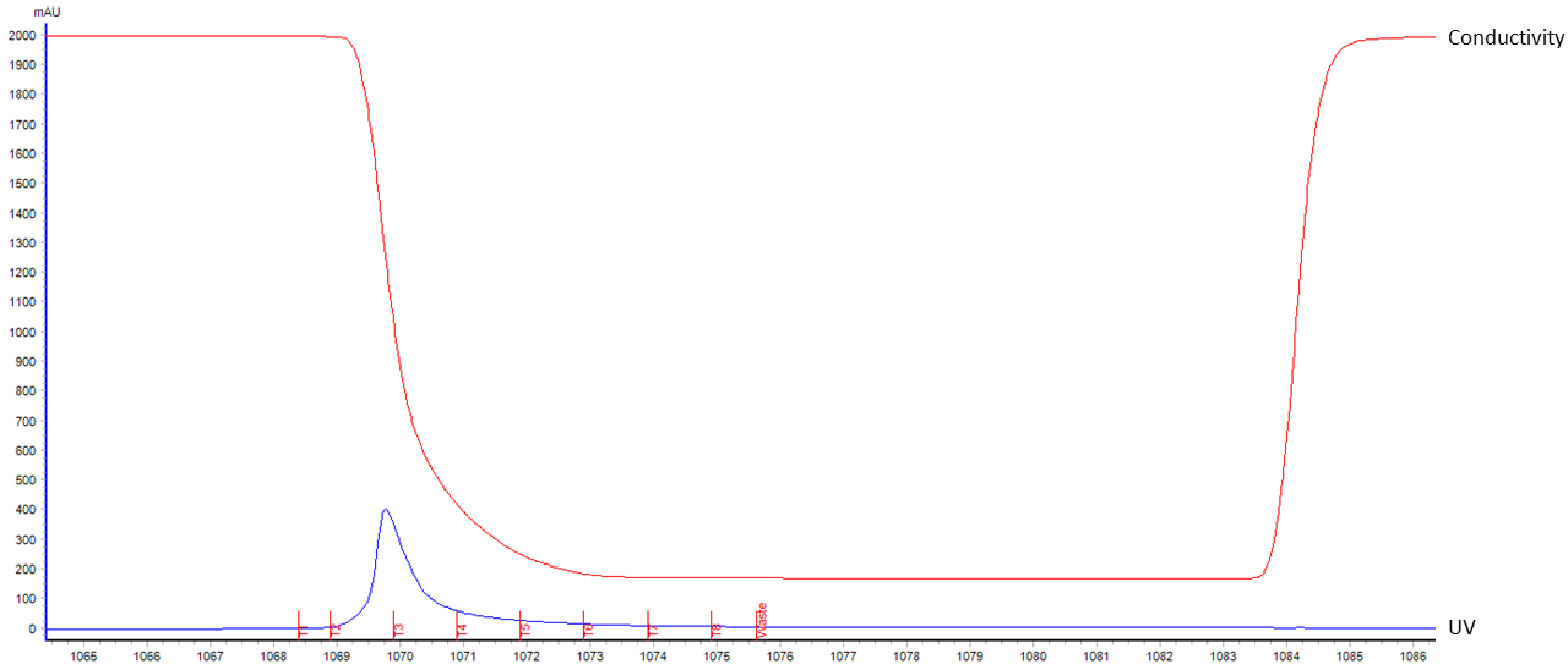

Figure 5-4 Human serum purification using OX21 affinity chromatography.
Human FI was purified from plasma using the ÄKTA Start protein purification system with a 1 mL OX-21 Column. UV trace produced upon elution of with 0.1 M Glycine, pH 2.7.

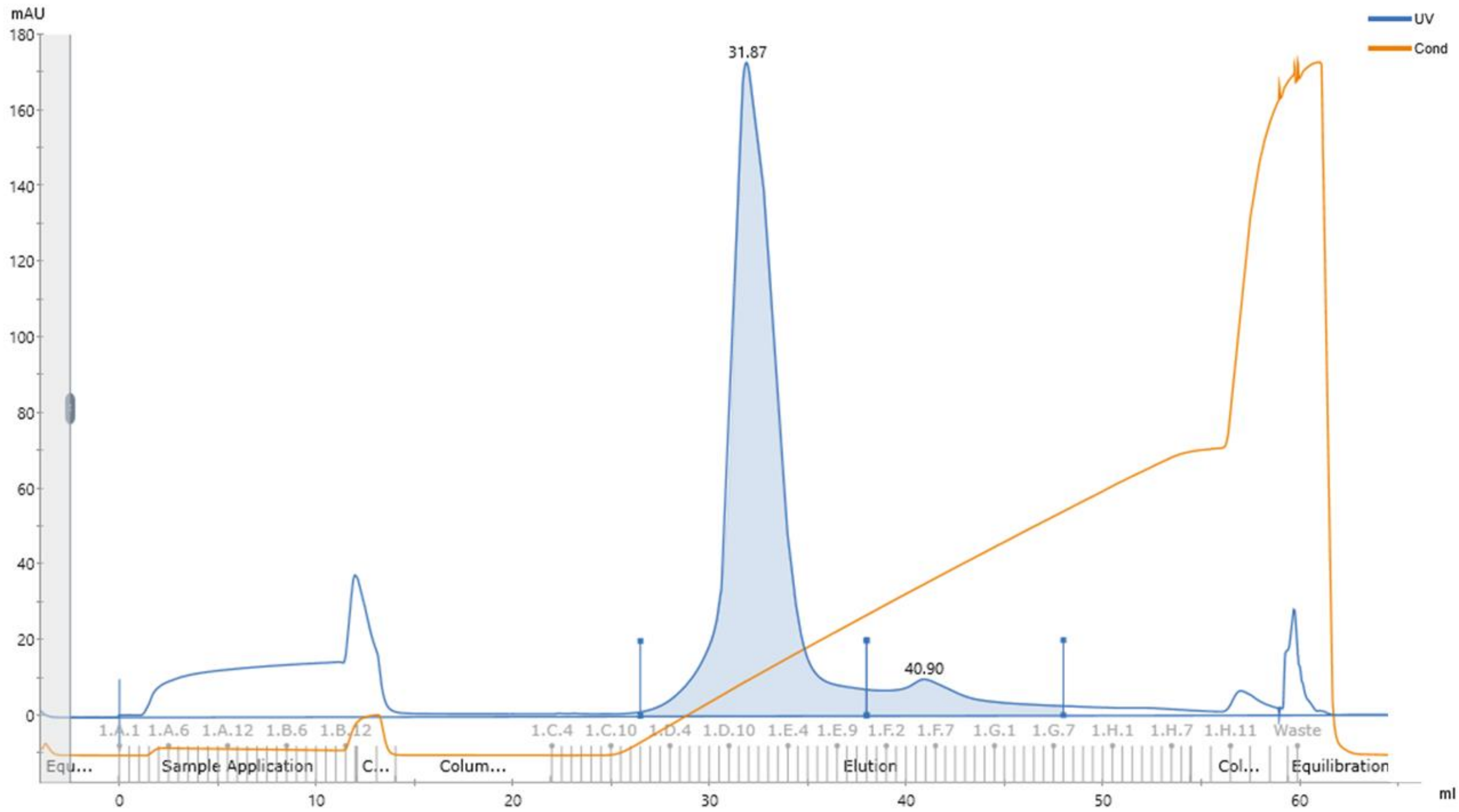

Figure 5-5 IEX chromatography of serum FI and Pro-I using a Mono S column.
Chromogram of Mono S ion-exchange chromatography purification of plasma purified FI at pH 6.

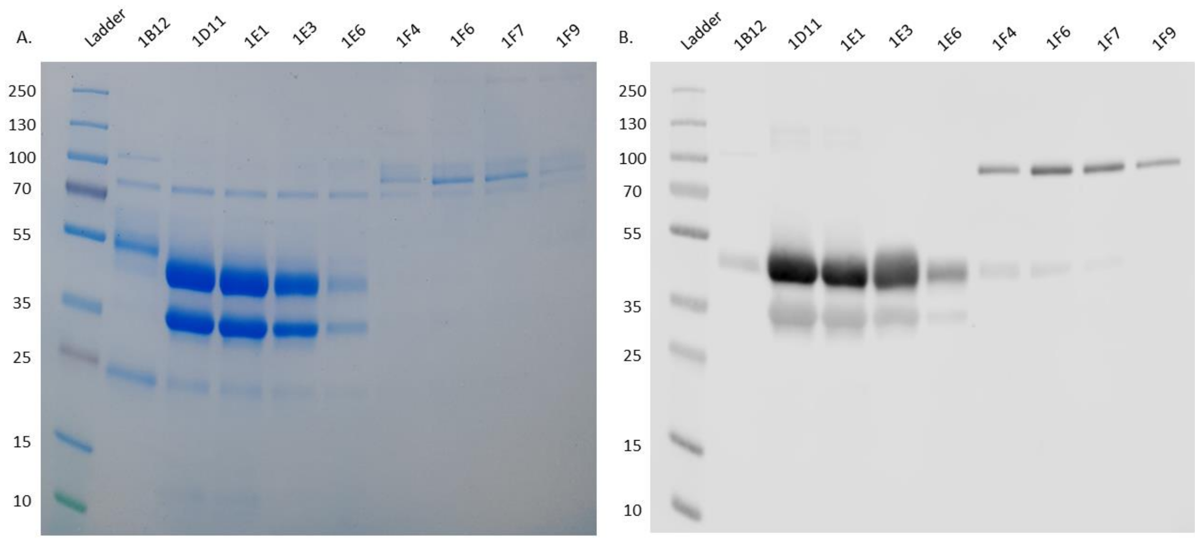

Figure 5-6 SDS PAGE and Western Blot of Mono S purified serum FI and Pro-I under reducing conditions.
Reducing SDS PAGE and Western Blot of Mono S peak fractions. (A) Reducing SDS PAGE of peak fractions from Mono S purification of plasma FI stained with Coomassie Blue. (B) Reducing Western Blot of peak fractions from Mono S purification of plasma FI. Detected with sheep polyclonal anti-human Factor I.

5.3.2. Fluid-Phase Cofactor Activity

To assess the functional activity of both recombinant and plasma purified Pro-I, a fluid-phase C3b cofactor assay was performed using the peak fractions. In the first instance, FH1-4 was chosen as the cofactor over full-length FH in preparation for subsequent BIAcore experiments. The resulting products from a 30-minute incubation at 37°C were run on an SDS PAGE gel under reducing conditions (Figure 5-7). Both recombinant and plasma FI had similar activity to the control FI with regards to C3b α' chain breakdown and C3b α1 formation. In contrast, both recombinant and plasma Pro-I were more comparable to the C3b+FH1-4 only control with respect to the C3b α' chain breakdown. There was however some C3b α1 produced for the Pro-I preparations, indicating C3b α' cleavage. To confirm the reduced activity of the Pro-I, densitometry was also performed (Figure 5-8). Using the C3b β chain to provide a loading control, it was evident that the Pro-I had reduced C3b cleavage, with approximately 50% of the α' chain remaining compared to ~5% remaining when using FI. Additionally, no notable difference in activity was observed between the recombinant and the plasma purified proteins.

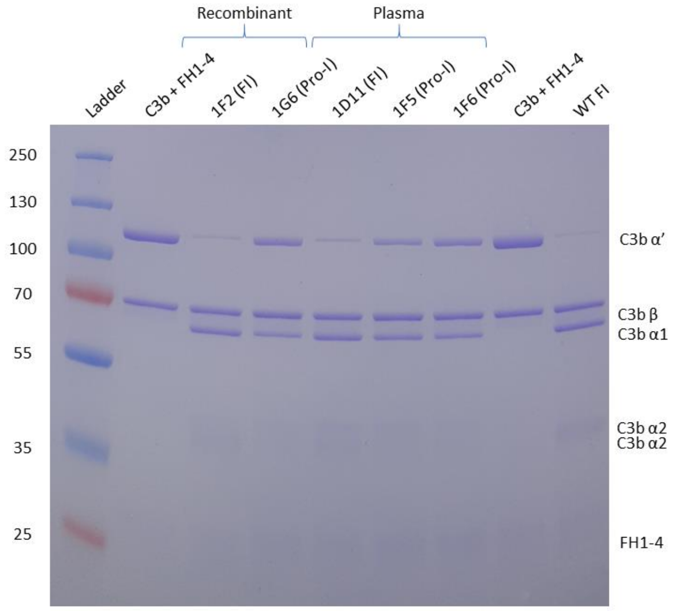

Figure 5-7 SDS PAGE visualisation of the fluid-phase cofactor (FH1-4) activity of recombinant and serum purified FI and Pro-I.

SDS PAGE showing proteolytic activity of recombinant FI/Pro-I and plasma purified FI/Pro-I peak fractions. Activity assessed by the ability of Factor I in combination with its cofactor FH1-4, to cleave C3b to its inactive form iC3b. C3b cleavage was indicated by the appearance of α1 and the two α2 bands. All samples were ran under reducing conditions with a PageRuler Prestained Protein ladder (10 – 250 kDa).

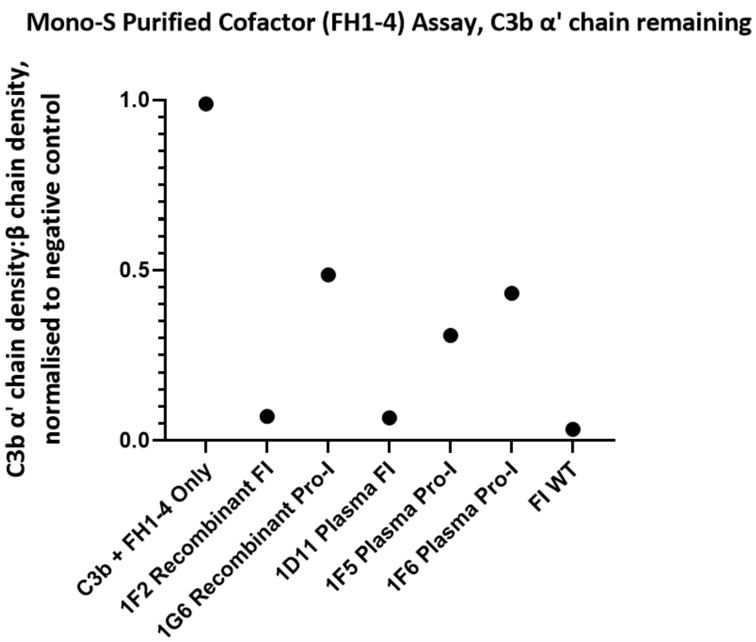

Figure 5-8 C3b α' chain degradation analysis of FH1-4 cofactor activity for recombinant and serum purified FI and Pro-I.

Plotted is the density of C3b α’ chain remaining (y-axis) after incubation of recombinant and serum purified FI and Pro-I, with C3b and FH1-4 over a duration of 60 mins at 37°C during a fluid-phase cofactor assay. The density of the α’ chain band was normalised to the density of the β chain band, before the resultant figure was normalised to a negative control containing no FI, giving a proportion of α’ chain remaining compared to the no FI control.

To investigate whether the cofactor activity observed for the Pro-I was due to FI contamination (Figures 5-3 and 5-6), the cofactor assay was repeated using highly purified fractions as determined by SDS PAGE and Western Blot. Using these highly purified proteins, it was clear that Pro-I has no C3b cleavage activity, with an absence of C3b α' chain degradation and a lack of appearance of the C3b α1 band (Figure 5-9).

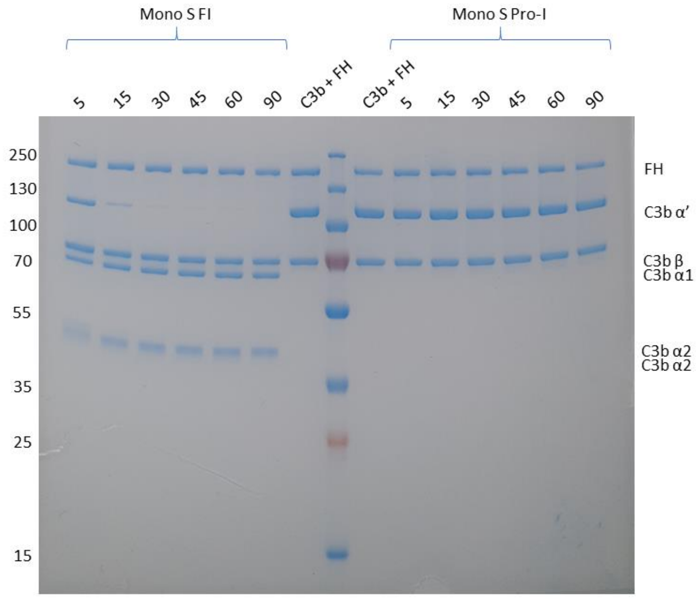

Figure 5-9 SDS PAGE visualisation of the fluid-phase cofactor (FLFH) activity of recombinant and serum purified FI and Pro-I, over time.
SDS PAGE showing proteolytic activity of recombinant FI and Pro-I across a range of timepoints (5 – 90 minutes). Activity assessed by the ability of Factor I/ Pro-I in combination with its cofactor FH, to cleave C3b to its inactive form iC3b. C3b cleavage was indicated by the appearance of α1 and the two α2 bands. All samples were ran under reducing conditions with a PageRuler Prestained Protein ladder (10 – 250 kDa).

5.3.3. AP TMC Formation Using Pro-I

To elucidate the lack of cleavage activity associated with Pro-I, its ability to form the AP trimolecular complex was assessed using surface plasmon resonance (SPR) (Figure 5-10). Typically, this process is complicated by cleavage of the substrate C3b by active FI, however using a methodology developed within the National Renal Complement Therapeutics Centre the AP TMC can be formed on the surface of a BIAcore chip to provide a real-time readout of complex formation.

Initially 1000 resonance units (RU) of C3b was coupled to the surface of a CM5 chip, before injections of Pro-I or FI, either individually or in combination with FH1-4. FH1-4 was chosen as the cofactor for the BIAcore experiments to minimise retention on the chip surface, due to the "stickiness" associated with the stronger C3b binding site located in CCPs 19 and 20 (Hellwage *et al.*, 2001; Schmidt *et al.*, 2008; Pechtl *et al.*, 2011).

To provide a control for TMC formation, FI was also produced using a *CFI* backbone which had been mutated at position S525A. The introduction of the S525A mutation has been previously reported to inhibit the serine protease activity of FI, and therefore enables TMC modelling by overcoming issues associated with substrate C3b cleavage (Xue *et al.*, 2017). The incorporation of this mutation and its role within the formation of the TMC on the BIAcore will be explored later within this chapter.

The injection of S525A FI with FH1-4 onto the C3b coupled surface revealed the formation of a complex as identified by a significant increase in SPR. The formation of this complex demonstrated the synergistic action of both proteins within the TMC, as when these proteins were injected individually, FH1-4 produced a much smaller bimolecular complex (3.8 RU vs 23 RU), and S525A FI didn't bind at all. In contrast to the TMC formed using S525A FI, the WT FI rapidly formed the complex (4RU) before demonstrating a steady state reaction whereby there was a cycle of rapid TMC formation, substrate C3b cleavage, and TMC dissociation.

When assessing the generation of the TMC by Pro-I, neither recombinant (CHO) or plasma purified Pro-I were able to form the complex. Both preparations showed no interaction with the C3b surface in the presence of FH1-4, indicating an inability to bind to the C3b:FH1-4 bimolecular complex.

The results from the cofactor assays and the TMC building on the BIAcore demonstrate that Pro-I is completely inactive with respect to C3b cleavage. This inactivity is likely due to the stereochemical constraints enforced by the presence of the RRKR linker, which inhibit binding to C3b:FH complexes. These findings highlight a requirement for Pro-I removal when performing functional assessments of FI, as the proportion of Pro-I present within a preparation would have a significant impact on the apparent activity of FI. This is particularly important when assessing the impact of genetic variants, as the impact of any functional defects may be subtle.

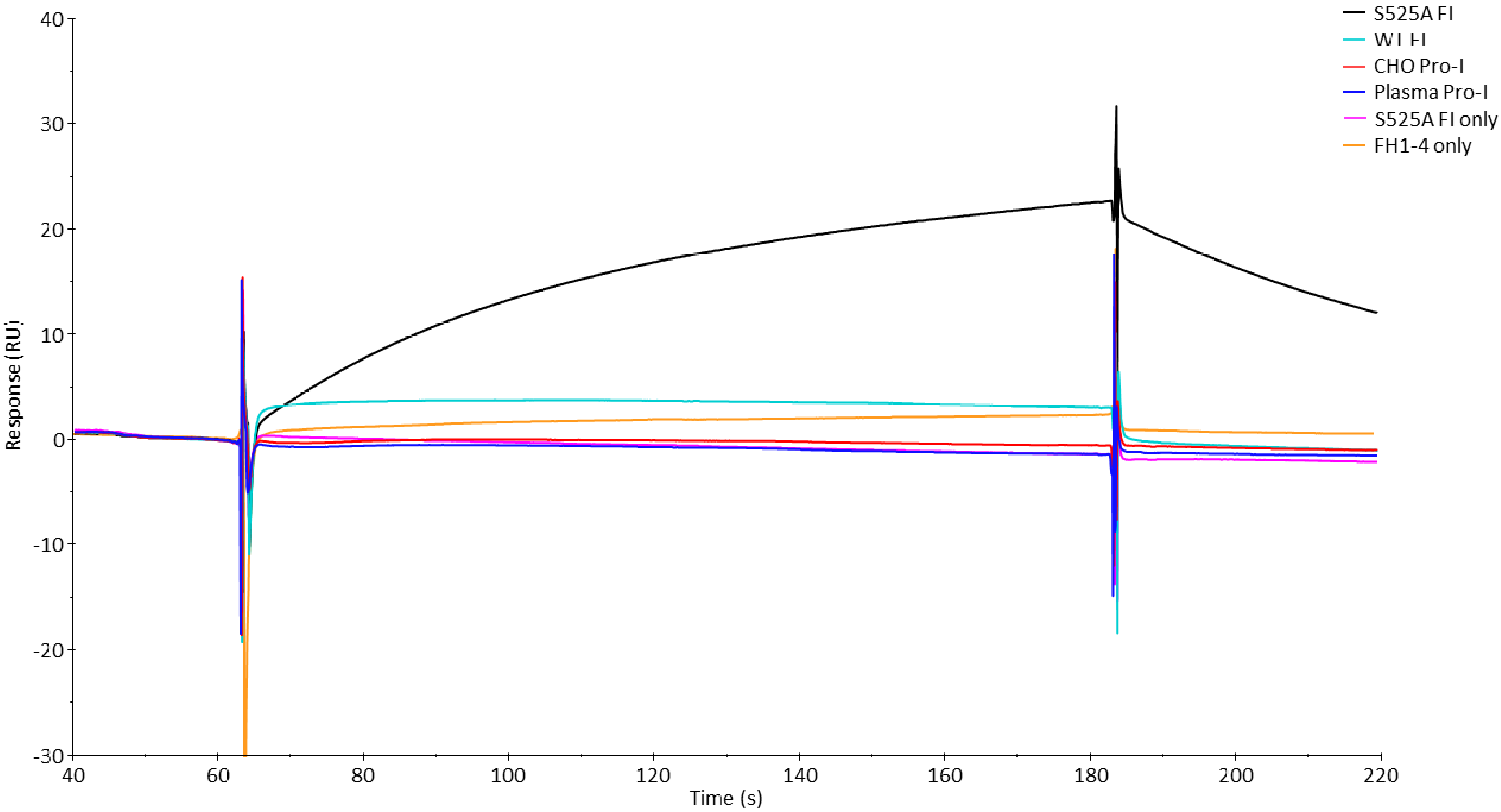

Figure 5-10 Formation of AP regulatory TMC on a physiologically coupled C3b surface using FI, Pro-I and FH1-4.

Displayed is a sensorgram produced in the BIAevaluation software S200 (GE) after injection of WT FI, recombinant Pro-I or serum purified Pro-I in combination with FH1-4, onto a C3b coupled CM5 chip surface. Time (x-axis, seconds) is plotted versus response (RU) after normalisation by injection over a blank flow cell.

5.3.4. Internal Ribosomal Entry Site (IRES) Vector

Previous methods to address the issue of Pro-I contamination outlined in this thesis have had limited success. The most effective method was the Mono S separation of Pro-I from FI, however, this was inefficient due to the quantity of Pro-I produced. Previous efforts to minimise Pro-I contamination produced compositions that lacked purity or required downstream processing. To overcome these issues of incomplete Pro-I processing using the current methods, a vector was developed consisting of *CFI* and the serine endoprotease *Furin*.

5.3.4.1. Incubation with Furin

Previous work within the National Renal Complement Therapeutics Centre (NRCTC) by Dr Seema Sharma had demonstrated that recombinant Pro-I could be cleaved by the addition of Furin post-purification to generate a pure FI protein (Figure 5-11). Whilst this method was effective at removing the Pro-I contamination the additional steps required added extra time and cost to protein production, in addition to limiting the utility of this method for *in vitro* FI production only.

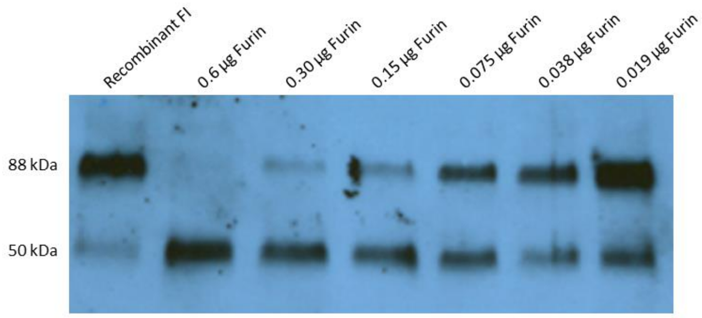

Figure 5-11 Western Blot of recombinant FI incubated with varying Furin concentrations.
Reducing western blot of recombinant FI incubated with increasing concentrations of Furin. Detected with sheep polyclonal anti-human Factor I.

5.3.4.2. IRES Vector Design

To circumvent the issues associated with the addition of Furin post-purification, a vector was designed which encoded both *Furin* and *CFI* to generate fully processed FI. Previous embodiments of this work have centred on co-transfection with Furin and *CFI* (Wong *et al.*, 1995), however these expressions did not lead to a completely pure product. When designing the vector for bicistronic expression, both IRES (Pelletier and Sonenberg, 1988) and self-cleaving 2A peptides (Ryan, King and Thomas, 1991) were considered. The IRES functions by enabling 5'-cap-independent binding of the 40S ribosomal subunits to initiate internal translation (Jackson, Hellen and Pestova, 2010) whereas the 2A sequences enable bicistronic translation by facilitating ribosomal skipping of a glycyl-prolyl peptide bond due to steric hinderance at the C-terminus of the 2A, leading to a separation of the 2A sequence and the downstream peptide (Liu *et al.*, 2017). Whilst it has been shown that 2A peptide sequences lead to a higher level of downstream protein expression in comparison to the IRES (Kim *et al.*, 2011), an IRES element was chosen as this unbalanced expression was desirable in this context. By positioning the *Furin* gene upstream of the IRES element (Figure 5-12), this would lead to an excess of Furin for the proteolytic processing of Pro-I to FI, resulting in a completely pure product. To increase the expression of the final product in cell lines containing a T antigen, a simian virus 40 (SV40) late polyadenylation tail was also included (Carswell and Alwine, 1989).

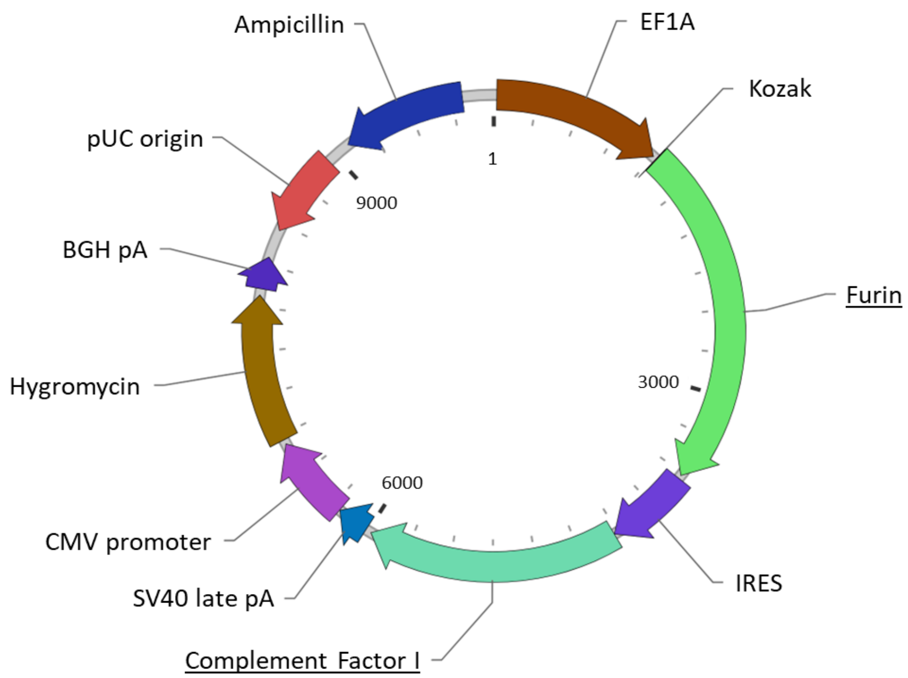

Figure 5-12 Plasmid map of Furin-IRES-*CFI* vector.
The Fur gene is responsible for the Furin enzyme which cleaves the RRKR linker found in pro-I. The internal ribosomal entry site (IRES) initiates translation in a cap-independent manner, allowing synthesis of two proteins from a single bicistronic mRNA. The *CFI* gene codes for the protein complement factor I. Human eukaryotic translation elongation factor 1 α1 (EF1A) is a strong promotor. The Kozak translation initiation sequence facilitates translation of the ATG start codon downstream from this sequence. The Simian virus 40 late polyadenylation signal (SV40 late pA) allows transcription termination and polyadenylation of transcribed mRNA. Human cytomegalovirus immediate early enhancer (CMV) is a strong promoter for the downstream hygromycin resistance gene, which enables cells to be resistant to hygromycin B, aiding selection. The Bovine growth hormone polyadenylation signal (BGH pA) acts similarly to the SV40 and allows for transcription termination and polyadenylation of mRNA transcribed by RNA polymerase II. pUC origin of replication facilitates plasmid replication in *E. coli* and regulates high-copy number plasmids. The ampicillin gene enables *E. coli* to be resistant to ampicillin. The plasmid is 10187 bp in size.

5.3.4.3. Comparison of FI Expression in HEK293T and CHO

To determine the optimum cell line for FI expression using the *CFI* IRES vector, the vector cDNA was used to transfect both HEK293T and CHO cells. Transfection of the *CFI* cDNA led to successful secretion of FI by both cell lines as determined by a dot blot for human FI. Following selection with hygromycin, an ELISA was performed to determine the best cell line for FI expression (Figure 5-13). The amount of FI secreted when using the HEK293T was approximately 28 times more than that achieved by the transfected CHO cells. HEK293T were therefore chosen as the expression system for generating the rare genetic *CFI* variants for functional testing.

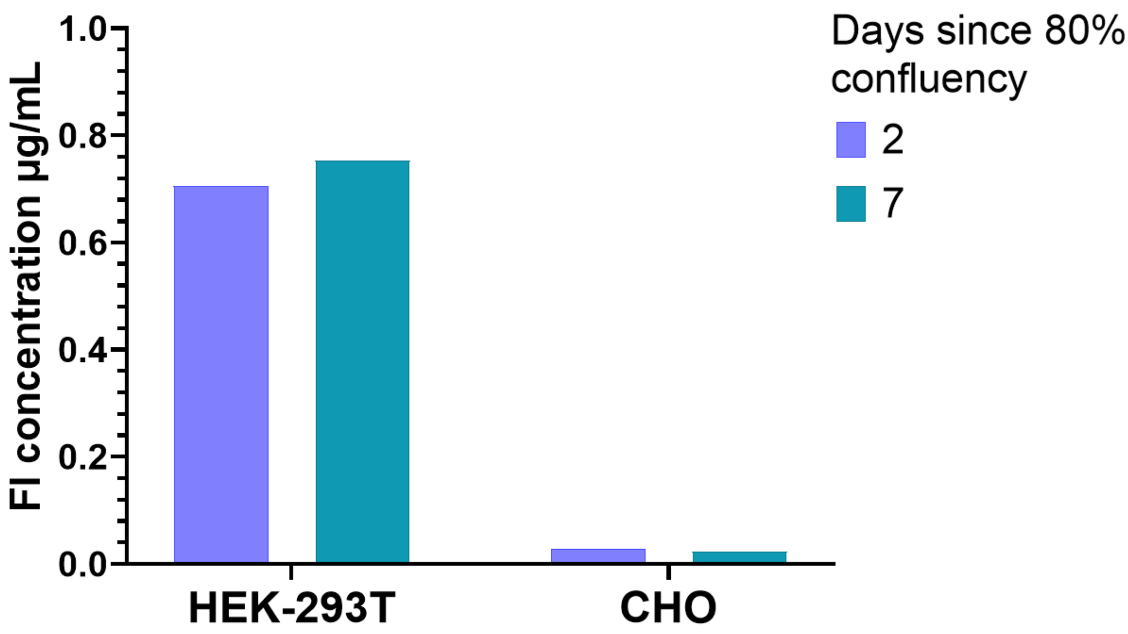

Figure 5-13 FI titre from the stable transfection of HEK293T and CHO cells with IRES FI vector as determined by ELISA.

FI ELISA of recombinant FI generated using the IRES vector in HEK-293T cells and CHO cells. FI concentration interpolated from Comptech FI standard curve. FI concentration assessed at 2 days and 7 days following the cells reaching 80% confluency.

5.3.5. Production of FI Variants

As mentioned in Chapter 3, three rare FI variants were chosen based upon their prevalence in the literature, their OR, their CADD scores, the position within the AP TMC, and the impact that these mutations had on steric hindrance and polarity. Using site-directed mutagenesis, the *CFI* gene in the *CFI* IRES vector was modified to introduce each variant. In addition to the AMD associated variants, the S525A FI mutation used for the generation of crystal structures (Xue *et al.*, 2017) was also introduced to the *CFI* backbone to facilitate the modelling of each variant within the TMC on the BIAcore (double mutant proteins: R406H/S525A; K441R/S525A and P553S/S525A) .

5.3.5.1. Sequencing of *CFI* Variants

Following SDM using the mutagenesis primers in Appendix 2, the modified plasmid cDNA was extracted from *E. coli* transformed with each *CFI* variant. The cDNA was then Sanger sequenced by Eurofins Genomics using the sequencing primers in appendix 3. Sequencing results were downloaded from Eurofins and analysed using Sequencher V5.0 by comparing to the wild-type *CFI* reference sequence (Y00318.1) to provide the sequencing traces (Figure 5-14). Each *CFI* sequence was checked for correct incorporation of the desired mutations and for the presence of any additional point mutations. Once the sequences were validated, the cDNA was then used for transfection into HEK293T cells.

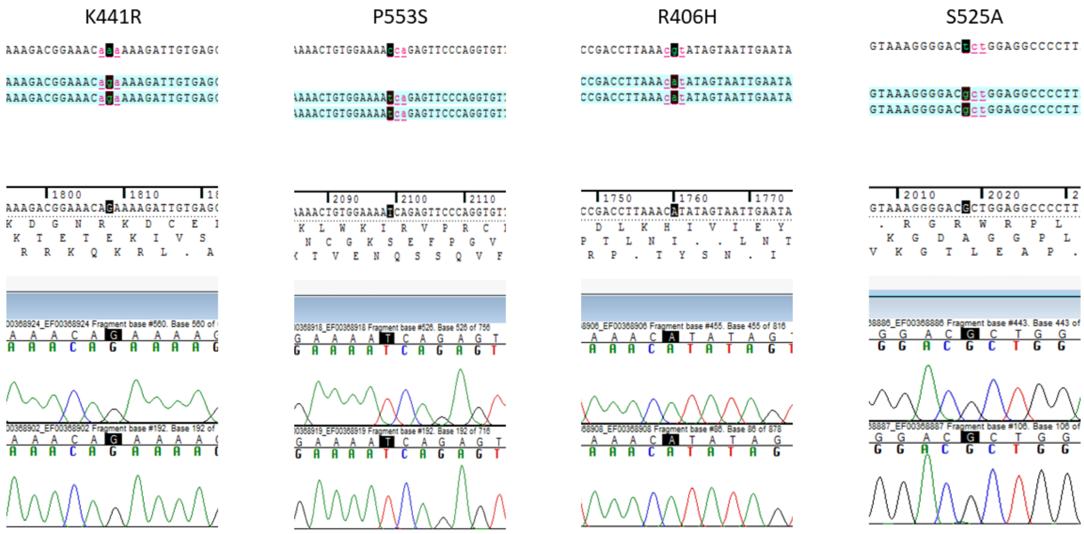

Figure 5-14 Sequencing of *CFI* variants within the IRES vector.
CFI nucleotide sequences and chromatograms made in Sequencher v5.0 resulting from Sanger sequencing of all successfully mutated, *CFI* variant -containing DNA constructs.

5.3.5.2. FI Variant Protein Production

Once the HEK293T cells were transfected with the variant cDNA, the cells were allowed to grow for three days in the absence of hygromycin. After 36 hours, the supernatants were collected and the FI expression determined by ELISA. Each variant produced a similar amount of FI (~20 ng/mL) except for R406H on the WT backbone, where the transfection was unsuccessful (Figure 5-15). Following the period of transient expression, 400 µg/mL of hygromycin was added to the transfected cells to select for successful incorporation of the

CFI IRES vector. After seven days, the supernatant was harvested, and an ELISA performed (Figure 5-16). Both the WT and S525A versions of P553S and K441R produced a similar amount of FI (~5 ng/mL), whereas R406H/S525A produced an expression of 38 ng/mL FI. The transfection of WT R406H was repeated, and a stable FI expressing colony was generated. Due to the variability in expression when using a bulk culture, each FI variant was diluted to monoclonality before expanding to multilayer flasks for FI production.

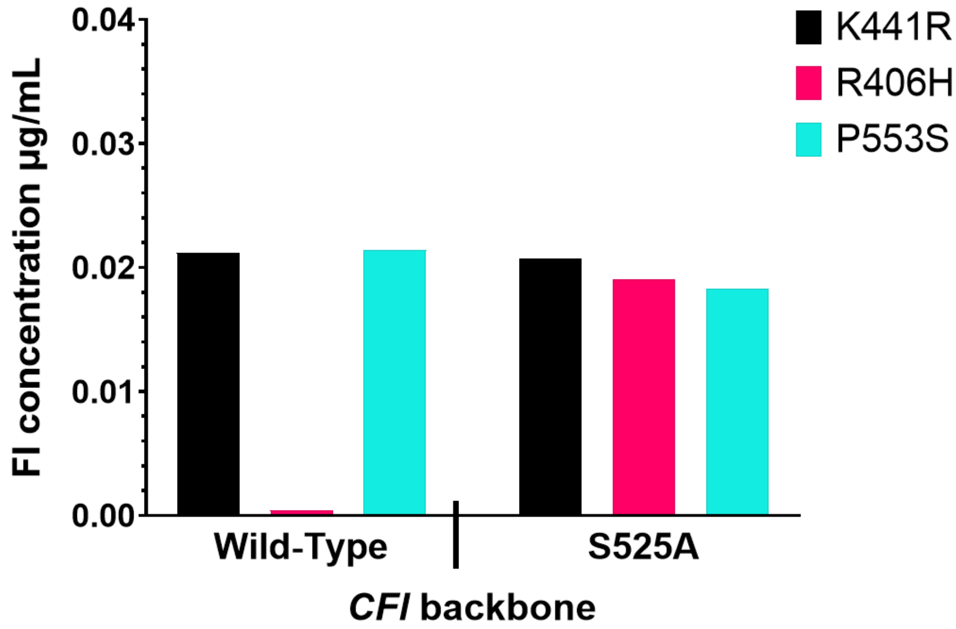

Figure 5-15 FI variant titre produced by transient transfection as measured by ELISA.
FI ELISA of recombinant FI variants generated using the IRES vector in HEK-293T cells, following transient transfection. FI concentration interpolated from Comptech FI standard curve.

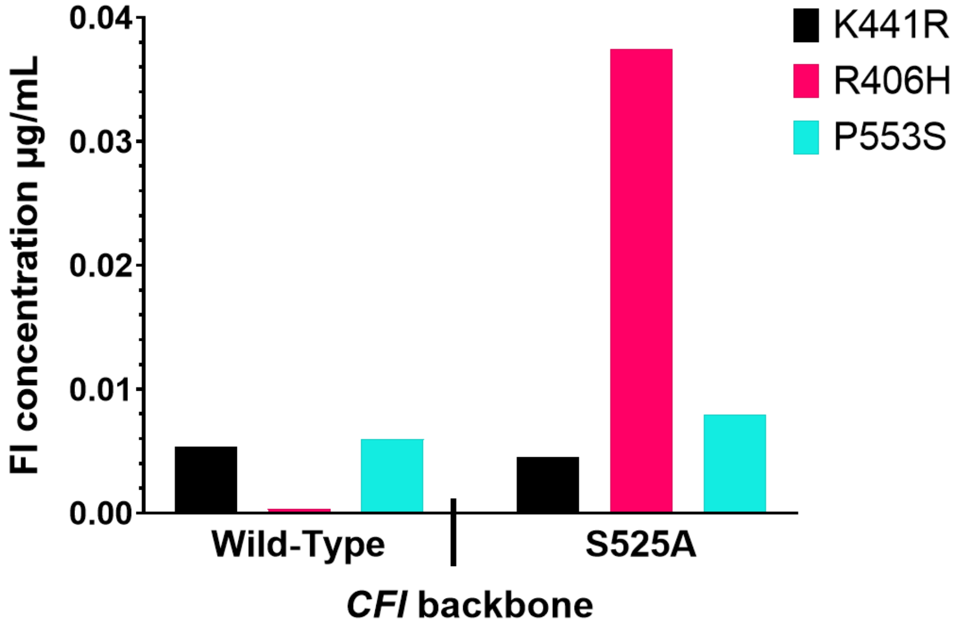

Figure 5-16 FI variant titre produced by stable transfection as measured by ELISA.
FI ELISA of recombinant FI variants generated using the IRES vector in HEK-293T cells, following transfection and selection with hygromycin. FI concentration interpolated from Comptech FI standard curve.

5.3.6. Purification

Each FI variant and control was purified from 600 mL supernatant using the method outlined in Methods 2.1.5. A separate 1 mL OX-21 column was used for each variant to eliminate the risk of cross contamination. Figure 5-17 shows the representative UV traces obtained from the purification of each variant on the WT backbone. The peak UV absorbance measured for each FI protein was variable, with wild-type FI (Figure 5-17A) producing the highest reading (295 mAU) and P553S (Figure 5-17D) producing the least (58 mAU). Regardless of the amplitude of the UV peak observed, the supernatant was passed over each column twice, to ensure complete depletion of FI. The same procedure was followed for the purification of the S525A backbone variants, with R406H producing the largest UV peak, and P553S producing the smallest. Following purification, the peak fractions for each protein were collated and buffer exchanged into PBS using a PD-10 column prior to analysis.

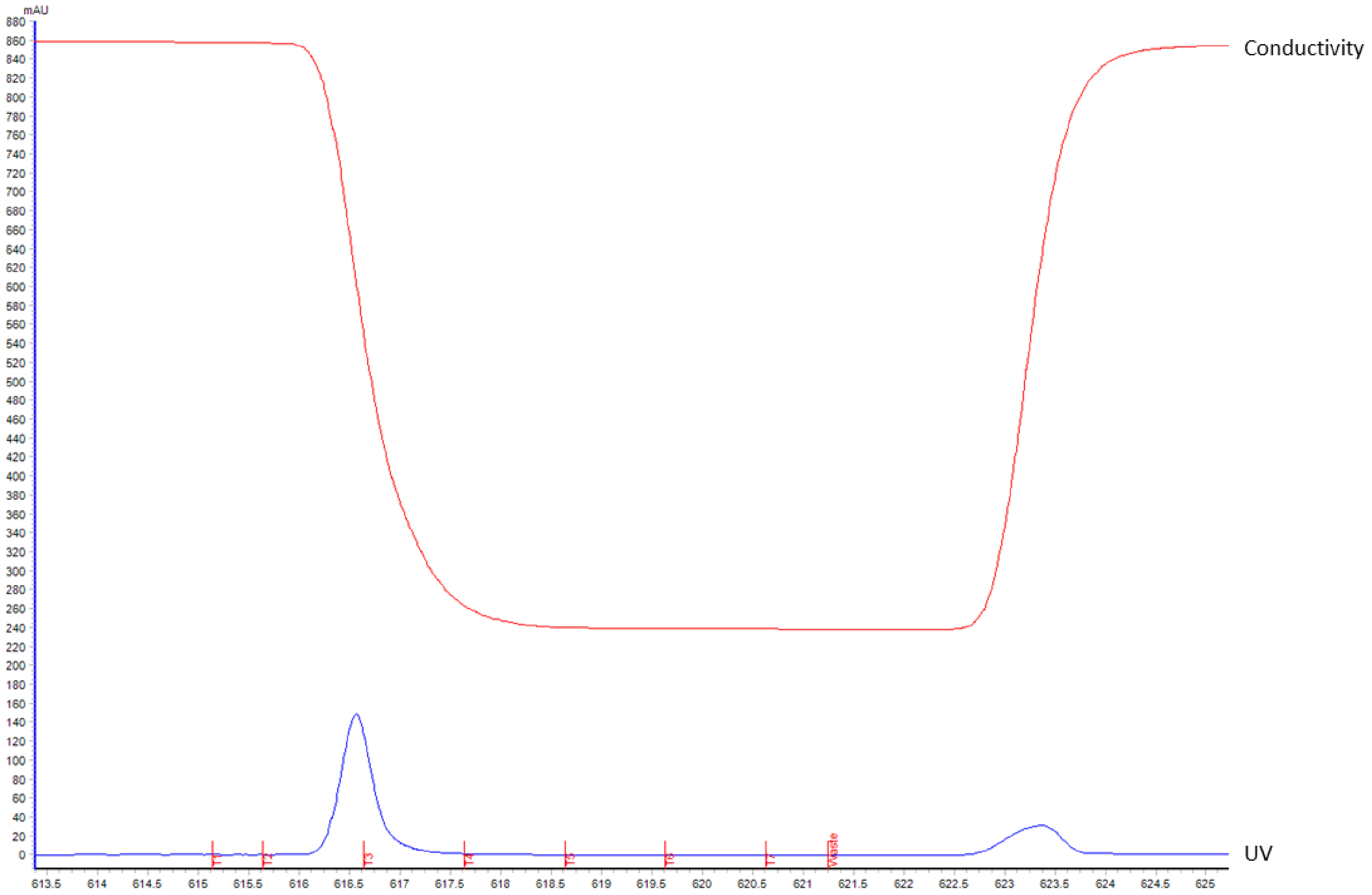

Figure 5-17A UV trace obtained during the purification of WT FI produced using the *CFI* IRES vector.

FI was purified from cell culture supernatant using the ÄKTA Start protein purification system with a 1 mL OX-21 Column. UV trace produced upon elution of with 0.1 M Glycine, pH 2.7.

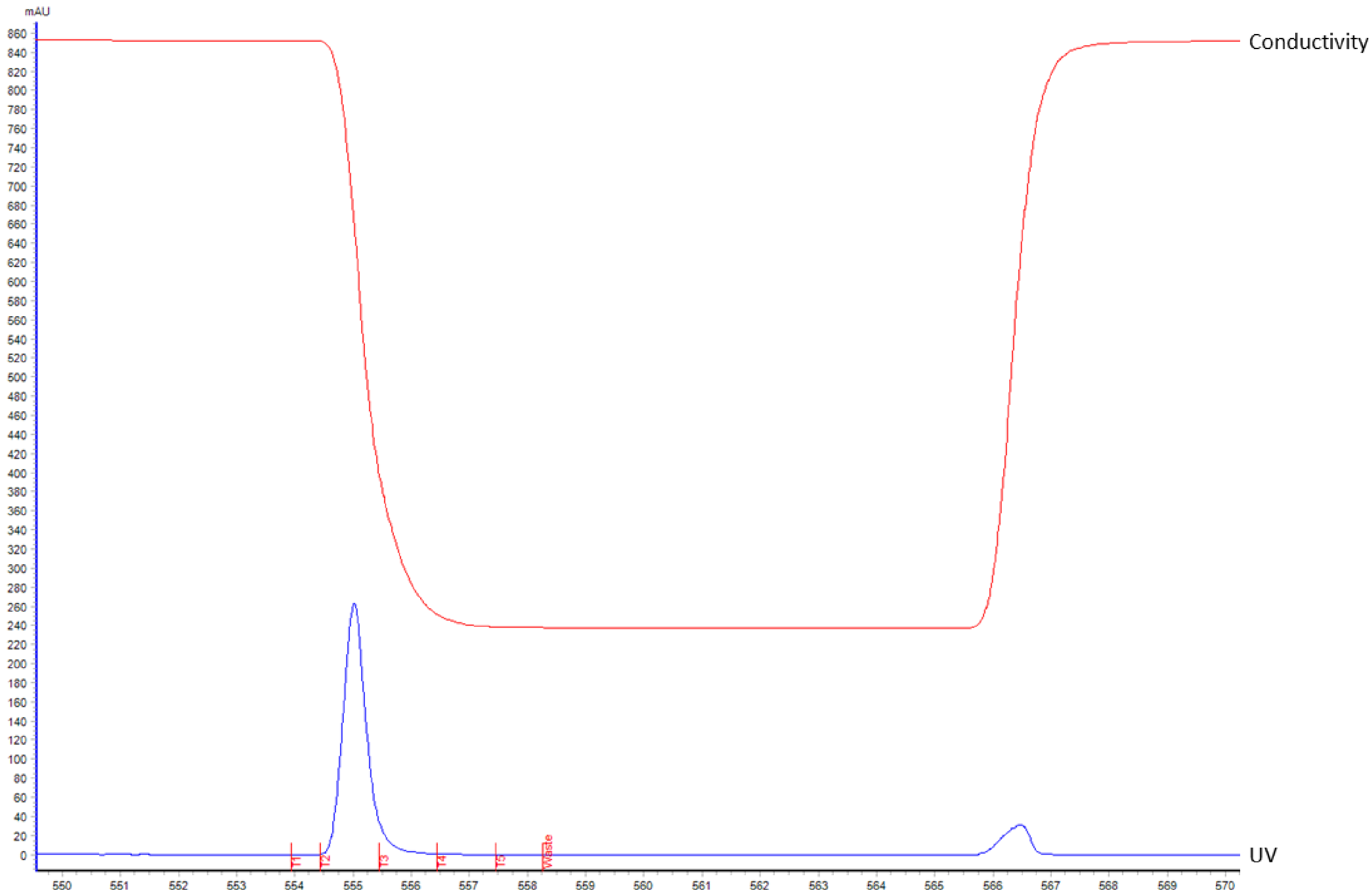

Figure 5-18B UV trace obtained during the purification of R406H FI produced using the *CFI* IRES vector.

FI was purified from cell culture supernatant using the ÄKTA Start protein purification system with a 1 mL OX-21 Column. UV trace produced upon elution of with 0.1 M Glycine, pH 2.7.

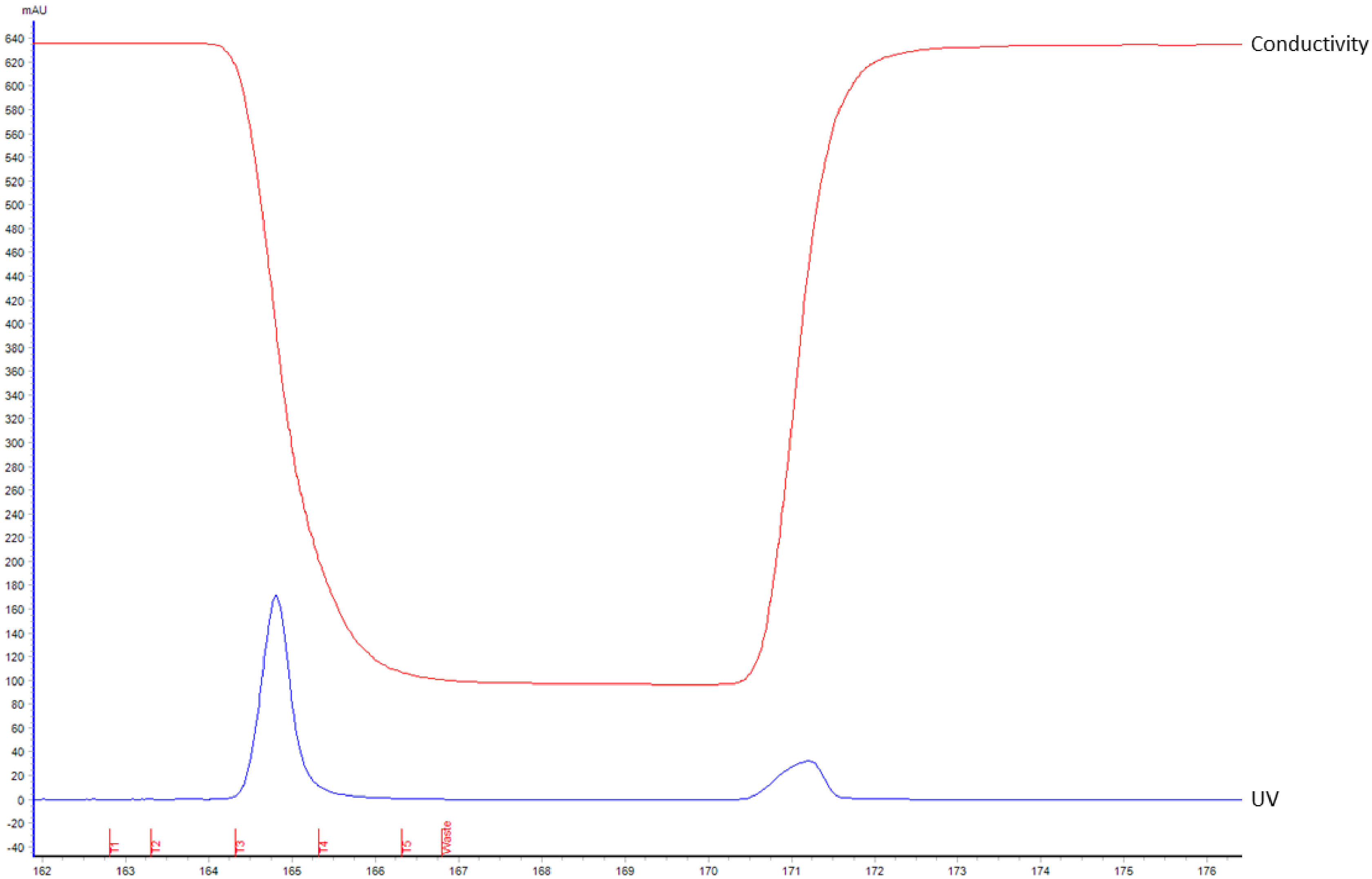

Figure 5-19C UV trace obtained during the purification of K441R FI produced using the *CFI* IRES vector.

FI was purified from cell culture supernatant using the ÄKTA Start protein purification system with a 1 mL OX-21 Column. UV trace produced upon elution of with 0.1 M Glycine, pH 2.7.

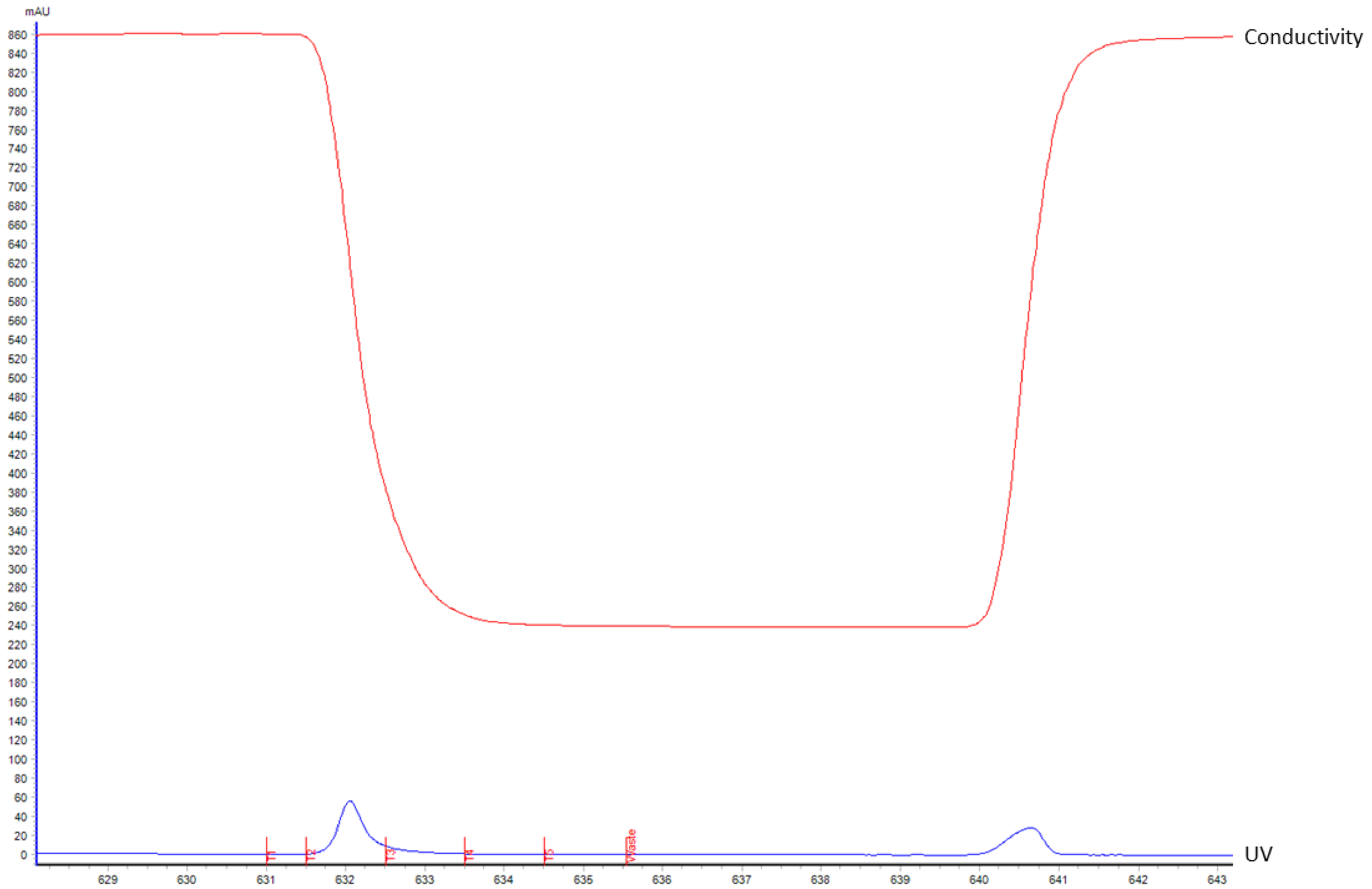

Figure 5-20D UV trace obtained during the purification of P553S FI produced using the *CFI* IRES vector.

FI was purified from cell culture supernatant using the ÄKTA Start protein purification system with a 1 mL OX-21 Column. UV trace produced upon elution of with 0.1 M Glycine, pH 2.7.

5.3.6.1. Analysis of SDS PAGE and Western Blotting

After purification, the resulting FI proteins were assessed by SDS PAGE stained with Coomassie and analysed by Western Blot, to confirm identity and to determine the presence of any contaminants. In the first instance, the three variants were compared to a serum purified wild-type FI protein standard (Comptech FI) on an SDS PAGE. As demonstrated in Figure 5-18, each of the three variants produced one band at ~88 kDa under non-reducing conditions and two bands at 50 kDa and at ~35 kDa respectively, under reducing conditions. The band at 50 kDa, represents the heavy chain of FI, and the band at ~35 kDa is for the light chain. For both conditions, the purified proteins exhibited high purity, with no evidence of breakdown products or any contaminating species. When compared to the reference FI, the recombinant proteins were slightly smaller in size, indicating a potential difference in glycosylation.

Due to the difference in size compared to the reference FI, an SDS PAGE and Western Blot were performed using recombinant WT FI as the positive control (Figure 5-19). On both the SDS PAGE and the Western Blot, the expected band at 88 kDa under non-reducing conditions, and two bands at ~50 kDa and ~35 kDa under reducing conditions were observed. There was no evidence of a ~90 kDa band, representative of Pro-I, in any of the preparations when reduced, confirming complete conversion of Pro-I to FI when using the *CFI* IRES vector.

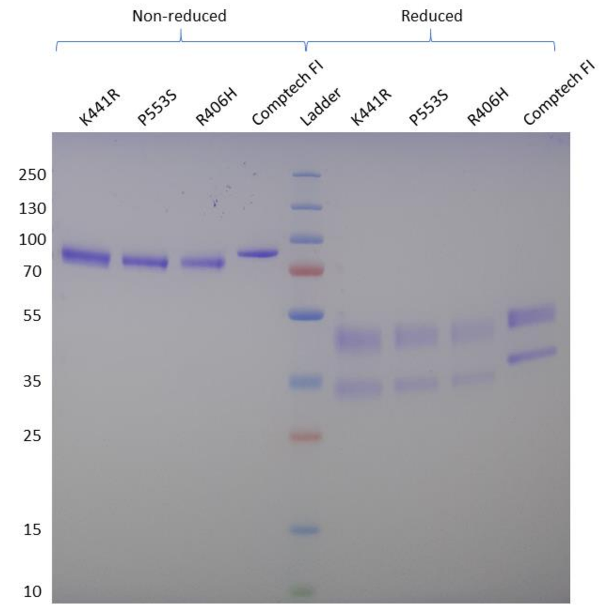

Figure 5-21 SDS PAGE visualisation of purified FI variants under non-reducing and reducing conditions.
SDS PAGE of purified FI variants and Comptech FI under non-reducing and reducing conditions, stained with Coomassie Blue.

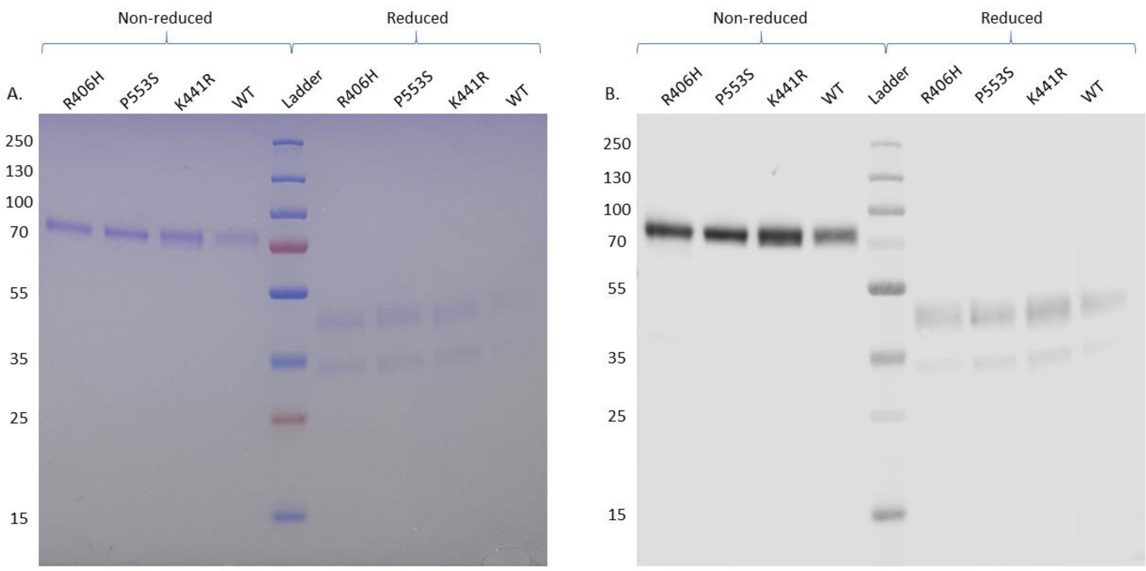

Figure 5-22 SDS PAGE and Western Blot of purified IRES FI.

SDS PAGE and Western Blot of purified FI variants and WT recombinant FI under non-reducing and reducing conditions. (A) SDS PAGE of purified FI variants and WT recombinant FI under non-reducing and reducing conditions stained with Coomassie Blue. (B) Western Blot of purified FI variants and WT recombinant FI under non-reducing and reducing conditions. Detected with sheep polyclonal anti-human Factor I.

5.3.6.2. Deglycosylation of IRES FI

To examine whether differing glycosylation patterns were responsible for the difference in molecular weight observed for the IRES FI compared to the serum purified FI (Comptech), both proteins were deglycosylated using the enzyme PNGase F. PNGase F is an endoglycosidase which cleaves the glycans from complex oligosaccharides between the innermost *N*-Acetylglucosamine (GlcNAc) and asparagine residues, such as those found on FI (Maley *et al.*, 1989). In the native form, serum purified FI had a molecular weight of 88 kDa, and IRES FI had a molecular weight of ~80 kDa. By incubating with PNGase F, a reduction in molecular weight was observed for both species, with the band for the native proteins shifting from ~88 kDa to ~62 kDa (Figure 5-20). This was consistent with the removal of the N-linked glycans from both chains, as the expected molecular weight for non-glycosylated FI is 62,878 Da (Tsiftsoglou *et al.*, 2006). As both species had the same observed molecular weight following PNGase F treatment, this demonstrated that the difference in size observed on the SDS-PAGE was solely attributed to variations in glycosylation. Furthermore, previous work by Tsiftsoglou *et al.* (2006) has demonstrated that FI glycans do not serve any functional role in the interactions between C3b and FH, providing confidence that the IRES FI can be used as a surrogate for serum FI, in spite of a differing glycosylation pattern.

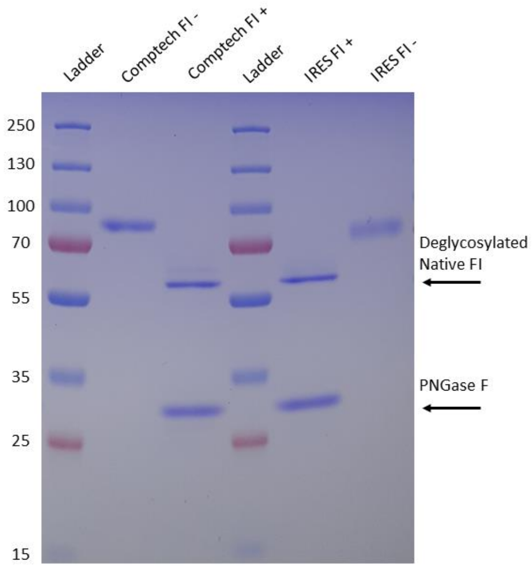

Figure 5-23 SDS PAGE visualisation of deglycosylated IRES FI compared to Comptech FI.
IRES FI and Comptech FI were deglycosylated using the Protein Deglycosylation Mix, according to manufacturer's instructions. 2 µg of IRES FI and Comptech FI were used per well. Samples run against a PageRuler Prestained Protein ladder (10 – 250 kDa). Control lanes contained no PNGase F.

5.3.7. Fluid-Phase Cofactor Assay

One of the main mechanisms for determining the functional activity of FI is through the use of fluid-phase cofactor activity assays. As AMD is predominantly considered a disease of the alternative pathway (Tan, Rickman and Katsanis, 2016), the cofactor assays performed in this chapter will be centred around the cleavage of C3b, in the presence of a variety of FI cofactors.

5.3.7.1. Cleavage of C3b by FI and Its Cofactors

There are three sites on C3b where FI can proteolytically cleave (Figure 1-4). The first and second cleavage sites of C3b are at Arg1303–Ser1304 and Arg1320–Ser1321, respectively, and can be cleaved in the presence of all of the FI cofactors, such as FH, FHL-1, MCP (CD46) and CR1 (CD35); however, the third and final cleavage site at Arg954–Glu955, can only be achieved in the presence of CR1. Following the formation of a C3b-cofactor complex, FI cleaves the first scissile bond and causes the breakdown of the C3b α' chain (114 kDa) into the α1 (68 kDa) and α2 (46 kDa) chains. Cleavage of this first bond induces flexibility within the C3b molecule, allowing repositioning of the second scissile bond into the FI active site. When this second site is cleaved, the fragment C3f (3 kDa), is released from the α2 chain (43 kDa), forming iC3b. Release of C3f enables unfolding of the CUB domain and the extension of a flexible peptide chain in α1 that facilitates the docking of the third scissile bond into the FI catalytic site (Xue *et al.*, 2017). In the presence of CR1, the final cleavage results in the release of C3dg (39 kDa) from α1 (29 kDa), forming the molecule C3c. C3dg is then further degraded by trypsin-like enzymes into the fragments C3d and C3g (Lachmann, Lay and Seilly, 2018).

5.3.7.2. Analysis of Cofactor Activity

Since all the cofactors can degrade C3b to iC3b in the presence of functional FI, FI activity was assessed by the extent of α' chain breakdown after a set period of time, as determined by approximately 50% α' chain remaining. The resulting breakdown products were then analysed by SDS PAGE stained with Coomassie. To provide a quantitative measure of FI activity, each cofactor assay was performed in triplicate and densitometry was used to determine the proportion of the α' chain remaining. Since the C3b β chain remains intact during FI mediated cleavage of C3b, the density of this chain was therefore used for normalisation to provide an inter-assay control. The activity of each variant was also compared to the negative (C3b + cofactor only) control to account for any C3b α' chain degradation which had occurred prior to incubation with FI.

5.3.7.3. IRES vs Serum Purified FI

In the first instance, the C3b cleavage ability of WT FI generated using the IRES vector was compared to that of serum purified FI in the presence of FH (Figure 5-21). Over the course of one hour, there was no noticeable difference in α' chain breakdown for either WT protein, with the α1 chain appearing clearly after 15 minutes, and the α2 chains appearing after 45 minutes for both proteins. At the end point, the remaining α' chain for each FI was normalised to the β chain and compared by densitometry. The amount of α' chain remaining was approximately equal for both origins of FI, demonstrating that IRES FI could be used to model human FI in fluid-phase cofactor activity assays.

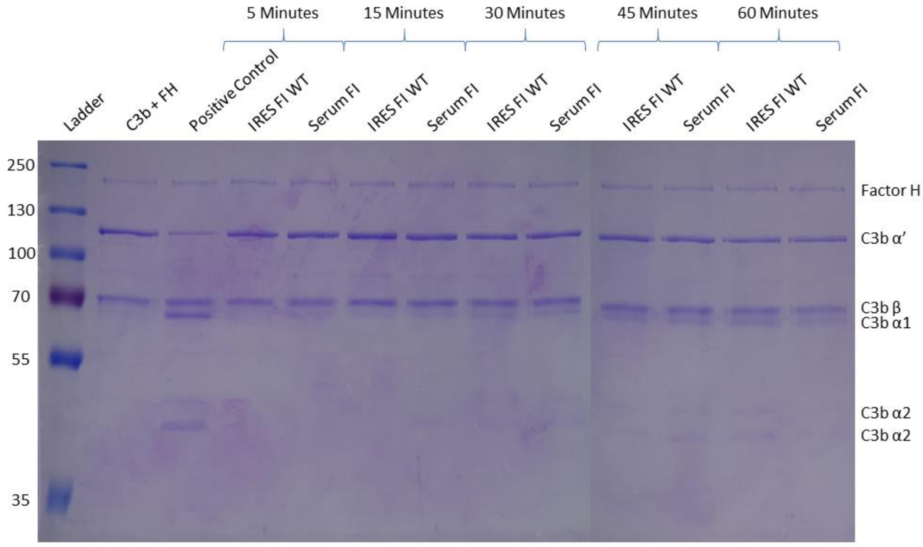

Figure 5-24 SDS PAGE visualisation of the fluid-phase cofactor (FLFH) activity of IRES FI compared to serum purified FI, over time.

SDS PAGE showing proteolytic activity of IRES FI and serum purified FI across a range of timepoints (5 – 60 minutes). Activity assessed by the ability of Factor I in combination with its cofactor FH, to cleave C3b to its inactive form iC3b. C3b cleavage was indicated by the appearance of α1 and the two α2 bands. All samples were ran under reducing conditions with a PageRuler Prestained Protein ladder (10 – 250 kDa).

5.3.7.4. Fluid-Phase Cofactor Assay with Full-Length FH (FLFH)

Following the confirmation of WT IRES FI activity, fluid-phase activity assays were performed for each of the selected variants using FLFH as the cofactor first. After resolving the breakdown products on an SDS PAGE gel (Figure 5-22) there was no distinct difference in activity for each of the variants when compared to the WT, with respect to α' chain breakdown and α1 chain generation. Additionally, each variant was able to cleave C3b to iC3b, as indicated by the presence of the smaller α2 chain. To confirm this finding, densitometry and statistical analysis were used to provide a quantitative measure of activity for each of the variants.

Using densitometry and statistical analysis with an n of 3, a difference in activity for one of the variants was identified (Figure 5-23). The P553S variant demonstrated a significant difference in activity when compared to the WT ($P < 0.05$), with this variant exhibiting a reduced ability to cleave the α' chain of C3b in the presence of FLFH. This reduction in activity was only observed for P553S, with the other two variants demonstrating a similar activity to the WT protein in this analysis. None of the variants demonstrated a difference in the generation of the smaller C3b fragments, with both the variants and the WT producing both α2 chains at 46 and 43 kDa.

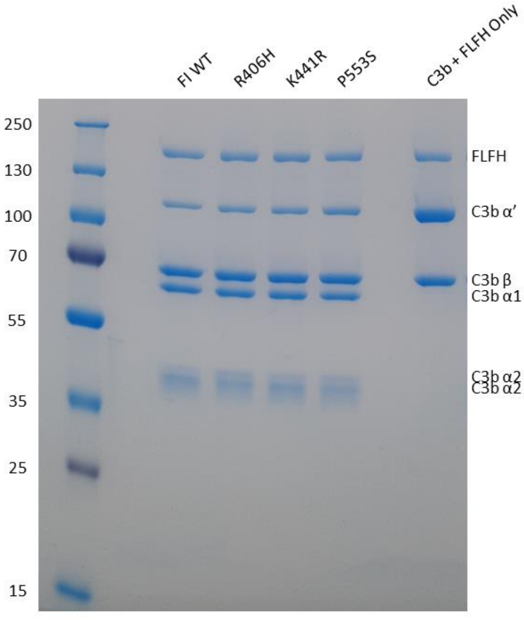

Figure 5-25 SDS PAGE for visualisation of the full length FH cofactor assay for the FI variants.
SDS-PAGE for visualisation of the full length FH cofactor assay for FI variants. Displayed is a Coomassie stained reducing SDS-PAGE gel run to separate the products of an FI fluid phase cofactor assay with FLFH. The α' (114kDa), β (68kDa), α1 (68kDa) and α2 (46 and 43kDa) C3b fragments can be seen clearly as labelled on the right side of the image, with the molecular weight marker and associated sizes on the left-hand side. Each lane represents the separation of an individual reaction mixture, each including a different FI variant, as labelled at the top of the image.

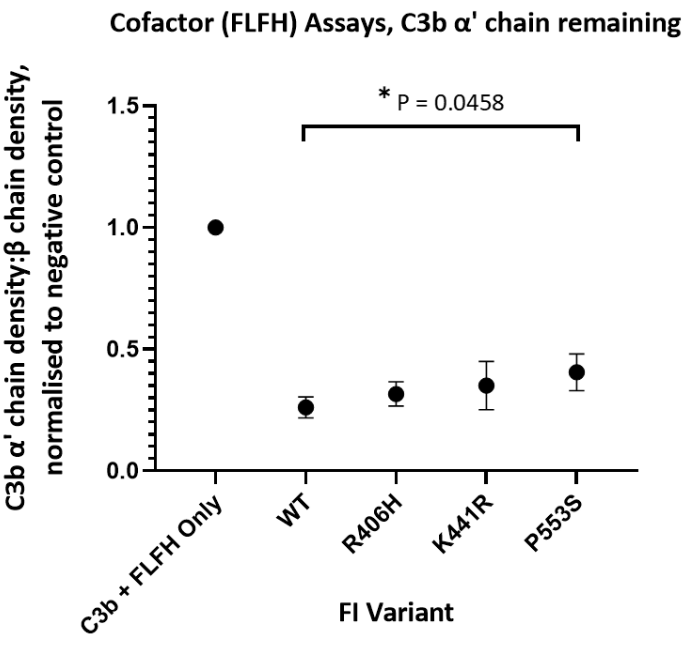

Figure 5-26 C3b α' chain degradation analysis of the FLFH cofactor assay for FI variants.
Plotted is the density of C3b α' chain remaining (y-axis) after incubation of recombinant purified FI with C3b and FH over a duration of 15 mins at 37°C during a fluid-phase cofactor assay. The density of the α' chain band

was normalised to the density of the β chain band, before the resultant figure was normalised to a negative control containing no FI, giving a proportion of α' chain remaining compared to the no FI control. The normalised density for each variant was given as the mean, with SEM as error bars and compared to the mean of the WT using a standard t-test (for n of 3 for all variants).

5.3.7.5. Fluid-Phase Cofactor Assay with FH1-4

The variants were then tested in a fluid-phase assay with FH1-4 as the cofactor using the same method as before. Qualitatively there were no differences in activity between the variants and the WT (Figure 5-24). There were also no noticeable differences in the generation of the breakdown fragments, with α1 and the two α2 chains being produced by each variant.

To determine whether the qualitative similarities remained following normalisation, densitometry and statistical analysis were performed (Figure 5-25). There was no significant difference in activity between the variants and WT FI identified. Again, there was also no difference in the generation of the α2 fragments.

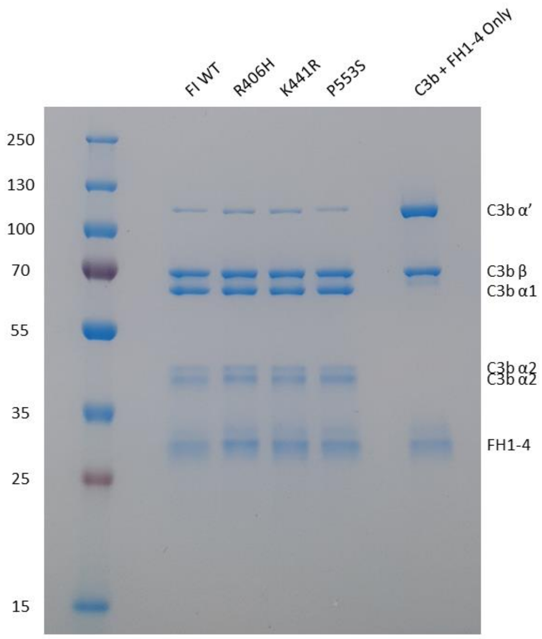

Figure 5-27 SDS-PAGE for visualisation of the FH1-4 cofactor assay for FI variants.
SDS-PAGE for visualisation of the FH1-4 cofactor assay for FI variants. Displayed is a Coomassie stained reducing SDS-PAGE gel run to separate the products of an FI fluid phase cofactor assay with FH1-4. The α' (114kDa), β (68kDa), α1 (68kDa) and α2 (46 and 43kDa) C3b fragments can be seen clearly as labelled on the right side of the image, with the molecular weight marker and associated sizes on the left-hand side. Each lane represents the separation of an individual reaction mixture, each including a different FI variant, as labelled at the top of the image.

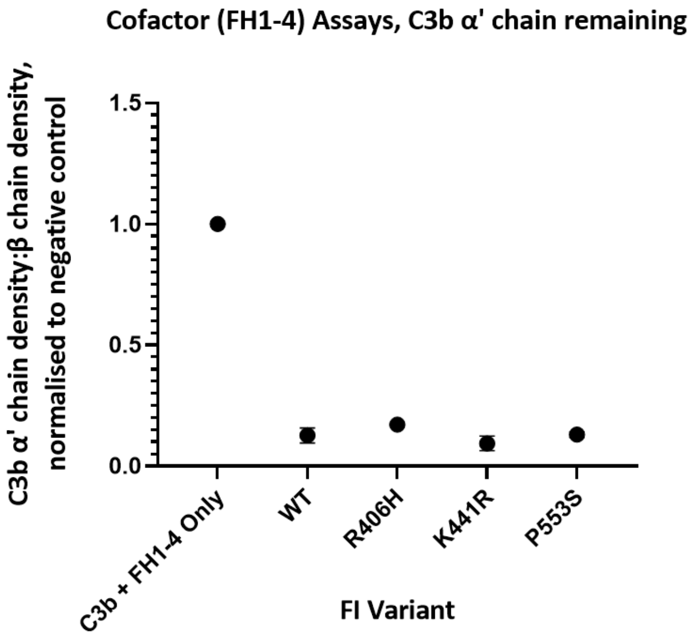

Figure 5-28 C3b α' chain degradation analysis of the FH1-4 cofactor assay for FI variants.
Plotted is the density of C3b α' chain remaining (y-axis) after incubation of recombinant purified FI with C3b and FH1-4 over a duration of 15 mins at 37°C during a fluid-phase cofactor assay. The density of the α' chain band was normalised to the density of the β chain band, before the resultant figure was normalised to a negative control containing no FI, giving a proportion of α' chain remaining compared to the no FI control. The normalised density for each variant was given as the mean, with SEM as error bars and compared to the mean of the WT using a standard t-test (for n of 3 for all variants).

5.3.7.6. Fluid-Phase Cofactor Assay with FHL-1

Next, the variants were tested in a fluid-phase assay with FHL-1 as the cofactor. Similarly to FH1-4, there were no marked visual differences in activity between the variants and the WT (Figure 5-26). However, for P553S the smaller α2 chain did seem to be slightly reduced when compared to the other variants, potentially indicating a reduction in cleavage of the second scissile bond. Although due to the resolution of the gel, densitometry could not be performed on the α2 band to support this observation.

Once assessed by densitometry and normalised to the β chain, no statistical differences in activity for P553S or the other variants were identified (Figure 5-27). Unfortunately, due to the similarity in size between FHL-1 (49 kDa) and the larger α2 chain, the resolution of the gel was not enough to perform densitometry on this chain. However, following normalisation to the β chain there were no significant differences in the production of the smaller α2 chain for each of the variants.

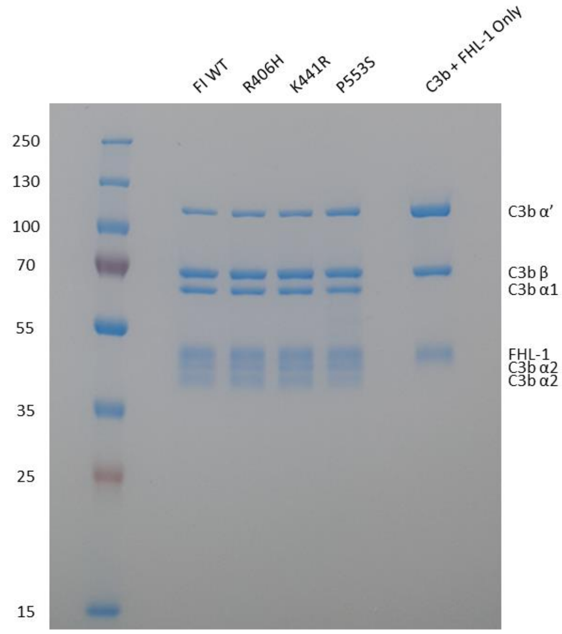

Figure 5-29 SDS-PAGE for visualisation of the FHL-1 cofactor assay for FI variants.

SDS-PAGE for visualisation of the FHL-1 cofactor assay for FI variants. Displayed is a Coomassie stained reducing SDS-PAGE gel run to separate the products of an FI fluid phase cofactor assay with FHL-1. The α' (114kDa), β (68kDa), α1 (68kDa) and α2 (46 and 43kDa) C3b fragments can be seen clearly as labelled on the right side of the image, with the molecular weight marker and associated sizes on the left-hand side. Each lane represents the separation of an individual reaction mixture, each including a different FI variant, as labelled at the top of the image.

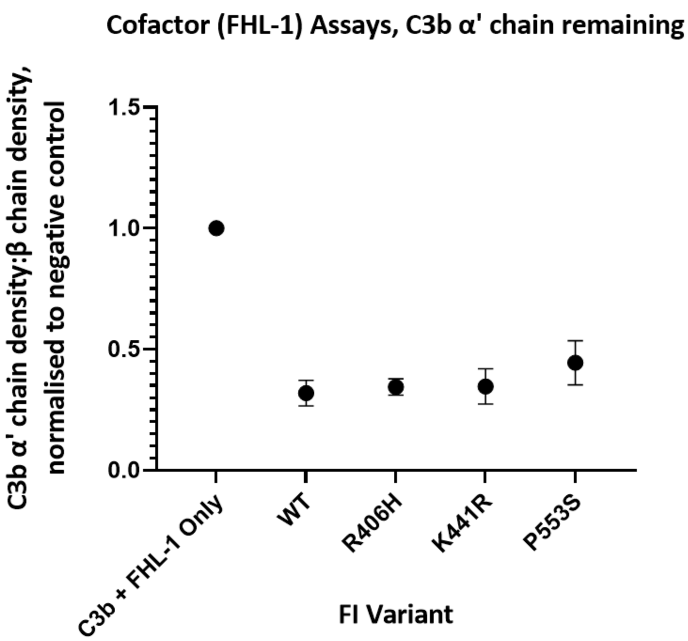

Figure 5-30 C3b α' chain degradation analysis of the FHL-1 cofactor assay for FI variants.

Plotted is the density of C3b α' chain remaining (y-axis) after incubation of recombinant purified FI with C3b and FHL-1 over a duration of 15 mins at 37°C during a fluid-phase cofactor assay. The density of the α' chain band was normalised to the density of the β chain band, before the resultant figure was normalised to a negative control containing no FI, giving a proportion of α' chain remaining compared to the no FI control. The normalised density for each variant was given as the mean, with SEM as error bars and compared to the mean of the WT using a standard t-test (for n of 3 for all variants).

5.3.7.7. Fluid-Phase Cofactor Assay with MCP

Following on from the FH associated cofactors, MCP was the next cofactor used for the fluid-phase C3b breakdown assay (Figure 5-28). As before, there were no large differences in activity observed, however R406H did appear to generate a greater proportion of both α1 and the smaller α2 breakdown products as visualised on the SDS PAGE gel, when compared to both the WT and the other variants.

To corroborate these findings, densitometry and statistical analysis were performed as before (Figure 5-29). There was no statistical difference in activity observed for R406H or K441R when compared to the WT, however P553S was significantly less active than the WT with regards to α' chain breakdown ($P < 0.05$). The generation of the 43 kDa α2 fragment was also assessed by densitometry (Figure 5-30). R406H appeared to generate iC3b faster than WT in the presence of MCP, however due to the large variability, this was not conclusive. Supporting the findings from the α' chain cleavage, P553S also generated the least amount of iC3b.

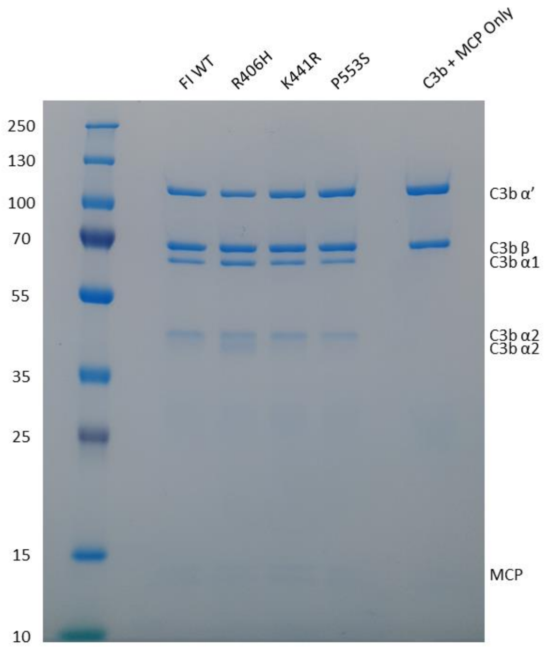

Figure 5-31 SDS-PAGE for visualisation of the MCP cofactor assay for FI variants.
SDS-PAGE for visualisation of the MCP cofactor assay for FI variants. Displayed is a Coomassie stained reducing SDS-PAGE gel run to separate the products of an FI fluid phase cofactor assay with MCP. The α' (114kDa), β (68kDa), α1 (68kDa) and α2 (46 and 43kDa) C3b fragments can be seen clearly as labelled on the right side of the image, with the molecular weight marker and associated sizes on the left-hand side. Each lane represents the separation of an individual reaction mixture, each including a different FI variant, as labelled at the top of the image.

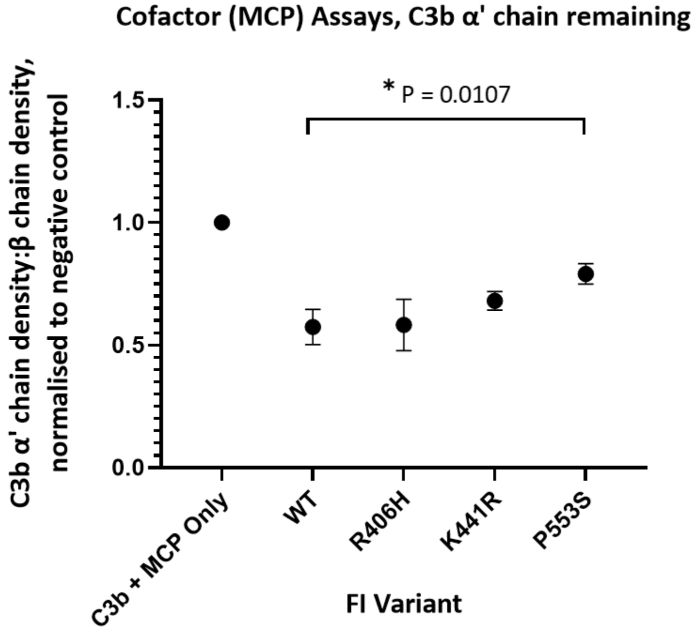

Figure 5-32 C3b α′ chain degradation analysis of the MCP cofactor assay for FI variants.
Plotted is the density of C3b α′ chain remaining (y-axis) after incubation of recombinant purified FI with C3b and MCP over a duration of 15 mins at 37°C during a fluid-phase cofactor assay. The density of the α′ chain band was normalised to the density of the β chain band, before the resultant figure was normalised to a negative control containing no FI, giving a proportion of α′ chain remaining compared to the no FI control. The normalised density for each variant was given as the mean, with SEM as error bars and compared to the mean of the WT using a standard t-test (for n of 3 for all variants).

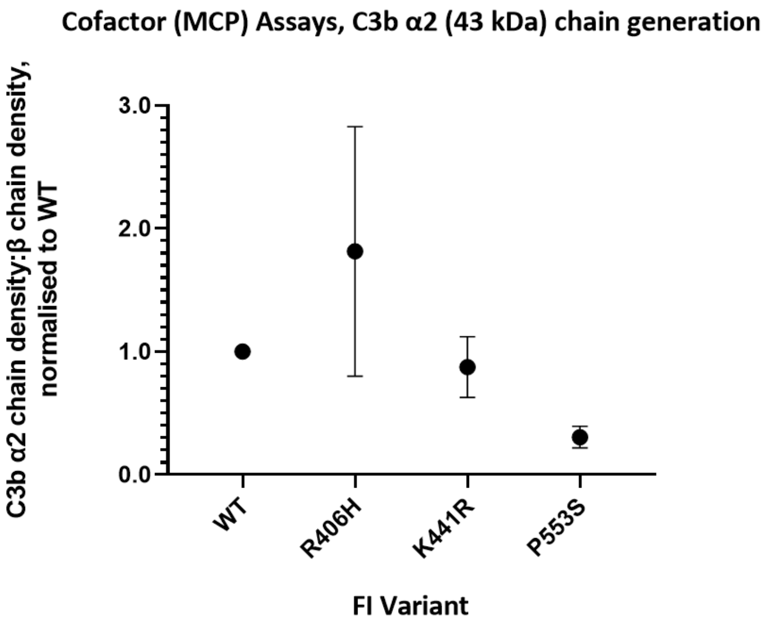

Figure 5-33 C3b α2 chain generation analysis of the MCP cofactor assay for FI variants.
Plotted is the density of C3b α2 chain (43kDa) generated (y-axis) after incubation of each FI variant (x-axis) with C3b and MCP for 15 mins at 37°C during a fluid phase cofactor assay. The density of the α2 chain band was normalised to the density of the β chain band in each individual test, before the resultant figure for each variant was normalised to the result for the WT positive control, giving a ratio of α2 chain generated compared to the WT result.

5.3.7.8. Fluid-Phase Cofactor Assay with soluble CR1

The final cofactor used for the assessment of fluid-phase C3b breakdown, was sCR1 (Figure 5-31). There were no large changes α' chain cleavage, however, for P553S there was more α' chain remaining when compared to the WT. P553S also demonstrated reduced activity with regards to production of the α2 chains. When using sCR1 as the cofactor, FI can cleave the third scissile bond to produce C3dg. Each variant was able to generate this final cleavage product, however, there was less C3dg produced by P553S likely due to its decreased activity.

To further assess the difference in activity between the variants and the WT, densitometry and statistical analysis was performed for n of 3 replicates. Whilst there was no significant difference between R406H and K441R and the WT, P553S was statistically different ($P < 0.05$), demonstrating a reduction in α' chain cleavage for this variant (Figure 5-32). There was also a notable decrease in the generation of the smaller α2 chain for P553S relative to the WT, providing further evidence that this variant was less active than the WT in the presence of sCR1 (Figure 5-33). Both K441R and R406H performed similarly to the WT with regards to the generation of the 43 kDa α2 chain, although the average normalised density for K441R was slightly less than that of R406H (0.849 vs 0.917). Whilst each variant was able to generate C3dg, the resolution of the 39 kDa band on the SDS PAGE gel was not sufficient to provide reliable densitometric assessment.

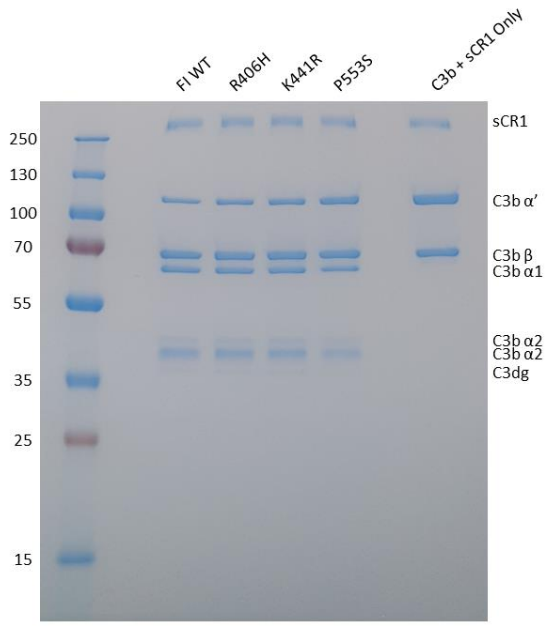

Figure 5-34 SDS-PAGE for visualisation of the sCR1 cofactor assay for FI variants.

SDS-PAGE for visualisation of the sCR1 cofactor assay for FI variants. Displayed is a Coomassie stained reducing SDS-PAGE gel run to separate the products of an FI fluid phase cofactor assay with sCR1. The α' (114kDa), β (68kDa), α1 (68kDa) and α2 (46 and 43kDa) C3b fragments can be seen clearly as labelled on the right side of the image, with the molecular weight marker and associated sizes on the left-hand side. Each lane represents the separation of an individual reaction mixture, each including a different FI variant, as labelled at the top of the image.

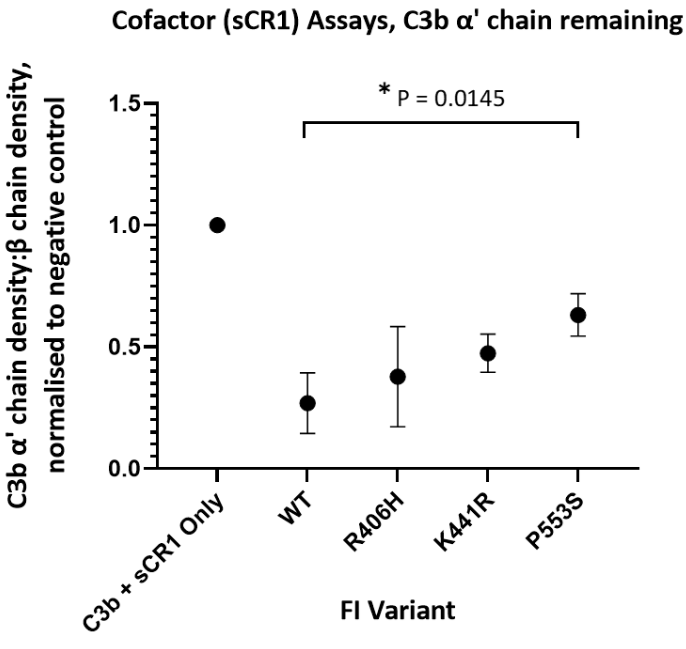

Figure 5-35 C3b α' chain degradation analysis of the sCR1 cofactor assay for FI variants.

Plotted is the density of C3b α' chain remaining (y-axis) after incubation of recombinant purified FI with C3b and sCR1 over a duration of 15 mins at 37°C during a fluid-phase cofactor assay. The density of the α' chain band was normalised to the density of the β chain band, before the resultant figure was normalised to a negative control containing no FI, giving a proportion of α' chain remaining compared to the no FI control. The normalised density for each variant was given as the mean, with SEM as error bars and compared to the mean of the WT using a standard t-test (for n of 3 for all variants).

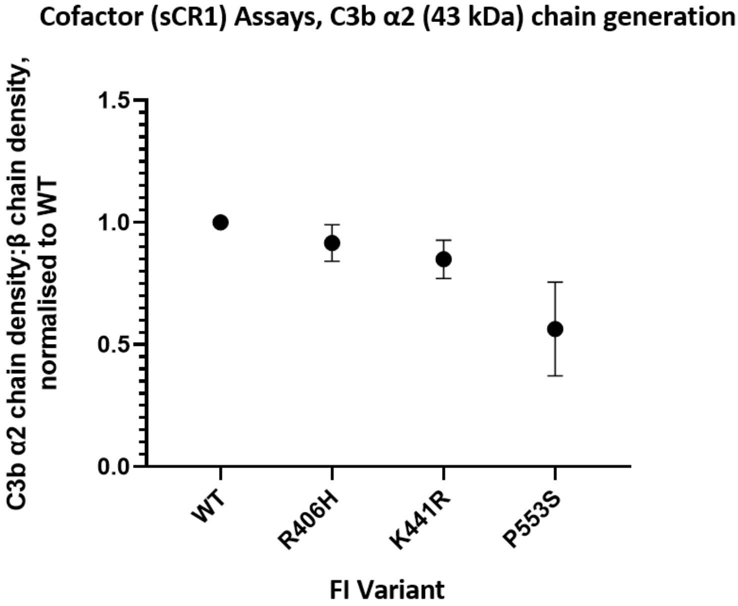

Figure 5-36 C3b α2 chain generation analysis of the sCR1 cofactor assay for FI variants.
Plotted is the density of C3b α2 chain (43kDa) generated (y-axis) after incubation of each FI variant (x-axis) with C3b and sCR1 for 15 mins at 37°C during a fluid phase cofactor assay. The density of the α2 chain band was normalised to the density of the β chain band in each individual test, before the resultant figure for each variant was normalised to the result for the WT positive control, giving a ratio of α2 chain generated compared to the WT result.

5.3.7.9. Summary of Cofactor Assay Results

Overall, only P553S demonstrated a significant reduction in activity across a range of cofactors. Both R406H and K441R exhibited a similar activity to the WT in the fluid-phase with regards to α' chain degradation for all of the cofactors tested. In most instances the WT was the most active, followed by R406H and K441R, with P553S being the least active variant. For all cofactors, the first cleavage of the α' chain appeared to be the rate-limiting step, due to the fact that if the α' chain cleavage was reduced, then the generation of the 43 kDa α2 chain was also reduced; with the one exception occurring for R406H with MCP.

5.3.8. Haemolytic AP Cofactor Activity on C3b-Coated Sensitised Sheep Erythrocytes

The effect of the rare genetic variants on FI-mediated proteolytic cleavage of C3b into iC3b in the presence of FLFH, was then assessed on the surface of C3b-coated activated sheep erythrocytes. Supporting the evidence from the fluid-phase cofactor assays, each variant demonstrated the ability to cleave C3b into iC3b, to protect an activated surface from complement-mediated lysis upon the addition of guinea pig serum. There was no significant difference in the concentration of each variant required to achieve 50% protection from lysis compared to the WT (IC_{50} 1.34 nM) (Figure 5-34). However, K441R was marginally more protective than the WT (IC_{50} 1.32 nM), P553S performed similarly (IC_{50} 1.40 nM), and R406H was shown to be the least protective (IC_{50} 1.80 nM). This is in contrast to the results from the FH fluid-phase cofactor assay where P553S was significantly less active, however as each of the variants are still able to cleave C3b, the differences in activity between the variants may be lost due to the error within the assay.

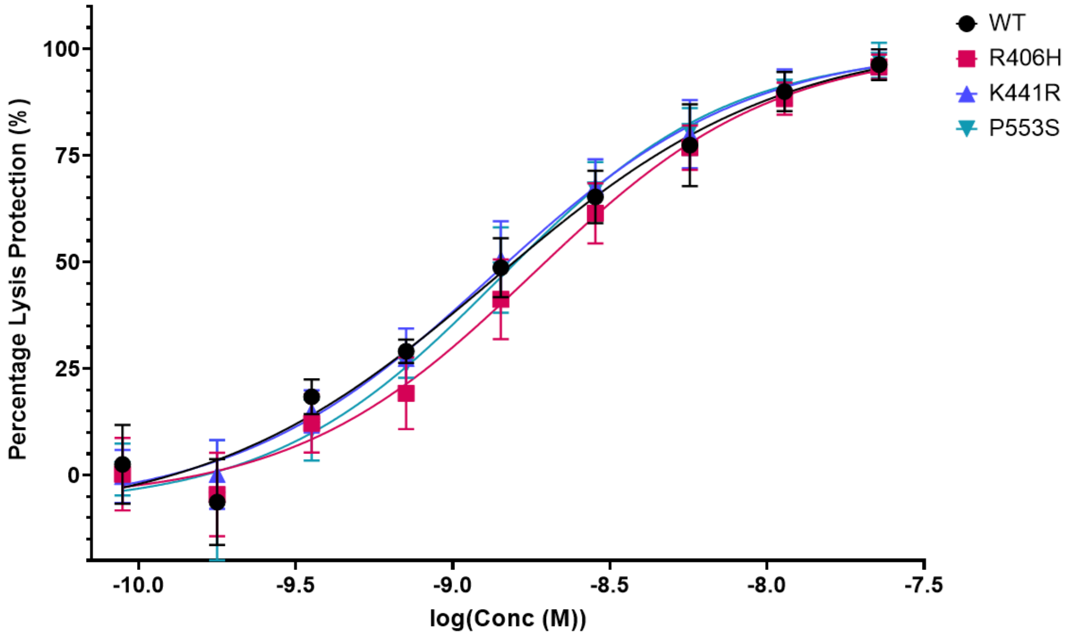

Figure 5-37 Haemolytic cofactor activity of the FI variants on sensitised sheep red blood cells.
C3b-coated activated sheep erythrocyte cofactor haemolysis assay. Percentage lysis protection plotted against log(Conc (M)) for each FI variant. Error bars show the standard deviation.

5.3.9. Trimolecular Complex (TMC) Formation

Since each of the previous assays were only able to demonstrate subtle differences in activity. BIAcore was used to model the impact that each variant had on the formation of the alternative pathway trimolecular complex, FI:FH:C3b, to gain a deeper understanding of the impact of these variants may have on FI function.

5.3.9.1. S525A FI

In most circumstances, assessment of AP TMC formation using SPR is complicated by the cleavage of the chip bound C3b substrate by the active FI protein. Following C3b cleavage, the TMC rapidly dissociates due to a lack of affinity by FI and FH for C3b after the loss of C3f. To overcome this issue, a catalytically inactivated form of FI was generated through the incorporation of the S525A mutation into the *CFI* IRES vector backbone.

5.3.9.1.1. S525A FI SDS PAGE

Following transfection into HEK293T and confirmation of FI expression by ELISA, S525A FI was purified from supernatant by affinity chromatography as before (Methods 2.1.5).

Figure 5-35 visualises the successful purification of S525A FI from supernatant as determined by SDS PAGE stained with Coomassie. Under both reducing and non-reducing conditions the bands migrated to the expected 88 kDa for the non-reduced protein, and to ~38 kDa and ~50 kDa, indicative of the FI light and heavy chains respectively, under reducing conditions. Again, through the use of the IRES vector, there was no evidence of any Pro-I contamination or any FI degradation.

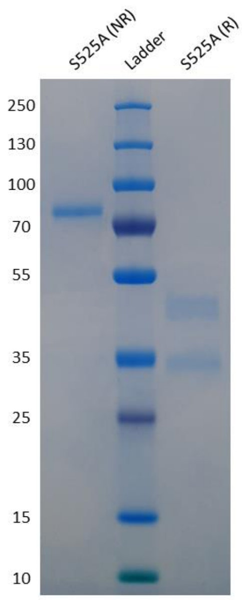

Figure 5-38 SDS PAGE of inactive FI (S525A) stained with coomassie blue.
SDS PAGE of reduced and non-reduced inactive FI stained with Coomassie Blue.

5.3.9.1.2. S525A FI Fluid-Phase Cofactor Activity

To confirm the inactivation of the serine protease domain, a fluid-phase cofactor assay was performed using full length FH. As before, proteolytic activity is determined by the degradation of C3b α' into the α1 and the two α2 chains. Figure 5-36 demonstrates that purified S525A is unable to cleave C3b and is comparable to the negative control, where there was no FI present. To quantify the observed lack of activity, densitometry was performed (Figure 5-37). Following normalisation to the negative control, S525A exhibited an equivalent lack of activity (~1).

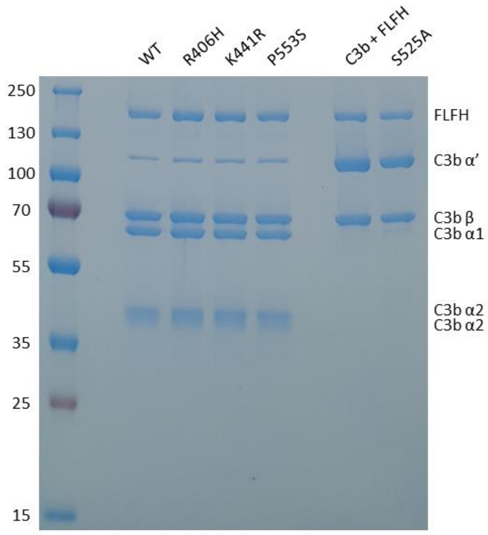

Figure 5-39 SDS-PAGE for visualisation of the FLFH cofactor assay for S525A FI.

SDS-PAGE for visualisation of the full length FH cofactor assay for inactive FI vs active variants. Displayed is a Coomassie stained reducing SDS-PAGE gel run to separate the products of an FI fluid phase cofactor assay with FLFH. The α' (114kDa), β (68kDa), α1 (68kDa) and α2 (46 and 43kDa) C3b fragments can be seen clearly as labelled on the right side of the image, with the molecular weight marker and associated sizes on the left-hand side. Each lane represents the separation of an individual reaction mixture, each including a different FI variant, as labelled at the top of the image.

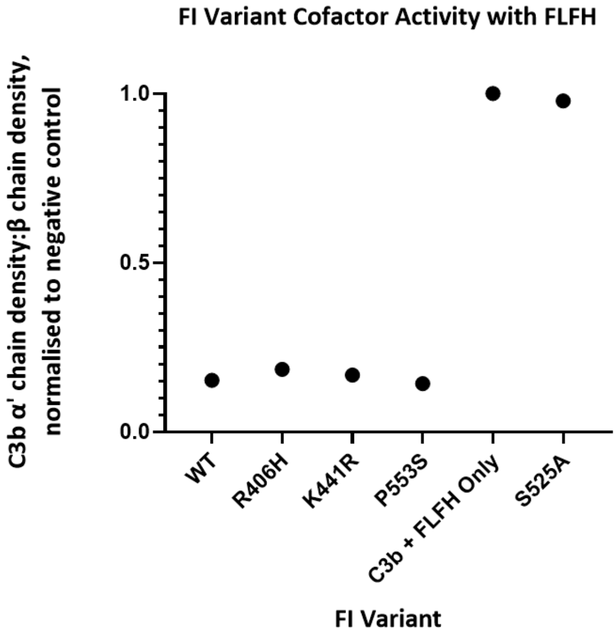

Figure 5-40 C3b α' chain degradation analysis of the FLFH cofactor assay for S525A FI.

Plotted is the density of C3b α' chain remaining (y-axis) after a 60 minute incubation of inactive FI vs active variants with C3b and FLFH at 37°C during a fluid-phase cofactor assay. The density of the α' chain band was normalised to the density of the β chain band, before the resultant figure was normalised to a negative control containing no FI, giving a proportion of α' chain remaining compared to the no FI control.

5.3.9.1.3. Amidolytic Assay

To further validate the inactivation of FI by the S525A mutation, an amidolytic assay was performed using the synthetic FI substrate Boc-Asp(OBzl)-Pro-Arg-7-Amino-4-

methylcoumarin (AMC). Previously, Tsiftsoglou and Sim had demonstrated that FI can cleave AMC derivatives in the absence of a cofactor, therefore facilitating an assessment of protease activity independent of cofactor interactions (Tsiftsoglou and Sim, 2004). By cleaving the substrate the fluorogenic AMC molecule is released, enabling assessment of substrate cleavage following excitation at 355nm and monitoring the emission at 460 nm. The activity of FI was determined by the change in emission per minute at the linear portion of the emission curve (ΔOD) (Figure 5-38). WT FI was shown to have an ΔOD of 3.685 at 0.5 µM and 2.524 at 0.25 µM. In comparison to active FI, S252A had an ΔOD of 0.08046 and was equivalent to that of the WT when using the inhibitor, Pefabloc-SC, previously shown to completely inhibit substrate cleavage (Tsiftsoglou and Sim, 2004).

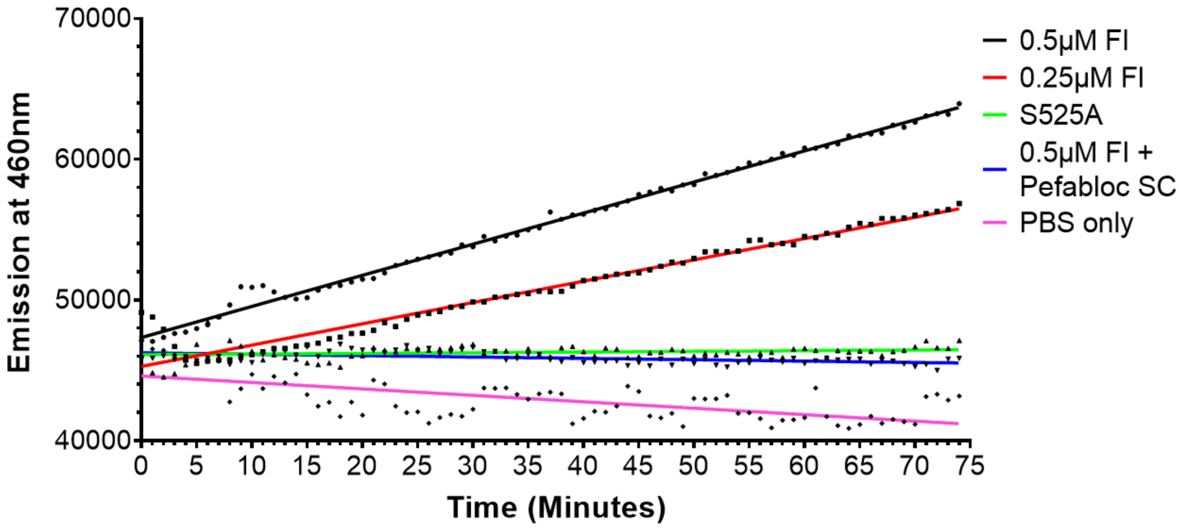

Figure 5-41 Comparison of Boc-Asp(OBzl)-Pro-Arg-AMC cleavage by WT and S525A FI.
Activity of FI in the absence of cofactor as determined by the release of fluorogenic AMC substrate. Emission at 460nm plotted against time.

Taken together, the results from the fluid-phase cofactor assay and the amidolytic assay demonstrate that the S525A mutation renders WT FI inactive, irrelevant of the substrate or cofactor used.

5.3.9.1.4. Production of FI variants on the S525A *CFI* backbone

To study the impact that each variant had on the formation of the TMC using the BIAcore, SDM was used to introduce each variant onto the IRES-*CFI* S525A backbone. Following transfection into HEK293T, the presence of secreted FI was confirmed by ELISA. The highest expressing colonies where then diluted to monoclonality before scaling-up. Each variant was purified as described previously. Figure 5-39 shows the purified double mutant proteins under reducing conditions. The heavy and light chain for all variants migrated to the expected 50 kDa and ~38 kDa, and there was no evidence of Pro-I contamination.

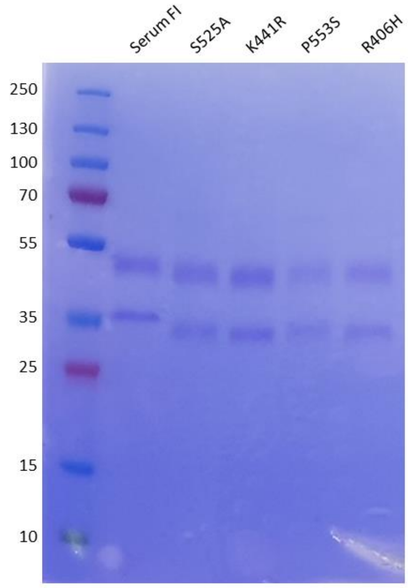

Figure 5-42 Reducing SDS PAGE stained with coomassie of purified inactive variants.
Reducing SDS PAGE of all inactive variants compared to serum purified FI stained with Coomassie Blue.

5.3.9.1.5. Confirmation of Variant Inactivation using Fluid-Phase Cofactor Assays with FLFH

Fluid-phase cofactor assays were performed in the presence of full length FH for each of the double mutated variants to confirm the inactivation of the serine protease domain. Figure 5-40 is a representative gel demonstrating the lack of C3b cleavage observed for each of the double mutated proteins at a selection of time-points. After 60 minutes, there was no detectable presence of either the α1, or the two α2 chains for any of the variants, confirming their catalytic inactivation.

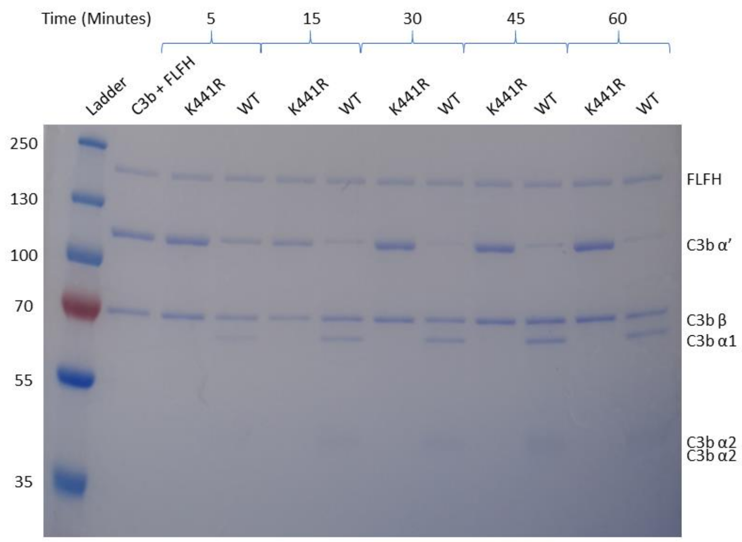

Figure 5-43 . Representative SDS-PAGE for visualisation of the FLFH cofactor assay for inactive FI variants.
Representative SDS-PAGE for visualisation of the full length FLFH cofactor assay for active FI vs inactive variants. Displayed is a Coomassie stained reducing SDS-PAGE gel run to separate the products of an FI fluid phase cofactor assay with FLFH. The α' (114kDa), β (68kDa), α1 (68kDa) and α2 (46 and 43kDa) C3b fragments can be seen clearly as labelled on the right side of the image, with the molecular weight marker and associated sizes on the left-hand side. Each lane represents the separation of an individual reaction mixture.

5.3.10. Surface Plasmon Resonance Analysis of TMC Formation

To supplement the standard complement functional analysis techniques, a novel, real-time analysis of FI variants in the formation of the AP regulatory trimolecular complex was performed.

5.3.10.1. SPR Analysis of the Interaction of FI Variants with Amine Coupled C3b

In the first instance, 1000 RU of C3b was immobilised on the surface of a CM5 sensor chip using amine coupling. Following immobilisation, each of the FI variants and FH1-4 were individually flowed over the chip surface to assess their interaction with the bound C3b (Figure 5-41). Neither the FI nor the FH1-4 exhibited any notable binding to the surface, with the SPR signal staying under 5 RU for all samples. Corresponding with the start and the end of the injection for each of the samples, there was a sharp rise and fall in RU. Since FI requires a cofactor to bind C3b (Xue *et al.*, 2017), in the absence of FH1-4, there is little/no interaction with the C3b bound on the chip. FH1-4, however, is expected to bind to C3b, albeit with a much lower affinity than full-length FH (Schmidt *et al.*, 2008). The FH1-4 exhibited a very similar profile to the FI variants, with fast on/off binding, indicating a very weak interaction with the C3b on the surface. Since amine coupling occurs in a random manner, this may explain the low binding response observed with FH1-4, as some of the C3b molecules are undoubtedly orientated in such a way that some of the FH1-4 binding sites are not available.

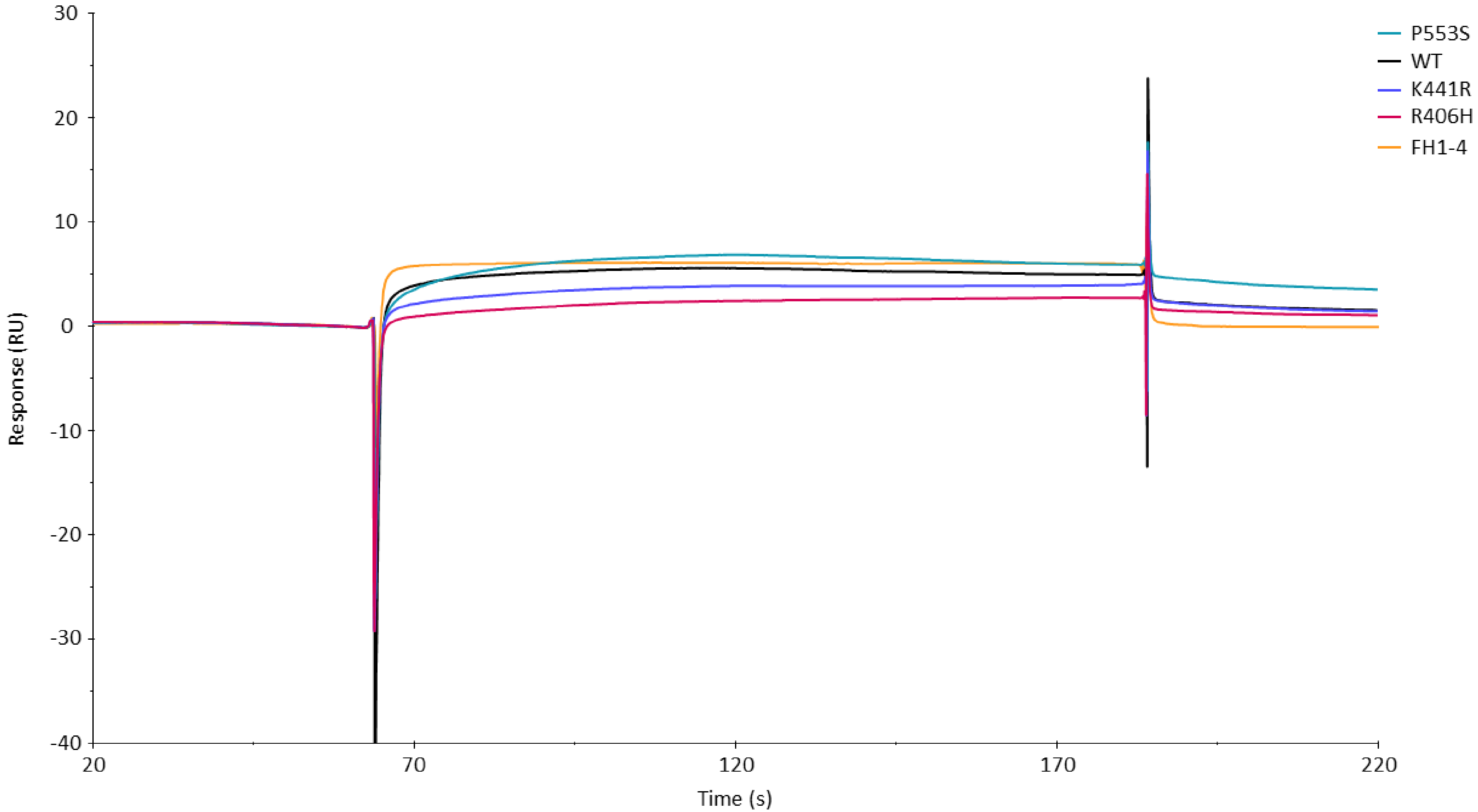

Figure 5-44 Analysis of FI or FH1-4 binding to amine coupled C3b surface.
Displayed is a sensorgram produced in the BIAevaluation software S200 (GE) after individual injections of each variant FI and FH1-4, onto a C3b coupled CM5 chip surface. Time (x-axis, seconds) is plotted versus response (RU) after normalisation by injection over a blank flow cell. Each sample was used at a concentration of 125 nM.

5.3.10.1.1. Real-time analysis of FI variants in the formation of the AP TMC

Following the initial separate injections of FI or FH1-4, the FI variants were co-injected with FH1-4 onto the amine coupled C3b surface revealing the formation of the TMC. Figure 5-42 demonstrates the large gradual increase in RU associated with TMC formation, followed by the slow dissociation of the complex at the end of the sample injection.

WT FI (WT/S525A) was used as the benchmark for normal TMC formation in this assay, and produced the largest response as measured by SPR (25.9 RU) after injection at 62.5 nM. In concordance with the previous functional data, K441R produced an almost identical response to that of the WT protein (25.6 RU, 99% of WT). R406H showed a notable reduction in efficacy (18.9 RU), producing a response that was 73% that of the WT, providing a contrast to the previous functional data which demonstrated no significant difference in activity. Meanwhile, P553S exhibited a marked decrease in TMC formation, producing a response that was 48% less than that of the WT protein (13.4 RU). Strengthening the results from the fluid-phase cofactor assays whereby P553S was the only variant to demonstrate a significant reduction in C3b cleavage activity.

To confirm that the differences in SPR observed for each of the FI variants was a result of the mutations and not a loss of C3b surface stability, the AP convertase, C3bBb, was formed at the start and the end of each experiment. Figure 5-43 demonstrates the formation of the convertase at the start of the experiment (convertase 1), the formation of the convertase at the end of the experiment (convertase 2), and the formation of the convertase following cleavage of the surface using active WT FI (convertase 3). Comparing the SPR signal for convertase 1 and 2, there was a 6% loss of surface activity at the end of the experiment compared to the start; likely due to the regeneration conditions used between each sample. For convertase 3 however, the difference in surface activity following cleavage with active WT FI was substantial. Comparing the response for convertase 2 and convertase 3, there was a 27% reduction in surface activity, rendering the chip unusable for further comparisons of TMC or convertase formation. Overall, this highlighted the necessity for the inactivation of the serine protease domain with the S525A mutation, to not only to enable analysis of TMC formation, but to also protect the chip surface from FI cleavage. As the difference in surface activity between the start and the end of the experiment was minimal with the inactivated FI variants, it was therefore possible to compare the activity of all three variants using the same chip surface.

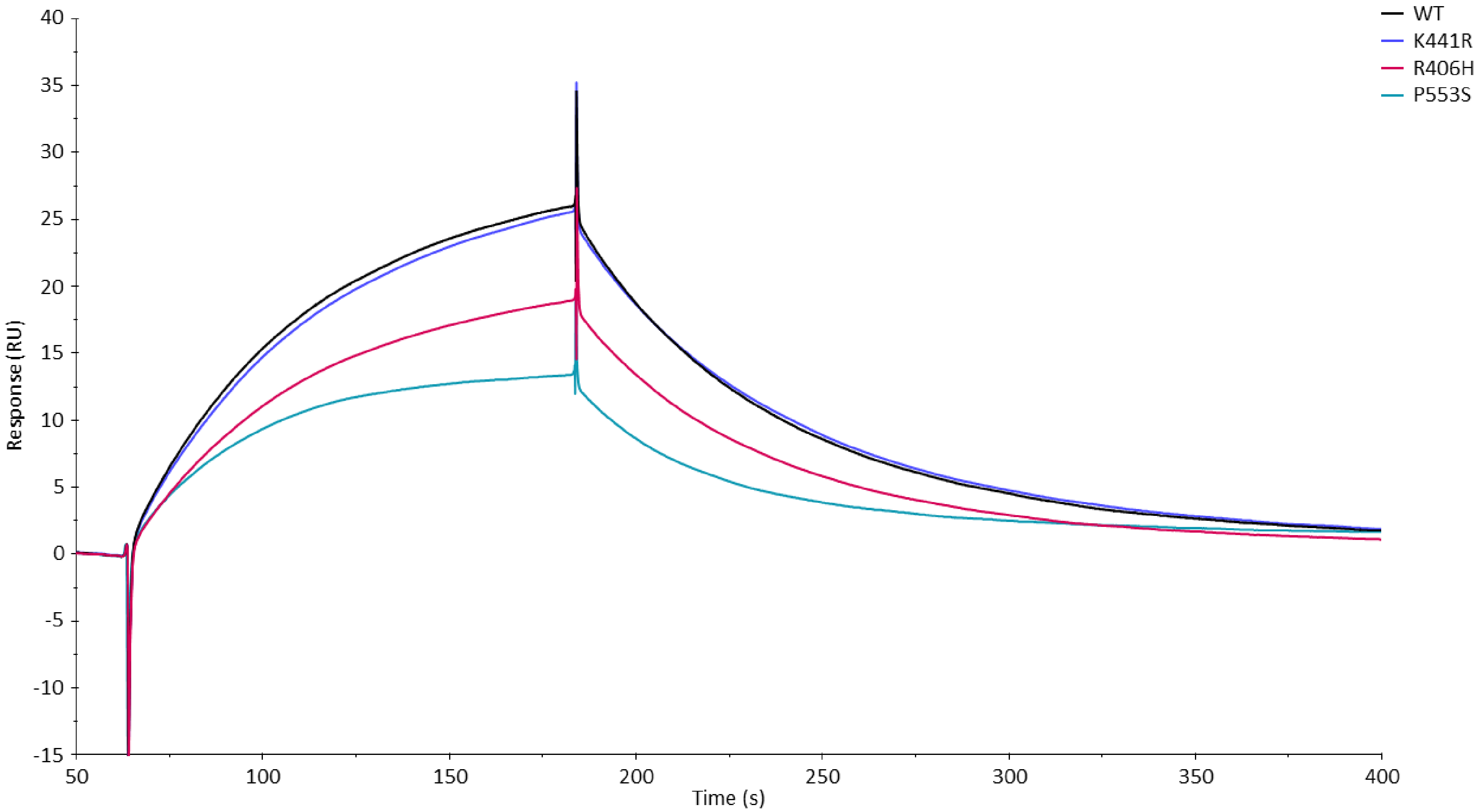

Figure 5-45 TMC building at 62.5 nM for each FI variant on an amine coupled C3b surface.

Displayed is a sensorgram produced in the BIAevaluation software S200 (GE) after injection of variant FI with FH1-4, onto a C3b coupled CM5 chip surface. Time (x-axis, seconds) is plotted versus response (RU) after normalisation by injection over a blank flow cell.

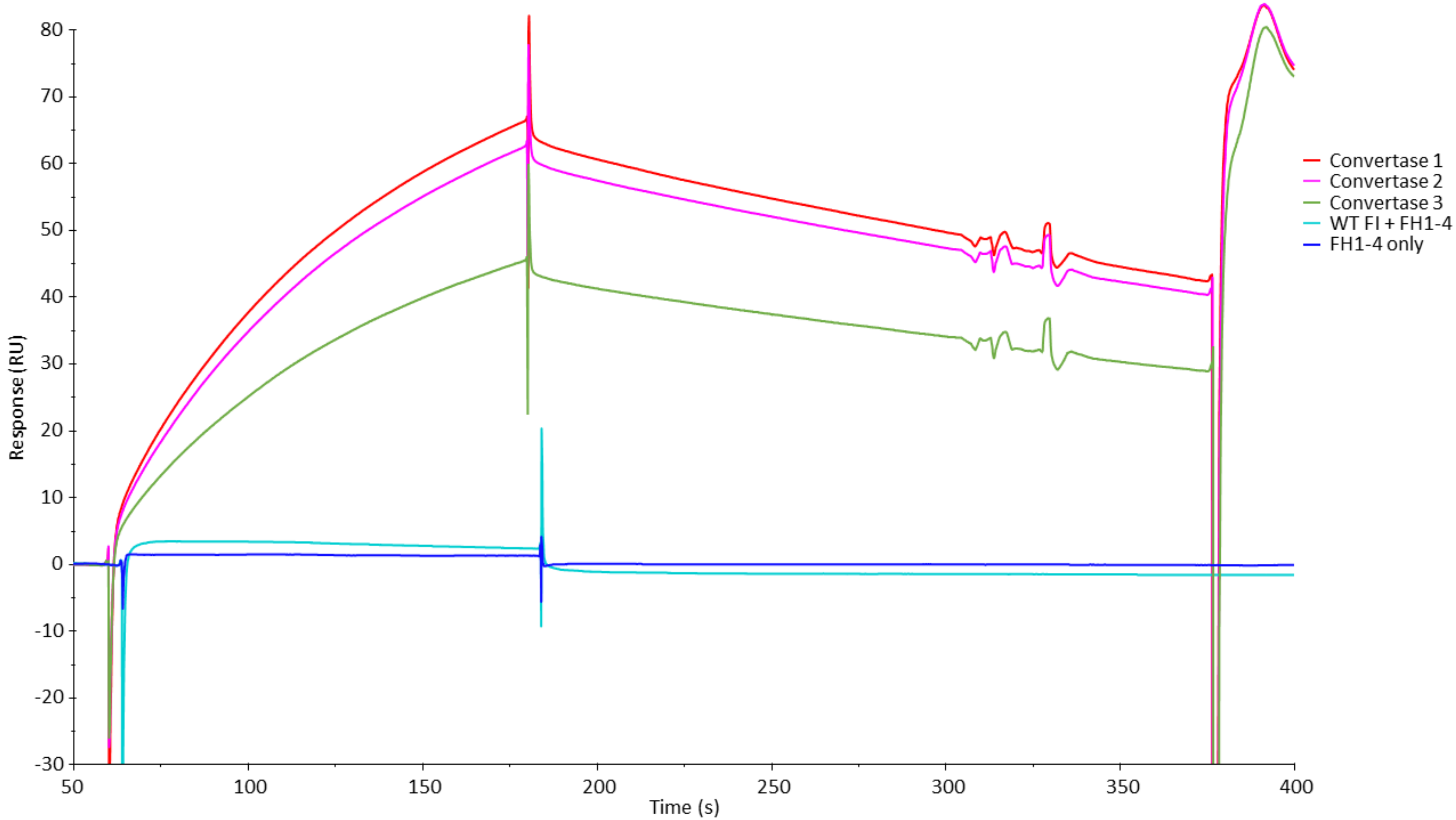

Figure 5-46 Analysis of convertase building before and after TMC formation on an amine coupled C3b surface.

Displayed is a sensorgram produced in the BIAevaluation software S200 (GE) before and after the formation of the TMC. Time (x-axis, seconds) is plotted versus response (RU) after normalisation by injection over a blank flow cell. (Convertase 1) C3 convertase before TMC building. (Convertase 2) C3 convertase after S525A variants TMC builds. (Convertase 3) C3 convertase after WT TMC build. (WT FI + FH1-4) Active TMC formation. (FH1-4 only) FH1-4 indicted individually prior to WT TMC build.

5.3.10.1.2. Effect of FI Concentration on TMC Binding

To confirm that the results of the assay were replicable, different concentrations of each FI variant were injected with a constant concentration of FH1-4 (125 nM). Figure 5-44 shows that the relative response for each FI variant across different concentrations was comparable. Typically, WT and K441R produced the largest responses, followed by R406H, with P553S producing the smallest response. At a concentration of 250 nM, however, both K441R and R406H deviated from this trend, and generated a response marginally larger than the WT. Although this is unlikely to be physiologically relevant as circulating levels of FH are in excess of FI (Geerlings *et al.*, 2017).

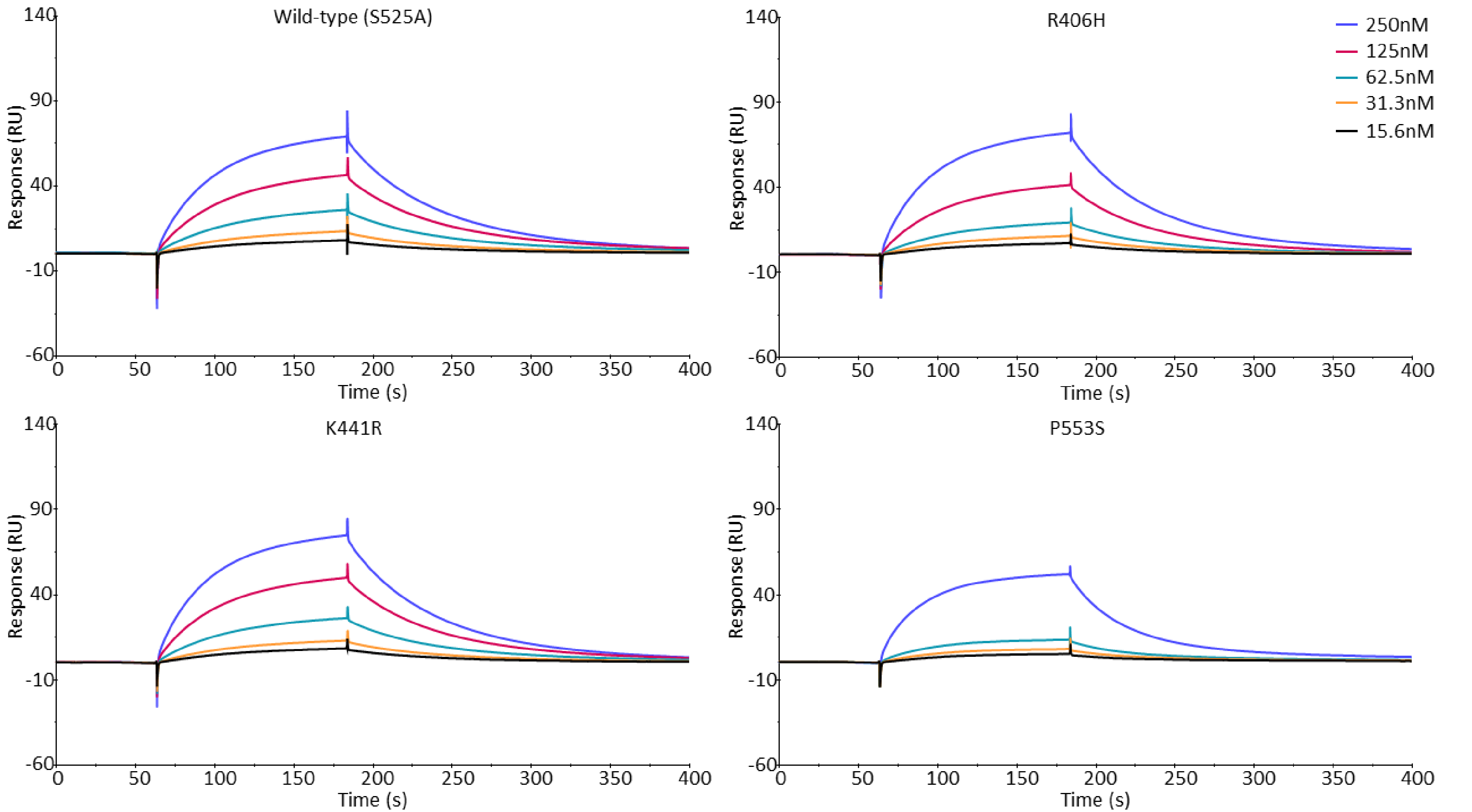

Figure 5-47 Analysis of the effect that concentration has on TMC building for FI variants on an amine coupled C3b surface.

Displayed is a sensorgram produced in the BIAevaluation software S200 (GE) after injections of each variant FI with FH1-4, onto a C3b coupled CM5 chip surface at different concentrations. Time (x-axis, seconds) is plotted versus response (RU) after normalisation by injection over a blank flow cell.

5.3.10.2. SPR Analysis of the Interaction of FI Variants with Physiologically immobilised C3b

To validate the results of the TMC building assay on the amine coupled surface, the method was repeated on a new surface, whereby the C3b was physiologically immobilised through nucleophilic attack. To produce the physiologically relevant surface, a small nidus of C3b (100 RU) was first immobilised by amine coupling. Once coupled, FB and FD were used to build the AP C3 convertase (C3bBb) on the chip-bound C3b, enabling C3 cleavage. Following the injection of C3, the convertase cleaves C3 to C3b, resulting in its immobilised onto the chip surface, through nucleophilic attack on the internal thioester. This process of convertase formation and C3 cleavage was repeated serval times, until 1000 RU of C3b was covalently immobilised on the chip.

Following immobilisation, each of the FI variants and FH1-4 were individually flowed over the chip surface to assess their interaction with the physiologically bound C3b (Figure 5-45). Again, none of the FI variants exhibited any notable binding to the surface in the absence of a cofactor, with 8 RU being the largest SPR signal generated. For FH1-4, however, there was a much larger response compared to the signal observed on the amine coupled C3b surface (26 RU vs 5 RU). This was likely due to the improved accessibility to C3b when physiologically immobilised.

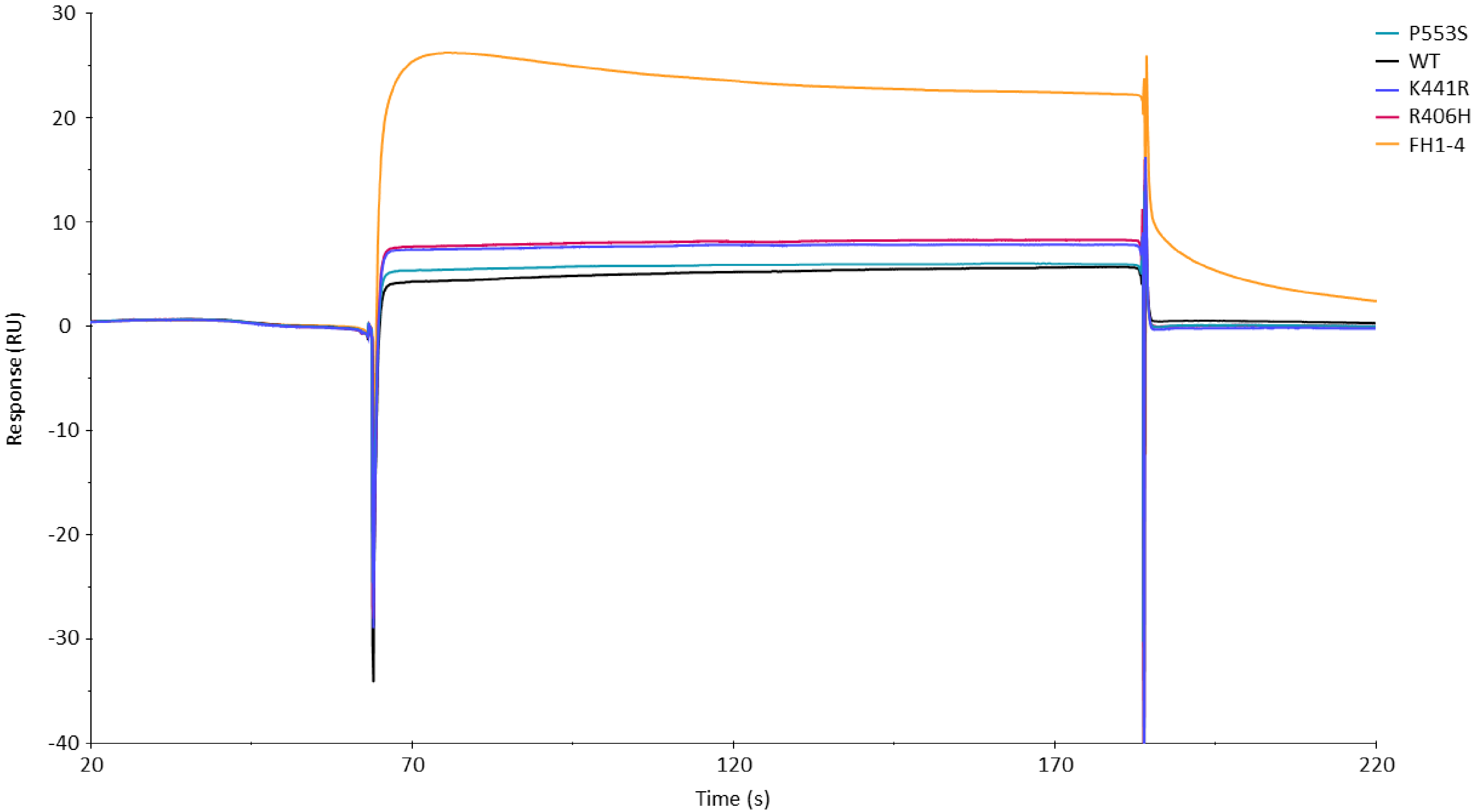

Figure 5-48 Analysis of FI variants binding to physiologically coupled C3b.
Displayed is a sensorgram produced in the BIAevaluation software S200 (GE) after individual injections of each variant FI and FH1-4, onto a C3b coupled CM5 chip surface. Time (x-axis, seconds) is plotted versus response (RU) after normalisation by injection over a blank flow cell. Each sample was used at a concentration of 125 nM.

5.3.10.2.1 Real-time analysis of FI variants in the formation of the AP TMC on Physiologically Coupled C3b

Following the individual injections of FI or FH1-4, the FI variants were co-injected with 125 nM of FH1-4 to form the TMC (Figure 5-46). Replicating the amine surface, TMC formation was demonstrated by a large gradual increase in RU, followed by a slow decrease at the end of the sample injection, indicating TMC dissociation.

As before, WT FI (WT/S525A) was used as the benchmark for normal TMC formation; producing the largest response as measured by SPR (97.5 RU) after injection at 62.5 nM. Similarly to the amine surface, P553S formed substantially less TMC compared to the WT (62.9 RU, 65% of WT). R406H, again, showed a reduction in efficacy in this assay, with a response that was 76% of that of the WT (74.6 RU). K441R on the other hand, was very similar to the WT, producing a response that was 94% of that of the WT (91.2 RU). The trend observed for each variant was in agreement with the results from the amine coupled surface, albeit with the physiologically coupled surface producing higher overall responses.

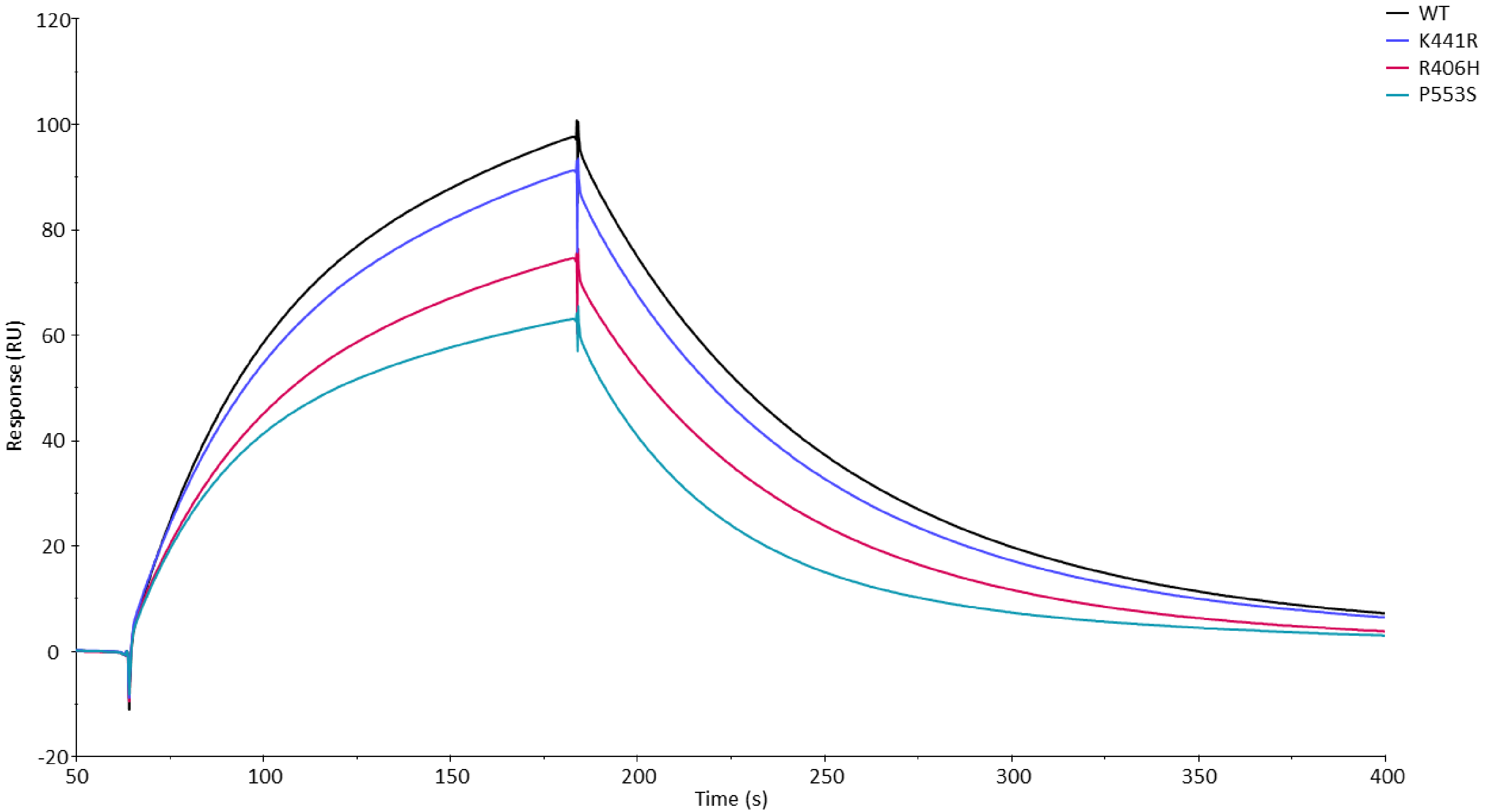

Figure 5-49 TMC building at 62.5nM for each FI variant on a physiologically coupled C3b surface.

Displayed is a sensorgram produced in the BIAevaluation software S200 (GE) after injection of variant FI with FH1-4, onto a C3b coupled CM5 chip surface. Time (x-axis, seconds) is plotted versus response (RU) after normalisation by injection over a blank flow cell.

5.3.10.2.2 Effect of FI Concentration on TMC Binding

To reproduce the results from the amine coupled surface, varying concentrations of each FI variant were compared in the presence of constant FH1-4 (125 nM) (Figure 5-47). On the physiologically coupled surface, the binding of the WT FI protein always resulted in the largest response, followed by K441R, then R406H and finally P553S. There was also a greater distinction between the WT and K441R at each concentration when compared to the amine coupled surface, however both still demonstrated a similar efficacy in TMC building at higher concentrations. R406H typically generated a response ~75% of the WT, and P553S ~62%, indicating a reduced efficacy at building the TMC for each of these variants.

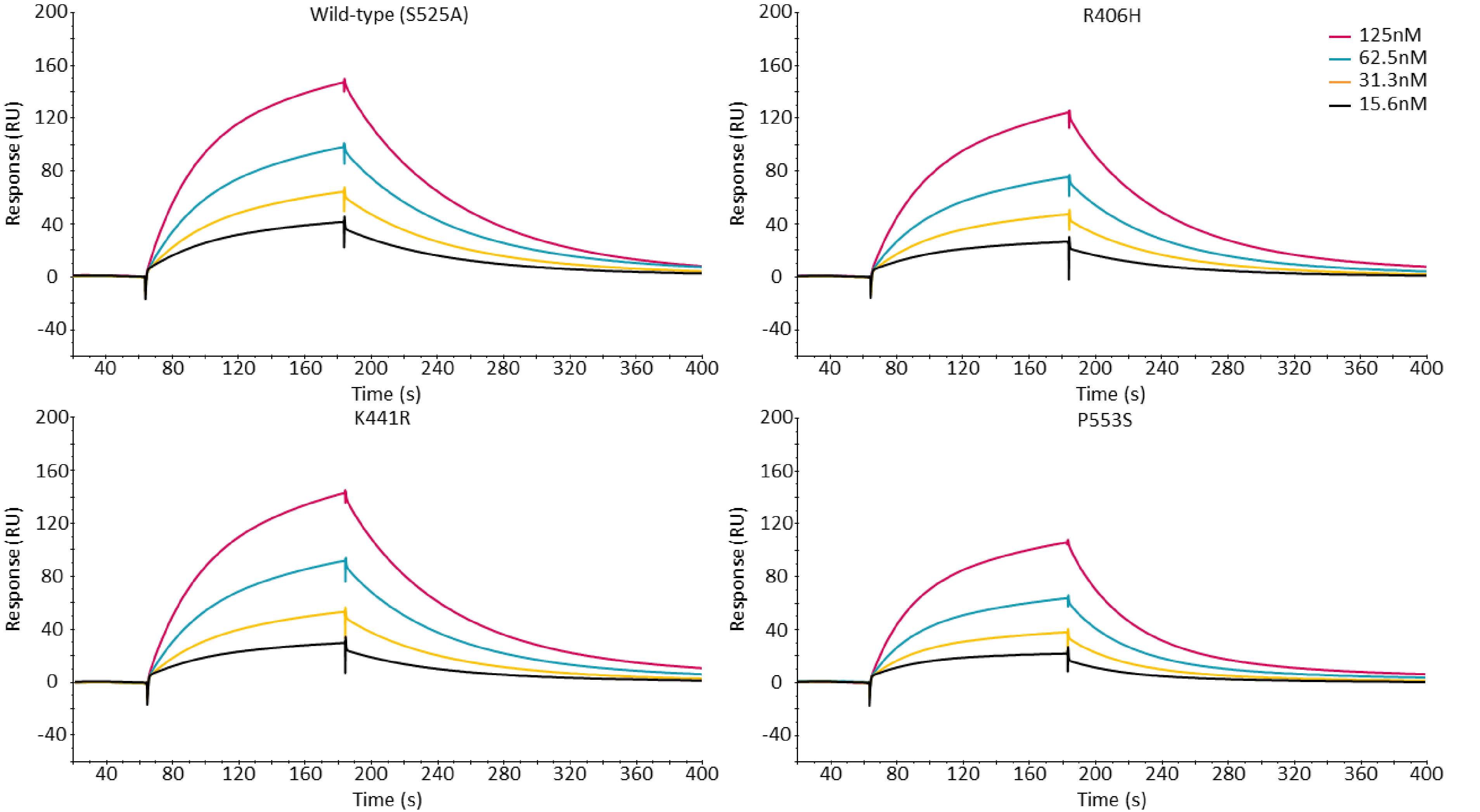

Figure 5-50 Analysis of the effect that concentration has on TMC building for FI variants on a physiologically coupled C3b surface.

Displayed is a sensorgram produced in the BIAevaluation software S200 (GE) after injections of each variant FI with FH1-4, onto a C3b coupled CM5 chip surface at different concentrations. Time (x-axis, seconds) is plotted versus response (RU) after normalisation by injection over a blank flow cell.

5.3.11. Summary of Functional Testing Results

The activities of each FI variant in a range of functional assays described in the previous sections are summarised in Table 5-1. Overall, it was clear that the P553S mutation had the greatest impact on FI function for each of the chosen variants. In the fluid phase, P553S demonstrated a significantly impaired ability to cleave the C3b α' chain in the presence of a variety of cofactors. There was also a notable decrease in the efficacy of building the alternative pathway TMC, despite exhibiting a normal function on the surface of activated C3b coated sheep erythrocytes. In most instances, K441R performed similarly to the WT when using FH and associated proteins as cofactors within fluid-phase assays. K441R appeared to have a slightly impaired ability to cleave the C3b α' chain in the presence of MCP and sCR1, however this did not reach significance in this study. K441R also demonstrated a marginally increased ability to cleave C3b on the surface of activated sheep erythrocytes, and formed the TMC approximately equivalent to WT on both amine and physiologically coupled surfaces. R406H exhibited an impaired ability to form the TMC on both amine and physiologically coupled surfaces and had the greatest IC_{50} for the degradation of C3b on activated sheep erythrocytes. In the fluid-phase, however, R406H performed similarly to WT across a range of cofactors.

Table 5-1 Summary table of functional analysis of CFI variants.

Factor I	**Cofactor Activity with FLFH (Average percentage of α' chain remaining after 15 minutes)**	**Cofactor Activity with FH1-4 (Average percentage of α' chain remaining after 15 minutes)**	**Cofactor Activity with FHL-1 (Average percentage of α' chain remaining after 15 minutes)**	**Cofactor Activity with MCP (Average percentage of α' chain remaining after 15 minutes)**	**Cofactor Activity with sCR1 (Average percentage of α' chain remaining after 15 minutes)**	**Haemolytic Cofactor activity on C3b-activated Sheep Erythrocytes (IC_{50} - 50% protection from lysis (nM))**	**TMC Max Response at 62.5nM (Thiol Coupled C3b)**	**TMC Max Response at 62.5nM (Amine Coupled C3b)**
WT	26.1	12.7	31.9	57.4	27.0	1.637	97.5	25.9
R406H	31.6	17.2	34.4	58.3	37.8	2.039	74.6	18.9
K441R	35.1	9.36	34.6	68.1	47.5	1.556	91.2	25.6
P553S	40.5 *(P = 0.0458)	13.0	44.4	79.1 *(P = 0.0107)	63.2 *(P = 0.0145)	1.664	62.9	13.4

5.4. Discussion

5.4.1. Functional Analysis of Pro-I

Pro-I was first identified by Goldberger *et al.* 1984 through the analysis of the biosynthesis of human FI in three hepatoma-derived cell lines, where they demonstrated that FI is first synthesised as a single chain precursor, that undergoes glycosylation and proteolytic cleavage to generate the two chained mature form (Goldberger *et al.*, 1984). Since then, most studies which involve the production of FI have focused on cleaving Pro-I to FI extracellularly, through co-transfection with Furin, the enzyme responsible for the cleavage of the RRKR linker which distinguishes the mature form of FI from the Pro-I form (Wong *et al.*, 1995; Xue *et al.*, 2017). A novel method to cleave Pro-I intracellularly has been developed during this project, that mimics the natural processing of FI (Goldbergers *et al.*, 1987), albeit with a higher rate of conversion, as indicated by the presence of Pro-I in serum (Section 1.3.1.2) (Goldberger *et al.*, 1987). Since this is the first identification of Pro-I in plasma, it is likely that the bulk of Pro-I undergoes proteolytic cleavage by Furin intracellularly and only a small proportion bypasses the postsynthetic processing. As Pro-I is fairly abundant in recombinant preparations of FI (Goldberger *et al.*, 1984; Wong *et al.*, 1995), there is also the possibility that a greater proportion of Pro-I is actually secreted into the plasma where it is then cleaved by Furin which has been “shed” into the extracellular milieu following autocleavage or activation by other proprotein convertases (Preininger *et al.*, 1999).

Despite efforts to maximise Pro-I cleavage, the functional activity of Pro-I had not previously been defined. Therefore prior to the generation of recombinant FI, the activity of Pro-I (which is typically present at ~20-50% in most preparations) was assessed. Chapter 4 outlined a novel method for the purification of Pro-I which has enabled its functional characterisation. Similarly to pro-C3, Pro-I behaved as a single component with a molecular weight of ~90 kDa, comparable to that of fully processed FI, and does not dissociate into the two chains upon reduction with 2-mercaptoethanol, yet is antigenically related (Minta, Ngan and Pang, 1979). When used in cofactor activity assays, Pro-I exhibited no ability to cleave C3b, due to an incapacity to form the AP TMC as determined by SPR. This inability to form the TMC is likely due to the presence of the RRKR linker, which confines the molecule to a linear conformation, preventing the 11° rotation of the heavy chain required for the allosteric activation of the SP light chain and further stabilisation of the TMC (Roversi *et al.*, 2011). The lack of proprotein serine protease activity is shared with Pro-FD. In MASP1/3 deficient mice their sera lacks the ability to activate the AP (Takahashi *et al.*, 2010) due to the inability to cleave Pro-FD to FD by MASP-3 (Dobó *et al.*, 2016). Furthermore, since Pro-I is completely inactive, patients with mutations within the RRKR linker that inhibit Furin cleavage, are more likely to suffer from diseases of uncontrolled complement regulation, such as AMD or aHUS. Within these individuals an elevated Pro-I levels may be a possible biomarker for disease, supporting the benefit of an antibody against Pro-I, as attempted in Chapter 4.

5.4.2. Functional Analysis of Rare Genetic Variants of FI

Overall, the results of the cofactor assays with 5 different cofactors for FI were consistent with one another, showing a similar trend, but not always reaching a similar the level of statistical significance. Each cofactor assays had a consistent number of replicates (i.e., 3), however, due to the reactions not being at end point, this increased variability with each cofactor exhibiting different reaction kinetics. Of the FH-derived cofactors, FLFH has the highest affinity for C3b (Kd 0.647 µM), followed by FHL-1 (Kd 1.520 µM) and finally FH1-4 (Kd 10-14 µM) (Harder *et al.*, 2016). sCR1 on the other hand demonstrates an affinity of 4.59 µM Kd (Ishii, 2018), and MCP 0.57 µM Kd (Martínez-Barricarte *et al.*, 2015). A stronger affinity for C3b, however, does not always equate to faster reaction kinetics. An example of this is that, whilst FLFH and miniFH have a similar binding affinity for C3b (0.647 µM vs 0.709 µM), FLFH demonstrates a significantly higher fluid-phase activity (Harder *et al.*, 2016). In these assays, the FH1-4 demonstrated the fastest degradation of the C3b α' chain, and MCP the least, despite MCP exhibiting a greater than 10-fold increase in affinity for C3b.

Whilst each of the variants assessed in this study have been commonly reported as benign, this is typically based upon *in silico* analysis by software such as PolyPhen2 (Seddon *et al.*, 2013; Kavanagh *et al.*, 2015; Osborne *et al.*, 2018). At the start of this project, only R406H had undergone functional testing using cofactor assays (Kavanagh *et al.*, 2008). Since then, further studies have analysed the functional consequences of R406H (Java *et al.*, 2019, 2020), P553S (Geerlings *et al.*, 2017; Java *et al.*, 2019, 2020) and K441R (Java *et al.*, 2020) in cofactor assays. All three variants have now also been characterised in a zebrafish model of retinal vasculogenesis (Tan *et al.*, 2017).

In Java *et al.* 2019, P553S demonstrated no statistically significant difference in the cleavage of the α′ chain or in the production of the α1, or the two α2 fragments, compared with WT. This finding was consistent with Geerlings *et al.* 2017 and Java *et al.* 2020, which showed that P553S had a similar capacity to degrade C3b to iC3b when compared to WT FI purified from noncarrier plasma. These conclusions are in contrast to the results presented in this chapter, as P553S was the only variant to show a significant reduction in the degradation of the C3b α′ chain when using a range of different cofactors. As Geerlings *et al.* 2017 took the assay to end-point (90 minutes incubation) and focused on the production of the second cleavage fragment of C3b, the results from this chapter are not suitable for a direct comparison. The results described by Java *et al.* 2019, are however more appropriate for comparison due to co-transfection with Furin, the shorter reaction time, and the activity measured by the percentage of α′ chain remaining. Despite this, the results reported conflict with those presented within this chapter. Java *et al.* demonstrated no significant difference in activity between WT FI and P553S, when using FH, MCP or CR1 as a cofactor. A potential explanation for the observed statistical difference in this study is that the reactions presented here are much more complete, when measured by normalised α′ chain remaining (57% remaining after 15 minutes for MCP, and 27% remaining after 15 minutes for sCR1), compared to those presented by Java *et al.* for MCP and CR1 (80% remaining after 30 minutes for MCP, and 50% remaining after 30 minutes for CR1). As is the case for the cofactor assays using sCR1 described in this thesis, it would have been useful if Java *et al* had been able to measure the production of the C3dg chain, as an assessment of P553S activity in the presence of CR1. However, this would require the reaction to be closer to completion and would therefore hinder the ability to assess differences in reaction kinetics between the variants, as there would be the potential to miss the activity of hyperactive variants.

As mentioned, R406H was the only variant to have undergone functional testing before the start of this project (Kavanagh *et al.*, 2008). In 2008, Kavanagh *et al.* wanted to establish the functional consequences of a representative subset of aHUS-associated mutants, one of which was R388H (R406H with the leader sequence). The R406H variant was reported as leading to no functional consequences, with the generation of the α1 band comparable to WT in the C3b cofactor assay, in addition to a kinetic analysis which also demonstrated rapid cleavage of the α′ chain comparable to WT. The C4b cleavage ability of R406H was also determined as comparable to WT. In this project, no C4b cofactor activity assays were performed for the chosen variants, as despite the presence of C4 (and C4a) in drusen (Schaft *et al.*, 1993; Loyet *et al.*, 2012), C4a levels are not significantly elevated in patients with AMD compared to the controls (Loyet *et al.*, 2012). Consequently, the CP and MBLP are not typically considered to be associated with AMD (Ricklin *et al.*, 2010). This project instead focused on functional testing in the AP only. Java *et al.* 2019, also investigated R406H and demonstrated a decreased rate of α' chain cleavage with both FH and CR1, yet normal functional activity with MCP (Java *et al.*, 2019). Again, the results from Java *et al.* 2019 contrast with the findings presented here and in Kavanagh *et al.* 2018, where R406H performed similarly to WT for all cofactor proteins. Despite, the lack of a significant difference in activity, R406H performed most similarly to WT when using MCP, and was slightly less active when using sCR1, FH, FHL-1 and FH1-4. Java *et al.*, also noticed a similar trend, and postulated that as the R406 side chain forms a stabilising salt bridge with the carboxy group of residue E123 of FH, a residue which is missing in MCP; this may therefore account for the difference in activity observed. Since the impact of this mutation is reduced in MCP, this may also account for the faster cleavage of the second scissile bond at R1320-S1321 (Roversi *et al.*, 2011; Xue *et al.*, 2017), as evidenced by a greater amount of α2 (43 kDa) produced compared to the WT, however an assay assessing the kinetics of this second cleavage would be required to confirm this finding.

In the assays presented in this chapter, K441R was not statistically different in activity compared to the WT across all the cofactors tested. This finding was consistent with Java *et al.* (2020) which demonstrated that K441R performed similarly to WT with respect to C3b cleavage (Java *et al.*, 2020). This finding is, on the surface, somewhat surprising as K441 forms a putative hydrogen bond with N136 of FH CCP2 and is located within a highly charged stretch of amino acids (residues 435–448) next to the critical loop structures 394–408 and 471–485 in the SP domain of FI, key for the hydrophobic binding of FH through CCP2 and CCP3. In addition, this highly charged region also plays a key part in the binding of MCP and CR1. Despite this, K441R performed similarly to WT with FH, MCP and CR1, with the addition of the four more residues between Cys129 and Cys141 in MCP and CR1 compared to FH, having little impact. One possible explanation for why this mutation exhibits a negligible effect is that the region where K441 resides is able to adjust its conformation and adapt to the pattern of charges present on the various cofactors, and since the Lysine to Arginine change maintains its positive charge, there is no significant detriment on the conformational rearrangements required to bind the variety of cofactors (Xue *et al.*, 2017).

Each variant assessed in this chapter was also functionally analysed by Tan *et al.* 2017 in a zebrafish model of retinal vasculogenesis, characterising all three variants as benign (Tan *et al.*, 2017). This *in vivo* model was initially utilised by van de Ven *et al.* 2013 to assess the highly penetrant Type 1 mutation G119R, associated with a high risk of AMD (OR = 22.20). In this study, the model showed defects in the morphology of hyaloid vessels in the developing retina introduced by G119, however when the arginine mutation associated with AMD was introduced at this position, the results were indistinguishable from controls, presenting a contrast with the activity observed on the cofactor assays (van de Ven *et al.*, 2013). Further to this, Tan *et al.* also treated K441R and P553S as negative controls due to a "high frequency in ExAC (Lek *et al.*, 2016) yet no association with AMD", although this disregards the association with AMD identified in other studies (Kavanagh *et al.*, 2015; Shoshany *et al.*, 2019; Java *et al.*, 2020) and also the impact these variants have in other diseases of complement dysregulation (Bienaime *et al.*, 2010; Bresin *et al.*, 2013). Fundamentally, assessments of vascular branching likely lack the sensitivity required to determine the impact of complement dysregulation introduced by these variants, although it may be useful in the analysis of genes associated with wet AMD, such as VEGF (Nasevicius, Larson and Ekker, 2000; Campa and Harding, 2011).

5.5. Conclusion

In conclusion, a novel method for generating completely processed recombinant FI with no Pro-I contamination has been developed. Using the designed IRES vector, fully process FI can be generated that is functionally equivalently to serum purified FI for use in functional analysis or potentially FI supplementation. This chapter has also demonstrated successful modelling of the three variants K441R, R406H and P553S on both a WT and S525A *CFI* backbone, which has enabled the most extensive analysis of these variants recorded in the literature. K441R, R406H, P553S all demonstrate proteolytic activity, and any defect is small, in comparison to the Type 1 variants described by Kavanagh *et al.* (2008). Only P553S repeatedly demonstrated a statistically reduced activity in the fluid-phase cofactor assays and a substantially reduced ability to form the TMC. There was no statistical difference between R406H or the WT protein in fluid-phase and surface-bound cofactor assays. R406H did however demonstrate slightly reduced TMC building ability, and it could be hypothesised that this may lead to reduced regulatory activity, albeit this is below the resolving capacity of the current assays. Further work will be required to confirm this. In all the assays presented here, K441R performed equivalently to the WT, and therefore further investigation is required to decipher the link between K441R and AMD. The work in this chapter has also confirmed that Pro-I is inactive and is incapable of forming TMC. As such, the results from previous recombinant analysis where there has been no addition of Furin, whether intracellular or extracellularly, will be dependent on the ratio of FI to Pro-I present.

Chapter 6. Discussion

AMD is a complex, multifactorial disease caused by a combination of risk factors which function together to define an individual's predisposition to AMD. These include ageing, race, environmental and lifestyle risk factors, and genetic predisposition. Numerous genetic associations between the complement system and AMD, have shown a clear involvement of the alternative and terminal pathways of complement, through both genetic and functional studies. Both rare and common genetic variants in *CFI* are significantly associated with increased AMD susceptibility, with rare variants carrying a particularly increased burden (Seddon *et al.*, 2013; van de Ven *et al.*, 2013; Fritsche *et al.*, 2016; Geerlings, de Jong and den Hollander, 2017).

Loss of function variants have the greatest impact on increasing the risk of AMD (Seddon *et al.*, 2013), and can be categorised into two subclasses: Type 1 and Type 2 (Kavanagh *et al.*, 2008; Kavanagh *et al.*, 2015). Type 1 variants are characterised by a quantitative deficiency of FI, in the serum or plasma, and Type 2 variants are associated with normal levels of FI in the plasma, but with functional defects resulting in impaired complement regulation. Low systemic FI levels are significantly associated with AMD (Kavanagh *et al.*, 2015; Hallam *et al.*, 2020), and provide a biomarker for FI dysfunction. Many genetic variants significantly associated with AMD however do not lead to low FI levels and have unclear functional consequences. By developing new assays for functional characterisation, we will not only improve our understanding of the impact of these rare genetic variants, but also provide further evidence to elucidate their role in the pathogenesis of AMD. Through the successful characterisation of Type 1 and Type 2 variants, this may facilitate a more personalised approach to AMD treatment in individuals experiencing complement dysregulation, either through FI supplementation or complement blockade.

This thesis therefore aimed to provide a robust functional analysis of three rare *CFI* variants nominally associated with AMD and normal FI levels (Kavanagh *et al.*, 2015; de Jong *et al.*, 2020; Hallam *et al.*, 2020). These were R406H, P553S and K441R, and their selection was based upon occurrence in the literature, *in silico* analysis and structural modelling within the AP regulatory trimolecular complex.

Of the three selected variants, only R406H had ever undergone previous functional analysis prior to the start of this project (Kavanagh *et al.*, 2008). However, it was still of interest for further interrogation due to its conflicting Polyphen-2 (possibly damaging) and CADD scores (benign); association with reduced disease burden (OR = 0.10) and location within the TMC. In R406H the histidine has a pK_a of ~6.5, and can therefore vary within the extracellular environment, shifting from protonated to neutral at a higher pH (Schönichen *et al.*, 2013). Due to the increased pH sensing caused by the variant, this may lead to alterations in FI function at areas of high metabolic activity such as the retina (Yang *et al.*, 2005) or the kidney (Hamm, Nakhoul and Hering-Smith, 2015) as a result of protonation at a lower environmental pH causing structural changes (Nordlund *et al.*, 2003). Since the arginine at p.406 is directly involved in the cofactor interaction, it was hypothesised that the introduction of a histidine at this position will cause a decrease in binding affinity of FI to the FH:C3b complex, and as a result of a pH-switching, depending on the environmental pH.

There were no prior studies assessing the functional significance of the rare variants P553S or K441R, however since the start of this thesis all three variants have now be functionally assessed (Geerlings *et al.*, 2017; Tan *et al.*, 2017; Java *et al.*, 2019, 2020). PolyPhen-2 predicted the impact of both P553S and K441R to be benign, whereas the CADD score considered P553S to be deleterious.

The P553S mutation involves changing a small nitrogen-containing ring (proline) for a small polar uncharged amino acid (serine). Whilst both amino acids are similar in size, they differ in conformation. The nitrogen-containing ring makes the proline structurally rigid, preventing the adoption of multiple conformations. Serine, on the other hand, is adaptable due to its small size and is typically well tolerated if switched for other small polar amino acids. Despite these fundamental differences in structure, serine may mimic proline through the formation of a hydrogen bond between the reactive hydroxyl group and the protein backbone (Betts and Russell, 2003), potentially reducing the impact of this mutation which may account for the benign prediction by PolyPhen-2. As residue P553 is located in the activation loop in close proximity to the catalytic triad (Geerlings *et al.*, 2018; Java *et al.*, 2019); it was therefore hypothesised that the P553S mutation may be deleterious through an alteration in the conformation of the activation loop impacting substrate binding to the FI active site.

In silico analysis predicted the K441R mutation to be the least impactful, with a CADD score of 0.001 and a PolyPhen-2 classification of benign. The K441R amino acid change means that a positively charged basic amino acid (lysine) is substituted for a positively charged basic amino acid (arginine). Whilst fairly similar in pK_a, ~10.5 vs ~12.5, the guanidinium group of arginine enables an increase in the possible number of electrostatic interactions, compared to lysine, which can in turn generates more stable ionic interactions (Sokalingam *et al.*, 2012). It was therefore hypothesised that this mutation may impact FI activity by modifying the enzyme-cofactor interaction through increased hydrogen bonding with FH at CCP2. Additionally, an increase in binding affinity for FH may result in a reduction of free FH for decay of the C3 convertase through decay accelerating activity (Weiler *et al.*, 1976) which could also contribute to a reduction in complement regulation in individuals with this FI mutation.

Overall, the primary driver for the analysis of each of the selected variants was their recurrence in a variety of AMD patient cohorts (Seddon *et al.*, 2013; Kavanagh *et al.*, 2015; Tan *et al.*, 2017; Geerlings *et al.*, 2018; Shoshany *et al.*, 2019; Hallam *et al.*, 2020). These variants have also been identified in patients with other diseases of complement dysregulation such as aHUS and C3G/MPGN (Fremeaux-Bacchi *et al.*, 2004; Fang *et al.*, 2008; Kavanagh *et al.*, 2008; Bienaime *et al.*, 2010; Caycı *et al.*, 2012; Kavanagh *et al.*, 2012; Bresin *et al.*, 2013; Fremeaux-Bacchi *et al.*, 2013; Zhang *et al.*, 2014; Geerlings *et al.*, 2018; Osborne *et al.*, 2018; Java *et al.*, 2019) which added further support to the potential pathogenic role of these variants.

Following the initial selection of the variants of interest, a method for the purification of functionally active FI was first developed, through an adaptation of the protocol outlined by Hsiung *et al.* (1982). By using an OX-21 column for affinity purification, FI could be purified from either plasma or cell culture supernatant via a two-step or one-step process, producing the protein in a conformationally correct and active form. Using the method outlined in this thesis, the plasma purified FI was significantly more pure than the product produced by Hsiung *et al.,* with no evidence of any contaminating species (Hsiung *et al.*, 1982). The resulting protein also maintained a similar fluid-phase C3b cleavage activity to Comptech FI, which is generated using conventional techniques (Fearon, 1977; Crossley and Porter, 1980; Morgan, 2000), indicating that this method could be used without any detriment to downstream functional assessments.

After the successful development of a protocol for FI purification, the production of recombinant FI was the next priority as access to patient plasma with the variants of interest was not possible and could contain a mixture of WT and mutant FI. The generation of recombinant FI was first described by Wong *et al.* (1995), and resulted in a product that was a mixture of Pro-I and mature FI, a finding in concordance with this project. The proportion of Pro-I to FI, varies depending on the cell line used, with the COS-1 cells producing 90% Pro-I, and the CHO-K1 cells producing 50% (Wong *et al.*, 1995). The results shown in this thesis demonstrate that the proportion of Pro-I in the final recombinant product was ~20% when using CHO cells.

Previous studies have suggested that Pro-I is an inactive form of FI, however this has never been proven (Kavanagh *et al.*, 2008; Wong *et al.*, 1995), despite its likely presence in all recombinant FI preparations generated in the absence of co-transfected Furin. Due to the similarities between Pro-I and FI, Pro-I may either act as another regulator of complement or could function as a complement activator by binding to the C3b-cofactor complex, preventing cofactor mediated cleavage. As a consequence, recombinant FI is typically cleaved through the use of co-transfected Furin (Wong *et al.*, 1995; Xue *et al.*, 2017; Java *et al.*, 2019), although this can lead to additional proteolysis at R315-R317 (Xue *et al.*, 2017).

This project therefore aimed to produce an antibody against Pro-I, to not only aid in the removal of Pro-I contamination from recombinant preparations but to also enable the purification and subsequent functional assessment of Pro-I. Further, the generation of an anti-Pro-I antibody could facilitate the measurement of Pro-I antigenic levels in human serum, providing another tool for the analysis of *CFI* variants which inhibit cleavage of the RRKR linker. In individuals with impaired Pro-I cleavage, an increased Pro-I level could provide a surrogate marker for decreased AP regulation or mask the correct classification of Type 1 *CFI* variants, due to cross-reactivity with FI antibodies.

Initially within this project, hybridoma generation through mouse immunisation was used to produce an anti-Pro-I antibody. Two approaches were considered for immunisation of the mice; the first was a peptide only approach, and the second, a combination of peptide and recombinant (CHO) FI, to provide epitopes against the full length Pro-I protein. The peptide contained the amino acid sequence; GVKNRMHI**RRKR**IVGGKRAQ, with the Pro-I linker region highlighted in bold. In both instances the peptide was conjugated to the carrier protein, KLH, an immunogenic protein xenogeneic to mammalian immune systems, to act as immunostimulant against the RRKR containing peptide (Curtis *et al.*, 1970; Plitnick and Herzyk, 2010; Swaminathan *et al.*, 2014). The peptide and the recombinant proteins were also prepared in the adjuvants, FCA and FIA to further induce a higher antibody titre

(Leenaars and Hendriksen, 2005), due to increased antigen retention at the injection site (Talmage and Dixon, 1953).

Despite the measures used to initiate a strong immune response towards the antigens of interest, both the peptide approach and the combination approach were unable to generate a strong immune response towards the peptide across all mice. There was however a strong response observed for some of the mice, highlighted by the generation of a polyclonal antiserum from one mouse, 633, which was able to detect non-reduced recombinant FI on a Western Blot and produce a strong signal towards the RRKR peptide on an ELISA. A potential reason for the reduced immune response, was the conservation of consensus residues within the Pro-I protein across man and mouse, with the linking peptide chain (RRKR) in human Pro-I, identical in mice (Minta *et al.*, 1996).

The fusion of immunised splenocytes with myeloma cells was used to produce numerous hybridomas (Köhler and Milstein, 1975). A total of 24 hybridomas were generated from the peptide only immunisation; of these, only 7 exhibited a differential response towards CHO FI, and once scaled up, only two continued to demonstrate a preference in binding to the peptide. 2G8 demonstrated low reactivity on the ELISA (0.02 Abs), and therefore only 5A2 was used for the Western Blot. However, no signal was produced by 5A2 under either reducing or non-reducing conditions.

In contrast to the peptide-only approach, the protein-peptide combination generated over 100 hybridomas which exhibited a positive response on the peptide. Despite the greater number of hybridomas generated, only colony 1B2 demonstrated the desired specificity towards the peptide with no signal against Comptech FI. Once diluted to monoclonality, two peptide specific hybridomas were taken forward for further characterisation (D5-C10 and D8-G5). Although both hybridomas originated from the same colony, they produced antibodies with different isotypes, with D5-C10 being an IgM and D8-G5 being an IgG_3. Once purified by affinity chromatography, neither antibody however was able to detect Pro-I on either a western blot or by ELISA.

In addition to the two peptide-specific hybridomas selected, the hybridoma 12E9 was also chosen as it demonstrated specificity towards FI. Once diluted to monoclonality the clone 12E9-C11 was determined to be of isotype IgG_3 and was purified using a Protein G column. When used in a Western Blot, 12E9-C11 was able to detect both recombinant and serum FI, particularly under non-reducing conditions. There was no evidence of Pro-I cross-reactivity when using this antibody. Promisingly, this specificity towards FI could facilitate its use in FI purification as either a primary purification antibody or for a polishing step, to separate FI from Pro-I. However, due to time constraints this use of 12E9-C11 was unable to be explored further.

A major drawback of the method described by Köhler and Milstein is that an assortment of monoclonal antibodies are produced with very different structural and functional features. IgM antibodies are very large and exist as a pentamer, whereas the IgG antibodies monomeric and much smaller (Janeway *et al.*, 2001). Both antibodies also demonstrate differing affinities to their target antigens, with IgG binding very strongly as a result of affinity maturation, whereas IgM antibodies are typically exhibit lower affinities, particularly in monomeric interactions, as they predominately produced before somatic hypermutation (Eisen, 2014). Ultimately, the final antibody specificity is predominately decided by chance, despite efforts to enhance the immune response to a particular antigen through either an immunostimulant or an adjuvant.

As the hybridoma approach was unsuccessful, an alternative method for producing a monoclonal antibody towards Pro-I, was therefore sought through collaboration with BioRad. BioRad uses a phage display approach with their HuCAL PLATINUM system to provide a more targeted method of antibody generation. However, before the library could be screened, the antigen, Pro-I, first had to be purified. To achieve this, three different methods were employed: Furin inhibition, use of a Furin deficient cell line and ion-exchange chromatography.

Furin inhibition was the first method explored. There are no natural protein inhibitors of Furin, however there are two classes of synthetic inhibitor available: peptide-based inhibitors and protein-based inhibitors. Of these, the most characterised are decanoyl-Arg-Val-Lys-Arg-chloromethylketone (dec-RVKR-cmk) (Henrich *et al.*, 2003; Remacle *et al.*, 2010) and α1-antitrypsin Portland (α1-PDX) (Benjannet *et al.*, 1997; Jean *et al.*, 1998). Dec-RVKR-cmk was chosen due to its high affinity (K_i ~2.0 nM), availability and the fact that it is often used as a reference molecule for Furin inhibition (Henrich *et al.*, 2003; Remacle *et al.*, 2010; Becker *et al.*, 2012). By transfecting CHO cells with pDEF-*CFI* DNA in the presence of the inhibitor, recombinant Pro-I was generated. This is the first instance in the literature for the generation and subsequent purification of this precursor species of FI. Despite the successful generation of the antigen, the low yield and high cost of the inhibitor meant that other methods for generating Pro-I were instead investigated.

To circumvent the requirement for the Furin inhibitor, a Furin-deficient cell line was utilised. The commercially available LoVo cell line (ATCC® CCL-229™) was chosen, due to its complete Furin inactivation by way of two mutations (Takahashi *et al.*, 1995). This cell line demonstrated no innate Pro-I production, and following transfection with pDEF-*CFI* DNA no protein was produced.

Finally, separation of FI and Pro-I through ion-exchange chromatography was explored. This method for Pro-I purification was based upon the difference in isoelectric point between Pro-I (7.38) and FI (6.49), attributed to the loss of the highly basic RRKR linker. Separation of the two proteins was first attempted using a Mono Q column, packed with a strong anion exchange resin. At a protein's pI, the protein has no net charge and will not interact with a charged medium. However, at a pH above its pI, the protein will bind to an anion (positive) exchanger and, at a pH below its pI, a cation (negative) exchanger. Due to this, recombinant FI was buffer exchanged into Tris-HCl at pH 7 and loaded onto the column. However, when the bound proteins were eluted using a sodium chloride gradient there was only one peak observed, indicating poor selectivity.

As both species bound well to the Mono Q column despite a theoretical preference of FI binding, a Mono S column was then used instead. At pH 6, both FI and Pro-I bound to the column and were eluted at two different salt concentrations, as indicated by two separate peaks on the UV chromatogram. When analysed by SDS PAGE and Western Blotting, the first peak was identified as FI and the second peak as Pro-I, indicating that at pH 6, FI had the lowest net charge of the two species and therefore was eluted at a lower ionic strength. Using this method, good separation was achieved for both species, albeit with some FI contamination in the Pro-I peak fractions, as identified by Western Blot. To improve selectivity a lower pH of 5.5 was tested, however both species bound more poorly to the column and there was no noticeable increase in separation.

As ion-exchange chromatography could be used to produce Pro-I with less than 30% FI contamination, this method was used to produce the antigen for HuCAL screening. The recombinant FI produced for the production run contained a greater proportion of Pro-I, indicating that the Pro-I expression may have overwhelmed the endogenous Furin in the transfected CHO cells (Cao *et al.*, 1996). Due to the increase in the amount of Pro-I, the fractions with the least amount of FI contamination could be selected whilst maintaining the desired amount of protein, for a completely pure product.

Once a method had been developed for the production and purification of Pro-I, the CRA, FI, was then produced using the method outlined in Chapter 3. These reagents were then sent to Bio-Rad to screen the HuCAL PLATINUM antibody library (Prassler *et al.*, 2011). After three rounds of panning, the phages isolated from each round were tested by ELISA to assess the enrichment of the binders towards Pro-I within the polyclonal pool. High enrichment phages were further screened by ELISAs to determine the specificity for Pro-I compared to FI. Bio-Rad staff screened two batches of Pro-I by this method, yet no phages were identified which exhibited the desired specificity for Pro-I.

Unfortunately, in this project, the development of an antibody against Pro-I was unsuccessful. However, a monoclonal antibody specific to FI was successfully generated, a chromatographical method for separating Pro-I from recombinant FI has been established, and two methods for producing and purifying Pro-I have been developed.

Following the development of a method for purifying Pro-I from both supernatant and plasma, the activity of Pro-I could then be assessed. Pro-I was first identified by Goldberger *et al.* 1984 through the analysis of the biosynthesis of human FI in three hepatoma-derived cell lines, where they demonstrated that FI is first synthesised as a single chain precursor, that undergoes glycosylation and proteolytic cleavage to generate the two chained mature form (Goldberger *et al.*, 1984). Purified Pro-I has a molecular weight of ~90 kDa, comparable to that of fully processed FI. Following reduction with β-mercaptoethanol, Pro-I does not dissociate into separate heavy and light chains like FI, but maintains a monomeric composition. When used in cofactor activity assays, Pro-I is unable to cleave C3b to iC3b. SPR was used to determine that the lack of proteolytic cleavage by Pro-I, was the result of an inability to form the AP regulatory TMC. It is therefore hypothesised that the presence of the RRKR linker confines the molecule to a linear conformation, preventing the 11° rotation of the heavy chain required for the allosteric activation of the SP light chain and further stabilisation of the TMC (Roversi *et al.*, 2011). The lack of proprotein serine protease activity is shared with Pro-FD. In MASP1/3 deficient mice their sera lacks the ability to activate the AP (Takahashi *et al.*, 2010) due to the inability to cleave Pro-FD to FD by MASP-3 (Dobó *et al.*, 2016). Further to the confirmation of its functional activity, this was also the first identification of Pro-I in human plasma. Since Pro-I is completely inactive, it could also provide an interesting biomarker in AMD or aHUS, as increased serum Pro-I levels may be indicative of AP dysregulation which occurs as a result of mutations within the RRKR linker of FI that prevent Furin cleavage. However further work would be required to explore this hypothesis. Additionally, the presence of Pro-I may also mask FI deficiencies due to antibody cross-reactivity between FI and Pro-I.

Additional to the analysis of Pro-I, a novel method to cleave Pro-I intracellularly was also developed during this project. A vector was designed which encoded both *Furin* and *CFI* to generate fully processed FI. Previous embodiments of this work have centred on co-transfection with Furin (Wong *et al.*, 1995), however these expressions do not always lead to a completely pure product, and can lead to additional proteolysis at R315-R317 (Xue *et al.*, 2017). Using an IRES element to enable synthesis of two proteins from a single bicistronic mRNA, fully processed FI was produced. The resulting protein was functionally equivalent to serum purified FI, differing only in glycosylation, which has been previously demonstrated to have no impact on FI function (Tsiftsoglou *et al.*, 2006).

Using the IRES vector, the three variants of interest K441R, R406H and P553S were produced for subsequent functional analysis. These mutations were hypothesised to lead to different degrees of dysfunction, as attributed by their differing ORs, and CADD scores, and therefore were assessed by multiple methods.

At the start of this project, only R406H had undergone functional testing using cofactor assays (Kavanagh *et al.*, 2008). Since then, further studies have analysed the functional consequences of R406H (Java *et al.*, 2019, 2020), P553S (Geerlings *et al.*, 2017; Java *et al.*, 2019, 2020) and K441R (Java *et al.*, 2020) in cofactor assays. All three variants have now also been characterised in a zebrafish model of retinal vasculogenesis (Tan *et al.*, 2017).

Java *et al.* 2019 found that P553S demonstrated no statistically significant difference in the cleavage of the α′ chain or in the production of the α1, or the two α2 fragments, compared with WT. This was consistent with results from Geerlings *et al.* 2017 and Java *et al.* 2020, which showed that P553S had a similar capacity to degrade C3b to iC3b when compared to WT FI in serum-based cofactor assays. However, the results from this thesis found that P553S was the only variant to show a significant reduction in the degradation of the C3b α′ chain when using a range of different cofactors. These cofactor activity results were also consistent with the SPR data, which demonstrated that P553S has a noticeably decreased ability to form the AP regulator TMC.

As mentioned previously, R406H was the only variant to have undergone functional testing prior to the start of this project (Kavanagh *et al.*, 2008). The R406H variant was suggested to have no functional consequences, with the generation of the α1 band comparable to WT in the C3b cofactor assay. This was in keeping with the results presented here, were R406H performed similarly to WT across a range of cofactors, both in the fluid-phase and on the surface of activated sheep erythrocytes. Java *et al.* 2019, however, also investigated R406H and demonstrated a decreased rate of α' chain cleavage with both FH and CR1, yet normal functional activity with MCP (Java *et al.*, 2019). This is potentially more in keeping with the results from the AP TMC formation, which demonstrated that R406H had a slightly reduced TMC building potential, and it could be hypothesised that this may lead to reduced regulatory activity. Although further work will be required to confirm this hypothesis.

In all of the assays outlined herein, K441R performed similarly to the WT across all the cofactors tested. This finding was consistent with Java *et al.* (2020) which demonstrated that K441R performed similarly to WT with respect to C3b cleavage (Java *et al.*, 2020). This was also supported in the AP TMC build, where it was able to form the TMC with a response equivalent to WT.

Each variant assessed in this thesis was also functionally assessed by Tan *et al.* (2017) in a zebrafish model of retinal vasculogenesis, characterising all three variants as benign (Tan *et al.*, 2017). Albeit this assays appears to lack the sensitivity to properly distinguish between mutants, as in the analysis of the Type 1 mutation G119R, the increase in vasculogenis was indistinguishable from controls, presenting a contrast with the activity observed on the cofactor assays (van de Ven *et al.*, 2013).

It is also important to note that all three variants were classified as Type 3 variants by Java *et al.* (2020). This newly proposed subclass of *CFI* variants is based upon normal FI antigen levels in serum, normal iC3b generation by cofactor assays, but inefficient cleavage of iC3b per unit of FI (Java *et al.*, 2020). This is an interesting concept as it may explain the differing results obtained from the R406H TMC formation and the cofactors assays, however further investigation would be required to support these findings using the assays described in this thesis.

Chapter 7. Conclusion

Three rare genetic variants of *CFI* nominally associated with AMD have been identified for further functional analysis. Their selection was based upon occurrence in the literature, *in silico* analysis and structural modelling within the AP TMC. Each of the three variants are secreted and are typically reported within the normal range for serum FI (Kavanagh *et al.*, 2015; de Jong *et al.*, 2020; Hallam *et al.*, 2020). To facilitate the functional analysis of these selected variants, a method for FI purification was devised based upon the purification of FI from human plasma. Using an OX-21 affinity column and gel filtration, human FI was purified with high purity and functional activity comparable to that of FI purified by conventional methods. Recombinant FI was generated using a pDEF-*CFI* vector for expression in CHO cells. The vector was modified to remove an incorporated polyhistidine tag as an OX-21 column could be utilised for both plasma and recombinant FI purification. The purified protein showed no evidence of aggregation or degradation, with the expected Pro-I present as the only contaminant. The recombinant protein was functionally active and cleaved the α' chain of C3b into both α1 and the two α2 chains in the presence of FH CCP1-4. Despite the confirmed cofactor activity of the recombinant FI, Pro-I contamination was still present.

To provide a mechanism to facilitate Pro-I removal, the development of an antibody against Pro-I was undertaken. Unfortunately, an anti-Pro-I antibody was unable to be generated using either hybridomas or phage display. However, based on these results, there is the potential to develop an antibody in the future. Due to the development of a method for Pro-I production, pure Pro-I is now available for use during the immunisation process. In addition, the full-length Pro-I protein would also improve the ELISA used for screening the hybridomas as it would enable the identification of antibodies for epitopes not located in the RRKR-peptide. Therefore, by using the findings made during this project, this could pave the way for the development of a Pro-I antibody. Additionally, monoclonal antibody specific to FI was also generated and may provide an alternative for recombinant FI purification without Pro-I contamination, however further work is required to confirm this.

Through the purification of Pro-I, it has been confirmed that Pro-I is completely inactive and is incapable of forming the AP regulatory TMC. As such, the results from previous recombinant analysis where there has been no addition of Furin, will be dependent on the ratio of FI to Pro-I present. The presence of Pro-I in plasma has also been identified for the first time, and high levels of Pro-I may provide a biomarker for complement dysregulation.

Additionally, a novel method for generating completely processed recombinant FI with no Pro-I contamination has been developed. Using the designed IRES vector, fully processed FI can be generated that is functionally equivalent to serum purified FI for use in functional analysis or potentially FI supplementation. Through the modelling of the three variants K441R, R406H and P553S on both an active and inactive FI backbone, this has enabled the most extensive analysis of these variants recorded in the literature. K441R, R406H, P553S all demonstrate proteolytic activity, and any defect is small, in comparison to the Type 1 variants described by Kavanagh *et al.* (2008). Only P553S repeatedly demonstrated a statistically reduced activity in the fluid-phase cofactor assays and was in keeping with the reduced TMC formation. There was no statistical difference between R406H or the WT protein in fluid-phase and surface-bound cofactor assays. R406H did however demonstrate slightly reduced TMC building potential, and it could be hypothesised that this may lead to reduced regulatory activity, albeit this is below the resolving capacity of the current assays. Further work will be required to confirm this. In all the assays presented here, K441R performed equivalently to the WT, and therefore further investigation is required to decipher the link between K441R and AMD.

Chapter 8. Future Work

Therefore, based on the results of this study, the following would be interesting to investigate:

1. Examination of other *CFI* variants either nominally or significantly associated AMD, using the functional assays described herein.
2. Generate a column using 12E9-C11 for the purification of recombinant FI to determine whether this antibody could be used for the purification of FI without Pro-I contamination.
3. Make an anti-Pro-I antibody by repeating the hybridoma generation process using full-length Pro-I as the antigen.
4. Make an aptamer against Pro-I for use in AMD patient screening to determine antigenic Pro-I levels.
5. Generate the CP regulatory TMC (C4b:C4BP:FI) on the BIAcore to explore the impact of *CFI* variants within the CP.
6. Use the MicroVue iC3b EIA Enzyme Immunoassay to measure iC3b levels following the cofactor assays described here, to confirm the finding by Java *et al.* (2020) that K441R, P553S and R406H should be categorised as Type 3 variants.

References

Adzhubei, I. A. *et al.* (2010) 'A method and server for predicting damaging missense mutations', *Nature Methods*. Nature Publishing Group, 7(4), pp. 248–249. doi: 10.1038/nmeth0410-248.

Age-Related Eye Disease Study Research Group (1999) 'The Age-Related Eye Disease Study (AREDS): design implications. AREDS report no. 1', *Controlled clinical trials*, 20(6), pp. 573–600. doi: 10.1016/s0197-2456(99)00031-8.

Age-Related Eye Disease Study Research Group (2000) 'Risk factors associated with age-related macular degeneration. A case-control study in the age-related eye disease study: Age-Related Eye Disease Study Report Number 3.', *Ophthalmology*, 107(12), pp. 2224–2232. doi: 10.1016/s0161-6420(00)00409-7.

Alfaleh, M. A. *et al.* (2020) 'Phage Display Derived Monoclonal Antibodies: From Bench to Bedside', *Frontiers in Immunology*. Frontiers Media S.A., p. 1986. doi: 10.3389/fimmu.2020.01986.

Altmann, T. *et al.* (2020) 'Complement factor I deficiency: A potentially treatable cause of fulminant cerebral inflammation', *Neurol Neuroimmunol Neuroinflamm*. 2020/02/27. Neurol Neuroimmunol Neuroinflamm, 7(3), p. e689. doi: 10.1212/nxi.0000000000000689.

Araújo, A. P. U. *et al.* (2000) 'Influence of the Histidine Tail on the Structure and Activity of Recombinant Chlorocatechol 1,2-Dioxygenase', *Biochemical and Biophysical Research Communications*. Academic Press, 272(2), pp. 480–484. doi: 10.1006/BBRC.2000.2802.

Armento, A., Ueffing, M. and Clark, S. J. (2021) 'The complement system in age-related macular degeneration', *Cellular and Molecular Life Sciences*. Springer, 78(10), pp. 4487–4505. doi: 10.1007/S00018-021-03796-9.

Awate, S., Babiuk, L. A. and Mutwiri, G. (2013) 'Mechanisms of action of adjuvants', *Frontiers in Immunology*. Frontiers Media S.A., 4, p. 114. doi: 10.3389/fimmu.2013.00114.

Becker, G. L. *et al.* (2012) 'Highly potent inhibitors of proprotein convertase furin as potential drugs for treatment of infectious diseases', *Journal of Biological Chemistry*. American Society for Biochemistry and Molecular Biology Inc., 287(26), pp. 21992–22003. doi: 10.1074/jbc.M111.332643.

Benjannet, S. *et al.* (1997) 'α1-antitrypsin portland inhibits processing of precursors mediated by proprotein convertases primarily within the constitutive secretory pathway', *Journal of Biological Chemistry*. J Biol Chem, 272(42), pp. 26210–26218. doi: 10.1074/jbc.272.42.26210.

Betts, M. J. and Russell, R. B. (2003) 'Amino Acid Properties and Consequences of Substitutions', *Bioinformatics for Geneticists*. John Wiley & Sons, Ltd, pp. 289–316. doi: 10.1002/0470867302.CH14.

Bienaime, F. *et al.* (2010) 'Mutations in components of complement influence the outcome of Factor I-associated atypical hemolytic uremic syndrome'. doi: 10.1038/ki.2009.472.

Bird, A. C. *et al.* (1995) 'An international classification and grading system for age-related maculopathy and age-related macular degeneration', *Survey of Ophthalmology*, 39(5), pp. 367–374. doi: https://doi.org/10.1016/S0039-6257(05)80092-X.

Boon, C. J. F. *et al.* (2008) 'Basal laminar drusen caused by compound heterozygous variants in the CFH gene.', *American Journal of Human Genetics*, 82(2), pp. 516–523. doi: 10.1016/j.ajhg.2007.11.007.

Booth, W. T. *et al.* (2018) 'Impact of an N-terminal Polyhistidine Tag on Protein Thermal Stability', *ACS Omega*. American Chemical Society, 3(1), pp. 760–768. doi: 10.1021/ACSOMEGA.7B01598.

Bornemann, K. D. *et al.* (1995) 'Roles of heavy and light chains in IgM polymerization', *Proceedings of the National Academy of Sciences of the United States of America*. National Academy of Sciences, 92(11), pp. 4912–4916. doi: 10.1073/pnas.92.11.4912.

Bourne, R. R. A. *et al.* (2021) 'Trends in prevalence of blindness and distance and near vision impairment over 30 years: an analysis for the Global Burden of Disease Study', *The Lancet Global Health*. Elsevier, 9(2), pp. e130–e143. doi: 10.1016/S2214-109X(20)30425-3.

Bourne, R. R. A. *et al.* (2021) 'Causes of blindness and vision impairment in 2020 and trends over 30 years, and prevalence of avoidable blindness in relation to VISION 2020: The Right to Sight: An analysis for the Global Burden of Disease Study', *The Lancet Global Health*. Elsevier, 9(2), pp. e144–e160. doi: 10.1016/S2214-109X(20)30489-7.

Bresin, E. *et al.* (2013) 'Combined complement gene mutations in atypical hemolytic uremic syndrome influence clinical phenotype', *Journal of the American Society of Nephrology*. J Am Soc Nephrol, 24(3), pp. 475–486. doi: 10.1681/ASN.2012090884.

Camous, L. *et al.* (2011) 'Complement alternative pathway acts as a positive feedback amplification of neutrophil activation', *Blood*, 117(4), pp. 1340–1349. doi: 10.1182/blood-2010-05-283564.

Campa, C. and Harding, S. (2011) 'Anti-VEGF compounds in the treatment of neovascular age related macular degeneration', *Current drug targets*. Curr Drug Targets, 12(2), pp. 173–181. doi: 10.2174/138945011794182674.

Cao, J. *et al.* (1996) 'Membrane type matrix metalloproteinase 1 activates pro-gelatinase A without furin cleavage of the N-terminal domain', *Journal of Biological Chemistry*. Elsevier, 271(47), pp. 30174–30180. doi: 10.1074/jbc.271.47.30174.

Carson, M. *et al.* (2007) 'His-tag impact on structure', *Acta crystallographica. Section D, Biological crystallography*. Acta Crystallogr D Biol Crystallogr, 63(Pt 3), pp. 295–301. doi: 10.1107/S0907444906052024.

Carswell, S. and Alwine, J. C. (1989) *Efficiency of Utilization of the Simian Virus 40 Late Polyadenylation Site: Effects of Upstream Sequences*, *MOLECULAR AND CELLULAR BIOLOGY*. Available at: https://journals.asm.org/journal/mcb.

Catterall, C. F. *et al.* (1987) 'Characterization of primary amino acid sequence of human complement control protein factor I from an analysis of cDNA clones', *Biochemical Journal*. 1987/03/15, 242(3), pp. 849–856. doi: 10.1042/bj2420849.

Caycı, F. S. *et al.* (2012) 'Eculizumab therapy in a child with hemolytic uremic syndrome and CFI mutation', *Pediatric Nephrology*. Springer, 27(12), pp. 2327–2331. doi: 10.1007/S00467-012-2283-9.

Chirco, K. R. *et al.* (2017) 'Structural and molecular changes in the aging choroid: implications for age-related macular degeneration', *Eye*. Nature Publishing Group, 31(1), pp. 10–25. doi: 10.1038/eye.2016.216.

Cho, E. *et al.* (2001) 'Prospective study of dietary fat and the risk of age-related macular degeneration', *The American Journal of Clinical Nutrition*, 73(2), pp. 209–218. doi: 10.1093/ajcn/73.2.209.

Chong, E. W.-T. *et al.* (2009) 'Fat consumption and its association with age-related macular degeneration.', *Archives of Ophthalmology*. United States, 127(5), pp. 674–680. doi: 10.1001/archophthalmol.2009.60.

Clackson, T. *et al.* (1991) 'Making antibody fragments using phage display libraries', *Nature*. Nature Publishing Group, 352(6336), pp. 624–628. doi: 10.1038/352624a0.

Clark, S. J. *et al.* (2014) 'Identification of Factor H–like Protein 1 as the Predominant Complement Regulator in Bruch's Membrane: Implications for Age-Related Macular Degeneration', *The Journal of Immunology*, 193(10), pp. 4962 LP – 4970. doi: 10.4049/jimmunol.1401613.

Clark, S. J. *et al.* (2017) 'Bruch's Membrane Compartmentalizes Complement Regulation in the Eye with Implications for Therapeutic Design in Age-Related Macular Degeneration', *Frontiers in Immunology*. Frontiers Media S.A., 8(DEC), p. 1778. doi: 10.3389/fimmu.2017.01778.

Coleman, A. L. *et al.* (2010) 'Impact of age-related macular degeneration on vision-specific quality of life: Follow-up from the 10-year and 15-year visits of the Study of Osteoporotic Fractures', *American Journal of Ophthalmology*. 2010/08/05, 150(5), pp. 683–691. doi: 10.1016/j.ajo.2010.05.030.

Corominas, J. *et al.* (2018) 'Whole-Exome Sequencing in Age-Related Macular Degeneration Identifies Rare Variants in COL8A1, a Component of Bruch's Membrane.', *Ophthalmology*, 125(9), pp. 1433–1443. doi: 10.1016/j.ophtha.2018.03.040.

Cortes, C. *et al.* (2012) 'Local release of properdin in the cellular microenvironment: Role in pattern recognition and amplification of the alternative pathway of complement', *Frontiers in Immunology*. Frontiers, 3(JAN), p. 412. doi: 10.3389/FIMMU.2012.00412/BIBTEX.

Crabb, J. W. *et al.* (2002) 'Drusen proteome analysis: An approach to the etiology of age-related macular degeneration', *Proceedings of the National Academy of Sciences*, 99(23), pp. 14682 LP – 14687. doi: 10.1073/pnas.222551899.

Crossley, L. G. and Porter, R. R. (1980) 'Purification of the human complement control protein C3b inactivator', *Biochemical Journal*. Portland Press, 191(1), pp. 173–182. doi: 10.1042/BJ1910173.

Cunha-Vaz, J., Bernardes, R. and Lobo, C. (2010) 'Blood-Retinal Barrier', *European Journal of Ophthalmology*. SAGE Publications, 21(6_suppl), pp. 3–9. doi: 10.5301/EJO.2010.6049.

Curcio, C. A. *et al.* (1993) 'Aging of the human photoreceptor mosaic: evidence for selective vulnerability of rods in central retina.', *Investigative Ophthalmology & Visual Science*, 34(12), pp. 3278–3296.

Curcio, C. A., Medeiros, N. E. and Millican, C. L. (1996) 'Photoreceptor loss in age-related macular degeneration.', *Investigative Ophthalmology & Visual Science*. United States, 37(7), pp. 1236–1249.

Curtis, J. E. *et al.* (1970) 'The human primary immune response to keyhole limpet haemocyanin: interrelationships of delayed hypersensitivity, antibody response and *in vitro* blast transformation.', *Clinical and Experimental Immunology*. Wiley-Blackwell, 6(4), pp. 473–47391. Available at: /pmc/articles/PMC1712800/?report=abstract (Accessed: 1 June 2021).

Delcourt, C. *et al.* (1998) 'Smoking and Age-related Macular Degeneration: The POLA Study', *Archives of Ophthalmology*, 116(8), pp. 1031–1035. doi: 10.1001/archopht.116.8.1031.

Delori, F. C., Goger, D. G. and Dorey, C. K. (2001) 'Age-related accumulation and spatial distribution of lipofuscin in RPE of normal subjects.', *Investigative Ophthalmology & Visual Science*. United States, 42(8), pp. 1855–1866.

Dewan, A. *et al.* (2006) 'HTRA1 promoter polymorphism in wet age-related macular degeneration.', *Science*. United States, 314(5801), pp. 989–992. doi: 10.1126/science.1133807.

Dobó, J. *et al.* (2016) 'MASP-3 is the exclusive pro-factor D activator in resting blood: the lectin and the alternative complement pathways are fundamentally linked', *Scientific Reports*. Nature Publishing Group, 6(1), pp. 1–12. doi: 10.1038/srep31877.

Duvvari, M. R. *et al.* (2014) 'Analysis of rare variants in the C3 gene in patients with age-related macular degeneration.', *PLoS ONE*, 9(4), p. e94165. doi: 10.1371/journal.pone.0094165.

Edwards, A. O. *et al.* (2005) 'Complement factor H polymorphism and age-related macular degeneration.', *Science (New York, N.Y.)*. United States, 308(5720), pp. 421–424. doi:

10.1126/science.1110189.

Eisen, H. N. (2014) ‘Affinity enhancement of antibodies: how low-affinity antibodies produced early in immune responses are followed by high-affinity antibodies later and in memory B-cell responses’, *Cancer immunology research*. Cancer Immunol Res, pp. 381–392. doi: 10.1158/2326-6066.CIR-14-0029.

Fagerness, J. A. *et al.* (2009) ‘Variation near complement factor I is associated with risk of advanced AMD’, *European Journal of Human Genetics*. 2008/08/06. Nature Publishing Group, 17(1), pp. 100–104. doi: 10.1038/ejhg.2008.140.

Fang, C. J. *et al.* (2008) ‘Membrane cofactor protein mutations in atypical hemolytic uremic syndrome (aHUS), fatal Stx-HUS, C3 glomerulonephritis, and the HELLP syndrome’, *Blood*. American Society of Hematology, 111(2), pp. 624–632. doi: 10.1182/BLOOD-2007-04-084533.

Fearon, D. T. (1977) ‘Purification of C3b Inactivator and Demonstration of Its Two Polypeptide Chain Structure’, *The Journal of Immunology*, 119(4), pp. 1248–1252.

Feher, J. *et al.* (2006) ‘Mitochondrial alterations of retinal pigment epithelium in age-related macular degeneration’, *Neurobiology of Aging*, 27(7), pp. 983–993. doi: https://doi.org/10.1016/j.neurobiolaging.2005.05.012.

Ferris, F. L. *et al.* (2005) ‘A simplified severity scale for age-related macular degeneration: AREDS Report No. 18.’, *Archives of Ophthalmology*, 123(11), pp. 1570–1574. doi: 10.1001/archopht.123.11.1570.

Ferris, F. L. *et al.* (2013) ‘Clinical classification of age-related macular degeneration.’, *Ophthalmology*. United States, 120(4), pp. 844–851. doi: 10.1016/j.ophtha.2012.10.036.

Fitch, C. A. *et al.* (2015) ‘Arginine: Its pKa value revisited’, *Protein Science*. Blackwell Publishing Ltd, 24(5), pp. 752–761. doi: 10.1002/pro.2647.

Flaxel, C. J. *et al.* (2020) ‘Age-Related Macular Degeneration Preferred Practice Pattern®’, *Ophthalmology*. Ophthalmology, 127(1), pp. P1–P65. doi: 10.1016/J.OPHTHA.2019.09.024.

Frank, R. N. *et al.* (2000) ‘Race, iris color, and age-related macular degeneration’, *Transactions of the American Ophthalmological Society*, 98, pp. 109–117. Available at: https://pubmed.ncbi.nlm.nih.gov/11190014.

Fremeaux-Bacchi, V. *et al.* (2004) ‘Complement factor I: a susceptibility gene for atypical haemolytic uraemic syndrome’, *Journal of Medical Genetics*. BMJ Publishing Group Ltd, 41(6), pp. e84–e84. doi: 10.1136/JMG.2004.019083.

Fremeaux-Bacchi, V. *et al.* (2013) ‘Genetics and outcome of atypical hemolytic uremic syndrome: a nationwide French series comparing children and adults’, *Clinical Journal of the American Society of Nephrology*. Clin J Am Soc Nephrol, 8(4), pp. 554–562. doi: 10.2215/CJN.04760512.

Friedman, D. S. *et al.* (1999) ‘Racial differences in the prevalence of age-related macular degeneration: the Baltimore Eye Survey.’, *Ophthalmology*. United States, 106(6), pp. 1049–1055. doi: 10.1016/S0161-6420(99)90267-1.

Fritsche, L. G. *et al.* (2010) ‘An imbalance of human complement regulatory proteins CFHR1, CFHR3 and factor H influences risk for age-related macular degeneration (AMD)’, *Human Molecular Genetics*. Hum Mol Genet, 19(23), pp. 4694–4704. doi: 10.1093/HMG/DDQ399.

Fritsche, L. G. *et al.* (2013) ‘Seven new loci associated with age-related macular degeneration’, *Nature Genetics*. Nature Publishing Group, 45(4), pp. 433–439. doi: 10.1038/ng.2578.

Fritsche, L. G. *et al.* (2016) ‘A large genome-wide association study of age-related macular degeneration highlights contributions of rare and common variants’, *Nature Genetics*, 48(2), pp. 134–143. doi: 10.1038/ng.3448.

Gasteiger, E. *et al.* (2005) ‘Protein identification and analysis tools on the ExPASy server’, *The Proteomics Protocols Handbook*. Humana Press, pp. 571–607. Available at: http://www.springer.com/life+sciences/biochemistry+%26+biophysics/book/978-1-58829-343-5 (Accessed: 18 April 2023).

Geerlings, M. J. *et al.* (2017) ‘The functional effect of rare variants in complement genes on C3b degradation in patients with age-related macular degeneration’, *JAMA Ophthalmology*. American Medical Association, 135(1), pp. 39–46. doi: 10.1001/jamaophthalmol.2016.4604.

Geerlings, M. J. *et al.* (2018) ‘Genotype-phenotype correlations of low-frequency variants in the complement system in renal disease and age-related macular degeneration’, *Clinical Genetics*. John Wiley & Sons, Ltd, 94(3–4), pp. 330–338. doi: 10.1111/CGE.13392.

Geerlings, M. J., de Jong, E. K. and den Hollander, A. I. (2017) 'The complement system in age-related macular degeneration: A review of rare genetic variants and implications for personalized treatment', *Molecular Immunology*. Elsevier Ltd, 84, pp. 65–76. doi: 10.1016/j.molimm.2016.11.016.

Gleeson, P. J. *et al.* (2016) 'Chromosomal rearrangement—A rare cause of complement factor I associated atypical haemolytic uraemic syndrome', *Immunobiology*. Netherlands, 221(10), pp. 1124–1130. doi: 10.1016/j.imbio.2016.05.002.

Gold, B. *et al.* (2006) 'Variation in factor B (BF) and complement component 2 (C2) genes is associated with age-related macular degeneration.', *Nature Genetics*, 38(4), pp. 458–462. doi: 10.1038/ng1750.

Goldberger, G. *et al.* (1984) 'Biosynthesis and postsynthetic processing of human C3b/C4b inactivator (factor I) in three hepatoma cell lines', *Journal of Biological Chemistry*. 1984/05/25. Elsevier, 259(10), pp. 6492–6497. doi: 10.1016/S0021-9258(20)82168-1.

Goldberger, G. *et al.* (1987) 'Human complement factor I: analysis of cDNA-derived primary structure and assignment of its gene to chromosome 4', *Journal of Biological Chemistry*. 1987/07/25, 262(21), pp. 10065–10071. doi: 10.1016/S0021-9258(18)61076-2.

Gräslund, S. *et al.* (2008) 'Protein production and purification', *Nature Methods*. Nature Publishing Group, 5(2), pp. 135–146. doi: 10.1038/nmeth.f.202.

Hageman, G. S. *et al.* (2001) 'An integrated hypothesis that considers drusen as biomarkers of immune-mediated processes at the RPE-Bruch's membrane interface in aging and age-related macular degeneration.', *Progress in Retinal and Eye Research*. England, 20(6), pp. 705–732. doi: 10.1016/s1350-9462(01)00010-6.

Hageman, G. S. *et al.* (2005) 'A common haplotype in the complement regulatory gene factor H (HF1/CFH) predisposes individuals to age-related macular degeneration', *Proceedings of the National Academy of Sciences of the United States of America*, 102(20), pp. 7227 LP – 7232. doi: 10.1073/pnas.0501536102.

Haines, J. L. *et al.* (2005) 'Complement factor H variant increases the risk of age-related macular degeneration.', *Science*. United States, 308(5720), pp. 419–421. doi: 10.1126/science.1110359.

Hallam, T. M. *et al.* (2020) 'Rare Genetic Variants in Complement Factor I Lead to Low FI Plasma Levels Resulting in Increased Risk of Age-Related Macular Degeneration', *Investigative Ophthalmology & Visual Science*. The Association for Research in Vision and Ophthalmology, 61(6), pp. 18–18. doi: 10.1167/IOVS.61.6.18.

Hamm, L. L., Nakhoul, N. and Hering-Smith, K. S. (2015) 'Acid-Base Homeostasis', *Clinical Journal of the American Society of Nephrology*. American Society of Nephrology, 10(12), pp. 2232–2242. doi: 10.2215/CJN.07400715.

Hammond, C. J. *et al.* (2002) 'Genetic influence on early age-related maculopathy: a twin study.', *Ophthalmology*. United States, 109(4), pp. 730–736. doi: 10.1016/s0161-6420(01)01049-1.

Handa, J. T. *et al.* (1999) 'Increase in the advanced glycation end product pentosidine in Bruch's membrane with age.', *Investigative Ophthalmology & Visual Science*, 40(3), pp. 775–779.

Harder, M. *et al.* (2016) 'Comparative Analysis of Novel Complement-Targeted Inhibitors, MiniFH, and the Natural Regulators Factor H and Factor H-like Protein 1 Reveal Functional Determinants of Complement Regulation', *Journal of immunology (Baltimore, Md. : 1950)*. J Immunol, 196(2), pp. 866–876. doi: 10.4049/JIMMUNOL.1501919.

Harms, M. J. *et al.* (2008) 'A buried lysine that titrates with a normal pKa: Role of conformational flexibility at the protein-water interface as a determinant of pKavalues', *Protein Science*. Wiley, 17(5), pp. 833–845. doi: 10.1110/ps.073397708.

Harris, C. L. *et al.* (2005) 'Molecular dissection of interactions between components of the alternative pathway of complement and decay accelerating factor (CD55).', *The Journal of Biological Chemistry*. United States, 280(4), pp. 2569–2578. doi: 10.1074/jbc.M410179200.

Harris, C. L. *et al.* (2012) 'The complotype: dictating risk for inflammation and infection', *Trends in Immunology*. Elsevier, 33(10–10), p. 513. doi: 10.1016/J.IT.2012.06.001.

Harris, C. L. *et al.* (2018) 'Developments in anti-complement therapy; from disease to clinical trial.', *Molecular Immunology*. England, 102, pp. 89–119. doi: 10.1016/j.molimm.2018.06.008.

Harris, J. R. and Markl, J. (1999) 'Keyhole limpet hemocyanin (KLH): a biomedical review', *Micron*, 30(6), pp. 597–623. doi: https://doi.org/10.1016/S0968-4328(99)00036-0.

Hellwage, J. *et al.* (2001) 'The complement regulator factor H binds to the surface protein OspE of Borrelia burgdorferi', *The Journal of Biological Chemistry*. J Biol Chem, 276(11), pp. 8427–8435. doi: 10.1074/JBC.M007994200.

Henrich, S. *et al.* (2003) 'The crystal structure of the proprotein processing proteinase furin explains its stringent specificity', *Nature Structural Biology*. Nat Struct Biol, 10(7), pp. 520–526. doi: 10.1038/nsb941.

Hoogenboom, H. R. *et al.* (1991) 'Multi-subunit proteins on the surface of filamentous phage: Methodologies for displaying antibody (Fab) heavy and light chains', *Nucleic Acids Research*, 19(15), pp. 4133–4137. doi: 10.1093/nar/19.15.4133.

Hsiung, L. *et al.* (1982) 'Purification of human C3b inactivator by monoclonal-antibody affinity chromatography', *Biochemical Journal*. Portland Press, 203(1), pp. 293–298. doi: 10.1042/BJ2030293.

Hussain, A. A. *et al.* (2019) 'Study of association between the serum lipid profile and age-related macular degeneration in a tertiary care centre of Central UP', *International Journal of Research in Medical Sciences*, 7(4), pp. 1104–1108. Available at: https://www.msjonline.org/index.php/ijrms/article/view/6227 (Accessed: 23 September 2021).

Hussain, A. A. *et al.* (2010) 'Macromolecular diffusion characteristics of ageing human Bruch's membrane: Implications for age-related macular degeneration (AMD)', *Experimental Eye Research*. Academic Press, 90(6), pp. 703–710. doi: https://doi.org/10.1016/j.exer.2010.02.013.

Hussain, A. A., Rowe, L. and Marshall, J. (2002) 'Age-related alterations in the diffusional transport of amino acids across the human Bruch's-choroid complex', *Journal of the Optical Society of America A*. OSA, 19(1), pp. 166–172. doi: 10.1364/JOSAA.19.000166.

Hyman, L. *et al.* (2000) 'Hypertension, Cardiovascular Disease, and Age-Related Macular Degeneration', *Archives of Ophthalmology*, 118(3), pp. 351–358. doi: 10.1001/archopht.118.3.351.

Ishii, N. (2018) 'Folding and Binding Properties of Human Complement Receptor Type 1

Extracellular Domain', *Peripheral Membrane Proteins*. IntechOpen. doi: 10.5772/INTECHOPEN.75120.

Iyengar, S. K. *et al.* (2004) 'Dissection of genomewide-scan data in extended families reveals a major locus and oligogenic susceptibility for age-related macular degeneration.', *American Journal of Human Genetics*, 74(1), pp. 20–39. doi: 10.1086/380912.

Jackson, R. J., Hellen, C. U. T. and Pestova, T. V. (2010) 'The mechanism of eukaryotic translation initiation and principles of its regulation', *Nature Reviews Molecular Cell Biology 2010 11:2*. Nature Publishing Group, 11(2), pp. 113–127. doi: 10.1038/nrm2838.

Janeway, C. *et al.* (2001) 'The distribution and functions of immunoglobulin isotypes', in *Immunobiology: The Immune System in Health and Disease. 5th edition.* Garland Science. Available at: https://www.ncbi.nlm.nih.gov/books/NBK27162/ (Accessed: 3 June 2021).

Java, A. *et al.* (2019) 'A Multimodality Approach to Assessing Factor I Genetic Variants in Atypical Hemolytic Uremic Syndrome', *Kidney International Reports*. International Society of Nephrology, 4(7), pp. 1007–1017. doi: 10.1016/j.ekir.2019.04.003.

Java, A. *et al.* (2020) 'Functional Analysis of Rare Genetic Variants in Complement Factor I (CFI) using a Serum-Based Assay in Advanced Age-related Macular Degeneration', *Translational Vision Science & Technology*. Association for Research in Vision and Ophthalmology (ARVO), 9(9), p. 37. doi: 10.1167/tvst.9.9.37.

Jean, F. *et al.* (1998) 'α 1 -Antitrypsin Portland, a bioengineered serpin highly selective for furin: Application as an antipathogenic agent', *Proceedings of the National Academy of Sciences*. National Academy of Sciences, 95(13), pp. 7293–7298. doi: 10.1073/pnas.95.13.7293.

de Jong, S. *et al.* (2020) 'Effect of rare coding variants in the CFI gene on Factor I expression levels', *Human Molecular Genetics*. Oxford Academic, 29(14), pp. 2313–2324. doi: 10.1093/HMG/DDAA114.

Kang, K. T. and Kim, Y. C. (2019) 'Dietary Patterns and Age-Related Macular Degeneration in Korea: The Korea National Health and Nutrition Examination Survey 2010-2011.', *Scientific Reports*, 9(1), p. 8200. doi: 10.1038/s41598-019-44632-2.

Kassoff, A. *et al.* (2001) 'A Randomized, Placebo-Controlled, Clinical Trial of High-Dose

Supplementation With Vitamins C and E, Beta Carotene, and Zinc for Age-Related Macular Degeneration and Vision Loss: AREDS Report No. 8', *Archives of Ophthalmology*. American Medical Association, 119(10), pp. 1417–1436. doi: 10.1001/archopht.119.10.1417.

Kavanagh, D. *et al.* (2008) 'Characterization of mutations in complement factor I (CFI) associated with hemolytic uremic syndrome', *Molecular Immunology*. Pergamon, 45(1), pp. 95–105. doi: 10.1016/j.molimm.2007.05.004.

Kavanagh, D. *et al.* (2012) 'Factor I Autoantibodies in Patients with Atypical Hemolytic Uremic Syndrome: Disease-Associated or an Epiphenomenon?', *Clinical Journal of the American Society of Nephrology*, 7, pp. 417–426. doi: 10.2215/CJN.05750611.

Kavanagh, D. *et al.* (2015) 'Rare genetic variants in the CFI gene are associated with advanced age-related macular degeneration and commonly result in reduced serum factor I levels', *Hum Mol Genet*. 2015/03/20, 24(13), pp. 3861–3870. doi: 10.1093/hmg/ddv091.

Kevany, B. M. and Palczewski, K. (2010) 'Phagocytosis of retinal rod and cone photoreceptors', *Physiology*, 25(1), pp. 8–15. doi: 10.1152/physiol.00038.2009.

Keyt, B. A. *et al.* (2020) 'Structure, Function, and Therapeutic Use of IgM Antibodies', *Antibodies*. MDPI AG, 9(4), p. 53. doi: 10.3390/antib9040053.

Khan, J. C. *et al.* (2006) 'Smoking and age related macular degeneration: the number of pack years of cigarette smoking is a major determinant of risk for both geographic atrophy and choroidal neovascularisation', *British Journal of Ophthalmology*, 90(1), pp. 75 LP – 80. doi: 10.1136/bjo.2005.073643.

Kim, J. H. *et al.* (2011) 'High Cleavage Efficiency of a 2A Peptide Derived from Porcine Teschovirus-1 in Human Cell Lines, Zebrafish and Mice', *PLoS ONE*. Public Library of Science, 6(4), p. e18556. doi: 10.1371/JOURNAL.PONE.0018556.

Klaver, C. C. *et al.* (1998) 'Genetic risk of age-related maculopathy. Population-based familial aggregation study.', *Archives of Ophthalmology*. United States, 116(12), pp. 1646–1651. doi: 10.1001/archopht.116.12.1646.

Klein, M. L., Mauldin, W. M. and Stoumbos, V. D. (1994) 'Heredity and age-related macular degeneration. Observations in monozygotic twins.', *Archives of Ophthalmology*. United States, 112(7), pp. 932–937. doi: 10.1001/archopht.1994.01090190080025.

Klein, R. J. *et al.* (2005) ‘Complement factor H polymorphism in age-related macular degeneration.’, *Science*. United States, 308(5720), pp. 385–389. doi: 10.1126/science.1109557.

Klein, R., Klein, B. E. K. and Linton, K. L. P. (1992) ‘Prevalence of Age-related Maculopathy: The Beaver Dam Eye Study’, *Ophthalmology*, 99(6), pp. 933–943. doi: https://doi.org/10.1016/S0161-6420(92)31871-8.

Köhler, G. and Milstein, C. (1975) ‘Continuous cultures of fused cells secreting antibody of predefined specificity’, *Nature*, 256(5517), pp. 495–497. doi: 10.1038/256495a0.

Kortvely, E. *et al.* (2010) ‘ARMS2 Is a Constituent of the Extracellular Matrix Providing a Link between Familial and Sporadic Age-Related Macular Degenerations’, *Investigative Ophthalmology & Visual Science*, 51(1), pp. 79–88. doi: 10.1167/iovs.09-3850.

Kremlitzka, M. *et al.* (2018) ‘Functional analyses of rare genetic variants in complement component C9 identified in patients with age-related macular degeneration’, *Human Molecular Genetics*, 27(15), pp. 2678–2688. doi: 10.1093/hmg/ddy178.

Lachmann, P. J., Lay, E. and Seilly, D. J. (2018) ‘A novel and sensitive functional assay for complement Factor I based on the third proteolytic clip of C3b’, *Journal of Immunological Methods*. Elsevier, 457, pp. 30–32. doi: 10.1016/J.JIM.2018.03.013.

Lachmann, P. J. and Müller-Eberhard, H. J. (1968) ‘The Demonstration in Human Serum of “Conglutinogen-Activating Factor” and its Effect on the Third Component of Complement’, *The Journal of Immunology*, 100(4), pp. 691 LP – 698. Available at: http://www.jimmunol.org/content/100/4/691.abstract.

Leenaars, M. and Hendriksen, C. F. M. (2005) ‘Critical steps in the production of polyclonal and monoclonal antibodies: Evaluation and recommendations’, *ILAR Journal*. Institute for Laboratory Animal Research, 46(3), pp. 269–279. doi: 10.1093/ilar.46.3.269.

Lek, M. *et al.* (2016) ‘Analysis of protein-coding genetic variation in 60,706 humans’, *Nature*. Nature Publishing Group, 536(7616), pp. 285–291. doi: 10.1038/nature19057.

Liew, G. *et al.* (2016) ‘Validating the AREDS Simplified Severity Scale of Age-Related Macular Degeneration with 5- and 10-Year Incident Data in a Population-Based Sample’, *Ophthalmology*, 123(9), pp. 1874–1878. doi: https://doi.org/10.1016/j.ophtha.2016.05.043.

Liu, Z. *et al.* (2017) 'Systematic comparison of 2A peptides for cloning multi-genes in a polycistronic vector', *Scientific Reports*. Nature Publishing Group, 7(1), pp. 1–9. doi: 10.1038/s41598-017-02460-2.

Loyet, K. M. *et al.* (2012) 'Activation of the alternative complement pathway in vitreous is controlled by genetics in age-related macular degeneration', *Investigative Ophthalmology & Visual Science*. The Association for Research in Vision and Ophthalmology, 53(10), pp. 6628–6637. doi: 10.1167/iovs.12-9587.

Luibl, V. *et al.* (2006) 'Drusen deposits associated with aging and age-related macular degeneration contain nonfibrillar amyloid oligomers.', *The Journal of Clinical Investigation*, 116(2), pp. 378–385. doi: 10.1172/JCI25843.

Lutty, G. A. *et al.* (2010) 'Development of the human choriocapillaris', *Eye*. Nature Publishing Group, 24(3), pp. 408–415. doi: 10.1038/eye.2009.318.

Macular Society (2018) *Nearly 1.5m people in the UK are affected by macular disease - Macular Society*. Available at: https://www.macularsociety.org/about/media/news/nearly-15m-people-uk-are-affected-macular-disease/ (Accessed: 22 September 2021).

Maley, F. *et al.* (1989) 'Characterization of glycoproteins and their associated oligosaccharides through the use of endoglycosidases', *Analytical Biochemistry*. Academic Press, 180(2), pp. 195–204. doi: 10.1016/0003-2697(89)90115-2.

Martínez-Barricarte, R. *et al.* (2015) 'The molecular and structural bases for the association of complement C3 mutations with atypical hemolytic uremic syndrome', *Molecular Immunology*. Elsevier, 66(2), p. 263. doi: 10.1016/J.MOLIMM.2015.03.248.

McCafferty, J. *et al.* (1990) 'Phage antibodies: filamentous phage displaying antibody variable domains', *Nature*. Nature Publishing Group, 348(6301), pp. 552–554. doi: 10.1038/348552a0.

Merle, B. M. J. *et al.* (2019) 'Mediterranean Diet and Incidence of Advanced Age-Related Macular Degeneration: The EYE-RISK Consortium.', *Ophthalmology*. United States, 126(3), pp. 381–390. doi: 10.1016/j.ophtha.2018.08.006.

Meyers, S. M., Greene, T. and Gutman, F. A. (1995) 'A twin study of age-related macular degeneration.', *American Journal of Ophthalmology*. United States, 120(6), pp. 757–766. doi:

10.1016/s0002-9394(14)72729-1.

Milton, R. C. *et al.* (2005) 'Risk Factors for the Incidence of Advanced Age-Related Macular Degeneration in the Age-Related Eye Disease Study (AREDS): AREDS report no. 19', *Ophthalmology*. Elsevier, 112(4), pp. 533-539.e1. doi: 10.1016/J.OPHTHA.2004.10.047.

Minta, J. O. *et al.* (1996) 'cDNA cloning, sequencing and chromosomal assignment of the gene for mouse complement factor I (C3b/C4b inactivator): identification of a species specific divergent segment in factor I', *Molecular Immunology*. 1996/01/01, 33(1), pp. 101–112. doi: 10.1016/0161-5890(95)00116-6.

Minta, J. O. *et al.* (1998) 'Cloning and characterization of the promoter for the human complement factor I (C3b/C4b inactivator) gene.', *Gene*. Netherlands, 208(1), pp. 17–24. doi: 10.1016/s0378-1119(97)00632-x.

Minta, J. O., Fung, M. and Paramaswara, B. (1998) 'Transcriptional and post-transcriptional regulation of complement factor I (CFI) gene expression in Hep G2 cells by interleukin-6.', *Biochimica et biophysica acta*. Netherlands, 1442(2–3), pp. 286–295. doi: 10.1016/s0167-4781(98)00189-4.

Minta, J. O., Ngan, B.-Y. and Pang, A. S. D. (1979) 'Purification and Characterization of a Single Chain Precursor C3-Protein (PRO-C3) from Normal Human Plasma', *The Journal of Immunology*, 123(5).

Mitchell, P. *et al.* (1995) 'Prevalence of age-related maculopathy in Australia. The Blue Mountains Eye Study.', *Ophthalmology*. United States, 102(10), pp. 1450–1460. doi: 10.1016/s0161-6420(95)30846-9.

Morgan, B. P. (ed.) (2000) *Complement Methods and Protocols*, *Methods in Molecular Biology*. doi: 10.1017/CBO9781107415324.004.

Mullins, R. F. *et al.* (2000) 'Drusen associated with aging and age-related macular degeneration contain proteins common to extracellular deposits associated with atherosclerosis, elastosis, amyloidosis, and dense deposit disease.', *The FASEB Journal*. United States, 14(7), pp. 835–846.

Nasevicius, A., Larson, J. and Ekker, S. C. (2000) 'Distinct Requirements for Zebrafish Angiogenesis Revealed by a VEGF-A Morphant', *Yeast*. Hindawi Limited, 17(4), p. 294. doi:

10.1002/1097-0061(200012)17:4<294::aid-yea54>3.0.co;2-5.

Nicol, P. A. and Lachmann, P. J. (1973) ‘The alternate pathway of complement activation. The role of C3 and its inactivator (KAF)’, *Immunology*, 24(2), pp. 259–275. Available at: https://pubmed.ncbi.nlm.nih.gov/4632688.

Nilsson, S. C. *et al.* (2010) ‘Mutations in complement factor I as found in atypical hemolytic uremic syndrome lead to either altered secretion or altered function of factor I’, *European Journal of Immunology*. John Wiley & Sons, Ltd, 40(1), pp. 172–185. doi: 10.1002/eji.200939280.

Nordlund, H. R. *et al.* (2003) ‘Introduction of histidine residues into avidin subunit interfaces allows pH-dependent regulation of quaternary structure and biotin binding’, *FEBS Letters*. No longer published by Elsevier, 555(3), pp. 449–454. doi: 10.1016/S0014-5793(03)01302-4.

Osborne, A. J. *et al.* (2018) ‘Statistical Validation of Rare Complement Variants Provides Insights into the Molecular Basis of Atypical Hemolytic Uremic Syndrome and C3 Glomerulopathy’, *The Journal of Immunology*. American Association of Immunologists, 200(7), pp. 2464–2478. doi: 10.4049/JIMMUNOL.1701695.

Pangburn, M. K., Schreiber, R. D. and Muller-Eberhard, H. J. (1977) ‘Human complement C3b inactivator: isolation, characterization, and demonstration of an absolute requirement for the serum protein beta1H for cleavage of C3b and C4b in solution’, *Journal of Experimental Medicine*. 1977/07/01, 146(1), pp. 257–270. doi: 10.1084/jem.146.1.257.

Paramaswara, B. and Minta, J. O. (1999) ‘An initiator element and a proximal cis-acting sequence are essential for transcriptional activation of the complement factor I (CFI) gene’, *Gene*, 237(1), pp. 71–80. doi: https://doi.org/10.1016/S0378-1119(99)00304-2.

Pascolini, D. and Mariotti, S. P. (2012) ‘Global estimates of visual impairment: 2010’, *British Journal of Ophthalmology*. BMJ Publishing Group Ltd, 96(5), pp. 614–618. doi: 10.1136/BJOPHTHALMOL-2011-300539.

Pauleikhoff, D. *et al.* (1990) ‘Aging Changes in Bruch’s Membrane: A Histochemical and Morphologic Study’, *Ophthalmology*, 97(2), pp. 171–178. doi: https://doi.org/10.1016/S0161-6420(90)32619-2.

Pechtl, I. C. *et al.* (2011) ‘Disease-associated N-terminal complement factor H mutations perturb cofactor and decay-accelerating activities', *The Journal of Biological Chemistry*. J Biol Chem, 286(13), pp. 11082–11090. doi: 10.1074/JBC.M110.211839.

Pelletier, J. and Sonenberg, N. (1988) 'Internal initiation of translation of eukaryotic mRNA directed by a sequence derived from poliovirus RNA', *Nature*. Nature, 334(6180), pp. 320–325. doi: 10.1038/334320a0.

Perkins, S. J. and Smith, K. F. (1993) 'Identity of the putative serine-proteinase fold in proteins of the complement system with nine relevant crystal structures', *Biochemical Journal*. 1993/10/01, 295 (Pt 1, pp. 109–114. doi: 10.1042/bj2950109.

Plitnick, L. M. and Herzyk, D. J. (2010) 'The T-dependent antibody response to keyhole limpet hemocyanin in rodents.', *Methods in Molecular Biology*. Humana Press, 598, pp. 159–171. doi: 10.1007/978-1-60761-401-2_11.

Prassler, J. *et al.* (2011) 'HuCAL PLATINUM, a synthetic fab library optimized for sequence diversity and superior performance in mammalian expression systems', *Journal of Molecular Biology*. Academic Press, 413(1), pp. 261–278. doi: 10.1016/j.jmb.2011.08.012.

Preininger, A. *et al.* (1999) 'Strategies for recombinant Furin employment in a biotechnological process: complete target protein precursor cleavage', *Cytotechnology*. Springer, 30(1–3), p. 1. doi: 10.1023/A:1008030407679.

Provis, J. M. *et al.* (2005) 'Anatomy and development of the macula: specialisation and the vulnerability to macular degeneration', *Clinical and Experimental Optometry*. John Wiley & Sons, Ltd, 88(5), pp. 269–281. doi: 10.1111/J.1444-0938.2005.TB06711.X.

Ramrattan, R. S. *et al.* (1994) 'Morphometric analysis of Bruch's membrane, the choriocapillaris, and the choroid in aging.', *Investigative Ophthalmology & Visual Science*. United States, 35(6), pp. 2857–2864.

Rein, D. B. *et al.* (2022) 'Prevalence of Age-Related Macular Degeneration in the US in 2019', *JAMA Ophthalmology*. American Medical Association, 140(12), pp. 1202–1208. doi: 10.1001/JAMAOPHTHALMOL.2022.4401.

Remacle, A. G. *et al.* (2010) 'Selective and potent furin inhibitors protect cells from anthrax without significant toxicity', *International Journal of Biochemistry and Cell Biology*. NIH Public Access, 42(6), pp. 987–995. doi: 10.1016/j.biocel.2010.02.013.

Rentzsch, P. *et al.* (2019) 'CADD: predicting the deleteriousness of variants throughout the human genome', *Nucleic Acids Research*. Oxford Academic, 47(D1), pp. D886–D894. doi: 10.1093/NAR/GKY1016.

Ricklin, D. *et al.* (2010) 'Complement: a key system for immune surveillance and homeostasis', *Nature Immunology*. 2010/08/19. Nat Immunol, 11(9), pp. 785–797. doi: 10.1038/ni.1923.

Rivera, A. *et al.* (2005) 'Hypothetical LOC387715 is a second major susceptibility gene for age-related macular degeneration, contributing independently of complement factor H to disease risk ', *Human Molecular Genetics*, 14(21), pp. 3227–3236. doi: 10.1093/hmg/ddi353.

Rodriguez, E. *et al.* (2014) 'New functional and structural insights from updated mutational databases for complement factor H, Factor I, membrane cofactor protein and C3', *Bioscience Reports*, 34(5), pp. 635–649. doi: 10.1042/BSR20140117.

Roumenina, L. T. *et al.* (2019) 'Context-dependent roles of complement in cancer', *Nature Reviews Cancer*. Nature Research, pp. 698–715. doi: 10.1038/s41568-019-0210-0.

Roversi, P. *et al.* (2011) 'Structural basis for complement factor I control and its disease-associated sequence polymorphisms', *Proceedings of the National Academy of Sciences*. 2011/07/20, 108(31), pp. 12839–12844. doi: 10.1073/pnas.1102167108.

Ruddy, S. and Austen, K. F. (1969) 'C3 Inactivator of Man: I. Hemolytic Measurement by the Inactivation of Cell-Bound C3', *The Journal of Immunology*, 102(3), pp. 533 LP – 543. Available at: http://www.jimmunol.org/content/102/3/533.abstract.

Ryan, M. D., King, A. M. Q. and Thomas, G. P. (1991) 'Cleavage of foot-and-mouth disease virus polyprotein is mediated by residues located within a 19 amino acid sequence', *Journal of General Virology*. Microbiology Society, 72(11), pp. 2727–2732. doi: 10.1099/0022-1317-72-11-2727.

Sarks, S. H. *et al.* (1999) 'Early drusen formation in the normal and aging eye and their relation to age related maculopathy: a clinicopathological study', *British Journal of Ophthalmology*, 83(3), pp. 358 LP – 368. doi: 10.1136/bjo.83.3.358.

Schaft, T. L. van der *et al.* (1993) 'Early stages of age-related macular degeneration: an immunofluorescence and electron microscopy study.', *British Journal of Ophthalmology*. BMJ

Publishing Group Ltd, 77(10), pp. 657 LP – 661. doi: 10.1136/bjo.77.10.657.

Schmidt, C. Q. *et al.* (2008) 'A new map of glycosaminoglycan and C3b binding sites on factor H', *Journal of Immunology*. J Immunol, 181(4), pp. 2610–2619. doi: 10.4049/JIMMUNOL.181.4.2610.

Schönichen, A. *et al.* (2013) 'Considering Protonation as a Post-translational Modification Regulating Protein Structure and Function', *Annual review of biophysics*. NIH Public Access, 42(1), p. 289. doi: 10.1146/ANNUREV-BIOPHYS-050511-102349.

Schrödinger, L. and DeLano, W. (2020) 'PyMOL'. Available at: http://www.pymol.org/pymol.

Schultz, N. M. *et al.* (2021) 'Global Burden of Dry Age-Related Macular Degeneration: A Targeted Literature Review', *Clinical Therapeutics*. Elsevier Inc., 43(10), pp. 1792–1818. doi: 10.1016/j.clinthera.2021.08.011.

Seddon, J. M. *et al.* (2013) 'Rare variants in CFI, C3 and C9 are associated with high risk of advanced age-related macular degeneration', *Nature Genetics*. 2013/09/17. Nat Genet, 45(11), pp. 1366–1370. doi: 10.1038/ng.2741.

Seddon, J. M., Ajani, U. A. and Mitchell, B. D. (1997) 'Familial aggregation of age-related maculopathy.', *American Journal of Ophthalmology*. United States, 123(2), pp. 199–206. doi: 10.1016/s0002-9394(14)71036-0.

Shiang, R. *et al.* (1989) 'Mapping of the human complement factor I gene to 4q25', *Genomics*, 4(1), pp. 82–86. doi: https://doi.org/10.1016/0888-7543(89)90318-2.

Shoshany, N. *et al.* (2019) 'Rare Genetic Variants in Jewish Patients Suffering from Age-Related Macular Degeneration'. doi: 10.3390/genes10100825.

Smith, G. P. (1985) 'Filamentous fusion phage: Novel expression vectors that display cloned antigens on the virion surface', *Science*. American Association for the Advancement of Science, 228(4705), pp. 1315–1317. doi: 10.1126/science.4001944.

Sokalingam, S. *et al.* (2012) 'A Study on the Effect of Surface Lysine to Arginine Mutagenesis on Protein Stability and Structure Using Green Fluorescent Protein', *PLoS ONE*. Public Library of Science, 7(7), p. e40410. doi: 10.1371/JOURNAL.PONE.0040410.

Swaminathan, A. *et al.* (2014) 'Keyhole limpet haemocyanin - A model antigen for human immunotoxicological studies', *British Journal of Clinical Pharmacology*. Blackwell Publishing

Ltd, 78(5), pp. 1135–1142. doi: 10.1111/bcp.12422.

Tachibana, H., Seki, K. and Murakami, H. (1993) ‘Identification of hybrid-type carbohydrate chains on the light chain of human monoclonal antibody specific to lung adenocarcinoma’, *Biochimica et biophysica acta*. Biochim Biophys Acta, 1182(3), pp. 257–263. doi: 10.1016/0925-4439(93)90067-B.

Takahashi, M. *et al.* (2010) ‘Essential role of Mannose-binding lectin-associated serine protease-1 in activation of the complement factor D’, *Journal of Experimental Medicine*. The Rockefeller University Press, 207(1), pp. 29–37. doi: 10.1084/JEM.20090633.

Talmage, F. J. and Dixon, F. J. (1953) ‘The influence of adjuvants on the elimination of soluble protein antigens and the associated antibody responsesi’, *Journal of Infectious Diseases*. J Infect Dis, 93(2), pp. 176–180. doi: 10.1093/infdis/93.2.176.

Tan, P. L. *et al.* (2017) ‘Systematic functional testing of rare variants: Contributions of CFI to age-related macular degeneration’, *Investigative Ophthalmology & Visual Science*. Association for Research in Vision and Ophthalmology, 58(3), pp. 1570–1576. doi: 10.1167/iovs.16-20867.

Tan, P. L., Rickman, C. B. and Katsanis, N. (2016) ‘AMD and the alternative complement pathway: genetics and functional implications’. doi: 10.1186/s40246-016-0079-x.

Terman, A. and Brunk, U. T. (1998) ‘Lipofuscin: mechanisms of formation and increase with age.’, *APMIS : acta pathologica, microbiologica, et immunologica Scandinavica*. Denmark, 106(2), pp. 265–276. doi: 10.1111/j.1699-0463.1998.tb01346.x.

Thielges, M. C. *et al.* (2011) ‘Influence of Histidine Tag Attachment on Picosecond Protein Dynamics’, *Biochemistry*. American Chemical Society, 50(25), pp. 5799–5805. doi: 10.1021/BI2003923.

Thurman, J. M. *et al.* (2013) ‘Detection of complement activation using monoclonal antibodies against C3d’, *Journal of Clinical Investigation*, 123(5), pp. 2218–2230. doi: 10.1172/JCI65861.

Tseng, M.-H. *et al.* (2018) ‘Serum complement factor I is associated with disease activity of systemic lupus erythematosus’, *Oncotarget*. Impact Journals, 9(9), pp. 8502–8511. doi: 10.18632/ONCOTARGET.23907.

Tsiftsoglou, S. A. *et al.* (2005) 'The Catalytically Active Serine Protease Domain of Human Complement Factor I', *Biochemistry*. American Chemical Society, 44(16), pp. 6239–6249. doi: 10.1021/bi047680t.

Tsiftsoglou, S. A. *et al.* (2006) 'Human complement factor I glycosylation: structural and functional characterisation of the N-linked oligosaccharides.', *Biochimica et biophysica acta*. Netherlands: Elsevier, 1764(11), pp. 1757–1766. doi: 10.1016/j.bbapap.2006.09.007.

Tsiftsoglou, S. A. and Sim, R. B. (2004) 'Human Complement Factor I Does Not Require Cofactors for Cleavage of Synthetic Substrates', *The Journal of Immunology*. The American Association of Immunologists, 173(1), pp. 367–375. doi: 10.4049/jimmunol.173.1.367.

van de Ven, J. *et al.* (2013) 'A functional variant in the CFI gene confers a high risk of age-related macular degeneration', *Nature Genetics*. Nat Genet, 45(7), pp. 813–817. doi: 10.1038/NG.2640.

Vingerling, J. R. *et al.* (1995) 'The prevalence of age-related maculopathy in the Rotterdam Study.', *Ophthalmology*. United States, 102(2), pp. 205–210. doi: 10.1016/s0161-6420(95)31034-2.

Vyse, T. J. *et al.* (1994) 'The Organization of the Human Complement Factor I Gene (IF): A Member of the Serine Protease Gene Family', *Genomics*, 24(1), pp. 90–98. doi: https://doi.org/10.1006/geno.1994.1585.

Wagner, E. K. *et al.* (2016) 'Mapping rare, deleterious mutations in Factor H: Association with early onset, drusen burden, and lower antigenic levels in familial AMD.', *Scientific Reports*, 6, p. 31531. doi: 10.1038/srep31531.

Wang, A. L. *et al.* (2009) 'Changes in Retinal Pigment Epithelium Related to Cigarette Smoke: Possible Relevance to Smoking as a Risk Factor for Age-Related Macular Degeneration', *PLoS ONE*. Public Library of Science, 4(4), p. e5304. doi: 10.1371/JOURNAL.PONE.0005304.

Watson, R. *et al.* (2015) 'Autoantibodies to CD59, CD55, CD46 or CD35 are not associated with atypical haemolytic uraemic syndrome (aHUS)', *Molecular Immunology*. 2014/08/21, 63(2), pp. 287–296. doi: 10.1016/j.molimm.2014.07.017.

Weiler, J. *et al.* (1976) 'Control of the amplification convertase of complement by the plasma protein beta1H', *Proceedings of the National Academy of Sciences of the United States of*

America. Proc Natl Acad Sci U S A, 73(9), pp. 3268–3272. doi: 10.1073/PNAS.73.9.3268.

Wong, M. J. *et al.* (1995) 'Processing of human factor I in COS-1 cells co-transfected with factor I and paired basic amino acid cleaving enzyme (PACE) cDNA', *Molecular Immunology*, 32(5), pp. 379–387. doi: 10.1016/0161-5890(94)00151-P.

Wong, W. L. *et al.* (2014) 'Global prevalence of age-related macular degeneration and disease burden projection for 2020 and 2040: a systematic review and meta-analysis', *The Lancet Global Health*. Lancet Glob Health, 2(2). doi: 10.1016/S2214-109X(13)70145-1.

Woodell, A. and Rohrer, B. (2014) 'A mechanistic review of cigarette smoke and age-related macular degeneration.', *Advances in Experimental Medicine and Biology*. Springer New York LLC, 801, pp. 301–307. doi: 10.1007/978-1-4614-3209-8_38.

Xu, X. *et al.* (2020) 'Regional differences in the global burden of age-related macular degeneration', *BMC Public Health*. BioMed Central, 20(1), pp. 1–9. doi: 10.1186/S12889-020-8445-Y.

Xue, X. *et al.* (2017) 'Regulator-dependent mechanisms of C3b processing by factor I allow differentiation of immune responses', *Nature Structural & Molecular Biology*. 2017/07/04. Nature Publishing Group, 24(8), pp. 643–651. doi: 10.1038/nsmb.3427.

Yang, Z. *et al.* (2005) 'Mutant carbonic anhydrase 4 impairs pH regulation and causes retinal photoreceptor degeneration', *Human Molecular Genetics*. Oxford Academic, 14(2), pp. 255–265. doi: 10.1093/HMG/DDI023.

Yu, Y. *et al.* (2011) 'Association of Variants in the LIPC and ABCA1 Genes with Intermediate and Large Drusen and Advanced Age-Related Macular Degeneration', *Investigative Ophthalmology & Visual Science*, 52(7), pp. 4663–4670. doi: 10.1167/iovs.10-7070.

Zauner, G. *et al.* (2013) 'Glycoproteomic analysis of antibodies', *Molecular & cellular proteomics : MCP*. Mol Cell Proteomics, 12(4), pp. 856–865. doi: 10.1074/MCP.R112.026005.

Zhan, X. *et al.* (2013) 'Identification of a rare coding variant in complement 3 associated with age-related macular degeneration.', *Nature Genetics*, 45(11), pp. 1375–1379. doi: 10.1038/ng.2758.

Zhang, Y. *et al.* (2014) 'Defining the Complement Biomarker Profile of C3 Glomerulopathy', *Clinical Journal of the American Society of Nephrology*. American Society of Nephrology, 9(11), p. 1876. doi: 10.2215/CJN.01820214.

Zhang, Y. *et al.* (2015) 'Very high cell density perfusion of CHO cells anchored in a non-woven matrix-based bioreactor', *Journal of Biotechnology*. J Biotechnol, 213, pp. 28–41. doi: 10.1016/J.JBIOTEC.2015.07.006.

Zhong, T. Y. *et al.* (2016) 'Hemocyanins Stimulate Innate Immunity by Inducing Different Temporal Patterns of Proinflammatory Cytokine Expression in Macrophages', *The Journal of Immunology*, 196(11), pp. 4650 LP – 4662. doi: 10.4049/jimmunol.1501156.

Publications and Presentations

Papers Under Preparation

Hallam T.M.[1], **Cox T.E.[1]**, Smith-Jackson K., Brocklebank V, Baral A.J., Tzoumas N, Steel D.H, Wong E.K.S., Shuttleworth V.G., Lotery A.J., Harris C.L., Marchbank K.J, Kavanagh D. A novel method for real-time analysis of the complement C3b:FH:FI complex reveals dominant negative CFI variants in Age-related Macular Degeneration. Frontiers in Immunology.

Kamala O, Malik T. H., Hallam T. M., **Cox T.E.**, Yang Y, Vyas F, Luli S, Connelly C, Gibson B, Smith-Jackson K, Denton H, Pappworth I. Y., Huang L, Kavanagh D, Pickering M. C., & Marchbank K. J. Homodimeric Minimal Factor H: *In vivo* Tracking and Extended Dosing Studies in Factor H Deficient Mice. Frontiers in Immunology.

Cox T.E., Kavanagh D, Marchbank K.J. *et al.* Functional analysis of Pro-I, the precursor to Factor I. (Manuscript in preparation).

Published Papers

Gleeson P.J.[1], Wilson V[1], **Cox T.E.[1]**, Sharma S.D., Smith-Jackson K, Strain L, Lappin D, McHale T, Kavanagh D[1], Goodship T.H.J.[1] Chromosomal rearrangement – a rare cause of *complement factor I* associated atypical haemolytic uraemic syndrome (2016). Immunobiology, 221(10), 1124-1130.

Wong E.K.S., Hallam T.M., Brocklebank V, Walsh P.R., Smith-Jackson K, Shuttleworth V.G., **Cox T.E.**, Anderson H.E., Barlow P.N, Marchbank K.J, Harris C.L., Kavanagh D. Functional Characterization of Rare Genetic Variants in the N-Terminus of Complement Factor H in aHUS, C3G, and AMD (2020). Frontiers in Immunology, 11: 602284.

McMahon O, Hallam T.M., Patel S, Harris C.L., Menny A, Zelek W.M., Widjajahakim R, Java A, **Cox T.E.**, Tzoumas N, Steel D.H.W., Shuttleworth V.G., Smith-Jackson K, Brocklebank V, Griffiths H, Cree A.J., Atkinson J.P., Lotery A.J., Bubeck D, Morgan B.P., Marchbank K.J., Seddon J.M., Kavanagh D. The rare C9 P167S risk variant for age-related macular degeneration increases polymerization of the terminal component of the complement cascade (2021). Human Molecular Genetics. 30(13): 1188-1199.

Cox T.E., Marchbank K.J., Kavanagh D., Harris C. Patent for the generation of fully mature human complement factor I protein.

Oral Presentations

- June 2018, Immunology North-East, Durham UK
- November 2017, North-East Postgraduate Conference, Newcastle UK
- May 2017, Newcastle University Academic Medicine Society Conference, Newcastle UK
- June 2016, North-East Renal Research Symposium, Newcastle UK

Poster Presentations

- November 2019, North-East Postgraduate Conference, Newcastle UK
- May 2018, MRC DTP Conference, Manchester UK

Appendix 1: Immunisation peptide amino acid sequence homology

Amino acid sequence homology for human and mouse *CFI* in the region spanned by the immunisation peptide. Differing amino acids are highlight in red.

Human	G	V	K	N	R	M	H	I	R	R	K	R	I	V	G	G	K	R	A	Q
Mouse	G	V	K	R	N	T	H	T	R	R	K	R	V	I	G	G	K	P	A	N

Appendix 2: Primers for site-directed mutagenesis

Mutagenesis primers were HPLC-purified from Integrated DNA Technologies. The mutated base pairs have been capitalised.

Variant	Forward Primer	Reverse Primer
R406H	ggatacaccccgaccttaaacAtatagtaattgaatacgtg	cacgtattcaattactataTgtttaaggtcggggtgtatcc
K441R	tgaaatgaaaaaagacggaaacaGaaaagattgtgagctgc	gcagctcacaatcttttCtgtttccgtctttttcatttca
P553S	ggaaaactgtggaaaaTcagagttcccaggtgtttacaccaaagtggc	gccactttggtgtaaacacctgggaactctgAttttccacagttttcc
S525A	cctgtaaaggggacGctggaggccccttagtctgtatggatgc	gcatccatacagactaaggggcctccagCgtcccctttacagg
STOP	ggccttttatttctcagtacaatgtaTAGgatgacgataagc	gcttatcgtcatcCTAtacattgtactgagaaataaaaggcc

Appendix 3: Sequencing primers

Primers for sequencing pDEF-*CFI* and *CFI* IRES vector.

Name	Primer sequence
CFI 1F TC	ccacttaaggttttgcaaggtc
CFI 1R TC	ctgtcaacaaaagagtttggaatg
CFI 2F TC	agtgtttccttgaagcatgg
CFI 3F TC	cagatgaaagcctgtgatgg
CFI 4F TC	atgccagtggaatcacctgt
CFI 5F TC	gctggggacgagaaaaagat
CFI 6R TC	tacattgtactgagaaataaaag